TRANSACTIONS
OF THE ASME
Series C

# Journal of HEAT TRANSFER

February 1960

RADIATION • CONDUCTION • CONVECTION • COMPLEX SYSTEMS • PHASE CHANGES AND MIXTURES • TRANSIENT PHENOMENA • THERMOPHYSICAL PROPERTIES • EXPERIMENTAL TECHNIQUES • THERMOMETRY • ANALOG METHODS • ANALYTICAL AND NUMERICAL METHODS • APPLICATIONS • DESIGN TECHNIQUES • HEAT EXCHANGERS • INSULATION • ECONOMIC FACTORS BIOTECHNOLOGY • ASTRONAUTICS

Published Quarterly by
THE AMERICAN SOCIETY OF MECHANICAL ENGINEERS

TRANSACTIONS
OF THE ASME
Series C

EDITORIAL DEPARTMENT

Editor, J. J. JAKLITSCH, JR.
Consulting Editor, LEO BLODGETT
Production, JEAN NORTH
Art Editor, HENRY BALFOUR

HEAT TRANSFER DIVISION

Chairman, H. A. JOHNSON
Secretary, S. OSTRACH
Consulting Editor, S. P. KEZIOS

OFFICERS OF THE ASME

President, W. L. CISLER
Secretary, O. B. SCHIER, II
Treasurer, E. J. KATES
Assistant Treasurer, H. J. BAUER

PUBLICATIONS COMMITTEE

Chairman, B. G. A. SKROTZKI
HENDLEY N. BLACKMON
R. D. MINDLIN
MARTIN GOLAND
VITO L. SALERNO
Junior Representatives
A. S. GOLDSTEIN
J. W. FOLLANSBEE

REGIONAL ADVISORY BOARD

Region I, H. M. ROGERS, JR.
Region II, GLENN R. FRYLING
Region III, F. J. HEINZE
Region IV, FRANCIS C. SMITH
Region V, H. M. CATHER
Region VI, C. R. EARLE
Region VII, M. S. UMBENHAUER
Region VIII, LINN HELANDER

Published quarterly by The American Society of Mechanical Engineers. Publication office at 20th and Northampton Streets, Easton, Pa. The editorial department is located at the headquarters of the Society, 29 West Thirty-Ninth Street, New York 18, N. Y. Cable address, "Mechaneer," New York. Price $3.00 a copy, $10.00 annually; to members, $1.50 a copy, $5.00 annually. Add 50 cents for postage to all countries outside the United States and Canada. Changes of address must be received at Society headquarters seven weeks before they are to be effective on the mailing list. Please send old as well as new address. . . . By-Law: The Society shall not be responsible for statements or opinions advanced in papers or . . . printed in its publications (B13, Par. 4). . . . Second-class mail privileges authorized at Easton, Penna. . . . This publication is authorized to be mailed at the special rates of postage prescribed by Section 132.122 . . . © Copyrighted, 1960, by The American Society of Mechanical Engineers. Reprints from this publication may be made on condition that full credit be given the Transactions of the ASME, Series C—Journal of Heat Transfer, and the author, and that date of publication be stated.

TRANSACTIONS OF THE ASME
is indexed by the Engineering Index, Inc.

# Journal of HEAT TRANSFER

VOL. 82 • SERIES C • NO. 1

February 1960

## CONTENTS

1 **Radiant Interchange Within an Enclosure**
*J. T. Bevans and R. V. Dunkle*

20 **Numerical Solutions to an Inverse Problem of Heat Conduction for Simple Shapes**
*G. Stolz, Jr.*

27 **Effect of Thermocouple Cavity on Heat Sink Temperature**
*J. V. Beck and H. Hurwicz*

37 **Freezing of a Growing Liquid Column**
*G. Horvay*

48 **Measurement of the Thermal Conductivities of Gases at High Temperatures**
*R. G. Vines*

53 **Laminar Transfer From Isothermal Spanwise Strips on a Flat Plate**
*H. H. Sogin*

64 **Spectral Characteristics of Fabrics From 1 to 23 Microns**
*R. V. Dunkle, F. Ehrenburg, and J. T. Gier*

**TECHNICAL BRIEFS**

71 **The Effect of Vapor Drag on Rotating Condensation**
*E. M. Sparrow and J. L. Gregg*

73 **Radiation Fin Effectiveness**
*J. G. Bartas and W. H. Sellers*

75 **A Tabulaton of the Function exp $X^2$ erfc X**
*J. E. Sunderland and R. J. Grosh*

TRANSACTIONS OF THE ASME Series B

Journal of
ENGINEERING FOR INDUSTRY

Volume 82 • Series B • Number 1

CONTENTS FOR FEBRUARY, 1960

1 Design and Analysis of Welded Pressure-Vessel Skirt Supports, by N. A. Weil and J. J. Murphy. (58—A-153)

15 Static Testing High-Pressure Piping Components, by T. G. Moore and E. J. Opersteny.

23 Tire Testing, by J. W. Hannell. (59—SA-48)

29 Nomographic Synthesis of Generator Linkages, by D. P. Adams. (59—SA-11)

41 The Effect of Presetting Helical Compression Springs, by T. J. Atterbury and W. B. Diboll, Jr. (59—SA-12)

47 A Quantitative Investigation of the Factors Which Influence the Fatigue Life of a V-Belt, by S. M. Marco, W. L. Starkey, and K. G. Hornung. (59—SA-18)

60 Edge Influence Coefficients for Toroidal Shells of Positive Gaussian Curvature, by G. D. Galletly. (59—Pet-2)

69 Edge Influence Coefficients for Toroidal Shells of Negative Gaussian Curvature, by G. D. Galletly. (59—Pet-3)

76 The Influence of Surface Residual Stress on Fatigue Limit of Titanium, by E. C. Reed and J. A. Viens. (59—Prod-1)

79 Shear-Zone Size, Compressive Stress, and Shear Strain in Metal-Cutting and Their Effects on Mean Shear-Flow Stress, by Dimitri Kececioglu. (59—Prod-3)

TRANSACTIONS OF THE ASME Series A

Journal of
ENGINEERING FOR POWER

Volume 82 • Series A • Number 1

CONTENTS FOR JANUARY, 1960

1 Development of a Three-Stage Liquid-Cooled Gas Turbine, by Sumner Alpert, R. E. Grey, and W. O. Flaschar. (59—GTP-1)

10 Effect of Ambient and Fuel Pressure on Spray Drop Size, by S. M. DeCorso. (59—GTP-3)

19 Presentation of a Blade-Design Method for Axial-Flow Turbines, Including Design and Test Results of a Typical Axial-Flow Stage, by F. Baumgartner and R. Amsler. (59—GTP-4)

27 The Basic Heat Transfer and Flow Friction Characteristics of Six Compact High-Performance Heat Transfer Surfaces, by W. M. Kays. (59—GTP-2)

35 Metallurgical Evaluation of Superheater-Tube Alloys After Six-Months' Exposure at Temperatures of 1100 to 1500 F, by C. L. Clark, J. J. B. Rutherford, A. B. Wilder, and M. A. Cordovi. (59—Pwr-1)

68 Blast-Furnace-Gas Cleaning for Iron and Ferromanganese Production, by J. S. Mackay and J. F. Kearns.

73 Influence Coefficients for Open-Crown Hemispheres, by G. D. Galletly. (59—SA-4)

TRANSACTIONS OF THE ASME Series D

Journal of
BASIC ENGINEERING

Vol. 81 • Series D • No. 4

CONTENTS FOR DECEMBER, 1959

433 Applications of Computer and Model Studies to Problems Involving Hydraulic Transients, by I. W. McCaig and F. H. Jonker. (58—A-101)

446 Large Water-Level Displacements in the Simple Surge Tank, by A. W. Morris. (58—A-29)

455 Experience in the Use of the Gibson Method of Water Measurement for Efficiency Tests of Hydraulic Turbines, by N. R. Gibson. (58—A-78)

488 Free Discharge Through a Turbine Distributor, Case, and Draft Tube, by R. A. Sutherland. (58—A-76)

493 Symposium on Welded Spiral Cases From the Manufacturer's Viewpoint. (58—A-60)

505 Dériaz Type Reversible Pump-Turbine Installation at Sir Adam Beck-Niagara Forebay Pumped Storage Project, by A. E. Aeberli. (58—A-77)

521 Reversible Pump-Turbines for Sir Adam Beck-Niagara Pumping-Generator Station, by P. Dériaz and J. G. Warnock. (58—A-108)

534 Some Hydraulic Features of Puntledge Generating Plant, by A. W. Lash and R. E. Passmore. (58—A-100)

543 Application of Boundary-Layer Theory in Turbomachinery, by H. Schlichting.

552 Radial Equilibrium in Supersonic Compressors, by A. G. Hammitt and S. M. Bogdonoff. (58—A-110)

559 Résumé of the Supersonic-Compressor Research at NACA Lewis Laboratory, by W. W. Wilcox, E. R. Tysl, and M. J. Hartmann. (58—A-177)

569 Application and Analysis of a Computer Control System, by Irving Lefkowitz and D. P. Eckman. (58—A-281)

578 The Response of Pneumatic Transmission Lines to Step Inputs, by C. B. Schuder and R. C. Binder. (58—A-136)

585 A General Approach to the Practical Solution of Creep Problems, by A. Mendelson, M. H. Hirschberg, and S. S. Manson. (58—A-98)

599 Multiaxial Creep Studies on Inconel at 1500 F, by C. R. Kennedy, W. O. Harms, and D. A. Douglas. (58—A-193)

610 Creep-Rupture Strength of Austenitic Cr-Ni-Mo Steels in Sheet and Bar Form, by G. V. Smith, F. Garofalo, R. W. Whitmore, and R. R. Burt. (58—A-102)

617 Correlation of High Temperature Creep and Rupture Data, by Hans Conrad. (58—A-96)

629 Comparison of Parameter Methods for Extrapolating High-Temperature Data, by R. M. Goldhoff. (58—A-121)

645 Tests on Deflection of Flat Oval Bourdon Tubes, by G. Kardos. (58—A-67)

651 Bending and Stretching of Corrugated Diaphragms, by R. F. Dressler. (58—A-62)

660 Electromagnetic Flowmeter Primary Elements, by V. P. Head. (58—A-126)

669 The Distribution of Contact Pressures in the Rolling of Metals, by C. W. MacGregor and R. B. Palme. (58—A-260)

681 The Effects of Friction in the Rolling of Metals, by M. D. Stone.

TRANSACTIONS OF THE ASME
Series E

Journal of
APPLIED MECHANICS

Vol. 81 • Series E • No. 4

CONTENTS FOR DECEMBER, 1959

TECHNICAL PAPERS

477 Boundary-Layer Solution for a Flow in a Diverging Passage Having a Swirl Component, M. A. Sinbel. (59—APMW-14)

485 Slow Rotatory Motion of a Circular Disk About One of Its Diameters in a Viscous Fluid, R. P. Kanwal. (59—APMW-6)

488 Thermal Stresses Owing to a Hot Spot in a Rectangular Strip, C. W. Nelson. (59—A-8)

491 Impact and Moving Loads on a Slightly Curved Elastic Half Space, A. C. Eringen and J. C. Samuels. (59—A-2)

499 Stability of Forced Oscillations With Nonlinear Second-Order Terms, Chi-Neng Shen. (59—A-19)

503 On Inertia Effects in a Transient Thermoelastic Problem, Eli Sternberg and J. G. Chakravorty. (59—APM-9)

510 Coupled Torsional and Longitudinal Vibrations of a Thin Bar, R. C. Di Prima. (59—A-18)

513 Production of Rotation in a Confined Liquid Through Translational Motion of the Boundaries, R. R. Berlot. (59—A-15)

517 Nonlinear Creep Deformations of Columns of Rectangular Cross Section, H. H. Bleich and O. W. Dillon, Jr. (59—A-1)

526 Forced Vibrations of a Circular Plate, Herbert Reismann. (59—A-9)

528 On the Propagation of Shock Waves in a Nonhomogeneous Elastic Medium, Eli Sternberg and J. G. Chakravorty. (59—APMW-17)

537 The Frequency of Flexural Vibration of Rectangular Orthotropic Plates With Clamped or Supported Edges, R. F. S. Hearmon. (59—APM-8)

541 Axially Symmetric Extensional Vibrations of a Circular Disk With a Concentric Hole, O. G. Gustafsson and T. R. Kane. (59—A-32)

546 Analysis of a Nonlinear Mechanical System With Three Degrees of Freedom, S. A. Hovanessian. (59—APM-29)

549 Stresses in an Ellipsoidal Rotor in a Centrifugal Force Field, M. A. Goldberg and Michael Sadowsky. (59—A-4)

553 Carrying Capacity of Elastic-Plastic Shells With Various End Conditions, Burton Paul. (59—APM-16)

561 Extensional Vibrations of Elastic Plates, R. D. Mindlin and M. A. Medick. (59—APM-4)

570 Triaxial Tension at the Head of a Rapidly Running Crack in a Plate, J. M. Frankland. (59—APM-11)

573 Viscous Flow Through Tubes of Multiply Connected Cross Sections, F. A. Gaydon and H. Nuttall. (59—APM-28)

577 On the Accuracy of Some Shell Solutions, G. D. Galletly and J. R. M. Radok. (59—APM-30)

584 The Drag on Spheres and Cylinders in a Stream of Dust-Laden Air, Thomas Gillespie and A. W. Gunter. (59—APM-14)

587 Elastic Flexible Cable in Plane Motion Under Tension, Wen-Hsiung Li. (59—A-6)

594 Incremental Stress-Strain Law Applied to Work-Hardening Plastic Materials, Chintsun Hwang. (59—APM-15)

599 On the Plastic Flow of Coulomb Solids Beyond Original Failure, A. W. Jenike and R. T. Shield. (59—A-7)

603 The Free Vibrations of Grillages, J. P. Ellington and H. McCallion. (59—APMW-12)

608 Piping Flexibility Analysis by Stiffness Matrix, L. H. Chen. (59—APM-24)

613 A Photoelastic Approach to Transient Stress Problems Employing Low-Modulus Materials, J. W. Dally, W. F. Riley, and A. J. Durelli. (59—A-10)

621 Rupture Characteristics of Safety Diaphragms, N. A. Weil. (59—APMW-3)

625 Bending of Isosceles Right Triangular Plates, H. J. Fletcher. (59—APMW-19)

629 Developments in the Application of the Grid Method to Dynamic Problems, A. J. Durelli, J. W. Dally, and W. F. Riley. (59—APMW-1)

635 The Solution of Elastic Stability Problems With the Electric Analog Computer, J. H. Shields and R. H. MacNeal. (59—APMW-20)

643 Symmetric Vortex Separation on Circular Cylinders and Cones, A. E. Bryson. (59—APMW-13)

649 Thermoelastic Problem for a Transversely Isotropic Hollow Sphere Embedded in an Elastic Medium, J. Nowinski. (59—APM-27)

651 Transient Analysis of Stress-Wave Penetration in Plates, Norman Davids. (59—A-16)

661 Transverse Flexure of a Semi-Infinite Thin Plate Containing an Infinite Row of Circular Holes, O. Tamate. (59—APMW-15)

666 Fundamental Frequency of a Thin, Flat Circular Plate Simply Supported Along a Circle of Abritrary Radius, R. Y. Bodine. (59—APMW-10)

669 BRIEF NOTES

689 DISCUSSION

696 BOOK REVIEWS

# Radiant Interchange Within an Enclosure

J. T. BEVANS[1]
R. V. DUNKLE[2]

## Part 1 Absorption and Emission Behavior of Gases

### Introduction

THIS IS THE FIRST of three papers relating to a general analysis of the radiant interchange within an enclosure filled with an absorbing and emitting medium, i.e., combustion products. The problem is approached initially by reviewing the basic physics of the absorption (or emission) of thermal radiation by gases (Part 1). The band approximations of Elsasser [6][3] are examined and compared with the experimental results of Howard, et al. [12]. The inapplicability of the exponential absorption law on a band energy or total energy basis is briefly discussed and the deviations from experiment pointed out. As an engineering approximation to the use of a monochromatic energy analysis, the absorption of gases on the band energy basis is incorporated in the geometrical interchange relationships between two surfaces.

In Part 2, the network method of Oppenheim [16] is used to derive the basic network relationships between one node and the other nodes of an enclosure. This is first done on a monochromatic basis and then reduced to the band energy approximation using the results of Part 1. The usual method of analysis, the gray radiation approximation, is shown to follow from the band energy and to be generally an approximation of lesser accuracy. A reiterative method of solving the network node equations for as many nodes as deemed practicable is presented in Part 3 and specific solutions are given as examples. These examples are used to illustrate the relative accuracies of the band energy and the gray radiation approximations.

In order to obtain a solution of the enclosure problem, a number of assumptions have been required. These assumptions were necessitated by the inadequacy of present knowledge. Also, sufficient information does not exist regarding the radiative characteristics of materials to permit a numerical analysis of most enclosures. These gaps in analytical and physical knowledge are indicated and are promising areas for both theoretical and experimental study.

### Basic Transfer Equations

The general expression for the net attenuation of a beam of monochromatic energy in an absorbing and emitting medium is given by [6]:

$$dI_\nu = k_\nu(I_{b\nu} - I_\nu)dm \tag{1}$$

This relation implies the use of Kirchhoff's law equating the emission and absorption of the medium. A more familiar form of equation (1) may be obtained by assuming the emission of the medium to be zero:

$$dI_\nu = -k_\nu I_\nu dm \tag{1a}$$

The mass of the medium used in either of these expressions refers to the molecules which are active in the absorption or emission process at the frequency of the incident energy. This mass is related to the concentration of the active molecules in the path by:

$$dm = \rho dr \tag{2}$$

Equation (1) may be integrated for an isothermal homogeneous medium for the usual boundary conditions:

$$m = 0;\ I_\nu = I_{\nu 0} \tag{3a}$$

to give:

$$I_\nu = I_{b\nu}[1 - \exp(-k_\nu m)] + I_{\nu 0}[\exp(-k_\nu m)] \tag{3b}$$

The restriction to isothermal homogeneous media cannot be removed until a specification is made of the temperature dependency of $k_\nu$, $m$, and $I_{b\nu}$. The latter is known since it is given by Planck's law of ideal radiation; the first is a property of the medium; and the second is a variable of the particular problem. Specific conditions can be established which would permit the integration of this equation but a general form is not readily obtainable. Any approximate analysis of nonisothermal media must begin by satisfying the requirements of equation (1) or by ascertaining the magnitude and direction of the error by some method. The exponential factors appearing in equation (3b) are conveniently used to define the transmission and absorption (or emission) of the medium:

$$\tau_\nu = \exp(-k_\nu m) \tag{4}$$

$$\alpha_\nu = 1 - [\exp(-k_\nu m)] = 1 - \tau_\nu \tag{5}$$

As a first step in developing the radiation exchange equations, two surfaces separated by an absorbing and emitting medium will be considered (Fig. 1). The gas volume involved is that volume determined by the two areas and the outermost envelope formed by straight lines connecting the boundaries of the two areas. That is, for any point on surface one, the gas volume considered lies within the solid angle defined by surface two. The converse is true for any point on surface two. The intensity of radiation leaving an opaque surface consists of radiation emitted and reflected by the surface. The irradiation of surface one from the direction of surface two is given by:

$$\Gamma_{2\to 1} = \int_{A_1}\int_{A_2}\int_0^\infty (I_{b\nu}\alpha_\nu + I_{\nu 2}\tau_\nu)\frac{\cos\theta_1\cos\theta_2}{r^2}\,dA_1 dA_2 d\nu \tag{6a}$$

---

[1] Shell Development Company, Emeryville, Calif. Mem. ASME.
[2] Associate Professor, Mechanical Engineering Department, University of California, Berkeley, Calif.
[3] Numbers in brackets designate References at end of Part 3.

Contributed by the Heat Transfer Division of THE AMERICAN SOCIETY OF MECHANICAL ENGINEERS and presented at the ASME-AIChE Heat Transfer Conference, Storrs, Conn., August 9–12, 1959.
NOTE: Statements and opinions advanced in papers are to be understood as individual expressions of their authors and not those of the Society. Manuscript received at ASME Headquarters, April 29, 1959. Paper No. 59—HT-4.

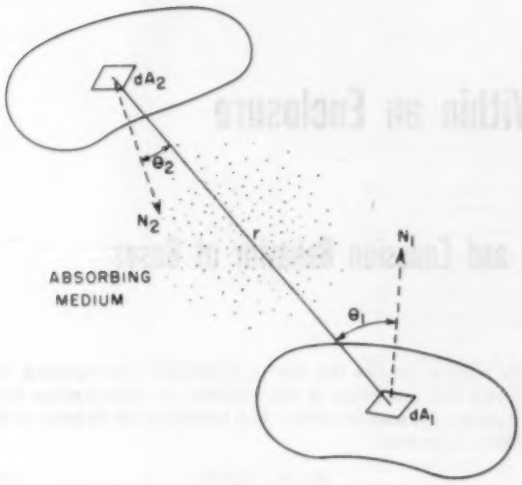


**Fig. 1 Geometry of radiation exchange between two surfaces with an absorbing medium**

Similarly for surface 2, the incident energy from the direction of surface 1 is:

$$\Gamma_{1\to 2} = \int_{A_1}\int_{A_2}\int_0^\infty (I_{b\nu}\alpha_\nu + I_{\nu 1}\tau_\nu)\frac{\cos\theta_1\cos\theta_2}{r^2}\,dA_1dA_2d\nu \tag{6b}$$

The irradiation of a surface from the direction of a second surface in an enclosure filled with an emitting medium is given by equation (6a) or (6b). This is composed of the radiation emitted by the medium and the transmitted radiation from the bounding surfaces. The emission from the gas is determined by the same geometry as the transmitted radiation. The radiation originating (emitted plus reflected) at either surface 1 or 2 and absorbed by the intervening medium is given by:

$$\Gamma_{(1+2)\to 2} = \int_{A_1}\int_{A_2}\int_0^\infty \alpha_\nu(I_{\nu 1} + I_{\nu 2})\frac{\cos\theta_1\cos\theta_2}{r^2}\,dA_1dA_2d\nu \tag{6c}$$

The net heat transfer to the medium by radiation is obtained by subtracting from equation (6c), the energy emitted by the medium and directly striking surface 1 or 2. The net energy exchange between the two surfaces is the difference between equations (6a) and (6b):

$$q_{1\to 2} = \int_{A_1}\int_{A_2}\int_0^\infty \tau_\nu(I_{\nu 1} - I_{\nu 2})\frac{\cos\theta_1\cos\theta_2}{r^2}\,dA_1dA_2d\nu \tag{7a}$$

This equation should be clearly understood to apply only to the net radiation flux between two surfaces and only for black surfaces does it represent the actual heat gained or lost by the surface. The radiosity of a surface is equal to $\pi$ times the intensity for a diffuse surface, and for a black surface (emissivity of unity) the radiosity becomes identical with the emissive power. The remainder of the discussion will be restricted to diffuse surfaces, although many of the relations given will be equally valid for nondiffuse conditions. Equation (7a) may be rewritten with the use of the relation between monochromatic radiosity and monochromatic intensity:

$$q_{1\to 2} = \int_{A_1}\int_{A_2}\int_0^\infty (J_{\nu 1} - J_{\nu 2})\tau_\nu\frac{\cos\theta_1\cos\theta_2}{\pi r^2}\,dA_1dA_2d\nu \tag{7b}$$

For a transmissivity of unity and black surfaces, i.e., the radiosity equals the monochromatic emissive power ($E_\nu$), this last expression becomes the conventional radiant interchange equation:

$$q_{1\to 2} = A_1F_{12}\sigma(T_1^4 - T_2^4) \tag{8a}$$

$$A_1F_{12} = A_2F_{21} = \int_{A_1}\int_{A_2}\frac{\cos\theta_1\cos\theta_2}{\pi r^2}\,dA_1dA_2 \tag{8b}$$

$$\sigma T^4 = \int_0^\infty E_\nu d\nu \tag{8c}$$

## Theoretical Gas Absorptivities or Transmissivities

Equation (3b) may be integrated over all frequencies to determine an absorption or transmission in terms of the concentration of the absorbing medium lying along a straight line path. The resulting expression may be substituted in equation (7a) since the integration with respect to the frequency is independent of geometry. This integration may be written as a transmissivity or an absorptivity, thus:

$$\tau = \frac{\int_0^\infty J_\nu[\exp(-k_\nu m)]d\nu}{\int_0^\infty J_\nu d\nu} \tag{9}$$

$$\alpha = \frac{\int_0^\infty J_\nu[1 - \exp(-k_\nu m)]d\nu}{\int_0^\infty J_\nu d\nu} \tag{10}$$

The transmissivity and absorptivity of a medium are quantities relating the effect of the medium upon the radiation from an external source. The expression for the emissivity of the medium is of the same form as that for the absorptivity but with the monochromatic emissive power corresponding to a Plankian radiator at the temperature of the medium substituted for the monochromatic radiosity of the external source. Therefore, in general, the total absorptivity and emissivity of a medium are only equal if the monochromatic radiosity of the source is equal to the monochromatic emissive power of a black body at the temperature of the medium at all frequencies where the medium absorbs radiation. The media of principal engineering interest are gases and the remaining discussion will be further restricted to these media.

The emission or absorption of radiation by a gas does not extend continuously over the whole spectrum as does that of a solid body. Instead, the emission or absorption of radiation is restricted to specific regions of the spectrum. A complete description of molecular spectra is beyond the requirements of this paper and only an approximate description is necessary to demonstrate the structure of this type of spectra.

The emission or absorption of energy by a gas is caused by changes in the energy levels of the molecules composing that gas, in accordance with Planck's law:

$$\Delta W = h\nu \tag{11}$$

The energy levels of a molecule may be written as the sum of the energies of the possible modes of oscillation:

$$W = W_e + W_v + W_r \tag{12}$$

The magnitudes of the electronic, vibrational, and rotational energies are such that as a generality, electronic transitions give rise to lines in the visible and shorter wave lengths, vibrational changes are in the infrared and rotational transitions are in the far infrared frequencies. However, the vibrational energy levels of a molecule are intimately coupled to the rotational levels and if the frequency of the energy has the correct value, a rotational transition may occur simultaneously with a vibrational transition.

Since the vibrational energies are much larger than the rotational energies, the frequency determined by the vibrational energy difference is dominant and the rotational differences cause perturbations of this basic frequency. As a result, the spectrum of a gas in the region of a vibrational frequency will be composed of a number of absorption lines in the vicinity of this vibrational frequency. This is commonly referred to as a vibration-rotation band and the individual absorption or emission lines within the band are the rotation lines. If more detailed information is desired, reference should be made to texts on molecular spectra [9].

The emission or absorption of energy by molecules as a result of electronic energy changes in combination with vibrational and rotational energy changes (the rotation energy changes are not necessarily required) give rise to lines in the ultraviolet, visible, and near infrared. This is the band spectra observed from a gas in a highly excited state, e.g., in shock tubes or flames. These bands consist of many lines closely spaced but occur in regions for which instrumentation of high resolving power is available. Possibly as a consequence, the analyses of these bands are generally restricted to the examination of the lines within the band relative to each other rather than to the band itelf. To the best of the authors' knowledge, these bands have not been studied in a manner similar to the studies of the vibration-rotation bands which will be described. At the present time, treatment of these electronics bands in a manner analogous to the procedure to be described for vibration-rotation bands is not possible. This is due to the lack of experimental and analytical information regarding the electronic bands.

These prefacing remarks were necessary to partially justify definitions of total line and band absorptions. A total line absorption would be for the total absorption of a single line, either rotation or electronic, and a total band absorption would apply to the total absorption of a vibrational-rotation band:

$$a_L = \frac{\int_{\Delta\nu_L} J_\nu[1 - \exp(-k_\nu m)]d\nu}{\int_{\Delta\nu_L} J_\nu d\nu} \tag{13}$$

$$a_B = \frac{\int_{\Delta\nu_B} J_\nu[1 - \exp(-k_\nu m)]d\nu}{\int_{\Delta\nu_B} J_\nu d\nu} \tag{14}$$

$$t_L = \frac{\int_{\Delta\nu_L} J_\nu[\exp(-k_\nu m)]d\nu}{\int_{\Delta\nu_L} J_\nu d\nu} \tag{15}$$

$$t_B = \frac{\int_{\Delta\nu_B} J_\nu[\exp(-k_\nu m)]d\nu}{\int_{\Delta\nu_B} J_\nu d\nu} \tag{16}$$

The total transmissivity and absorptivity of the gas [equations (9) and (10)] are given by:

$$\alpha = \frac{1}{\int_0^\infty J_\nu d\nu}\left\{\sum_1^\varphi a_{B\varphi}\int_{\Delta\nu_{B\varphi}} J_\nu d\nu + \sum_{L=1}^{\Psi} a_{L\Psi}\int_{\Delta\nu_{L\Psi}} J_\nu d\nu\right\} \tag{17}$$

$$\tau = \frac{1}{\int_0^\infty J_\nu d\nu}\left\{\sum_1^\varphi t_{B\varphi}\int_{\Delta\nu_{B\varphi}} J_\nu d\nu + \sum_{L=1}^{\Psi} t_{L\Psi}\int_{\Delta\nu_{L\Psi}} J_\nu d\nu\right\} \tag{18}$$

Inspection of the necessary equations will show the usual identities associated with the absorptivity and transmissivity have been retained:

$$a_L + t_L = 1 \tag{19a}$$

$$a_B + t_B = 1 \tag{19b}$$

$$\alpha + \tau = 1 \tag{19c}$$

Inclusion of both line and band absorptions in equations (17) and (18) permits the consideration of line and band effects which may occur in combustion and shock wave processes. For many engineering purposes, the importance of the line absorptions is negligible and only the influence of the bands must be considered.

**Absorption of a Single Isolated Line.** The determination of the absorption of a single line outside vibration-rotation band requires a specification of the variation of the absorption coefficient with frequency. This is generally accepted to be given by the Lorents equation:

$$k_\nu = \frac{s}{\pi}\left[\frac{\delta}{(\nu - \nu_o)^2 + \delta^2}\right] \tag{20}$$

where

$$S = \int_{-\infty}^{\infty} k_\nu d\nu \tag{21}$$

Substitution of equation (20) into equation (13) gives an equation which cannot be integrated without a specification of the frequency. However, Elsasser [6] observed that the expression could be integrated by assuming: (*a*) The absorption of the line is essentially complete in the interval $\Delta\nu_L$, i.e., $\Delta\nu_L \gg \delta$, and (*b*) the intensity of the incident energy is constant over the interval $\Delta\nu_L$. The second assumption permits the monochromatic emissive power to be removed from the integral and yields an integral in closed analytic form. The result for a homogeneous medium is:

$$a_L = \frac{2\pi\delta}{\Delta\nu_L}[J_o(i\beta) - iJ_1(i\beta)][\exp(-\beta)] \tag{22}$$

$$\beta = \frac{Sm}{2\pi\delta} \tag{23}$$

where $J_0$ and $J_1$ = Bessel functions of the zeroth and first order. This expression can be expanded to obtain values of the line absorption for small and large values of [6]:

$$\beta \ll 1; \quad a_L = \frac{Sm}{\Delta\nu_L} \tag{24a}$$

$$\beta \gg 1; \quad a_L = \frac{2}{\Delta\nu_L}(Sm\delta)^{1/2} \tag{24b}$$

The corresponding expressions for the transmission of a single line are:

$$t_L = 1 - \left\{\frac{2\pi\delta}{\Delta\nu_L}[J_o(i\beta) - J_1(i\beta)][\exp(-\beta)]\right\} \tag{25a}$$

$$t_L = 1 - \frac{Sm}{\Delta\nu_L}; \quad \beta \ll 1 \tag{25b}$$

$$t_L = 1 - \frac{2(Sm\delta)^{1/2}}{\Delta\nu_L}; \quad \beta \gg 1 \tag{25c}$$

The latter expressions should be compared with usual assumption of exponential transmission of a gas. Only for the case of small $\beta$ [equation (25*b*)] would the two agree in mathematical form.

The assumption of constant incident energy required by Elsasser to make this integration does not introduce serious error. The width of either an isolated rotational or a single electronic line is quite small, e.g., for a rotational line in the infrared, the width is

less than 0.01 micron. Consequently, the incident energy will not vary rapidly within such a small interval.

**The Absorption of a Band.**[4] A vibration rotation band is composed of a number of rotation lines spaced about a central frequency and the intensity of an individual line decreases with the distance of the line from this central frequency. The intensity of any specific line depends upon: (*a*) The probability of the energy transition and (*b*) the fraction of the total number of molecules in the required energy state for this transition. The first is dependent upon the molecular configuration of the molecule and the second is a function of the thermodynamic state of the gas.

The three gases of primary interest in engineering are carbon monoxide, carbon dioxide, and water vapor. The observed spectra of the first two are regular in appearance [2], whereas, the spectrum of the water molecule is quite irregular [19]. This irregularity arises from the overlapping of adjacent vibrational bands corresponding to two oscillation modes with central frequencies differing by less than the vibrational band widths. As a consequence, the theoretical analyses of carbon monoxide and carbon dioxide have been approached in a different manner than the analysis of water vapor.

The exact integration of the total absorption of carbon monoxide has been performed by Penner [17] using numerical computational techniques. Elsasser obtained an analytic band absorption for carbon dioxide which is also applicable to carbon monoxide, using an idealization of the spectrum [6]. The model considered was a band composed of periodic equal intensity lines uniformly spaced with frequency. This assumption permitted the absorption coefficient to be expressed as:

$$k_\nu = \sum_{\eta=-\infty}^{\eta=\infty} \frac{S}{\pi} \frac{\delta}{(\nu - \eta d)^2 + \delta^2} \tag{26}$$

In addition to the assumption given, the assumption made by Elsasser for a single line regarding the incident energy intensity-frequency distribution was also used, i.e., constant incident energy over the band width. Substitution of equation (26) into equation (14) gives for a homogeneous medium:

$$a_B = \sin h\gamma \int_\zeta^\infty [\exp(-\zeta \sin h\gamma \coth \gamma)][J_o(i\zeta)]d\zeta \tag{27}$$

$$\gamma = \frac{2\pi\delta}{d}; \quad \zeta = \frac{S}{d \sin h\gamma} \tag{28}$$

This gives for two particular cases:

$$d \gg \delta(\text{lines far apart}); \quad a_b = \text{erf}\left[\frac{(\pi Sm)^{1/2}}{d}\right] \tag{29}$$

$$d \ll \delta(\text{lines close together}); \quad a_b = \left[1 - \exp\left(\frac{Sm}{d}\right)\right] \tag{30}$$

The spectrum of the water molecule appears as a number of irregularly spaced absorption lines having an almost random intensity distribution [2]. Goody [8] observed from the experimental work of Randall, et al. [19] that the apparent random nature of the absorption was suitable for statistical analysis. Using this postulate and a Lorentz line shape [equation (20)], Goody obtained for the transmission of a water vapor band:

$$t_B = \exp\left[-\frac{Sm\delta}{d\left(\delta^2 + \frac{m\delta}{\pi}\right)^{1/2}}\right] \tag{31}$$

The integrated intensity ($S$) and the line spacing ($d$) are statistical quantities which must be determined from experiment and are not related to the physical geometry of the molecule by known functions. This analysis also assumed a constant incident energy within the frequency limits of the band.

The analyses by Goody and Elsasser have been the basis for extensive elaborations and studies in meteorology. The recent work of Plass, et al. [18] exemplifies such an extension of the Elsasser model. Unfortunately for the application to engineering problems, these analyses do not offer additional refinement of the basic relations obtained. The work of Goody and Elsasser do furnish an opportunity to speculate qualitatively upon the effect of pressure and temperature on gaseous absorption. In both the Elsasser and Goody analysis, the half-width ($\delta$) of the lines appears and the influence of temperature and pressure on this factor from simple collision theory for small concentrations may be written as [15]:

$$\delta = \delta_o \left(\frac{P}{P_o}\right)\left(\frac{T_o}{T}\right)^{1/2} \tag{32}$$

The reference half-width is dependent upon the nonactive molecules in the gas and upon the concentration of the active molecules, i.e., foreign broadening and self-broadening influences.

The integrated intensity of the lines ($S$) appearing in equations (28) and (31) are based upon an idealization of the spectra and are not related to the physical geometry of the molecules. However, if this factor may be considered to be representative of the true intensities in the manner of an average value, the effect of pressure and temperature may be considered qualitatively. As noted previously, the intensity of a rotational line in a vibration-rotation band is dependent upon the friction of the total number of active molecules in a specific energy state.[5] This fraction is determined by the partition function and is temperature dependent [9,17]. Quantitatively, a description of the effect of temperature upon the partition function is difficult. Qualitatively, the fraction of molecules having an energy which gives rise to the lines in the wings of the band is increased at the expense of the lines in the center of the band as the temperature is increased. This results in a broadening and flattening of the vibration-rotation band, i.e., temperature broadening.

The exact definition of the mass of the medium traversed by the radiation is given by equation (2) and is based upon the number of molecules per unit volume (concentration) multiplied by the path length. The quantity often used in the literature to represent $m$ neglects the effect of temperature upon the concentration and is the product of the partial pressure and the path length:

$$w = pr \tag{33}$$

The preferred definition is given by equation (2) where $\rho$ is obtained from the ideal gas law:

$$\rho = \frac{p}{RT} \tag{34}$$

Since all reported experimental measurements have been made under isothermal conditions, the temperature effect has been inherently removed as a factor. The definition given by equation (33) will be used in the remainder of the paper, but the more exact definition should not be ignored if nonisothermal conditions are to be considered.

Temperature affects the absorptivity of a band by changing

[4] The lines referred to in this section are the rotational lines which combine to make up the vibration-rotation band and should not be confused with a single rotation or electronic line discussed in the preceding section.

[5] The usual definition of the integrated intensity includes the total number of active molecules multiplied by this fraction. The total number of molecules has been included as a basic factor in the definition of $m$.

the half-width of the rotational lines composing the vibrational-rotational band; by altering the fraction of absorbers at the various possible energy levels which changes the relative intensities of the lines and the width of the band; and by affecting the concentration of the absorbers for a fixed partial pressure. The relative strength of two vibration bands is similarly affected by the temperature. The total pressure also affects the half-width of the rotational lines and for increased pressures may cause these lines to overlap. Another effect of total pressure is upon the number of absorbers in the radiation path for a fixed partial pressure. The magnitude and form of the corrections for band absorptivities necessary to account for these influences will require experimental investigation. Hottel [10] gives a procedure for correcting the emissivity (absorptivity) of certain gases for temperatures which has been corroborated theoretically by Penner [17]. However, the total emissivity includes the temperature dependency of the energy distribution of a Planckian radiator and the various absorption bands acting in toto. Consequently, the correction by Hottel cannot be used, ad hoc, for band absorptivities.

## Experimental Gaseous Absorptivities

No experimental determinations of the individual band absorptions of carbon monoxide, carbon dioxide, and water vapor have been reported which are adequate for engineering use, although total emissivities have been available for a number of years [10]. A comprehensive study of the individual bands would have to consider the variables: (*a*) Concentration of active molecules, (*b*) path length, (*c*) temperature, (*d*) total pressure, (*e*) effect of mixing of two or more active gases, and (*f*) effect of different nonactive, diluent gases. A study was recently reported by Howard, et al. [12] which considered to a greater or lesser degree, all of the variables given except temperature. This study was for meteorological purposes and is not adequate for most engineering applications. This work does provide an opportunity to ascertain the validity of the theoretical band absorptions. A summary of the range of variables considered by Howard and his co-workers is given in Table 1. The correlations obtained for both water vapor and carbon dioxide were of the two alternative forms:

$$a_B = cw^{1/2}(P + p)^b \tag{35}$$

$$a_B = C + D \log w + G \log (P + p) \tag{36}$$

The first expression is valid for band absorptions less than an experimentally determined value of absorption and the second is valid for absorptions greater than this value. If the value of $w$ were increased indefinitely, the absorption given by these correlations would not reach a limiting value as is physically necessary. Consequently, a third expression should exist for larger values of the variable $w$.

The form of equation (35) for the variable $w$ can be shown to follow from the Elsasser model by expanding equation (29) and retaining the first term of the expansion. A qualitative explanation for the form of equation (36) has been given by Elder and Strong [5]. The dependency of both equations upon total and partial pressure is attributed to the overlapping of adjacent lines, self-broadening, and total pressure broadening. Total pressure broadening follows from equation (32) but, experimentally, an exponent was found which was smaller than predicted theoretically. The partial pressure broadening enters the two expressions in a double dependency since theoretically and experimentally, self-broadening is stronger than total pressure broadening [12, 15]. The correlation of both carbon dioxide and water vapor with equations of the same form differs from the results indicated by the theories of Elsasser and Goody. The experimental results were matched satisfactorily to the theories of Elsasser and Goody for specific bands but the forms of the correlations chosen by Howard were found to be more accurate for both gases over a wider range of variables and the same form was retained for both gases. The constants of the correlations for the various bands are given in Table 2 to indicate the magnitudes and relative importance of the various bands. The band limits given were arbitrarily chosen by Howard and are not necessarily indicative of true physical limits. Howard, et al. [12] have also considered the

**Table 1 Range of variables for the study by Howard, et al. [12]**

All data obtained at a temperature of 531°F with a $N_2 - O_2$ mixture (corresponding to air) as a diluent.

| Band Nominal Center Wavelength (Microns) | Absorber Concentration (atmos. - ft.) | Partial Pressure Range of Absorber (atmos.) | Total Pressure (atmos.) |
|---|---|---|---|
| **A. Carbon Dioxide** | | | |
| 15 | 0.033 - 28.3 | 0.0003 - 0.026 | 0.026 - 0.98 |
| 5.2 | * | * | * |
| 4.8 | 0.30 - 51.3 | 0.001 - 0.013 | 0.001 - 0.97 |
| 4.3 | 0.26 - 51.3 | 0.001 - 0.066 | 0.011 - 1.0 |
| 2.7 | 0.16 - 56.8 | 0.001 - 0.045 | 0.001 - 1.0 |
| 2.0 | 3.5 - 283 | 0.01 - 0.099 | 0.01 - 1.0 |
| 1.6 | * | * | * |
| 1.4 | 17.7 - 283 | 0.066 - 0.099 | 0.099 - 1.0 |
| **B. Water** | | | |
| 6.3 | 0.44 - 66 | 0.0033 - 0.033 | 0.0033 - 0.98 |
| 3.2 | 0.09 - 101 | 0.0026 - 0.033 | 0.0026 - 1.0 |
| 2.7 | 0.44 - 167 | 0.0026 - 0.033 | 0.0026 - 1.0 |
| 1.87 | 1.32 - 167 | 0.004 - 0.051 | 0.004 - 0.97 |
| 1.38 | 2.2 - 79 | 0.004 - 0.037 | 0.007 - 0.97 |
| 1.1 | 4.0 - 44 | 0.004 - 0.037 | 0.013 - 0.97 |
| 0.94 | 8.8 - 101 | 0.007 - 0.037 | 0.013 - 0.97 |

*Not Given

**Table 2 Summary of results obtained by Howard, et al. [12]**

A. Carbon Dioxide

| Nominal Band Center Wavelength (Microns) | Band Limits (Microns) | "Weak" Band Fit C | "Weak" Band Fit g | "Weak" Band Fit Limit $a_B$ | "Strong" Band Fit C | "Strong" Band Fit D | "Strong" Band Fit G |
|---|---|---|---|---|---|---|---|
| 15 | 12.5 - 18.19 | 0.0126 | 0.44 | 20 | -0.272 | 0.220 | 0.188 |
| 5.2 | 5.05 - 5.35 | 0.00022 | 0.40 | 27 | —— | —— | —— |
| 4.8 | 4.63 - 5.05 | 0.00067 | 0.37 | 30 | —— | —— | —— |
| 4.3 | 4.0 - 4.63 | —— | —— | 15 | 0.0809 | 0.100 | 0.0926 |
| 2.7 | 2.63 - 2.87 | 0.0098 | 0.43 | 16 | -0.488 | 0.241 | 0.213 |
| 2.0 | 1.92 - 2.11 | 0.0011 | 0.39 | 18 | -1.191 | 0.307 | 0.253 |
| 1.6 | 1.53 - 1.67 | 0.00014 | 0.38 | 18 | —— | —— | —— |
| 1.4 | 1.38 - 1.50 | 0.00009 | 0.41 | 13 | —— | —— | —— |

B. Water

| Nominal Band Center Wavelength (Microns) | Band Limits (Microns) | "Weak" Band Fit C | "Weak" Band Fit g | "Weak" Band Fit Limit $a_B$ | "Strong" Band Fit C | "Strong" Band Fit D | "Strong" Band Fit G |
|---|---|---|---|---|---|---|---|
| 6.3 | 4.88 - 8.70 | 0.060 | 0.30 | 18 | -0.062 | 0.242 | 0.174 |
| 3.2 | 2.99 - 3.57 | 0.011 | 0.30 | 93 | —— | —— | —— |
| 2.7 | 2.27 - 2.99 | 0.045 | 0.32 | 19 | -0.063 | 0.232 | 0.142 |
| 1.87 | 1.69 - 2.06 | 0.021 | 0.30 | 25 | -0.232 | 0.211 | 0.131 |
| 1.38 | 1.25 - 1.54 | 0.016 | 0.30 | 23 | -0.369 | 0.307 | 0.132 |
| 1.1 | 1.08 - 1.20 | 0.0047 | 0.26 | 20 | —— | —— | —— |
| 0.94 | 0.87 - 0.99 | 0.0041 | 0.27 | 14 | —— | —— | —— |

Note: The "weak" band fit is of the form $a_B = cw^{1/2}(P + p)^b$ and is valid to the limiting value of absorptivity given. For absorptivities exceeding this limit, the "strong" band fit must be used: $a_B = C + D \log w + G \log (P + p)$.

problem of mixtures of carbon dioxide and water vapor which have overlapping spectra in certain frequency regions. The results for mixtures were correlated for only one band (2.7 microns):

$$a_B(H_2O + CO_2) = a_B(H_2O) + \epsilon a_B(CO_2) \tag{37}$$

The factor $\epsilon$ is empirically determined from experiment and is a function of the band absorption of the water vapor. This is similar to the correction given by Hottel [10] for the total absorption of a mixture of these two gases.

The experimental technique used by Howard, et al. [12] was based upon the theory of Nielsen, Thornton, and Dale [15] which predicted the band absorption to be independent of the resolving power of the spectrometer under certain limitations. The basic restriction of this theory is the requirement of a constant incident energy over the whole band. Experimentally, this was not found to be an important restriction if a source was chosen which did not vary significantly over the band, e.g., an ideal radiator at a high temperature. This condition corresponds to the theoretical restrictions of Elsasser and Goody.

The effect of temperature has not yet been measured experimentally but, as indicated previously, the expected behavior may possibly be of the form:

$$a_B = cw^{1/2}(P + p)^q \left(\frac{T_0}{T}\right)^s \tag{38a}$$

or

$$a_B = C + D \log w + G \log (P + p) + H \log \left(\frac{T_0}{T}\right) \tag{38b}$$

## Engineering Applications

The most important result obtained from the theoretical analyses of Elsasser and Goody and the limited experimental work of Howard, et al., is the nonexponential behavior of band absorption. Also, the form of the expression for absorption depends upon the value of the absorption and not directly upon the path length. For a given value of the variable $w$, the total absorption would be given by:

$$\alpha = \left(\frac{1}{\int_0^\infty J_\nu d\nu}\right)\left\{\sum_{B=1}^{B=\Phi_1} a_B \int_{\Delta\nu_B} J_\nu d\nu + \sum_{B=1}^{B=\Phi_2} a_B \int_{\Delta\nu_B} J_\nu d\nu + \sum_{L=1}^{L=\Psi} a_L \int_{\Delta\nu_L} J_\nu d\nu\right\} \tag{39}$$

An analogous expression for the transmission may be written using the definition presented previously. The absorption given by equation (39) does not include the bands which have reached maximum absorption but this can be adjusted by adding a third series and defining another total band absorption similar to equations (38a) and (38b). Equation (39) corresponds to the experimental total absorptions measured by Hottel [10] and the theoretical values computed by Penner [17] with $\Psi = 0$.

The foregoing definitions of band absorptivities and transmissivities may be applied to the problem of the net exchange between two surfaces separated by an absorbing medium. This results in the definition of geometrical band or line absorptivities and transmissivities:

$$(\bar{a}_B)_{\Phi_1} A_1F_{12} = \int_{A_1}\int_{A_2} (a_B)_{\Phi_1} \frac{\cos\theta_1 \cos\theta_2}{\pi r^2} dA_1 dA_2 \tag{40a}$$

$$(\bar{a}_B)_{\Phi_2} A_1F_{12} = \int_{A_1}\int_{A_2} (a_B)_{\Phi_2} \frac{\cos\theta_1 \cos\theta_2}{\pi r^2} dA_1 dA_2 \tag{40b}$$

$$(\bar{a})_L A_1F_{12} = \int_{A_1}\int_{A_2} a_L \frac{\cos\theta_1 \cos\theta_2}{\pi r^2} dA_1 dA_2 \tag{40c}$$

The expressions for the transmissivities can be written by substituting band or line transmissivities for the absorptivities. Then, by the use of equations (19a) and (19b), the relationship between transmission and absorption is found to be continued:

$$(\bar{a}_B + \bar{t}_B)_{\Phi_1} = 1 \tag{41a}$$

$$(\bar{a}_B + \bar{t}_B)_{\Phi_2} = 1 \tag{41b}$$

$$\bar{a}_L + \bar{t}_L = 1 \tag{41c}$$

Similarly, the total geometrical absorption and transmission may be written:

$$\bar{\alpha}_{12}A_1F_{12} = \left(\frac{1}{\int_0^\infty J_\nu d\nu}\right)\left\{\sum_{B=1}^{B=\Phi_1} \bar{a}_B \int_{\Delta\nu_B} J_\nu d\nu + \sum_{B=1}^{B=\Phi_2} \bar{a}_B \int_{\Delta\nu_B} J_\nu d\nu + \sum_{L=1}^{L=\Psi} \bar{a}_L \int_{\Delta\nu_L} J_\nu d\nu\right\} \tag{42a}$$

$$\bar{\tau}_{12}A_1F_{12} = \left(\frac{1}{\int_0^\infty J_\nu d\nu}\right)\left\{\sum_{B=1}^{B=\Phi_1} \bar{t}_B \int_{\Delta\nu_B} J_\nu d\nu + \sum_{B=1}^{B=\Phi_2} \bar{t}_B \int_{\Delta\nu_B} J_\nu d\nu + \sum_{L=1}^{L=\Psi} \bar{t}_L \int_{\Delta\nu_L} J_\nu d\nu\right\} \tag{42b}$$

$$\bar{\alpha} + \bar{\tau} = 1 \tag{42c}$$

Substitution of the foregoing expressions into equation (6b) gives:

$$q_{1-2} = A_1F_{12}\left[\int_0^\infty (J_{\nu 1} - J_{\nu 2})d\nu\right] - A_1F_{12}\left[\bar{\alpha}_{12}\int_0^\infty J_{\nu 1}d\nu - \bar{\alpha}_{21}\int_0^\infty J_{\nu 2}d\nu\right] \tag{43a}$$

or

$$q_{1-2} = A_1F_{12}\left[\bar{\tau}_{12}\int_0^\infty J_{\nu 1}d\nu - \bar{\tau}_{21}\int_0^\infty J_{\nu 2}d\nu\right] \tag{43b}$$

The integrated radiosity of a totally absorbing surface, i.e., an ideal radiator, is $\sigma T^4$ and equations (43a) and (43b) reduce to the conventional exchange equations for this condition. If there is no absorbing gas,

$$\bar{\tau}_{12} = \bar{\tau}_{21} = 1.$$

## Discussion

The problem of the effect of gaseous absorption upon the net exchange between two surfaces has been examined from present theory and from the limited available experimental information. The assumption of exponential absorption (Beer's law) for the attenuation of a band has been shown to be incorrect for a single line or for an assembly of such lines as occurs in a vibration band. The best available experimental data indicates the absorption of a band follows a square-root function of the optical "thickness" ($w$) for a weak absorption and a logarithmic function for a strong absorption. The logarithmic dependency for large values of $w$ may be shown with existing data for gaseous absorption [10]. For example, a plot of the logarithm of total absorption versus $w$ for $CO_2$ at a constant temperature yields a straight line for $w$ greater than 0.5 atmosphere-foot. This corresponds to equation (39) with $\Phi_1$ and $L$ equal to zero.

The various bands of a specific gas for a given temperature and pressure will not all behave according to only one of these two

types of functions. Consequently, the behavior of the gas over the whole energy spectrum will be a mixture of these two functions, superimposed upon unity transmission in those regions of the spectrum where the gas is not active. The total effect of the gas must be considered therefore as the sum of the effects of the individual bands. The complexity of this approach is readily apparent since the number of computations necessary are multiplied by the number of vibration bands occurring.

An advantage is gained, however, by considering the band or line absorptivities ($a_B$ or $a_L$) or the geometrical band or line absorptivities ($\bar{a}_B$ or $\bar{a}_L$). Theory which has been substantiated by experiment shows that these quantities are not strongly dependent upon the source but are primarily functions of the temperature of the absorbing medium. The source dependency is introduced when the comparable total factors are considered, i.e., $\alpha$ or $\bar{\alpha}$. This is important in the computation techniques available for analysis.

The calculations of gaseous absorption are complicated when complex reflecting geometrical configurations are considered. The network technique by Oppenheim [16] is well suited to this. In the last part, a procedure of solution will be described which is amenable to either band or digital computer calculation.

The use of band absorptions for gases and computations using this information also requires the use of spectral emittances and reflectances for the surfaces involved. Information of this type is not available in quantity but a recent paper [1] has described a method for performing such measurements. The importance of considering spectral emittance rather than total for calculating the net exchange between surfaces with no intervening absorbing medium has been demonstrated by Goodman [7]. The use of band absorptions for calculations, rather than total absorptions, is only an additional step beyond the work of Goodman. The data for band absorptions for carbon monoxide, carbon dioxide, and water as a function of temperature and total pressure are not now available but an experimental program has been initiated to partially eliminate this deficiency.

The importance of the nonexponential absorption upon the present methods of analysis is difficult to assess. An example will be given in a subsequent paper of the errors involved for a simple geometry. The historical work by Hottel and his coworkers [10] remains the best and only engineering approach presently available. Penner [17] computed the total emissivity of carbon monoxide by considering the individual contributions of each line in the several vibration bands and has confirmed theoretically the experimental measurements of Hottel. However, the assumption of exponential attenuation for such analyses as the volume emission of a gas [13] is questionable.

## Nomenclature for Part 1

(The units of the various quantities should be in a consistent system of units.)

$A$ = area
$C$ = constant, equation (36)
$D$ = constant, equation (36)
$E$ = emissive power of an ideal radiator
$F$ = geometrical form factor
$G$ = constant, equation (36)
$H$ = constant, equation (38$b$)
$I$ = intensity of radiation
$J$ = radiosity
$P$ = total pressure
$R$ = universal gas constant
$S$ = integrated intensity, equation (21)
$T$ = absolute temperature
$W$ = energy ($\Delta W$ = energy change)
$a$ = total absorptivity of a single line or band, equations (13) and (14)
$c$ = constant, equation (35)
$d$ = spacing between adjacent lines, equation (26)
$g$ = constant, equation (35)
$h$ = Planck's constant, $6.623 \times 10^{-27}$ erg-sec
$k$ = absorption coefficient
$m$ = mass per unit area of the radiating components in the medium lying in the path of the radiation
$p$ = partial pressure
$q$ = heat rate
$r$ = path length traversed by the radiation beam
$t$ = total transmissivity of a single line or band, equations (13) and (14)
$w$ = optical thickness, equation (33)
$y$ = constant, equation (38$a$)
$\bar{a}$ = geometrical absorptivity, equation (40)
$\bar{t}$ = geometrical transmissivity, equation (41)
$\Gamma$ = radiation passing from one surface to another
$\Phi_1$ = number of vibration-rotation bands having $w^{1/2}$ behavior
$\Phi_2$ = number of vibration-rotation bands having log $w$ behavior
$\Psi$ = number of lines external to a vibration-rotation band
$\alpha$ = total absorptivity
$\beta$ = parameter, equation (23)
$\gamma$ = parameter, equation (28)
$\delta$ = line half width
$\epsilon$ = correction factor, equation (37)
$\zeta$ = parameter, equation (28)
$\eta$ = number of lines, equation (26)
$\theta$ = angle
$\nu$ = frequency
$\pi$ = 3.14159 . . .
$\rho$ = density of the absorbing (or emitting) medium in the radiation path
$\sigma$ = Stefan-Boltzmann constant = $0.1714 \times 10^{-8}$ Btu/hr ft$^2$ (deg R)$^4$
$\tau$ = total transmissivity
$\varphi$ = total number of vibration-rotation bands
$\Delta\nu$ = frequency width, i.e., the frequency region within which absorption (or transmission) is complete
$\bar{\alpha}$ = total geometrical absorption, equation (42$a$)
$\bar{\tau}$ = total geometrical transmission, equation (42$b$)

Subscripts

$B$ = vibration-rotation band
$L$ = line
$O$ = incident
$b$ = ideal (black body) radiation
$e$ = electronic
$o$ = center or reference
$r$ = rotational
$v$ = vibrational
1, 2 = designate surface
3 = medium
1 + 2 = surface 1 plus 2
1 − 2 = from surface 1 to 2
$\nu$ = single frequency (monochromatic)

R. V. DUNKLE[2]
J. T. BEVANS[1]

# Part 2 General Interchange Equations

## Introduction

THIS IS THE second paper of three dealing with the solution of the radiant exchange within an enclosure containing an absorbing medium.

The starting point of the analysis to be given is the network analogy for radiative heat transfer given by Oppenheim [16]. The network analogy utilizes a resistive network to represent the interplay between the geometrical and physical characteristics of the radiation exchange system. An illustration of the conductances coupling two surfaces of an enclosure containing an absorbing medium is given in Fig. 2(*a*) for monochromatic radiation. The two surface node potentials ($E_{\nu,1}$ and $E_{\nu,2}$) are the monochromatic emissive powers of the two surfaces, respectively. The radiosities of the surfaces are given $J_{\nu,1}$ and $J_{\nu,2}$ and are the potentials of the inner nodes of the network.[6] The quantity $W_{\nu,nm}$ is the monochromatic emissive power of the medium lying between the nodes 1 and 2 in accordance with the description given in Part 1 for the radiant exchange between two surfaces.

The solution of the simple system given in Fig. 2(*a*) may be obtained quickly by basic electric network concepts. The direct solution of a system of only four or five nodes can become complicated and tedious and recourse is generally made to matrix algebra. A reiterative (relaxation) procedure for approaching a solution to a multinode network will be given in the final part. Prior to this, however, a generalized network for an enclosure will be used to examine the physical bases for solution and the approximations necessary to obtain the solution.

## Monochromatic Energy Analysis

Consider a radiation system of $M$ surfaces with a part or all of the $M$ surfaces forming an enclosure; the balance of the $M$ surfaces lie within this enclosure. An absorbing and/or emitting medium is contained within the enclosure. The number of surfaces is not specified, the aggregate surfaces of the enclosure are considered to have been subdivided into $M$ surfaces such that each of the $M$ surfaces is isothermal; each is assumed to follow Lambert's law of diffuse radiation and to be in equilibrium with its surrounds (i.e., no heat storage). The radiation characteristics of the medium are assumed to be isotropic and the medium to be in equilibrium. The $n$th node of such a system is shown in Fig. 2(*b*). The potentials of the gas nodes have been labeled by the subscript referring to the surface which determines this node in conjunction with surface $n$ (i.e., $W_{nm} = W_m$).

The sum of the currents flowing into node $n$ must be equal to zero by Kirchhoff's law of electrical networks or since the currents are equivalent to the heat fluxes, by the conservation of energy. If this is done, the following expression is found ($n \leq m$):

$$A_n \frac{e_{\nu,n}}{r_{\nu,n}} (E_{\nu,n} - J_{\nu,n}) = \sum_{m=1}^{M} (J_{\nu,n} - J_{\nu,m}) \bar{\tau}_{\nu,nm} A_n F_{nm} + \sum_{m=1}^{M} (J_{\nu,n} - W_{\nu,m}) \bar{\alpha}_{\nu,nm} A_n F_{nm} \quad (44)$$

Solving for the radiosity of the $n$th node ($J_{\nu,n}$) gives:

$$J_{\nu,n} \sum_{m=1}^{M} [\bar{\tau}_{\nu,nm} A_n F_{nm} + \bar{\alpha}_{\nu,nm} A_n F_{nm}] + J_{\nu,n} A_n \left(\frac{e_{\nu,n}}{r_{\nu,n}}\right) = A_n \left(\frac{e_{\nu,n}}{r_{\nu,n}}\right) E_{\nu,n} + \sum_{m=1}^{M} J_{\nu,m} \bar{\tau}_{\nu,nm} A_n F_{nm} + \sum_{m=1}^{M} W_{\nu,m} \bar{\alpha}_{\nu,nm} A_n F_{nm} \quad (45)$$

This equation may be simplified by noting:

$$\bar{\tau}_{\nu,nm} A_n F_{nm} + \bar{\alpha}_{\nu,nm} A_n F_{nm} = A_n F_{nm} \quad (46a)$$

$$\sum_{m=1}^{M} A_n F_{nm} = A_n \quad (46b)$$

Equation (45) then reduces to:

$$J_{\nu,n} A_n \left[1 + \left(\frac{e_{\nu,n}}{r_{\nu,n}}\right)\right] = A_n \left(\frac{e_{\nu,n}}{r_{\nu,n}}\right) E_{\nu,n} + \sum_{m=1}^{M} J_{\nu,m} A_n F_{nm} - \sum_{m=1}^{M} J_{\nu,m} \bar{\alpha}_{\nu,nm} A_n F_{nm} + \sum_{m=1}^{M} W_{\nu,m} \bar{\alpha}_{\nu,nm} A_n F_{nm} \quad (47)$$

[6] The term node will hereafter refer to an inner node such as $J_{\nu,1}$; surface node will designate a network point with a potential such as $E_{\nu,1}$; and gas node will be used for such points as $W_{\nu,12}$.

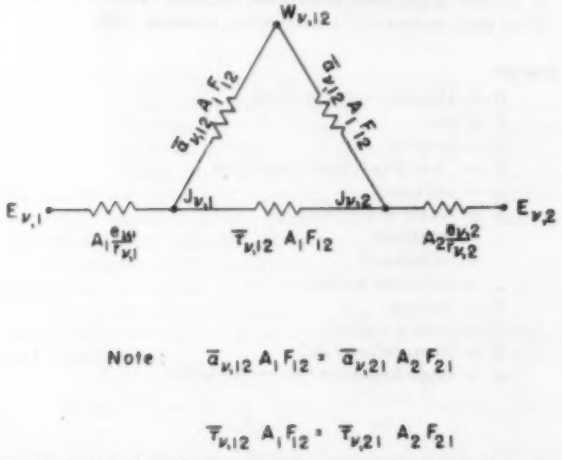


Fig. 2(*a*) Mutual conductances coupling two surface nodes in an enclosure containing an absorbing medium

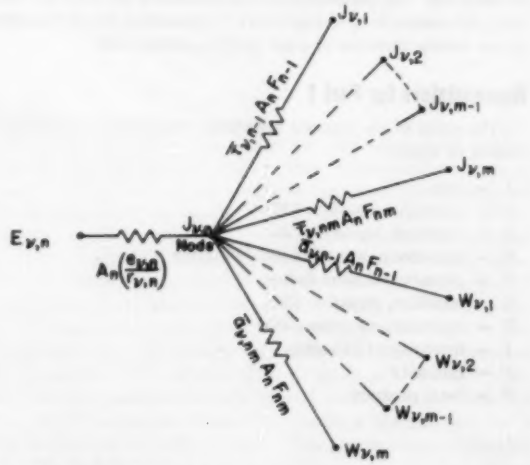


Fig. 2(*b*) The *n*th node of a radiation network for an enclosure containing an absorbing medium

An alternate procedure of analysis may be developed from equation (47) and is given in the Appendix. The method to be given in the main text retains the definitions given in the first part.

The total radiant energy is given by integration of equation (47) over all frequencies:

$$\int_0^\infty J_{\nu,n}A_n\left[1+\left(\frac{e_{\nu,n}}{r_{\nu,n}}\right)\right]d\nu = \int_0^\infty A_n\left(\frac{e_{\nu,n}}{r_{\nu,n}}\right)E_{\nu,n}\,d\nu + \sum_{m=1}^{M}\int_0^\infty J_{\nu,m}A_nF_{nm}d\nu - \sum_{m=1}^{M}\int_0^\infty J_{\nu,m}\bar{\alpha}_{\nu,nm}A_nF_{nm}d\nu + \sum_{m=1}^{M}\int_0^\infty W_{\nu,n}\bar{\alpha}_{\nu,nm}A_nF_{nm}d\nu \quad (48)$$

This expression represents an exact formulation of the energy interchange at node $n$. The solution depends upon the evaluation of the various integrals and the simultaneous solutions of the $M$ equations of which equation (48) is the $n$th. Assuming the radiant properties to be independent of frequency will give the "gray" radiation case. The approximation which is between the extremes of the exact and the gray cases, is the band energy approximation based upon the definitions given in the preceding paper Prior to presenting this, the total energy balance within the system should be obtained. Consider equation (44) summed over all nodes:

$$\sum_{n=1}^{M}A_n\left(\frac{e_{\nu,n}}{r_{\nu,n}}\right)(E_{\nu,n}-J_{\nu,n}) = \sum_{n=1}^{M}\sum_{m=1}^{M}(J_{\nu,n}-J_{\nu,m})\bar{\tau}_{\nu,nm}A_nF_{nm} + \sum_{n=1}^{M}\sum_{m=1}^{M}(J_{\nu,n}-W_{\nu,m})\bar{\alpha}_{\nu,nm}A_nF_{nm} \quad (49)$$

This expression assumes there is no energy storage within the system since equilibrium was assumed for the surfaces and the medium.

The definition of the monochromatic heat flow from the surface to the node used to derive equation (44) was:

$$q_{\nu,n} = A_n\left(\frac{e_{\nu,n}}{r_{\nu,n}}\right)(E_{\nu,n}-J_{\nu,n}) \quad (50)$$

where the heat flowing *into* the node is taken as positive. Consequently, the right-hand side of equation (49) is the total monochromatic heat flowing *out* of all the nodes:

$$Q_\nu = \sum_{n=1}^{M}q_{\nu,n} \quad (51)$$

The first term on the right-hand side of equation (49) is equal to zero. The double sum will cause a reversal in the sign of the quantity within the parentheses and this term reduces to zero when combined with the identity valid for monochromatic energy, i.e.,

$$\bar{\tau}_{\nu,nm}A_nF_{nm} = \bar{\tau}_{\nu,mn}A_mF_{mn} \quad (52)$$

A simple expansion of this term for $M = 2$ will demonstrate this readily:

$$\sum_{n=1}^{2}\sum_{m=1}^{2}(J_{\nu,n}-J_{\nu,m})\bar{\tau}_{\nu,nm}A_nF_{nm} = (J_{\nu,1}-J_{\nu,1})\bar{\tau}_{\nu,11}A_1F_{11} + (J_{\nu,1}-J_{\nu,2})\bar{\tau}_{\nu,12}A_1F_{12} + (J_{\nu,2}-J_{\nu,1})\bar{\tau}_{\nu,21}A_2F_{21} + (J_{\nu,2}-J_{\nu,2})\bar{\tau}_{\nu,22}A_2F_{22} = 0$$

The second term on the right-hand side of equation (49) relates the radiosities of the various nodes and the emissive power of the enclosed medium. Considering first the radiosity portion of this term, the double sum is the sum over all nodes of the total geometrical absorption of the medium, i.e., the total monochromatic energy absorbed by the medium. Similarly, the total monochromatic emitted energy from the medium is represented by the remaining portion of this sum. The difference between these two factors is the total monochromatic energy *absorbed* by the medium:

$$Q_\nu = \sum_{n=1}^{M}q_{\nu,n} = \sum_{n=1}^{M}\sum_{m=1}^{M}(J_{\nu,n}-W_{\nu,m})\bar{\alpha}_{\nu,nm}A_nF_{nm} \quad (53)$$

No other sources or sinks were postulated and equation (53) merely states this in terms of the radiosities, heat fluxes, and radiant characteristics of the system. The right-hand side of equation (53) may be integrated over all frequencies:

$$\sum_{n=1}^{M}\int_0^\infty q_{\nu,n}d\nu = \sum_{n=1}^{M}\sum_{m=1}^{M}\int_0^\infty (J_{\nu,n}-W_{\nu,n})\bar{\alpha}_{\nu,nm}A_nF_{nm}d\nu \quad (54a)$$

or

$$\int_0^\infty Q_\nu d\nu = Q \quad (54b)$$

## Band Energy Approximation

As noted previously, equation (48) is an exact formulation of the radiation interchange problem. The solution of the $M$ simultaneous equations is a formidable one and requires a specification of the frequency characteristics of each factor in the equations plus the simultaneous solution of the equations. As an intermediate approximation between the exact solution and the assumption of gray radiation, the procedures of the first part may be used. This method has been termed the band energy approximation.

In order to apply these procedures in a systematic manner, equation (48) is rewritten in its complete form:

$$\int_0^\infty J_{\nu,n}A_n\left[1+\left(\frac{e_{\nu,n}}{r_{\nu,n}}\right)\right]d\nu = \int_0^\infty A_n\left(\frac{e_{\nu,n}}{r_{\nu,n}}\right)E_{\nu,n}d\nu + \sum_{m=1}^{M}\int_{A_n}\int_{A_m}\int_0^\infty J_{\nu,m}\frac{\cos\theta_n\cos\theta_m}{\pi R^2}\,dA_ndA_md\nu - \sum_{m=1}^{M}\int_{A_n}\int_{A_m}\int_0^\infty J_{\nu,m}\,\alpha_\nu\frac{\cos\theta_n\cos\theta_m}{\pi R^2}\,dA_ndA_md\nu + \sum_{m=1}^{M}\int_{A_n}\int_{A_m}\int_0^\infty W_{\nu,m}\frac{\cos\theta_n\cos\theta_m}{\pi R^2}\,dA_ndA_md\nu \quad (55)$$

The integration of equation (55) over all frequencies is written as the sum of integrals over frequency intervals (bands). These intervals are the natural subdivisions determined by the absorption (or emission) characteristics of the intervening medium. The media of usual interest in engineering are gases and the procedures outlined in the first paper are applicable. The entire spectrum is divided, therefore, into $\Omega$ intervals of which $\omega_1$ intervals have no absorption and $\omega_2$ intervals have absorption.[7] Thus the $\omega_2$ intervals are the line absorptions and vibration-rotation frequency bands. The energy within each division must be conserved and equation (55) may be written in general form for one interval as

[7] In application, certain $\omega_1$ intervals may be further subdivided if the spectral characteristics of the surfaces vary rapidly within one or more of the $\omega_1$ intervals.

$$\int_{\Delta\nu_\omega} J_{\nu,n}A_n\left[1+\left(\frac{e_{\nu,n}}{r_{\nu,n}}\right)\right]d\nu = \int_{\Delta\nu_\omega} A_n\left(\frac{e_{\nu,n}}{r_{\nu,n}}\right)E_{\nu,n}d\nu + \sum_{m=1}^{M}\int_{A_n}\int_{A_m}\int_{\Delta\nu_\omega} J_{\nu,m}\frac{\cos\theta_n\cos\theta_m}{\pi R^2}dA_n dA_m d\nu - \sum_{m=1}^{M}\int_{A_n}\int_{A_m}\int_{\Delta\nu_\omega} J_{\nu,m}\alpha_\nu\frac{\cos\theta_n\cos\theta_m}{\pi R^2}dA_n dA_m d\nu + \sum_{m=1}^{M}\int_{A_r}\int_{A_m}\int_{\Delta\nu_\omega} W_{\nu,m}\alpha_\nu\frac{\cos\theta_n\cos\theta_m}{\pi R^2}dA_n dA_m d\nu \quad (56)$$

where

$$\Omega = \omega_1 + \omega_2 = \Sigma\omega$$

$$\alpha = 0 \quad \text{for} \quad \omega = \omega_1 \quad (57)$$

The last three terms of equation (57) are simplified by the use of the following expressions from the first part:

$$a = \frac{\int_{\Delta\nu_\omega}\alpha_\nu d\nu}{\Delta\nu_\omega} \cong \frac{\int_{\Delta\nu_\omega} J_\nu\alpha_\nu d\nu}{\int_{\Delta\nu_\omega} J_\nu d\nu} \quad (58)$$

where the factor $a$ is a function of the path length $R$ and

$$\bar{a}_{nm}A_nF_{nm} = \int_{A_n}\int_{A_m} a\frac{\cos\theta_n\cos\theta_m}{\pi R^2}dA_n dA_m \quad (59)$$

This gives for these three terms:

$$\sum_{m=1}^{M}\int_{A_n}\int_{A_m}\int_{\Delta\nu_\omega} J_{\nu,m}\frac{\cos\theta_n\cos\theta_m}{\pi R^2}dA_n dA_m d\nu = \sum_{m=1}^{M} A_nF_{nm}\int_{\Delta\nu_\omega} J_{\nu,m}d\nu \quad (60)$$

$$\sum_{m=1}^{M}\int_{A_n}\int_{A_m}\int_{\Delta\nu_\omega} J_{\nu,m}\alpha_\nu\frac{\cos\theta_n\cos\theta_m}{\pi R^2}dA_n dA_m d\nu = \sum_{m=1}^{M}\bar{a}_{nm}A_nF_{nm}\int_{\Delta\nu_\omega} J_{\nu,m}d\nu \quad (61)$$

$$\sum_{m=1}^{M}\int_{A_n}\int_{A_m}\int_{\Delta\nu_\omega} W_{\nu,m}\alpha_\nu\frac{\cos\theta_n\cos\theta_m}{\pi R^2}dA_n dA_m d\nu = \sum_{m=1}^{M}\bar{a}_{nm}A_nF_{nm}\int_{\Delta\nu_\omega} W_{\nu,m}d\nu \quad (62)$$

These approximations are based upon the following assumptions:

1 The radiosity or emissive power varies slowly within the interval.

2 The radiosities of the various nodes follow Lambert's "cosine" law. The second assumption is inherent in the network method of analysis but is no more restrictive than other present methods of analysis.

The remaining two terms require the definition of two new quantities involving the emittance and reflectance properties of the surfaces. Using the same assumptions as for the gaseous absorptivities, these quantities are:

$$\left(\frac{1}{\rho}\right)_{\omega,n} = \frac{\int_{\Delta\nu_\omega}\left(\frac{1}{r_{\nu,n}}\right)d\nu}{\Delta\nu_\omega} \cong \frac{\int_{\Delta\nu_\omega} J_{\nu,n}\left(\frac{1}{r_{\nu,n}}\right)d\nu}{\int_{\Delta\nu_\omega} J_\nu d\nu} = \frac{\int_{\Delta\nu_\omega} J_{\nu,n}\left[1+\left(\frac{e_{\nu,n}}{r_{\nu,n}}\right)\right]d\nu}{\int_{\Delta\nu_\omega} J_{\nu,n}d\nu} \quad (63)$$

$$\gamma_{\omega,n} = \frac{\int_{\Delta\nu_\omega}\left(\frac{e_{\nu,n}}{r_{\nu,n}}\right)d\nu}{\Delta\nu_\omega} \cong \frac{\int_{\Delta\nu_\omega} E_{\nu,n}\left(\frac{e_{\nu,n}}{r_{\nu,n}}\right)d\nu}{\int_{\Delta\nu_\omega} E_{\nu,n}d\nu} \quad (64)$$

The remaining terms of equation (56) become, with the aid of these definitions:

$$\int_{\Delta\nu_\omega} J_{\nu,n}A_n\left[1+\left(\frac{e_{\nu,n}}{r_{\nu,n}}\right)\right]d\nu = \frac{A_n}{(\rho)_{\omega,n}}\int_{\Delta\nu_\omega} J_{\nu,n}d\nu \quad (65)$$

$$\int_{\Delta\nu_\omega} A_n\left(\frac{e_{\nu,n}}{r_{\nu,n}}\right)E_{\nu,n}d\nu = \gamma_{\omega,n}A_n\int_{\Delta\nu_\omega} E_{\nu,n}d\nu \quad (66)$$

Substitution of the appropriate foregoing relations in equation (56) yields:

$$\frac{A_n}{(\rho)_{\omega,n}}\int_{\Delta\nu_\omega} J_{\nu,n}d\nu = \gamma_{\omega,n}A_n\int_{\Delta\nu_\omega} E_{\nu,n}d\nu + \sum_{m=1}^{M} A_nF_{nm}\int_{\Delta\nu_\omega} J_{\nu,m}d\nu - \sum_{m=1}^{M}\bar{a}_{nm}A_nF_{nm}\int_{\Delta\nu_\omega} J_{\nu,m}d\nu + \sum_{m=1}^{M}\bar{a}_{nm}A_nF_{nm}\int_{\Delta\nu_\omega} W_{\nu,m}d\nu \quad (67)$$

There will be $\omega_2$ equations having the form of equation (67) and $\omega_1$ equations without the last two terms, which must be solved. The $\Omega$ equations are connected by the temperatures and/or heat fluxes of the various nodes, e.g., the monochromatic emissive power of node $n$ in one frequency interval is related by the temperature of that node to the monochromatic emissive power of the other frequency intervals. The heat flow of a node for a specific band is given by:

$$q_{\omega,n} = \int_{\Delta\nu_\omega} q_{\nu,n}d\nu = \gamma_{\omega,n}A_n\left[\int_{\Delta\nu_\omega} E_{\nu,n}d\nu - \int_{\Delta\nu_\omega} J_{\nu,n}d\nu\right] \quad (68)$$

The total band energy may be obtained by starting with equation (49) and proceeding with the same approximations as used to obtain equation (55). This gives:

$$Q_\omega = \sum_{n=1}^{M} q_{\omega,n} = \sum_{n=1}^{M}\sum_{m=1}^{M}\bar{a}_{nm}A_nF_{nm}\left[\int_{\Delta\nu_\omega} J_{\nu,n}d\nu - \int_{\Delta\nu_\omega} W_{\nu,m}d\nu\right] \quad (69)$$

Certain comments are required regarding the approximations given by equations (63) and (64). When equation (64) is applied to determine the quantity $\gamma_{\omega,n}$, the monochromatic emissive power of the node may be used to determine this quantity more accurately than the definition given. The monochromatic emissive power is not always a known quantity for every surface. The definition given by equation (64) will permit general values of $\gamma_\omega$ to be determined from spectral emittance or reflectance data and these will be temperature dependent only as the temperature affects the spectral emittance and reflectance, i.e., independent of the temperature dependency of Planck's equation. This same argument holds for equation (63) and is more important to the analysis since the radiosity is generally unknown. The approxi-

mation given by equation (58) has already been discussed in the first paper. In each of these approximations [equations (63) and (64)], the accuracy is greater the smaller the frequency interval ($\Delta\nu_w$). Fortunately, the variation of spectral reflectance and emittance is usually small within the natural frequency intervals of $CO_2$ and $H_2O$ vapor (Part 1 and [1]). This physical behavior increases the accuracy of the approximation. Note should be made of the fact that neither equation (63) nor (64) correspond to physically observable quantities but arise from the method of analysis.

## Gray Radiation Approximation

The gray radiation approximation is the one most frequently used in analyses of radiant systems. The approximation is based upon the assumption of frequency independent radiation characteristics of the surfaces and the gases involved. This assumption is a result of the inadequate knowledge of the spectral behavior of these characteristics and is a necessity born from ignorance.

Equation (48) may be quickly reduced with the gray radiation assumption by simply dropping the subscript denoting frequency. Alternatively, an evaluation of this assumption may be obtained by simplifying equation (47) in a systematic manner to provide expressions which can be used to determine the errors involved. Multiplying equation (47) by the monochromatic reflectance and integrating over all frequencies gives:

$$\int_0^\infty J_{\nu,n}A_n d\nu = \int_0^\infty A_n e_{\nu,n}E_{\nu,n}d\nu + \sum_{m=1}^{M}\int_0^\infty r_{\nu,m}J_{\nu,m}A_nF_{nm}d\nu - \sum_{m=1}^{M}\int_0^\infty J_{\nu,m}r_{\nu,n}\bar{\alpha}_{\nu,nm}A_nF_{nm}d\nu + \sum_{m=1}^{M}\int_0^\infty W_{\nu,m}r_{\nu,n}\bar{\alpha}_{\nu,nm}A_nF_{nm}d\nu \quad (70)$$

The following expressions for the individual terms in equation (70) are now necessary to make the equation useful for computation:

$$A_nJ_n = \int_0^\infty A_nJ_{\nu,n}d\nu \quad (71)$$

$$A_ne_n\sigma T_n^4 = \int_0^\infty A_nE_{\nu,n}e_{\nu,n}d\nu \quad (72)$$

$${}_mr_nA_nF_{nm}J_m = \int_0^\infty r_{\nu,m}J_{\nu,m}A_nF_{nm}d\nu \quad (73)$$

$${}_mr_n\bar{a}'_{nm}A_nF_{nm}J_m = \int_0^\infty r_{\nu,m}J_{\nu,m}\bar{\alpha}_{\nu,nm}A_nF_{nm}d\nu \quad (74)$$

$${}_mr_n\bar{a}'_{nm}A_nF_{nm}\sigma T_{g,m}^4 = \int_0^\infty r_{\nu,n}W_{\nu,m}\bar{\alpha}_{\nu,nm}A_nF_{nm}d\nu \quad (75)$$

Equation (71) is actually a definition of the integrated radiosity and does not introduce an error in itself. Equation (72) is the definition of the total emittance of a surface:

$$e_n = \frac{\int_0^\infty E_{\nu,n}e_{\nu,n}d\nu}{\int_0^\infty E_{\nu,n}d\nu} = \frac{1}{\sigma T_n^4}\int_0^\infty E_{\nu,n}e_{\nu,n}d\nu \quad (76)$$

Equation (73), however, does introduce an approximation which cannot be evaluated. The spectral energy distribution of the radiosities of the various nodes is not known nor can it be determined by this analysis since the analysis is predicated on a total integrated energy. Instead, a further approximation is introduced by writing:

$${}_mr_n = {}_nr_m = r_n = 1 - e_n \quad (77)$$

Equation (77) is the first term requiring the use of the gray radiation assumption.

A similar series of approximations are necessary in equations (74) and (75) with the added complication of the gaseous absorptivities. Each factor in the two equations is considered to be independent of the others. Thus the geometrical absorption factor ($\bar{a}_{nm}'$) is based upon the concept of mean beam lengths which in turn is derived from a specified transmission law. The geometrical shape factor ($A_nF_{nm}$) is obtained from calculations made without absorption of the intervening medium and corrected for absorption by the factor $\bar{a}_{nm}'$. The reflectance of the surface is determined separately in a manner analogous to equation (77). These factors may be written as:

$${}_mr_n\bar{a}_{nm}'A_nF_{nm}J_m = \left[\frac{\int_0^\infty E_{\nu,n}r_{\nu,n}d\nu}{\int_0^\infty E_{\nu,n}d\nu}\right]\left[\int_0^\infty J_{\nu,m}d\nu\right]\left[\int_{A_n}\int_{A_m}\int_0^\infty \alpha_\nu \frac{\cos\theta_n\cos\theta_m}{\pi R^2}\,dA_n dA_m d\nu\right] \quad (78)$$

An identical equation may be obtained for the gas by substituting $W_{\nu,m}$ for $J_{\nu,m}$ in the last bracketed term. The quantity $\bar{a}_{nm}'A_nF_{nm}$ is generally evaluated by the procedures given by Hottel [10]. In brief, the procedure uses a "mean beam length" to determine the effective path of the radiation and this in turn is used to determine the emission and/or absorption of the gas from data collected by "parallel beam" experiments. The geometrical shape factor ($A_nF_{nm}$) for the two surfaces with no intervening medium is then multiplied by this absorption factor to obtain the product $\bar{a}_{nm}'A_nF_{nm}$. Recently, Hottel and Cohen [11] have made an important step toward improving the values of the geometrical factor. The absorption factor was introduced within the shape factor integral as a part of the integrand and values of the integral determined numerically.

The gray radiation approximation may be written using the terminology given in equations (71) through (75) but with the additional approximations outlined in the discussion:

$$A_nJ_n = e_n\sigma T_n^4 + \sum_{m=1}^{M} r_nA_nF_{nm}J_m - \sum_{m=1}^{M} r_n\bar{a}_{nm}'A_nF_{nm}J_m + \sum_{m=1}^{M} r_n\bar{a}_{nm}'A_nF_{nm}\sigma T_{g,m}^4 \quad (79)$$

The total energy balance for this approximation is:

$$\sum_{n=1}^{M} q_n = \sum_{n=1}^{M}\sum_{m=1}^{M} \bar{a}_{nm}'A_nF_{nm}(J_m - \sigma T_{g,m}^4) \quad (80)$$

## Discussion

Three methods of analysis of the radiant interchange within an enclosure have been presented in order of increasing approximation and decreasing complexity. The first is an exact formulation of the problem [equation (47) or (48)] and is only restricted by the assumption of Lambert's law (diffuse radiation). Unfortunately, application of this method to a physical situation is a practical impossibility. Solution of the $M$ expressions given by equation (47) would require a solution at each frequency with the number of solutions approaching infinity. Solution by means of equation (48) is not feasible since the integrations required include factors which are not sufficiently described physically as a function of frequency and temperature (e.g., the gaseous absorption factor $\alpha_\nu$) and/or include factors which are to be determined (e.g., the radiosity $J_{\nu,m}$). These expressions do provide the initial step in making the approximations necessary for a practical solution and, consequently, a measure of the errors involved.

The second procedure is the band energy approximation as given by equation (67). The various approximations used in this analysis are based upon the fundamental assumption used in the theoretical analysis of gaseous absorption and verified experimentally, i.e., the absorption may be adequately described by assuming the incident energy to be constant over the band. Equations (63) and (64) are extensions of this assumption to the radiant characteristics of the surfaces. Since the frequency dependency of these factors is generally less than that of a gas, this extension should be at least as valid. The effect of this assumption is to treat the radiant system as gray over small frequency intervals and to approach the actual system [equation (48)] in a series of steps rather than in one large one [equation (79)].

The band energy approximation may be improved by using the monochromatic emissive power of the surfaces in combination with the spectral characteristics of the surface as indicated in the first expression of equation (64). The monochromatic emissive power of the surface may also be used as an approximation in equation (63). If this is done, however, the values of $\gamma_\omega$ and $\rho_\omega$ become doubly temperature dependent as noted previously.

The application of the band energy method is not possible within present knowledge. Neither the magnitude nor the functional behavior of the absorption within the various frequency intervals has been studied experimentally over the range of variables required for an engineering analysis. Methods of measuring the spectral characteristics of the surfaces are feasible and a limited amount of information is available [1].

The final technique of analysis described is the one most commonly used in calculation of radiant exchange, the gray radiation approximation. This procedure assumes that all of the surfaces and the gas have absorption characteristics independent of frequency. The number of equations which must be solved simultaneously is reduced to $M$ and only one set is involved.

The assumption of frequency independent characteristics is obviously wrong whenever a gaseous medium is included. The errors involved are significant for the case without the gas [3] and the supposition must be made that a gas would add to these errors. The inaccuracies of the methods presently available for evaluating the geometrical absorption factors are not known. Until an analysis is made based upon the band energy approximation, the errors of the geometrical absorption factors cannot be estimated.

The particular case of refractory surfaces (surface with $q_n = 0$) commonly used in the gray radiation analysis must be imposed as a special condition for the band energy approximation. For a specific band, the refractory surface does not exist except as a very special case, since by definition a refractory surface is:

$$\sum_{\omega}^{\Omega} q_{\omega,n} = 0 \tag{81}$$

Equation (79) for the case of a refractory surface becomes:

$$\sigma T_n^4 = \sum_{m=1}^{M} A_n F_{nm} J_m - \sum_{m=1}^{M} \bar{a}_{nm}' A_n F_{nm} J_m + \sum_{m=1}^{M} \bar{a}_{nm}' A_n F_{nm} \sigma T_{g,m}^4 \tag{82}$$

The total energy balance provides a means for separately checking a solution of either the gray or band energy approximation. In addition, a primary condition given for many physical problems is the total energy provided by combustion gases. For the band energy approximation, the total energy *emitted* by the gases is obtained from equation (69):

$$H = -\sum_{\omega}^{\Omega} Q_{\omega,n} = \sum_{n=1}^{M} \sum_{m=1}^{M} \bar{a}_{nm} A_n F_{nm} \left[ \int_{\Delta\nu_\omega} W_{\nu,m} d\nu - \int_{\Delta\nu_\omega} J_{\nu,m} d\nu \right] \tag{83}$$

The analogous expression for the gray radiation approximation is found directly from equation (81):

$$H = -Q = \sum_{n=1}^{M} \sum_{m=1}^{M} \bar{a}_{nm}' A_n F_{nm} (\sigma T_{g,m}^4 - J_m) \tag{84}$$

Solution of the $M$ simultaneous equations may be secured by established methods of matrix algebra. These methods become difficult and time consuming for even digital computers as the number of nodes are increased. An alternative method of solution will be described which is analogous to a relaxation of the system of equations. This method approaches the solution of the equations by a series of approximations and permits the selection of a desired accuracy of solution. This technique and numerical examples of its application will be described in the final part.

## APPENDIX

The band energy approximation may be obtained in a form slightly different from that given in the text. This alternative derivation requires approximations of slightly different form but of no greater degree of approximation than those given in the text. The choice of the two forms is subject to the particular conditions of a problem since conditions are conceivable whereby the method given here would be preferable to that of the text.

The initial starting point is equation (47) of the text which has been altered by multiplying by the monochromatic reflectivity of node $n$:

$$J_{\nu,n} A_n = A_n \varepsilon_{\nu,n} E_{\nu,n} + \sum_{m=1}^{M} r_{\nu,m} J_{\nu,m} A_n F_{nm} - \sum_{m=1}^{M} r_{\nu,m} J_{\nu,m} \bar{\alpha}_{\nu,nm} A_n F_{nm} + \sum_{m=1}^{M} r_{\nu,m} W_{\nu,m} \bar{\alpha}_{\nu,nm} A_n F_{nm} \tag{85}$$

Proceeding in the same manner as before, the band energy equation for node $n$ and frequency interval $\Delta\nu_\omega$ may be obtained:

$$\begin{aligned} \int_{\Delta\nu_\omega} J_{\nu,n} A_n d\nu = {} & \int_{\Delta\nu_\omega} A_n \varepsilon_{\nu,n} E_{\nu,n} d\nu \\ & + \sum_{m=1}^{M} \int_{A_n} \int_{A_m} \int_{\Delta\nu_\omega} r_{\nu,m} J_{\nu,m} \frac{\cos\theta_n \cos\theta_m}{\pi R^2} d\nu dA_m dA_n \\ & - \sum_{m=1}^{M} \int_{A_n} \int_{A_m} \int_{\Delta\nu_\omega} r_{\nu,n} J_{\nu,m} \alpha_\nu \frac{\cos\theta_n \cos\theta_m}{\pi R^2} d\nu dA_m dA_n \\ & + \sum_{m=1}^{M} \int_{A_n} \int_{A_m} \int_{\Delta\nu_\omega} r_{\nu,n} W_{\nu,m} \alpha_\nu \frac{\cos\theta_n \cos\theta_m}{\pi R^2} d\nu dA_m dA_n \end{aligned} \tag{86}$$

The approximations given by equations (58) through (62) are, for this system:

$$a = \frac{\int_{\Delta\nu_\omega} \alpha_\nu d\nu}{\Delta\nu_\omega} \cong \frac{\int_{\Delta\nu_\omega} r_\nu J_\nu \alpha_\nu d\nu}{\int_{\Delta\nu_\omega} r_\nu J_\nu d\nu} \tag{87}$$

$$\bar{a}_{nm}A_nF_{nm} = \int_{A_n}\int_{A_m} a\,\frac{\cos\theta_n\cos\theta_m}{\pi R^2}\,dA_n dA_m \quad (88)$$

$$r_{\omega,n} = \frac{\int_{\Delta\nu_\omega} r_{\nu,n}J_{\nu,n}d\nu}{\int_{\Delta\nu} J_{\nu,n}d\nu}; \quad r_{\omega,n} \cong r_{\omega,m} \quad (89)$$

$$\sum_{m=1}^{M}\int_{A_n}\int_{A_m}\int_{\Delta\nu_\omega} r_{\nu,m}J_{\nu,m}\,\frac{\cos\theta_n\cos\theta_m}{\pi R^2}\,dA_n dA_m d\nu \cong \sum_{m=1}^{M} A_nF_{nm}r_{\omega,n}\int_{\Delta\nu_\omega} J_{\nu,m}d\nu \quad (90)$$

$$\sum_{m=1}^{M}\int_{A_n}\int_{A_m}\int_{\Delta\nu_\omega} r_{\nu,m}J_{\nu,m}\alpha_\nu\,\frac{\cos\theta_n\cos\theta_m}{\pi R^2}\,dA_n dA_m d\nu \cong \sum_{m=1}^{M} \bar{a}_{nm}A_nF_{nm}r_{\omega,n}\int_{\Delta\nu_\omega} J_{\nu,m}d\nu \quad (91)$$

$$\sum_{m=1}^{M}\int_{A_n}\int_{A_m}\int_{\Delta\nu_\omega} r_{\nu,n}W_{\nu,m}\alpha_\nu\,\frac{\cos\theta_n\cos\theta_m}{\pi R^2}\,dA_n dA_m d\nu \cong \sum_{m=1}^{M} \bar{a}_{nm}A_nF_{nm}r_{\omega,n}\int_{\Delta\nu_\omega} W_{\nu,m}d\nu \quad (92)$$

The approximations involving the spectral characteristics of the surface [equations (63) through (66)] are not required as before. These have been replaced by a fundamental approximation involving the product of the spectral reflectance of node $n$ and the radiosity of surface $m$ or gas node $m$. This also replaces the assumption involving the constancy of the incident energy over the gaseous absorption band. That is:

$$\frac{\int_{\Delta\nu_\omega}\alpha_\nu d\nu}{\Delta\nu_\omega} \cong \frac{\int_{\Delta\nu_\omega} r_{\nu,m}J_{\nu,n}\alpha_\nu d\nu}{\int_{\Delta\nu_\omega} r_{\nu,n}J_{\nu,n}d\nu}$$

replaces

$$\frac{\int_{\Delta\nu_\omega}\alpha_\nu d\nu}{\Delta\nu_\omega} \cong \frac{\int_{\Delta\nu_\omega} J_{\nu,n}\alpha_\nu d\nu}{\int_{\Delta\nu_\omega} J_{\nu,n}d\nu}$$

Analogous relations hold for the other approximations.

The inherent difficulty of this derivation is the lack of knowledge regarding the spectral reflectance of the $m$ surfaces in a particular problem. The frequency variability of the absorption characteristics of the gas are sufficiently established to approximate the absorption within a band under the assumption of incident energy varying as a black body. In the text this has been extended to the radiosity of the various nodes. The validity of this extrapolation is subject to serious question since the absorption of a gas is not uniform within a band and a distortion of the frequency-energy distribution is automatically introduced in the radiosities. The addition of the spectral reflectance as a factor to this compounds the unknowns within the approximation. The spectral variation of the reflectance could increase the distortion of the radiosity frequency variation just as well as reduce it. As noted in the text, the spectral reflectance for many surfaces is uniform within a limited frequency band so as not to affect the approximation. This cannot be taken as a generality for all surfaces or for all frequency intervals to provide a firm basis for including the reflectance as a factor in the approximation. When an absorbing medium is not involved, this procedure would not incur this difficulty.

The reduction of equation (86) to a form analogous to equation (67) gives:

$$\int_{\Delta\nu_\omega} A_nJ_{\nu,n}d\nu = A_n\varepsilon_{\omega,n}\int_{\Delta\nu_\omega} E_{\nu,n}d\nu + \sum_{m=1}^{M} A_nF_{nm}r_{\omega,n}\int_{\Delta\nu_\omega} J_{\nu,m}d\nu - \sum_{m=1}^{M} \bar{a}_{nm}A_nF_{nm}r_{\omega,n}\int_{\Delta\nu_\omega} J_{\nu,m}d\nu + \sum_{m=1}^{M} \bar{a}_{nm}A_nF_{nm}r_{\omega,n}\int_{\Delta\nu_\omega} W_{\nu,m}d\nu \quad (93)$$

This expression must be solved for each node and for each $\Delta\nu_\omega$ as previously. The gray radiation approximation follows from this relation by assuming the spectral characteristics of the surface to be independent of frequency.

## Nomenclature for Part 2

$A$ = area of surface; $A_n$ = area of surface $n$

$E$ = emissive power; $E_{\nu,n}$ = monochromatic emissive power of surface $n$

$F$ = geometrical shape factor; $F_{nm}$ is defined by the following expression:

$$A_nF_{nm} = \int_{A_n}\int_{A_m} \frac{\cos\theta_n\cos\theta_m}{\pi R^2}\,dA_n dA_m$$

$H$ = total energy emitted by the enclosed medium; see equation (83) or (84)

$J$ = radiosity of the surface; $J_{\nu,n}$ = monochromatic radiosity of surface $n$

$M$ = total number of surfaces composing a specific enclosure

$Q$ = net energy flowing from all surface nodes, equation (54b); $Q_\nu$ = monochromatic energy, equation (51); $Q_\omega$ = energy within the band, equation (69)

$R$ = length of the line joining the two differential areas of surfaces $A_n$ and $A_m$

$T$ = absolute temperature; $T_n$ = absolute temperature of surface $n$, $T_{g,m}$ = absolute temperature of the medium (gas) involved in the exchange of energy between surfaces $n$ and $m$

$W$ = emissive power of the medium; $W_{\nu,m}$ = monochromatic emissive power of the medium involved in the exchange of energy between surfaces $n$ and $m$

$a$ = band absorption of the absorbing medium, equation (58); $\bar{a}_{nm}$ = geometrical band absorption, equation (59); $\bar{a}_{nm}'$ = gray radiation approximation of the absorption of intervening medium, equation (74) or (75)

$\varepsilon$ = emittance of the surface; $\varepsilon_{\nu,n}$ = monochromatic emittance of surface $n$; $\varepsilon_n$ = total emittance of surface $n$, equation (26)

$m$ = number of surfaces composing a general enclosure; for a specific enclosure $m = 1, 2, 3, \ldots M$

$n$ = a specific surface of the enclosure

$q$ = energy flow; $q_{\nu,n}$ = monochromatic energy from the surface node $n$ to the inner node $n$ of the radiation network, equation (50); $q_{\omega,n}$ = band energy from a surface $n$, equation (68)

$r$ = reflectance; $r_{\nu,n}$ = monochromatic reflectance of surface $n$; ${}_mr_n$ = gray radiation approximation reflectance of surface $n$ which is a function of the radiosity of surface $m$, equation (74) and (75); $r_n = {}_mr_n$ for $m = n$, equation (27)

$\alpha$ = absorptivity of the intervening medium; $\alpha_\nu$ = monochromatic absorptivity; $\bar{\alpha}_{\nu,nm}$ = geometrical monochromatic absorptivity of the medium between surfaces $n$ and $m$, i.e.,

$$\alpha_{\nu,nm} = \frac{1}{A_n F_{nm}} \int_{A_n} \int_{A_m} \alpha_\nu \frac{\cos\theta_n \cos\theta_m}{\pi R^2} dA_n dA_m$$

$\gamma$ = band energy approximation to the ratio of emittance and reflectance; $\gamma_\omega = \gamma$ for a specific band, equation (64)

$\Delta$ = difference; $\Delta\nu_\omega$ = frequency interval for a specific band

$\theta$ = angle between the normal and the line $R$; $\theta_n$ = value at the surface $n$

$\nu$ = frequency; $\Delta\nu_\omega$ = frequency interval for $\omega$

$\pi$ = 3.14159 . . .

$\rho$ = the quantity analogous to reflectance required by the band energy approximation; $(\rho)_{\omega,n}$ defined by equation (63) for the specific band $n$ and surface $m$

$\tau$ = transmissivity of the intervening medium; $\tau$ = monochromatic transmissivity; $\tau_\nu + \alpha_\nu = 1$

$\Omega$ = total number of frequency intervals ($\Delta\nu$) used in subdividing the energy spectrum for the band energy approximation; $\Omega = \omega_1 + \omega_2$

$\omega$ = specific frequency intervals ($\Delta\nu$) used to subdivide the energy spectrum; $\omega_1$ = intervals with no absorption by the intervening medium; $\omega_2$ = intervals with absorption by the intervening medium

R. V. DUNKLE[2]
J. T. BEVANS[1]

# Part 3 A Method for Solving Multinode Networks and a Comparison of the Band Energy and Gray Radiation Approximations

THE FIRST PART in this series reviewed the principles of gaseous absorption and emission of thermal radiation. The second developed the analysis of the radiant interchange within an enclosure using the concepts of the network analogy. This final part will be used to demonstrate the application of the procedures discussed in the first two and to illustrate the errors involved in the band energy and gray radiation approximations.

The solution of a simple cubical enclosure will be used to illustrate the relaxation or reiterative method of solving the multinode network. The inadequacy of present knowledge of the radiation characteristics of surfaces and gaseous media plus the desire to demonstrate the procedure in a direct manner dictated the use of a simple system for the example. The last part of the paper presents a comparison of the band energy and gray radiation approximations for a gaseous medium between two parallel infinite surfaces. These examples are an extension of the analysis given by Goodman [7] and provide magnitudes of the errors involved in the basic methods of analysis of radiation exchange for specific systems. These errors are in addition to those introduced by the uncertainties in the radiation characteristics of the surfaces and media within the radiant system.

## Relaxation (Reiterative) Solution of a Radiation Network [14]

The example selected to demonstrate the method of solution is a cubical enclosure (box) with a heated top, a cooled floor, and refractory walls. The assumption of gray radiation and no absorbing medium will be made in order to reduce the number of computations. The top is assumed to be at a temperature of 2000 F and to have an emittance of 0.90; the bottom is maintained at 1000 F and has an emittance of 0.60. The temperature distribution of the side walls will be approximated by dividing these walls into four horizontal bands of equal area. The geometrical system is illustrated in Fig. 3 and the equivalent radiation network is given in Fig. 4. The temperature distribution over each of these six areas (top, bottom, and four bands) is assumed to be uniform as required by the network method.

The six equations which must be solved are obtained for this problem from the expressions given in the Appendix of Part 2, rearranged to give the radiosity of the $n$th surface in terms of the radiosities of all other surfaces. The radiosity of a gray, heat-transfer surface of uniform temperature and irradiation, is given in terms of its emissive power and the radiosities of all other surfaces within the enclosure by:

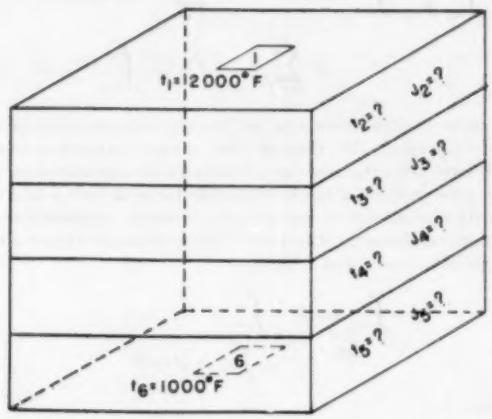


Fig. 3 Cube with refractory walls used as an example for the reiterative method

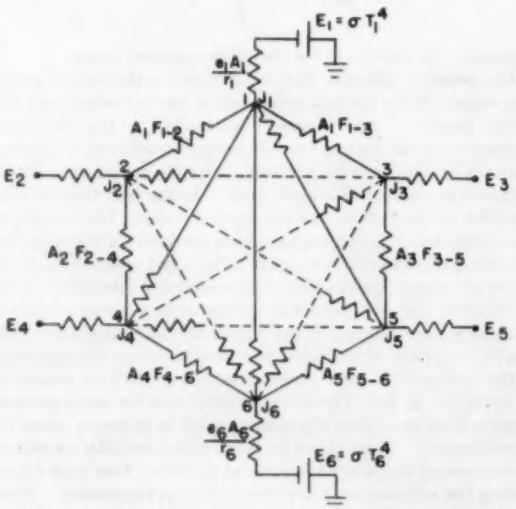


Fig. 4 Radiation network for system shown in Fig. 3

$$J_n = \left(\frac{\epsilon_n}{1 - r_n F_{nn}}\right) E_n + \left(\frac{r_n}{1 - r_n F_{nn}}\right) \sum_{\substack{m=1 \\ (n \neq m)}}^{M} J_m F_{nm} \quad (94)$$

The heat flux from this surface is expressed as:

$$(q/A)_n = \left(\frac{\epsilon_n}{r_n}\right)(E_n - J_n) = (1 - F_{nn})J_n - \sum_{\substack{m=1 \\ (n \neq m)}}^{M} J_m F_{nm} \quad (95)$$

The comparable equations for the four refractory surfaces must be modified by the definition of a refractory surface, i.e., $(q/A)_n = 0$ or $E_n = J_n$. Using these conditions gives:

$$J_n = \left(\frac{1}{1 - F_{nn}}\right) \sum_{\substack{m=1 \\ (n \neq m)}}^{M} J_m F_{nm} \quad (96)$$

In an enclosure of $M$ surfaces, there will be a total of $M$ equations of the form of either equation (94) or (96) The particular form will be determined by the conditions of the surface, i.e., whether a heat-transfer surface or a refractory one. The procedure of solution is initiated by assuming radiosities for all nodes and then, starting with node 1, solving for the radiosity of node 1 using the assumed radiosities for nodes 2 through $M$ and the pertinent equation for this node. This new value of the radiosity of node 1 is used along with the assumed radiosities for nodes 3 through $M$ to find a new value for the radiosity of node 2. The procedure is continued until new values for the radiosities of all nodes have been found. A second trial is made by repeating the computation with these new radiosities and the trials continued until the desired accuracy is achieved. This accuracy may be established in a number of ways such as requiring for each node the difference between the radiosities of successive trials to be less than a fixed percentage of the last trial radiosity. Accuracy may also be determined using the heat flux computed from the radiosity and emissive power of the node. The convergence of the procedure described is rapid and generally only a few trials are necessary for a moderate accuracy. Judicious guessing from experience of the initial radiosities will reduce the number of trials required.

This procedure is rapidly applied to the sample problem. The potentials (radiosities) of all six internal nodes are unknown as are the currents in the internal conductances. The currents to the external nodes of surfaces 1 and 6 are equal and opposite since the remaining surfaces are assumed to be refractory and no other heat sources or sinks exist in the system. The external potentials of nodes 1 and 6 are fixed while the potentials of the remaining nodes are "floating." The expressions for the radiosity of nodes 1 and 6 for the particular conditions of the example are obtained from equation (94):

$$J_1 = 56{,}664 + 0.10 \sum_{m=2}^{6} J_m F_{1-m} \quad (97)$$

$$J_6 = 3{,}100 + 0.60 \sum_{m=1}^{5} J_m F_{6-m} \quad (98)$$

Similar expressions for the remaining nodes are obtained from equation (96). The expression for node 2 is, for example:

$$J_2 = 1.316 \sum_{\substack{m=1 \\ m \neq 2}}^{6} J_m F_{2-m} \quad (99)$$

**Table 3 Solution of radiation network shown in Fig. 3**

| NODE PAIR n-m | $F_{nm}$ | $\epsilon_n$ | TRIAL 1 $J_n$ | TRIAL 1 $J_n F_{nm}$ | TRIAL 2 $J_n$ | TRIAL 2 $J_n F_{nm}$ |
|---|---|---|---|---|---|---|
| 1-2 | 0.380 | 50,000 | 19,000 | 46,000 | 17,500 | |
| 1-3 | 0.205 | 40,000 | 8,200 | 37,300 | 7,650 | |
| 1-4 | 0.135 | 30,000 | 4,050 | 30,800 | 4,160 | |
| 1-5 | 0.080 | 20,000 | 1,600 | 25,200 | 2,020 | |
| 1-6 | 0.200 | 10,000 | 2,000 | 25,100 | 5,020 | |
| | | $\sum$ | 34,850 | | 36,350 | |
| | $\left(\frac{r_1}{1-r_1F_{1-1}}\right)$ | $\sum$ | 3,485 | | 3,635 | |
| | | $\epsilon_1 E_1$ | 56,664 | | 56,664 | |
| | | $J_1$ | 60,150 | | 60,299 | |
| 2-1 | 0.380 | 60,150 | 24,000 | 60,300 | 23,900 | |
| 2-3 | 0.175 | 40,000 | 7,000 | 37,300 | 6,520 | |
| 2-4 | 0.070 | 30,000 | 2,100 | 30,800 | 2,160 | |
| 2-5 | 0.055 | 20,000 | 1,100 | 25,200 | 1,390 | |
| 2-6 | 0.080 | 10,000 | 800 | 25,100 | 2,000 | |
| | | $\sum$ | 35,000 | | 35,970 | |
| | | $J_2$ | 46,000 | | 47,400 | |
| 3-1 | 0.205 | 60,150 | 12,300 | 60,300 | 12,400 | |
| 3-2 | 0.175 | 46,000 | 8,050 | 47,400 | 8,300 | |
| 3-4 | 0.175 | 30,000 | 5,250 | 30,800 | 5,400 | |
| 3-5 | 0.070 | 20,000 | 1,400 | 25,200 | 1,760 | |
| 3-6 | 0.135 | 10,000 | 1,350 | 25,100 | 3,400 | |
| | | $\sum$ | 28,350 | | 31,260 | |
| | | $J_3$ | 37,300 | | 41,100 | |
| 4-1 | 0.135 | 60,150 | 8,120 | 60,300 | 8,150 | |
| 4-2 | 0.070 | 46,000 | 3,220 | 47,400 | 3,330 | |
| 4-3 | 0.175 | 37,300 | 6,520 | 41,100 | 7,200 | |
| 4-5 | 0.175 | 20,000 | 3,500 | 25,200 | 4,400 | |
| 4-6 | 0.205 | 10,000 | 2,050 | 25,100 | 5,150 | |
| | | $\sum$ | 23,400 | | 28,230 | |
| | | $J_4$ | 30,800 | | 37,100 | |
| 5-1 | 0.080 | 60,150 | 4,800 | 60,300 | 4,830 | |
| 5-2 | 0.055 | 46,000 | 2,530 | 47,400 | 2,600 | |
| 5-3 | 0.070 | 37,300 | 2,620 | 41,100 | 2,880 | |
| 5-4 | 0.175 | 30,800 | 5,400 | 37,100 | 6,500 | |
| 5-6 | 0.380 | 10,000 | 3,800 | 25,100 | 9,550 | |
| | | $\sum$ | 19,150 | | 26,360 | |
| | | $J_5$ | 25,200 | | 34,700 | |
| 6-1 | 0.200 | 60,150 | 12,030 | 60,300 | 12,100 | |
| 6-2 | 0.080 | 46,000 | 3,680 | 47,400 | 3,800 | |
| 6-3 | 0.135 | 37,300 | 5,040 | 41,100 | 5,550 | |
| 6-4 | 0.205 | 30,800 | 6,300 | 37,100 | 7,620 | |
| 6-5 | 0.380 | 25,200 | 9,600 | 34,700 | 13,200 | |
| | | $\sum$ | 36,650 | | 42,270 | |
| | $\left(\frac{r_6}{1-r_6F_{6-6}}\right)$ | $\sum$ | 22,000 | | 25,400 | |
| | | $\epsilon_6 E_6$ | 3,100 | | 3,100 | |
| | | $J_6$ | 25,100 | | 28,500 | |

| NODE PAIR n-m | $F_{nm}$ | TRIAL 7 $J_n$ | TRIAL 7 $J_n F_{nm}$ | TRIAL 8 $J_n$ | TRIAL 8 $J_n F_{nm}$ | |
|---|---|---|---|---|---|---|
| 1-2 | | 51,646 | 19,625 | 51,865 | 19,709 | $\left(\frac{r}{A}\right) = 16{,}090 \frac{Btu}{hr}\ ft^2$ |
| 1-3 | | 47,684 | 9,775 | 47,926 | 9,825 | |
| 1-4 | | 44,218 | 5,969 | 44,453 | 6,001 | $\left(\frac{r_1}{1-r_1F_{1-1}}\right) = 0.100$ |
| 1-5 | | 40,353 | 3,228 | 40,560 | 3,245 | |
| 1-6 | | 31,427 | 6,285 | 31,525 | 6,305 | |
| | $\sum$ | | 44,882 | | 45,085 | |
| | $\left(\frac{r_1}{1-r_1F_{1-1}}\right)\sum$ | | 4,488 | | 4,509 | |
| | $\epsilon_1 E_1$ | | 56,664 | | 56,664 | |
| | $J_1$ | | 61,152 | | 61,172 | |
| 2-1 | | 61,152 | 23,238 | 61,172 | 23,245 | |
| 2-3 | | 47,684 | 8,345 | 47,926 | 8,387 | $\left(\frac{1}{1-F_{2-2}}\right) = 1.316$ |
| 2-4 | | 44,218 | 3,095 | 44,453 | 3,112 | |
| 2-5 | | 40,353 | 2,219 | 40,560 | 2,231 | |
| 2-6 | | 31,427 | 2,514 | 31,525 | 2,522 | |
| | $\sum$ | | 39,411 | | 39,497 | |
| | $J_2$ | | 51,865 | | 51,978 | |
| 3-1 | | 61,152 | 12,536 | 61,172 | 12,540 | |
| 3-2 | | 51,865 | 9,076 | 51,978 | 9,096 | $\left(\frac{1}{1-F_{3-3}}\right) = 1.316$ |
| 3-4 | | 44,218 | 7,738 | 44,453 | 7,779 | |
| 3-5 | | 40,353 | 2,825 | 40,560 | 2,839 | |
| 3-6 | | 31,427 | 4,243 | 31,525 | 4,255 | |
| | $\sum$ | | 36,418 | | 36,509 | |
| | $J_3$ | | 47,926 | | 48,046 | |
| 4-1 | | 61,152 | 8,256 | 61,172 | 8,258 | |
| 4-2 | | 51,865 | 3,631 | 51,978 | 3,638 | $\left(\frac{1}{1-F_{4-4}}\right) = 1.316$ |
| 4-3 | | 47,926 | 6,367 | 48,046 | 6,408 | |
| 4-5 | | 40,353 | 7,062 | 40,560 | 7,098 | |
| 4-6 | | 31,427 | 6,443 | 31,525 | 6,462 | |
| | $\sum$ | | 33,779 | | 33,844 | |
| | $J_4$ | | 44,453 | | 44,565 | |
| 5-1 | | 61,152 | 4,892 | 61,172 | 4,894 | |
| 5-2 | | 51,865 | 2,853 | 51,978 | 2,859 | |
| 5-3 | | 47,926 | 3,355 | 48,046 | 3,363 | |
| 5-4 | | 44,453 | 7,779 | 44,565 | 7,799 | |
| 5-6 | | 31,427 | 11,942 | 31,525 | 11,980 | |
| | $\sum$ | | 30,821 | | 30,895 | |
| | $J_5$ | | 40,560 | | 40,658 | |
| 6-1 | | 61,152 | 12,230 | 61,172 | 12,234 | $\left(\frac{q}{A}\right)_6 = 15{,}878 \frac{Btu}{hr}\ ft^2$ |
| 6-2 | | 51,865 | 4,149 | 51,978 | 4,158 | |
| 6-3 | | 47,926 | 6,470 | 48,046 | 6,486 | $\left(\frac{r_6}{1-r_6F_{6-6}}\right) = 0.60$ |
| 6-4 | | 44,453 | 9,113 | 44,565 | 9,136 | |
| 6-5 | | 40,560 | 15,413 | 40,658 | 15,460 | |
| | $\sum$ | | 47,375 | | 47,446 | |
| | $\left(\frac{r_6}{1-r_6F_{6-6}}\right)\sum$ | | 28,425 | | 28,468 | |
| | $\epsilon_6 E_6$ | | 3,100 | | 3,100 | |
| | $J_6$ | | 31,525 | | 31,568 | |

The solution is shown in Table 3 using the following initial assumptions for the radiosities: $J_1 = 60{,}000$; $J_2 = 50{,}000$; $J_3 = 40{,}000$; $J_4 = 30{,}000$; $J_5 = 20{,}000$; $J_6 = 10{,}000$. Only trials 1, 2, 7, and 8 are shown in Table 3 for brevity. The difference between the values of trial 7 and 8 are seen to be less than 0.25 per cent indicating the values to be very close to the correct ones. An additional check shows the heat fluxes (currents) of surfaces 1 and 6 are equal within 1.3 per cent and for this particular example, the true value would be very near the arithmetic average of these two values.

The particular example chosen is not difficult to solve by established methods [10] and provides an opportunity for comparison. The equivalent circuit between nodes 1 and 6 may be drawn as shown in Fig. 5 where $A_1F_{1-6}$ is the value of the conductance between the two nodes. The value of this conductance given by Hottel [10] is:

$$F_{1-6} = 0.536$$

Using the results obtained on the eighth trial (Table 3), we have:

$$F_{1-6} = \frac{(q/A)_1}{J_1 - J_6} = \frac{15{,}980}{61{,}172 - 31{,}568} = 0.540$$

The comparison between these two values is satisfactory.

The radiosities of the four areas composing the walls of the enclosure may be used to determine the temperatures of these areas. Since these are refractory surfaces, the radiosities are equal to the emissive powers of a black body:

$$J = \sigma T^4$$

Calculation of these temperatures gives the following values:

$t_2 = 1884$ F $\qquad t_4 = 1797$ F

$t_3 = 1838$ F $\qquad t_5 = 1744$ F

These temperatures may be assumed to be the average values of the particular areas, or that temperature at the mid-height of the area. The equivalent radiant temperature of a surface is equal to the temperature of a black body which would have a total emissive power equal to the radiosity of the surface. This radiant temperature is the temperature which would be registered by a radiation pyrometer sighting at the surface. Errors using an optical pyrometer are liable to be even larger than when using a total radiation pyrometer, and the effect of nongrayness may either increase or decrease the error, depending upon the spectral characteristics of the surfaces and media in the system. For the problem just worked, the equivalent radiant temperatures found for the top and bottom surfaces are 1980 F and 1609 F, respectively. When compared with the true temperatures of 2000 F and 1000 F, the influence of the surface characteristics and of the surrounds upon radiation pyrometry is evident.

In the preceding example, either the emissive power (temperature) of a surface or the heat flow into the surface was known (zero for the refractory surfaces). This type of problem is a special case of a more general problem which may be considered. The unknowns in any problem must equal the number of nodes in order to insure a single solution. The number of known or specified quantities may be assigned to the nodes in any manner compatible with this restriction. Thus a node may have both the heat flux and the emissive power specified, either the heat flux or the emissive power may be given, or neither of these quantities may be given.

The application of the reiterative method to high speed digital computers is readily apparent and avoids the difficulty of matrix inversion required by other methods of solution of the radiation network. The limitation of the use of reiteration for hand calculation is the patience of the computer.

The use of the band energy approximation for nongray systems results in a large increase in the complexity of the problem. If the temperatures of all surfaces and the gas are known, the procedure is straightforward. Each band is solved separately, the heat-transfer rates are obtained for each surface by summing the bands for that specific surface. If only a few surfaces are involved, the radiation network can be solved analytically; but if many surfaces are involved, it is better to handle each band by the relaxation method as outlined for the gray system. If many bands and nodes are involved, the use of a computer is advisable.

If any of the surfaces in the system have specified heat rates (e.g., refractory surfaces with zero heat flux) and unknown temperature, or both unknown temperature and heat rate, the band energy approximation is much more difficult to apply. Particular attention should be given the refractory surfaces since the sum of the heat fluxes for all bands may be zero, but the value for any one band is not necessarily zero. The solution of a problem may be facilitated by first solving on the basis of gray conditions and using the results obtained to start the reiterative solution. This procedure should provide better initial estimates than experienced guesses for the unknown radiosities to be used to start the solution.

Solving an enclosure using the band energy approximation is presently restricted by the lack of adequate knowledge of the radiant characteristics of the surfaces and gaseous media. In addition, the complexity of such a solution would have obscured the procedure used in solving the network. Consequently, the reiterative method of solution has been separated from a discussion of the band energy and gray radiation approximations. This latter comparison has also been restricted to simple conditions in order to minimize the complexity.

## Comparison of the Band Energy and Gray Radiation Approximations

The first case to be considered is two infinite parallel plates separated by a nonabsorbing and nonemitting medium. The radiant exchange will be computed using the exact solution, the band energy approximation and the gray radiation approximations. This is similar to the analysis made by Goodman [7] for the exact solution and the gray radiation assumption. The exact solution and the band energy approximation differ only in the number and size of the frequency intervals used for a particular problem. When an absorbing medium is present, these intervals are determined by the characteristics of the medium and for this example the band limits of carbon dioxide have been used according to the work of Howard, et al. [12]. In addition, the "window" region between the wavelengths 5.3 and 12.5 microns (1870 to 800 $cm^{-1}$)

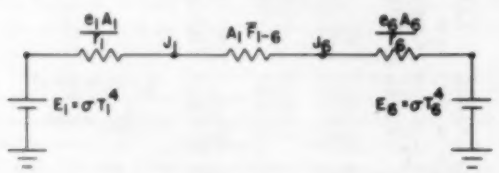


Fig. 5 Equivalent circuit for radiation network between surfaces 1 and 6 of the cube

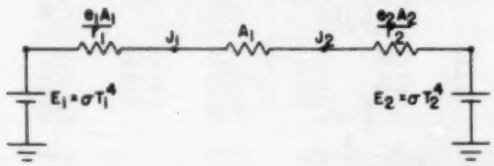


Fig. 6 Radiation circuit for parallel plates with no absorbing medium

has been subdivided into three regions. This procedure has been found to increase the accuracy of computations with an absorbing gas whenever a wide spectral region of zero absorption exists.

The radiation network for parallel plates consists of three conductances in series (Fig. 6) and the solution of this system on a monochromatic basis is:

$$q_{\nu,1-2} = \frac{A_1(E_{\nu,1} - E_{\nu,2})}{\frac{1}{\epsilon_{\nu,1}} + \frac{1}{\epsilon_{\nu,2}} - 1} = A_1 \mathfrak{F}_{\nu,1-2}(E_{\nu,1} - E_{\nu,2}) \quad (100)$$

The net exchange between the two surfaces is obtained by integrating equation (100) over all wavelengths using previously published procedures [3]:

$$q_{1-2} = \int_0^\infty q_{\nu,1-2}\,d\nu = A_1\sigma T_1^4 \int_0^\infty \mathfrak{F}_{\nu_1-2}\left(\frac{E_{\nu,1}}{\sigma T_1^5}\right) d\left(\frac{\nu}{T_1}\right) - A_1\sigma T_2^4 \int_0^\infty \mathfrak{F}_{\nu,1-2}\left(\frac{E_{\nu,2}}{\sigma T_2^5}\right) d\left(\frac{\nu}{T_2}\right) \quad (101)$$

The evaluation of equation (101) requires two numerical or graphical integrations, and it may be seen that a simple reciprocity relationship between the conductances from surface 1 to 2 and from surface 2 to 1 does not exist. This is in contrast with the gray radiation case where:

$$A_1 \int_0^\infty \mathfrak{F}_{\nu,1-2}\left(\frac{E_{\nu,1}}{\sigma T_1^5}\right) d\left(\frac{\nu}{T_1}\right) \cong A_1\mathfrak{F}_{1-2} \cong A_2\mathfrak{F}_{2-1} \quad (102)$$

The heat exchange for the gray radiation case is given by:

$$q_{1-2} = A_1\mathfrak{F}_{1-2}\sigma(T_1^4 - T_2^4) \quad (103)$$

The band energy approximation can be applied to this problem by replacing the integrals in equation (101) by the summation of individual band conductances. The band conductance in this case is approximated by using the arithmetic mean values of the emittances of each surface over the given band interval as indicated in equation (104).

$$\mathfrak{F}_{\Delta\nu,1-2} \cong \int_{\Delta\nu} \left[\frac{1}{\frac{1}{\epsilon_{\nu,1}} + \frac{1}{\epsilon_{\nu,2}} - 1}\right] d\nu \quad (104)$$

This approximation is slightly easier to use in the analytical expression for the conductance of this simple radiation circuit than the general expressions given in Part 2 of this paper for the multinode network. This approximation is also used later on for the parallel surfaces with absorbing gas between them.

Two examples of the evaluation of the net exchange are given in Table 5. In both cases, one surface was titanium alloy, C-110M which had been oxidized for 303 hours at 1000 deg F [1] and was assumed to have a temperature of 1260 F. The first example used a surface of the same material at 660 deg R. For these conditions, the following results were obtained:

$$\int_0^\infty \mathfrak{F}_{\nu,1-2}\left(\frac{E_{\nu,1}}{\sigma T_1^5}\right) d\left(\frac{\nu}{T_1}\right) = 0.486$$

$$\int_0^\infty \mathfrak{F}_{\nu,2-1}\left(\frac{E_{\nu,2}}{\sigma T_2^5}\right) d\left(\frac{\nu}{T_2}\right) = 0.300$$

Substitution of these values in equation (101) gives a net heat exchange of 2004 Btu/hr ft². The computation with the gray radiation approximation used the computed values given in the literature [1]. The results of these two methods of computation and the band energy approximation result is summarized in Table 5. Similar calculations using anodized aluminum for the colder surface are also presented in Table 5. The spectral data for both surfaces are shown in Fig. 7.

The results tabulated in Table 5 demonstrate the magnitude of the errors involved in the band energy approximation and the gray radiation approximation relative to the exact calculation. The errors given are indicative only and apply to the particular cases considered. No significance should be attached to the particular magnitudes shown as may be seen by the shift in the sign of the error in the two cases. However, in both instances the band energy approximation is significantly less in error.

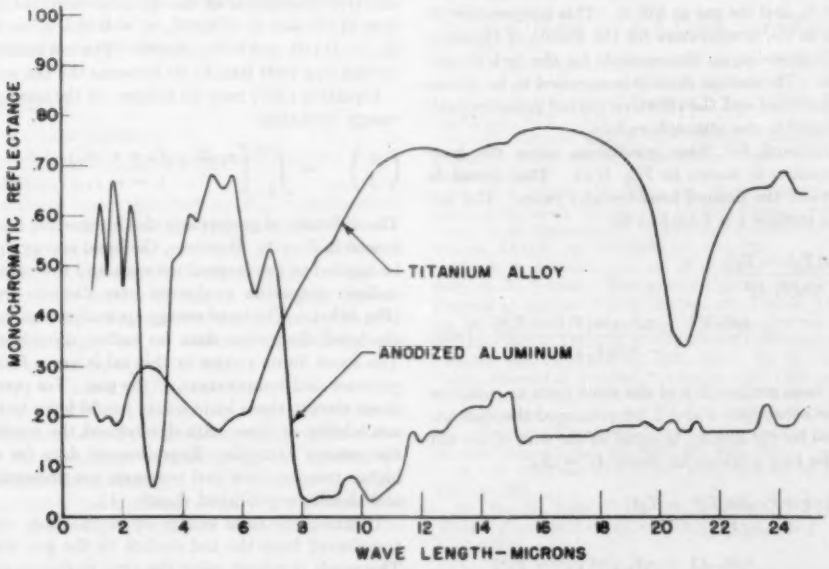


Fig. 7 Spectral reflectance of oxidized titanium alloy C-110 M(1) and anodized aluminum

**Table 4 Band intervals selected for calculations with carbon dioxide absorption [12]**

Path Length = 1 foot

Pressure (partial and total) = 1 atmosphere

Temperature = 532°R

| Nominal Wavelength -microns- | Band Limits Wave number $-cm^{-1}-$ | | Band Limits Wavelength -microns- | | Band Absorption $\frac{A_b}{}$ |
|---|---|---|---|---|---|
| 15 | 550 | 800 | 18.2 | 12.5 | 0.652 |
| | 800 | 1000 | 12.5 | 10.0 | — |
| | 1000 | 1433 | 10.0 | 6.97 | — |
| | 1433 | 1870 | 6.97 | 5.35 | — |
| 5.2 | 1870 | 1980 | 5.35 | 5.05 | 0.022 |
| 4.8 | 1980 | 2160 | 5.05 | 4.62 | 0.055 |
| 4.3 | 2160 | 2500 | 4.62 | 4.00 | 0.052 |
| | 2500 | 2680 | 4.00 | 3.87 | — |
| 2.7 | 2680 | 3800 | 3.87 | 2.63 | 0.0570 |
| | 3800 | 4750 | 2.63 | 2.10 | — |
| 2.0 | 4750 | 5200 | 2.10 | 1.92 | 0.109 |
| | 5200 | 6000 | 1.92 | 1.67 | — |
| 1.6 | 6000 | 6550 | 1.67 | 1.52 | 0.010 |
| | 6550 | 6650 | 1.52 | 1.50 | — |
| 1.4 | 6650 | 7250 | 1.50 | 1.38 | 0.0095 |

**Table 5 Comparison of band energy and gray radiation approximations with "exact" solution of radiation exchange between two infinite parallel surfaces**

| | Surface 1 | Surface 2 |
|---|---|---|
| Temperature | 800°F | 200°F |

A. Titanium Alloy C-110M (oxidized 303 hours at 1000°F)

| Method | Heat Transfer Rate | Per Cent Error |
|---|---|---|
| "Exact Solution" | 2004 Btu/hr ft² | — |
| Band Energy Approximation | 1977 Btu/hr ft² | -1.3 |
| Grey Radiation Approximation | 1400 | -30 |

B. Titanium Alloy C-110M (at 800°F) to Anodized Aluminum (at 200°F)

| Method | Heat Transfer Rate | Per Cent Error |
|---|---|---|
| "Exact" Solution | 1616 | — |
| Band Energy Approximation | 1626 | +1.2 |
| Grey Radiation Approximation | 2120 | +29 |

The final example will consider the case of parallel surfaces of the same titanium alloy as in the previous example separated by carbon dioxide gas. The hot surface is taken as 1500 deg R, the cold surface at 530 R, and the gas at 530 R. This temperature of 530 R corresponds to the temperature for the results of Howard, et al. [12] and is imposed upon the example by the lack of any other suitable data. The carbon dioxide is assumed to be at one atmosphere total pressure and the effective partial pressure path length product is equal to one atmosphere foot.

The radiation network for these conditions using the gray radiation approximation is shown in Fig. 8(*a*). This circuit is readily solved to yield the desired heat-transfer rates. The net radiation loss from surface 1 is found to be:

$$\left(\frac{q}{A}\right)_1 = \frac{\epsilon_1\epsilon_2\bar{\tau}_{1-g}\sigma(T_1^4 - T_2^4)}{1 - r_1r_2(\bar{\tau}_{1-g})^2} + \frac{\epsilon_1\bar{\alpha}_{1-g}(1 + r_2\bar{\tau}_{1-g})\sigma(T_1^4 - T_g^4)}{1 - r_1r_2(\bar{\tau}_{1-g})^2} \quad (105)$$

The net heat loss from surface 2 is of the same form as equation (105), but with the subscripts 1 and 2 interchanged throughout. The net heat gained by the gas, $q_g$, is equal to the sum of the net heat losses from the two surfaces or, since $A_1 = A_2$:

$$\left(\frac{q}{A}\right)_g = \frac{\epsilon_1\bar{\alpha}_{1-g}(1 + r_2\bar{\tau}_{1-g})\sigma(T_1^4 - T_g^4)}{1 - r_1r_2(\bar{\tau}_{1-g})^2} + \frac{\epsilon_2\bar{\alpha}_{1-g}(1 + r_1\bar{\tau}_{1-g})\sigma(T_2^4 - T_g^4)}{1 - r_1r_2(\bar{\tau}_{1-g})^2} \quad (106)$$

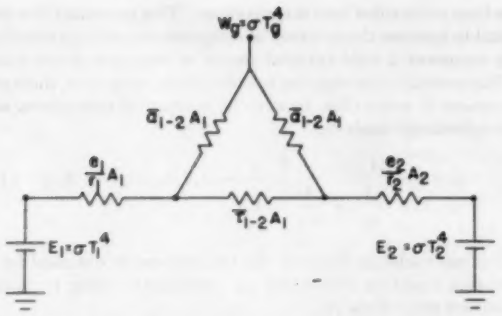


**Fig. 8(*a*) Radiation circuit for parallel plates with an absorbing medium: Gray radiation case**

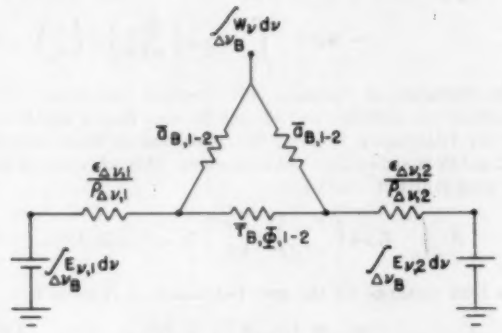


**Fig. 8(*b*) Radiation circuit for parallel plates with an absorbing medium: Band approximation**

For the conditions of this problem, $T_2 = T_g$ so that the heat transfer to the gas becomes:

$$\left(\frac{q}{A}\right)_{1-g} = \frac{\epsilon_1\bar{\alpha}_{1-g}(1 + r_2\bar{\tau}_{1-g})\sigma(T_1^4 - T_g^4)}{1 - r_1r_2(\bar{\tau}_{1-g})^2} \quad (107)$$

The values of the radiant properties of the two surfaces and the effective absorption of the medium were taken from the literature [1, 7] as: $\epsilon_1 = 0.655$, $r_1 = 0.345$, $\epsilon_2 = 0.560$, $r_2 = 0.440$, $\bar{\alpha}_{1-g} = 0.110$, and $\bar{\tau} = {}_{1-g}0.890$. The net exchange for these conditions was 1090 Btu/hr ft² between the hot surface and the gas.

Equation (107) may be written on the basis of monochromatic energy exchange:

$$\left(\frac{q}{A}\right)_{1-g} = \int_0^\infty \left[\frac{\epsilon_{\nu,1}\bar{\alpha}_{\nu,1-g}(1 + r_{\nu,2}\bar{\tau}_{\nu,1-g})(E_{\nu,1} - W_\nu)}{1 - r_{\nu,1}r_{\nu,2}(\bar{\tau}_{\nu,1-g})^2}\right] d\nu \quad (108)$$

The difficulty of performing this integration has already been discussed in Part 1. However, the band energy approximation may be applied to the original network and the various potentials and radiant properties evaluated over discrete frequency intervals [Fig. 8(*b*)]. The band energy approximation was computed using the band absorption data for carbon dioxide shown in Table 4. The band limits shown in this table are a function of the total pressure and temperature of the gas. For conditions other than those shown, these band limits would have to be adjusted. The availability of these data determined the conditions selected for the present example. Experimental data for carbon dioxide at higher temperatures and pressures are presently being measured and should be published shortly [4].

Utilizing the band energy approximation, the calculated heat transferred from the hot surface to the gas was 670 Btu/hr ft². The result obtained using the gray radiation approximation was 63 per cent greater than this. The result is in agreement with the

qualitative statement given by Hottel [10] to the effect the gray gas assumption will yield heat-transfer rates that are generally larger than the actual ones. An exception to this is the case of an enclosure with completely absorbing (black) walls where the gray assumption does not affect the results. Examination of equation (108) with $e_{\nu,1} = 1$, $r_{\nu,1} = 0$, and $r_{\nu,2} = 0$ will show that under the conditions of "black" surfaces, only the characteristics of the gas are important and these characteristics may be shown to correspond to the measured values reported in the literature [10].

## Discussion and Summary

The procedure for a reiterative or relaxation method for solving a multinode radiation network has been described and a simple example presented. The exact solution, band energy approximation, and gray radiation approximation have been compared for parallel surfaces with no absorbing intervening medium using two different surface combinations. In both cases, the band energy approximation was shown to be more accurate than the gray radiation method. A similar system with carbon dioxide gas as an absorbing medium between the parallel surfaces showed a difference of 63 per cent between the gray and the band energy approximations under the particular conditions selected.

The examples comparing the two methods for approximating the exchange have shown that the band energy method is the more accurate. Physically, this should be the general result, since the actual spectral characteristics of the surfaces are more correctly approximated. The band energy method is more laborious and time consuming and, consequently, will probably be restricted to problems requiring more accurate results than obtainable with the gray radiation assumption. The application will also be limited by the availability of the data required for such computations. However, the significant fact which should be noted is that the inaccuracy of the gray radiation approximation is in the method of analysis. Errors in the data used can be obscured by the errors of the method.

The relaxation method for reducing the solution of the network to a systematic procedure is more generally applied. This procedure is readily adaptable to either digital computers or hand calculation methods. Consequently, the analysis of complicated, multisurface enclosures can be performed with less restrictive limitations on the complexity of the system considered. The problem of matrix algebra, which can be difficult and intricate, is avoided by the relaxation or reiterative method.

## Nomenclature for Part 3

$A$ = area; $A_n$ = area of surface $n$

$E$ = emissive power; $E_{\nu,n}$ = monochromatic emissive power of surface $n$

$F$ = geometrical shape factor (see Part 2); $F_{nm}$ = geometrical shape factor of surface $n$ with respect to surface $m$

$\mathfrak{F}$ = factor relating geometry and radiant characteristics of two surfaces; $\mathfrak{F}_{\nu,1-2}$ = monochromatic value for surface 1 with respect to surface 2; $\mathfrak{F}_{\Delta\nu,1-2}$ = band energy approximation value of $\mathfrak{F}_{\nu,1-2}$ over the frequency interval $\Delta\nu$, equation (104); $\mathfrak{F}_{1-2}$ = value of $\mathfrak{F}_{\nu,1-2}$ integrated over all frequencies, equation (102)

$J$ = radiosity; $J_n$ = radiosity of surface $n$

$M$ = total number of surfaces composing a specific enclosure

$T$ = absolute temperature; $T_n$ = absolute temperature of surface $n$; $T_g$ = absolute temperature of the medium enclosed within the enclosure

$W$ = emissive power of the medium; $W_{\nu,m}$ = monochromatic emissive power of the medium involved in the exchange of energy between surfaces $n$ and $m$

$e$ = emittance of the surface; $e_{\nu,n}$ = monochromatic emittance of surface $n$; $e_n$ = total emittance of surface $n$, equation (76), Part 2

$m$ = number of surfaces composing a general enclosure; for a specific enclosure $m = 1, 2, 3, \ldots M$

$n$ = a specific surface of the enclosure

$q$ = energy flow; $q_{\nu,nm}$ = monochromatic energy flow between surface $n$ and $m$; $q_{nm}$ = total energy flow between surface $n$ and $m$

$t$ = temperature

$\alpha$ = absorptivity of the intervening medium; $\bar{\alpha}_{\nu,nm}$ = geometrical monochromatic absorptivity of the medium between surface $n$ and $m$ (see Part 2)

$\nu$ = frequency; $\Delta\nu$ = frequency interval for the band energy approximation

$\sigma$ = Stefan-Boltzmann constant

$\tau$ = transmissivity of intervening medium; $\bar{\tau}_{\nu,nm}$ = geometrical monochromatic absorptivity of the medium lying between surfaces $n$ and $m$; $\bar{\tau}_{\nu,nm} + \bar{\alpha}_{\nu,nm} = A_n F_{nm}$

## References


1 J. T. Bevans, J. T. Gier, and R. V. Dunkle, "Comparison of Total Emittances With Values Computed From Spectral Measurements," TRANS. ASME, vol. 80, 1958, pp. 1405–1416.

2 D. M. Dennison, *Reviews of Modern Physics*, vol. 3, 1931, pp. 280–345.

3 R. V. Dunkle, "Thermal-Radiation Tables and Applications," TRANS. ASME, vol. 76, 1954, pp. 549–552.

4 D. K. Edwards, PhD thesis, Department of Mechanical Engineering, University of California, Berkeley, Calif.

5 T. Elder and J. Strong, "Infrared Transmission of Atmospheric Windows," *Journal of The Franklin Institute*, vol. 255, 1953, pp. 189–208.

6 W. M. Elsasser, Harvard Meteorological Studies No. 6, Blue Hill Observatory, 1942.

7 S. Goodman, "Radiant-Heat Transfer Between Nongray Parallel Plates," *Journal of Research* (NBS), vol. 58, 1957, pp. 37–40.

8 R. N. Goody, *Quarterly Journal, Royal Meteorological Society*, vol. 78, 1952, p. 165.

9 G. Herzberg, "Molecular Spectra and Molecular Structure," vol. I and II, D. Van Nostrand Company, New York, N. Y., 1950 and 1954.

10 H. C. Hottel, "Heat Transmission," edited by W. H. McAdams, McGraw-Hill Book Company, Inc., New York, N. Y., third edition, chapter 4, 1955.

11 H. C. Hottel and E. S. Cohen, *Journal of the AIChE*, vol. 4, 1957, pp. 3–14.

12 J. N. Howard, D. C. Burch, and D. Williams, *Journal, Optical Society of America*, vol. 46, 1956, pp. 186, 237, 242, 334, 542.

13 M. Jakob, "Heat Transfer," vol. 1, John Wiley & Sons, Inc., New York, N. Y., 1949.

14 H. Jeffreys and B. S. Jeffreys, "Methods of Mathematical Physics," third edition, Cambridge University Press, Cambridge, England, 1956.

15 J. R. Nielsen, V. Thornton, E. B. Dale, "Absorption Laws for Gases in Infrared," *Reviews of Modern Physics*, vol. 16, 1944, p. 307.

16 A. K. Oppenheim, "Radiation Analysis by Network Method," TRANS. ASME, vol. 78, 1956, pp. 725–735.

17 S. S. Penner, *Journal of Applied Physics*, vol. 21, 1950, p. 685; S. S. Penner, "Emissivity Calculation for Diatomic Gases," *Journal of Applied Mechanics*, vol. 18, TRANS. ASME, vol. 73, 1951, pp. 53–58; S. S. Penner and D. Weber, *Journal of Applied Physics*, vol. 22, 1951, p. 1164; S. S. Penner and D. Weber, *Journal of Chemical Physics*, vol. 19, 1951, pp. 807, 1351; M. H. Ostrander and H. S. Tsien, *Journal of Applied Physics*, vol. 23, 1952, p. 250; S. S. Penner, "Emission of Radiation From Diatomic Gases—4," *Journal of Applied Physics*, vol. 23, 1952, pp. 825–837; S. S. Penner and A. Thomson, "Infrared Emissivities and Absorptivities of Gases," *Journal of Applied Physics*, vol. 28, 1957, pp. 614–623.

18 G. N. Plass and E. I. Fivel, *Journal of Meteorology*, vol. 12, 1955, p. 191.

19 H. M. Randall, D. M. Dennison, N. Ginsberg, and L. R. Weber, *Physical Review*, vol. 52, 1937, p. 160.

G. STOLZ, JR.
Senior Research Engineer, Heat and Mass Flow Analyzer Laboratory, Columbia University, New York, N. Y.

# Numerical Solutions to an Inverse Problem of Heat Conduction for Simple Shapes

*Numerical methods are presented for solving an inverse problem of heat conduction: Given an interior temperature versus time, find the surface heat flux versus time. The analysis is developed specifically for spheres; it applies to other simple shapes.*

*The system is treated as linear, permitting use of the superposition principle. The essence of the method is the numerical inversion of a suitable direct problem: Given a surface heat flux versus time, find an interior temperature versus time.*

*Care is required in selecting a time spacing for, if it is chosen too small in relation to the conditions, undesirable oscillation results.*

*Simplifying suggestions are presented, and the use of the methods are illustrated by examples.*

## Introduction

An inverse problem of transient heat conduction arises whenever a boundary condition such as surface heat flux versus time is sought from a knowledge of an interior condition such as temperature versus time. Such an inverse problem occurred as part of the co-operative Quenching Program [1, 2][1] at Columbia University, where obtaining heat flux and surface temperature data was one of the purposes of a number of experiments in which temperatures were measured inside a body being cooled.

In contrast with the inverse problem, the direct problem of transient heat conduction is relatively straightforward; in a direct problem the boundary conditions are known and the interior temperature is sought. Many cases appear in the literature [3]. To the author's knowledge no general treatment of the inverse problem has been given. For solving of the inverse problem a number of approximate procedures exist; some are:

(*a*) Trial and error, including electrical analog.

(*b*) Simplifying assumptions, when tenable, whereby the inverse problem becomes a direct one.

(*c*) Numerical inversion of a suitable direct problem.

[1] Numbers in brackets designate References at end of paper.

Contributed by the Heat Transfer Division and presented at the Semi-Annual Meeting, St. Louis, Mo., June 14–18, 1959, of The American Society of Mechanical Engineers.

Note: Statements and opinions advanced in papers are to be understood as individual expressions of their authors and not those of the Society. Manuscript received at ASME Headquarters, March 19, 1959. Paper No. 59—SA-20.

All three procedures have been used by the author. An electrical analog computer method (*a*) was abandoned because instrumentation problems delayed the work. A graphical procedure, based on a simplifying assumption (*b*) is in current use; it appears in the Appendix. The numerical inversion method (*c*) described in this paper has been in use since June, 1957 [4].

Several publications dealing with special simple methods (*b*) have appeared, many without mention of the restrictions implied. The first published use of a numerical inversion (*c*) seems to be in the recent paper of Mirsepassi [5], who presented charts for use with semi-infinite bodies. The inverse problem is dealt with as an illustration of graphical procedures, without mention of its derivation or possible limitations. These important questions are explored here in the development of a numerical procedure applicable to simple finite bodies.

Whatever method is used, the solution will suffer from an inherent uncertainty. In a heat-conduction system the effect of boundary conditions is always damped at interior points, and the inverse problem involves basically the extrapolation of the damped datum to the surface, and sometimes differentiation at the surface. The damped information cannot be completely recovered, but, as will be shown, this need not constitute a handicap.

**Statement of the Problem.** For simplicity the heat-conduction system will be treated as linear with the consequent advantages of the superposition principle. Constant physical properties and no internal heat generation will be assumed. While the development presented specifically applies to spheres, it can be easily extended to slabs and cylinders.

## Nomenclature

$A$ = area, sq ft
$c$ = specific heat, Btu/(lb)(deg F)
$F$ = response function, defined by equation (13)
$g$ = a constant, defined by equation (16)
$h$ = boundary conductance, Btu/hr, sq ft
$H$ = heat content, Btu
$j$ = index of series
$k$ = thermal conductivity, Btu/(hr)(ft)(deg F)
$N_{Bi}$ = Biot number = $hR/k$
$P$ = a function defined by equation (13)
$Q$ = total heat flow, Btu
$R$ = outer radius of sphere, ft
$r$ = distance from center, ft
$r_1, r_2$ = particular values of $r$
$T$ = a function defined by equation (13)
$u$ = unit step function
$V$ = volume, cu ft
$x_\nu$ = root of transcendental equation (12)
$Z$ = a constant = $\rho cV/A$, Btu/sq ft
$\alpha$ = thermal diffusivity, sq ft/hr
$\delta$ = difference operator
$\theta$ = temperature, deg F
$\lambda$ = time spacing, hr or sec
$\nu$ = index of series
$\rho$ = density, lb/cu ft
$\tau$ = time, hr or sec
$\phi$ = heat flux out of solid, Btu/(hr)(sq ft)
$\nabla^2$ = Laplacian operator

If the temperature of the body is initially uniform, and the temperature $\theta(r_1, \tau)$ at some interior point $r_1$ as a function of time is known, the statement of the inverse problem becomes

$$\alpha\nabla^2\theta(r, \tau) - \frac{\partial\theta}{\partial\tau}(r, \tau) = 0; \quad 0 \leq r < R \tag{1}$$

$$\frac{\partial}{\partial r}\theta(0, \tau) = 0 \tag{2}$$

$$\theta(r, 0) = \theta_i, \text{ constant} \tag{3}$$

$$\theta(r_1, \tau) = f(\tau); \quad 0 \leq r_1 < R \tag{4}$$

We seek the surface heat flux and surface temperature, $\phi(\tau) = -k\partial\theta(R, \tau)/\partial r$ and $\theta(R, \tau)$. Note that, if either of these is found, the other is readily established, and the two results may be combined as $\phi[\theta(R)]$.

To facilitate the solution of the problem set forth in equations (1) to (4), we consider first a related direct problem set up in such a way that it may be easily inverted.

## A Direct Problem

Suppose that equation (4) is replaced by equation (4*a*) which states: Instead of the interior temperature $\theta(r_1, \tau)$ being known, the heat flux $\phi(\tau)$ is known. Now $\theta(r, \tau)$ is sought.

$$-k\frac{\partial\theta(R, \tau)}{\partial r} = \phi(\tau) \tag{4a}$$

We can subdivide $\phi(\tau)$ into elements as follows:

$$\phi(\tau) = \sum_{j=0}^{n}\phi_j(\tau) \tag{5}$$

An element of temperature $\theta_j(r, \tau)$ corresponding to each $\phi_j(\tau)$ may be found by any convenient method—analytical, finite difference, electrical analog, or direct experiment. The desired temperature is composed from its elements

$$\theta(r, \tau) = \sum_{j=0}^{n}\theta_j(r, \tau) \tag{6}$$

More generally, if $F(r, \tau)/z$ is the solution of equations (1), (2), (3), and (4*a*) with $\phi(\tau) = -1$ and $\theta_i = 0$, then from Duhamel's theorem or the convolution theorem the solution of (1), (2), (3), and (4*a*) as written, i. e., with $\phi(\tau)$ arbitrary, is given by

$$[\theta_i - \theta(r, \tau)]Z = \frac{d}{d\tau}\int_0^\tau \phi(\tau - \tau')F(r, \tau')d\tau' = \int_0^\tau \phi(\mu)\frac{\partial}{\partial\tau}F(r, \tau - \mu)d\mu \tag{7}$$

For convenience the elements of heat flux $\phi_j(\tau)$ in equation (5) were chosen as steps $\delta\phi(j\lambda)$ at equal time intervals $\lambda$ and persisting thereafter; the argument denotes the time at which the increment in heat flux starts.

Thus

$$= n\lambda \tag{8}$$

and

$$\phi(\tau) = \phi(n\lambda) = \sum_{j=0}^{n}\delta\phi(j\lambda) \tag{9}$$[2]

[2] A more conventional but also more cumbersome notation would be $\phi(n\lambda) = \sum_{j=0}^{n} u[\tau - j\lambda]\delta\phi(j\lambda)$ where $u(\tau)$ is the unit step function.

Other heat flux elements were tried—straight lines, exponentials—but showed less desirable properties.

In performing the subdivision of equation (9) a good approximation results if a heat balance is realized at each step:

$$(1/A)Q(n\lambda) = \int_0^{n\lambda}\phi(\tau)d\tau = \lambda\sum_{j=0}^{n-1}\phi(j\lambda) \tag{10}$$

The temperature response to the step $\delta\phi(0)$ is for a sphere

$$\frac{[\theta_i - \theta(r, \tau)]Z}{\delta\phi(0)} = \tau + \frac{R^2}{\alpha}\left[\frac{1}{6}\left(\frac{r}{R}\right)^2 - \frac{1}{10}\right] - \frac{2}{3}\sum_{\nu=1}^{\infty}\frac{\sin(x_\nu r/R)}{(r/R)\sin x_\nu}\cdot\frac{\exp[-x_\nu^2\alpha\tau/R^2]}{x_\nu^2\alpha/R^2} \tag{11}$$

where $x_\nu$ is the $\nu$th positive root of the equation

$$x_\nu\cot x_\nu - 1 = 0 \tag{12}$$

The general form of equation (11) can be abbreviated

$$F(r, \tau) = \tau + P(r) + T(r, \tau) \tag{13}$$

where the "steady state" part is $\tau + P(r)$; the "transient" part, $T(r, \tau)$ becomes negligible after a short time.

The behavior of other simple shapes is similar. The response to a step in heat flux for a cylinder [6] and a slab [7] can be put in the form of equation (13).

Note that $\theta_i - \theta(r, \tau)$ in equation (11) is always proportional to $\delta\phi(0)$ whether the latter be positive or negative. Further, if the step in heat flux is shifted in time, the corresponding temperature is shifted in time by the same amount. Therefore, corresponding to any single increment of heat flux $\delta\phi(j\lambda)$ there is a temperature change at time $n\lambda$, given by

$$\theta_i - \theta(r, n\lambda) = \frac{1}{Z}\delta\phi(j\lambda)F[r, (n - j)\lambda] \tag{14}$$

The total temperature becomes, corresponding to equation (6)

$$\theta_i - \theta(r, n\lambda) = \frac{1}{Z}\sum_{j=0}^{n}\delta\phi(j\lambda)F[r, (n - j)\lambda] \tag{15}$$

This could be regarded as a finite difference form of equation (7).

A graphical illustration of the use of equation (15) appears in Fig. 1. The given heat flux, Fig. 1(*a*), is subdivided into elements, Fig. 1(*b*), and the corresponding temperature elements, Fig. 1(*c*), are summed to yield the total temperature, Fig. 1(*d*).

The evaluation of equation (15) is easily programmed either for a desk calculator or a digital computer. The response function $F$ need be obtained only once for each value of $r$. Since the arguments of the terms $\delta\phi$ and $F$ increase in reverse order, for desk calculation the functions are tabulated in reverse order and the sum obtained by accumulative multiplication. For a different value of $n\lambda$ the tables are shifted accordingly.

An interesting graphical procedure for the evaluation of equations of this type has been proposed by Mirsepassi [5].

Two additional shortcuts may speed the processing:

The transient part of the response function in equation (13) becomes negligible after a certain time $g\lambda$, called a long time in this context. For practical calculations $g\lambda$ would be given by

$$\alpha g\lambda/R^2 = 0.2 \tag{16}$$

If the times of the calculation exceed $g\lambda$, we split the summation in equation (15) into two parts, from $j = 0$ to $j = n - g$ and from $j = n - g + 1$ to $j = n$. In the first term $F[r, (n - j)\lambda]$ will contain only the steady-state part. Substitution of equations

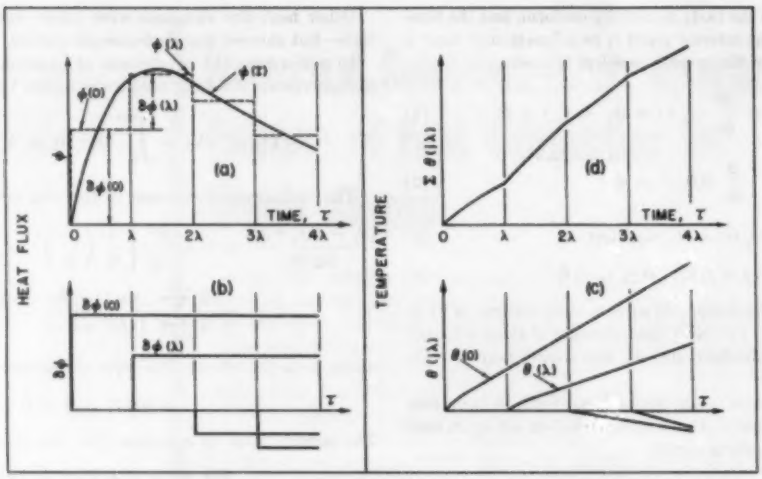


**Fig. 1 Graphical interpretation of superposition principle in equations (15) and (18); (a) total heat flux, (b) heat flux elements, (c) temperature elements, (d) total temperature**

(9) and (10) and rearrangement yields in place of equation (15)

$$\theta_i - \theta(r, n\lambda) = \frac{1}{Z}\left\{\frac{1}{A}\,Q[(n-g)\lambda] + F(r, g\lambda)\phi[(n-g)\lambda]\right\} + \frac{1}{Z}\sum_{j=n-g+1}^{n}\delta\phi(j\lambda)F[r,(n-j)\lambda] \quad (17)$$

A large number of terms have been replaced by two.

In some portions of the problem a time spacing coarser than $\lambda$ may save effort. This is done without altering the procedure by choosing integral multiples of $\lambda$ and setting the heat flux increments equal to zero at those times not of interest; then slight modification of equation (15) is needed.

No limitation need be put on the time spacing since a direct problem is involved. Smaller time spacing increases accuracy but may cost more.

In the next section, where the direct problem will be inverted, numerical considerations will set a lower limit on $\lambda$, in part dependent on the location of point $r_1$.

## Numerical Inversion of the Direct Problem

Returning to the main problem stated in equations (1) to (4), examination of equation (15) suggests a solution. Where in (15) $\theta(r, n\lambda)$ was the only unknown, now all of the values of $\delta\phi(j\lambda)$ are needed. After noting that $F(r, 0) = 0$, rearrangement yields

$$\delta\phi[(n-1)\lambda] = \left\{-\sum_{j=0}^{n-2}\delta\phi(j\lambda)F[r,(n-j)\lambda] + Z[\theta_i - \theta(r, n\lambda)]\right\}\Big/F(r, \lambda) \quad (18)$$

As any value of $\delta\phi(n\lambda)$ depends on all the previous heat flux increments, the solution has to be generated step-by-step from time zero.

Fig. 1 may be consulted for graphical interpretation. The information at hand is 1($d$), a measured temperature-time curve known at integral multiples of $\lambda$. We would like to subdivide it into components as shown in 1($c$), each of which will be a response to the heat flux increments 1($b$), which in turn can be summed to give the total heat flux 1($a$).

Now at the end of the first time interval $\lambda$ a temperature change $\theta_i - \theta(r, \lambda)$ has been observed. If it is agreed that a step change in heat flux occurring at time zero, $\delta\phi(0)$, caused this temperature change, then $\delta\phi(0)$ has the value:

$$\delta\phi(0) = Z[\theta_i - \theta(r, \lambda)]/F(r, \lambda) \quad (19)$$

At time $2\lambda$, $\delta\phi(0)$ would produce a temperature change given by $\delta\phi(0)F(r, 2\lambda)/Z$; it differs from the observed value, $\theta_i - \theta(r, 2\lambda)$. To account for the difference a new heat flux increment is started at time $\lambda$, which in the time from $\lambda$ to $2\lambda$ can produce the temperature change $[\theta_i - \theta(r, 2\lambda)] - \delta\phi(0)F(r, 2\lambda)/Z$. $\delta\phi(\lambda)$ becomes

$$\delta\phi(\lambda) = \{Z[\theta_i - \theta(r, 2\lambda)] - \delta\phi(0)F(r, 2\lambda)\}/F(r, \lambda) \quad (20)$$

In this way the entire heat flux time curve can be generated. Equation (18) might have been obtained by induction by continuing as in (19) and (20).

**Limitations of the Inverse Method.** As pointed out in the introduction, the calculation is based on truncated data which have been damped. Questions of the effect of experimental errors are considered separately and will be dealt with in the following. Improper selection of $\lambda$—too small for a given set of conditions—will lead to an undesirable oscillation. The oscillation shows up as an error which alternates in sign and may keep increasing in magnitude at each step. Even if oscillation is avoided, the solution will be approximate (determined within a certain range) as will be illustrated.

The oscillation stems from the character of the system. It will be recalled that heat conduction systems exhibit damping, i.e., at interior points the effect of any surface disturbance is delayed and diminished. Thus the effect of a heat flux change occurring at time $(n-1)\lambda$ may be undetected in the data at time $n\lambda$, if $\lambda$ is too small, and the calculation yields zero change in heat flux. In calculating the next heat flux element, the error is compensated, overcompensated if $\lambda$ is too small. Thus in succeeding times the error oscillates.

Whether the oscillation can become unbounded (unstable) and under what general conditions is not known at present. Regardless, it may become much larger in amplitude than the correct result; in such a case the answer is useless.

A general criterion for the optimum value of $\lambda$, or more generally $\alpha\lambda/R^2$, as a function of $r/R$ is under investigation. Usually

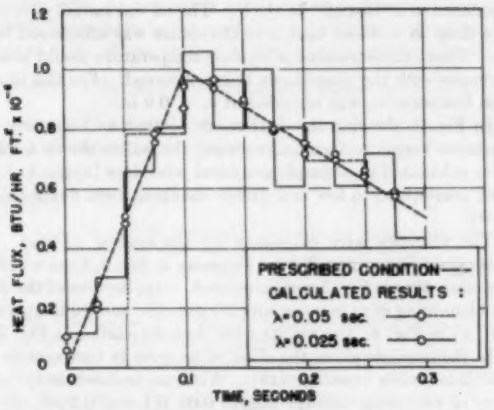


**Fig. 2 Results of performance test using equation (18) compared with exact result. Two different time spacings.**

a few trials will establish the optimum. As might be expected from the foregoing, the smaller the value of $r_1$, the larger $\lambda$ needs to be. Empirical results seem to show that $\lambda_{opt}$ is at or near the inflection point in the response function $F(r, \tau)$.

Oscillation may sometimes be reduced when the choice of $\lambda$ is not open, by proceeding stepwise in space. I.e., consider $r_2$—$R > r_2 > r_1$—to be a surface, the "boundary condition" found there becomes the datum for the second step, etc. But such bootstrap procedures do not improve the accuracy of the result sufficiently to warrant the effort.

The arbitrary choice of heat flux element as a step and time spacing $\lambda$ leads to a particular answer. A somewhat different answer would be obtained from a different choice. Fig. 2 shows the result of a performance test. The particular conditions represent a 1.0-in. radius silver sphere ($k$ = 207 Btu/(hr)(ft)(deg F), $\alpha$ = 5.33 sq ft/hr) subjected to the rather severe prescribed heat flux denoted by the dotted line. The temperatures at $r$ = 0.90 in. were obtained analytically and became the statement of the problem. Two different time spacings, $\lambda$ = 0.025 sec, $\lambda$ = 0.05 sec, were used to calculate the heat flux, which is plotted. The smoothed end results agree fairly well with the prescribed condition; the worst discrepancies occur at zero time and at the peak heat flux. It is shown that the results do differ somewhat. Further, for the shorter time spacing an oscillation is seen.

The effect of a single experimental error in a particular set of circumstances is readily determined by use of equation (18). Since the system is linear, the effect may be found directly after specifying a particular error by carrying out the operations indicated. Again the magnitude of the error depends on the choice of conditions. It diminishes as the location $r_1$ nears the surface.

The foregoing all points to one conclusion: When the choice of the location of the temperature probe is free, all other factors being equal, the best place to probe is close to the surface.

**Practical Details.** Some suggestions as to procedure have been presented in the section Direct Problem. The use of variable time spacing and the shortcut for long time—equation (17)—apply directly to equation (18).

The final heat flux, in the form of steps, may be smoothed by invoking a heat balance, equation (10). The smoothed values become the mid-points of the vertical segments; for more detail the mid-points of the horizontal segments may also be used.

An entire problem need not be handled by the inverse method if a simpler method can be applied. As the foregoing treatment implies an initial condition of uniform temperature (and zero heat flux initially), a minor revision is required:

According to equation (13) the response to a stationary or slowly changing heat flux becomes linear in time after a time $g\lambda$ given in (16). When the region of interest is preceded by a sufficiently long period of approximately constant cooling rate, the constant heat flux value that would produce this behavior is introduced to start the calculation. In this way the correct temperature profile is established. Since the inverse method deals with changes in temperature, such a procedure is possible and permits the calculation to be started at a suitable time other than zero.

**Illustrative Example.** For a specific application of the methods presented a quenching experiment is selected. The experiments themselves appear elsewhere [8]. A silver sphere, 1.0-in. radius, surface roughness 140 microinches, was heated to 1600 F and

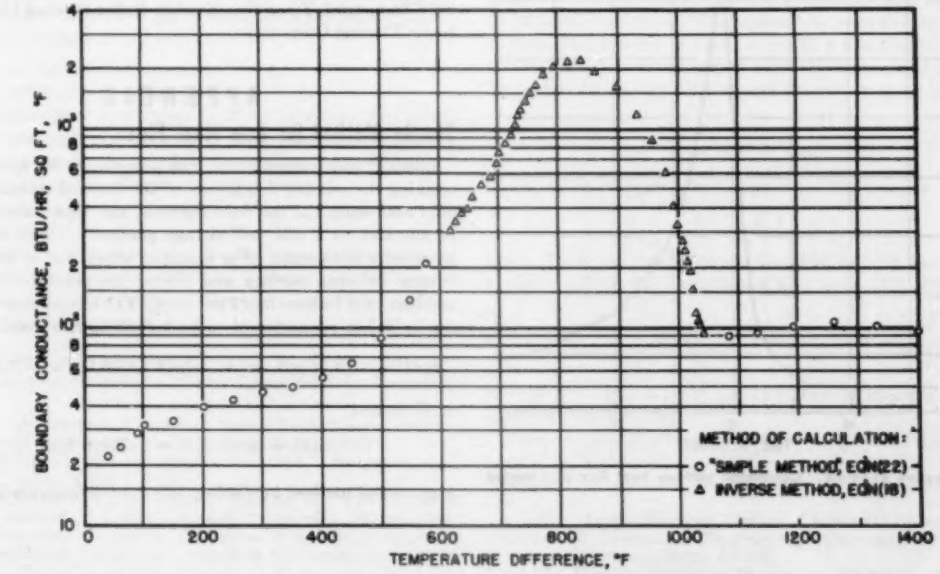
BOUNDARY CONDUCTANCE, BTU/HR, SQ FT, °F
TEMPERATURE DIFFERENCE, °F
METHOD OF CALCULATION:
○ "SIMPLE METHOD", EQN(22)
△ INVERSE METHOD, EQN(18)

**Fig. 3 Illustrative example. Boundary conductance versus surface temperature resulting from experimental cooling curve in Fig. 4.**

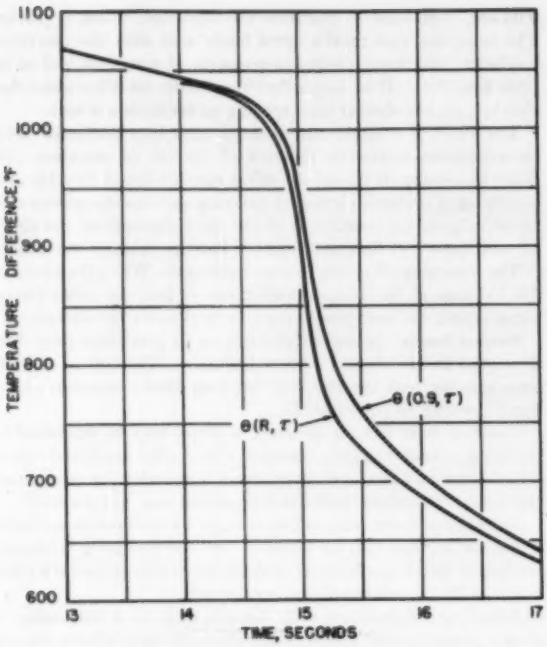


Fig. 4 Illustrative example. Experimentally measured interior temperature $\theta(0.9, \tau)$ and calculated surface temperature $\theta(R, \tau)$ versus time.

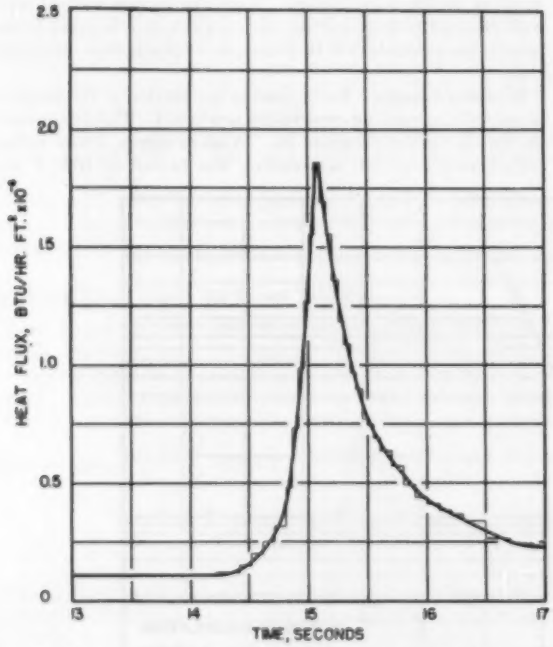


Fig. 5 Illustrative example. Calculated surface heat flux $\phi(\tau)$ versus time.

quenched in a "fast oil" at 110 F. The oil was initially quiescent in a deep 38 × 31-in. tank, and the sphere was submerged by 2.5 in. Direct measurement of surface temperature would interfere seriously with the phenomena being observed. For this illustration temperature was recorded at $r_1 = 0.9$ in.

In Fig. 3, showing the final result plotted as boundary conductance versus surface temperature, the points shown as circles were calculated by a simple graphical procedure (appendix) since they correspond to low and slowly changing heat fluxes ($N_{Bi} \leq 0.04$).

The triangles were calculated by the inverse method. The measured temperature $\theta(0.9, \tau)$ appears in Fig. 4, from which the heat flux $\phi(\tau)$ in Fig. 5 was calculated. Application of the direct problem using $\phi(\tau)$ in equation (15) gave the surface temperature $\theta(R, \tau)$ in Fig. 4; the results were then correlated as Fig. 3.

In the example given the effect of an error in temperature was calculated with equation (18). With an isolated temperature error of 1 F, using time spacings of 0.05, 0.1, and 0.2 sec, the corresponding maximum errors in heat flux, in millions of Btu/hr sq ft are 0.050, 0.024, and 0.013.

A complete calculation as illustrated requires approximately two man-days using a desk calculator. It is estimated that the use of a digital computer such as IBM 650 would replace one day by a few minutes.

## Acknowledgment

This work was performed at the Heat and Mass Flow Analyzer Laboratory at Columbia University; the following named individuals are present or past members of the laboratory. Dr. H. G. Landau generously gave advice at many stages of the investigation. He was also responsible for some of the mathematical developments. Mr. J. L. Sullivan performed much of the numerical work, aided by Mr. F. Ruf and Mrs. A. Heller. The author is indebted to Prof. V. Paschkis and Prof. C. F. Bonilla for their encouragement and patience, particularly during the early phases of the work. Grateful acknowledgment is made for the support of the following organizations: Caterpillar Tractor Co., Chrysler Corp., Curtiss-Wright Corp., Engineering Foundation, Frankford Arsenal, General Electric Co., Gulf Research & Development Co., Ladish Co., Libbey-Owens-Ford Glass Co., SKF Industries, Texas Co., Timken Roller Bearing Co., Westinghouse Electric Corporation.

# APPENDIX

## Simple Method for Low Heat Flux

Considerable computation can sometimes be spared by examining the relative magnitude of the thermal resistances of the fluid and solid. If the fluid controls, the Biot number $N_{Bi}$ will be low and, as a rule, will change gradually. The body will be practically isothermal. For example, when $N_{Bi} = 0.04$, the difference between surface and center temperature (referred to ambient) will be less than 2 per cent. The temperature, now $\theta(\tau)$, can be taken proportional to heat content $H(\tau)$ and

$$\phi(\tau) = -(1/A)dH/d\tau = -(\rho cV/A)d\theta/dt = -Zd\theta/d\tau \quad (21)$$

or, if desired,

$$h(\tau) = \phi(\tau)/\theta(\tau) = -Zd \ln \theta/d\tau \quad (22)$$

A graphical method for finding the time derivatives is described

by Hartree [9]. It consists of plotting $\theta$ or ln $\theta$ versus time and obtaining the normals to the curve using a straight edge with a reflecting surface. 98 per cent of the data recorded by the author can be processed in this way. It can be used whenever $\left|\frac{d\ln\theta}{d\tau}\right| < \frac{0.4k}{ZR}$ with accuracy of usually 1 per cent, and at somewhat more rapid cooling with decreasing accuracy.

## References


1 V. Paschkis and G. Stolz, Jr., "Quenching as a Heat-Transfer Problem," *Journal of Metals*, vol. 8, 1956, pp. 1074–1075.

2 V. Paschkis and G. Stolz, Jr., "How Measurements Lead to Effective Quenching," *Iron Age*, vol. 178, no. 21, Nov. 22, 1956, pp. 95–97.

3 H. S. Carslaw and J. C. Jaeger, "Conduction of Heat in Solids," Oxford University Press, London, England, 1947.

4 G. Stolz, Jr., C. F. Bonilla, and V. Paschkis, "Numerical Evaluation Techniques," Columbia University, Heat and Mass Flow Analyzer Laboratory, Quenching Program, Technical Report No. 5, November, 1957, No. CU-67-57-ORD-1621.

5 T. J. Mirsepassi, "Heat Transfer Charts for Time Variable Boundary Conditions—Part I: Semi-Infinite Solid," ASME Paper No. 58—SA-7.

6 Reference [3], p. 275.

7 A. B. Newman, "The Temperature-Time Relations Resulting From Electrical Heating of the Face of a Slab," *Trans. AIChE*, vol. 30, 1934, pp. 598–613.

8 G. Stolz, Jr., V. Paschkis, C. F. Bonilla, and G. Acevedo, "Thermal Considerations in Oil Quenching," to be published in *Journal of the Iron and Steel Institute*.

9 D. R. Hartree, "Numerical Analysis," Oxford University Press, London, England, 1952.


# DISCUSSION

## T. J. Mirsepassi[3]

The author is to be congratulated for his interesting presentation and useful study of an important problem of heat conduction.

On numerous occasions during recent years we have used this technique both numerically[4,5] and graphically[5,6] and have found it, quite in agreement with the author, a fast and accurate method especially adaptable to digital computers. Some cases were also calculated by the well-known arithmetic method of Schmidt. It was observed that the finite difference form of Duhamel's integral,[7] having the following advantages over the Schmidt method, is far better-suited for engineering applications:

1 Simplicity of calculation scheme.

2 Fewer arithmetical operations.

3 Independence of operations in direct problems, i.e., possibility of calculating temperature at a point inside the solid at any time without necessity to calculate for previous time intervals.

4 Lower probability of errors in calculation.

5 Errors, being local, are detected readily by comparison with the adjacent results.

6 Adaptability to desk calculators; i.e., the operator can carry out accumulative multiplications and register the final result only, while in Schmidt's method a large number of intermediate calculation must be registered.

The technique is by no means limited to simple shapes.[4,5,6] The temperature at the point of interest for an arbitrary boundary function can be readily calculated in an irregular configuration, provided that the temperature history at that point is known when the surface (or the ambient) temperature undergoes a step change. Since such problems are customarily solved by an analog computer, this technique results in (*a*) considerable saving of analog computer time, and (*b*) the possibility of solving response problems when the analog computer is no longer available.

[3] Director of Research Computer, Space Technology Division, Aerojet-General Corporation, Azusa, Calif. Mem. ASME.

[4] T. J. Mirsepassi, "Special Report No. 1375," Aerojet-General Corporation, Azusa, Calif.

[5] T. J. Mirsepassi, "Heat-Transfer Charts for Time-Variable Boundary Conditions," *British Chemical Engineering*, March, 1959.

[6] T. J. Mirsepassi, "Graphical Evaluation of a Convolution Integral," Mathematical Tables and Other Aids to Computation, July, 1959.

Equation (2),[3] equations (3) and (4),[4] and equation (3).[5]

## E. M. Sparrow[8]

Evidence attesting to the interest in the inverse problem of heat conduction may be found in an earlier publication on this subject entitled, "A Method for the Experimental Study of the Process of Heating a Solid Body," by N. V. Shumakov.[9] The problem which is posed there is the same one as is considered in the present paper, namely, to find the heat-transfer rate at the surface from unsteady temperature measurements in the interior. The technique used in the earlier paper is called The Method of Successive Intervals, and it is applied to the heat flow in a slab. Experimental temperature measurements are made, and these are used in conjunction with the analytical method to predict the surface heat transfer.

It would be interesting if the author would compare his approach with that of the earlier paper, pointing out the advantages or disadvantages of each. Also, it might be useful for him to apply his method to the slab to see if his surface heat-transfer predictions are consistent with those computed by Shumakov.

## Author's Closure

The interesting and valuable comments by the discussers are sincerely appreciated.

The Shumakov paper cited by Dr. Sparrow escaped attention until shortly before the oral presentation. The author is pleased to elaborate his verbal remarks.

Shumakov limits his treatment to a minimum dimensionless time spacing or Fourier number, $N_{Fo}{}^{*}$, of 0.5. For such long times the transient part of the response function $F(r, \tau)$ in equation (13) becomes negligible, and the remaining steady state part becomes linear in time. The author feels that an $N_{Fo}{}^{*}$ of 0.5 is too conservative; 0.3 is a safe limit, and in many cases 0.2 is satisfactory. Such a restriction does not apply to the present treatment. The author has been able to use dimensionless time spacing as small as 0.002, a hundred times shorter.

Equation (17) of this paper is readily specialized to yield the Shumakov treatment. We choose the time spacing long enough, i.e.,

$$\alpha\lambda/R^2 \geq N_{Fo}{}^{*} \tag{23}$$

which, when compared with equation (16), permits us to put

$$g = 1 \tag{24}$$

Using this in (17) and noticing that $F(r, 0) = 0$, the summation vanishes. With the definition of $Q(n\lambda)$ in (10) one obtains:

$$Z[\theta_L, -\theta(r, n\lambda)] = \phi[(n-1)\lambda]F(r, \lambda) + \lambda \sum_{j=0}^{n-2} \phi(j\lambda) \tag{25}$$

Except for differences of notation this is identical with Shumakov's equation (23).

Since the treatment is the same for "long times," Dr. Sparrow's suggestion to redo the Shumakov calculation was not followed, as identical results should be obtained. However, a much simpler

[8] NASA, Lewis Research Center, Cleveland, Ohio; at present Professor of Mechanical Engineering, University of Minnesota, Minneapolis. Assoc. Mem. ASME.

[9] Soviet Physics—Technical Physics (translated by American Institute of Physics), vol. 2, 1957, p. 771.

calculation is possible. If Shumakov's temperature-time data are replotted on semilog co-ordinates, one obtains very nearly a straight line, indicating a constant Biot number, $N_{Bi} \cong 0.42$. The corresponding heat flux versus time relation is within 10 per cent of the Shumakov prediction.

A more instructive comparison would perhaps be obtained by attempting to recalculate the results of Figs. 2 and 4 of this paper by the Shumakov technique. In the examples used, a Fourier number of 0.5 corresponds to a time spacing of 2.4 seconds. Thus the calculation leading to Fig. 2, which spans only 0.3 seconds, could not be done. Turning to Fig. 5, based on Fig. 4, we choose for convenience $\lambda = 2.5$ seconds and extrapolate the curves back by one second, permitting two time steps from 12 to 17 seconds. We obtain for the first time step a heat flux of 0.098 $\times 10^6$ Btu/hr, ft$^2$, quite close to the correct value. From 14.5 to 17 seconds the result is 0.57, a correct average value, but the essential feature of the physical process has been lost.

The pertinent comments of Dr. Mirsepassi, based on his experience with similar problems, are a welcome addition to the paper. Especially interesting is his suggestion that the techniques described can be applied not only to simple shapes, but to irregular configurations as well. One qualification appears warranted. The pertinent boundary condition—heat flux or surface temperature—must be expressed as a product of two functions, one of position alone, the other of time alone, e.g.,

$$\theta \text{ or } \frac{\partial \theta}{\partial n} = f(x, y, z, \tau) = f_1(x, y, z) f_2(\tau) \qquad \text{on } S \qquad (26)$$

where $\partial/\partial n$ indicates differentiation in the direction of the normal to the surface. In such a case Duhamel's theorem[10] leads to a convolution integral, in the usual sense, as in equation (7). There Dr. Mirsepassi's suggestion would apply. If, however, the boundary condition is not separable as in (26), the resulting form of Duhamel's theorem would not readily lend itself to this type of approximation.

It is of interest that in attacking the inverse problem, where heat flux was sought, neither Dr. Mirsepassi, using his graphical technique on a semi-infinite geometry, nor Shumakov encountered the numerical oscillation reported by the present author. For the long times used by Sumakov, one would not expect oscillations. It is possible that a semi-infinite body, where the response function has a different form, would not behave the same as the finite geometries considered in this paper.

In reply to some questions about alternate formulations for the inverse problem: More elaborate approximations to either the unknown function or the entire integrand in equation (7) are possible. The Laplace transform of the same equation could be inverted numerically. When $\phi(\tau)$ is the unknown, equation (7) is classed as a Volterra integral equation of the first kind. For a similar integral equation Hilderbrand[11] presents a least squares technique which ought to be of value in reducing numerical oscillation. The present approach is recommended by its relative simplicity, as Dr. Mirsepassi has also noted. Even simpler methods such as an extension of the analysis recently presented by Elrod[12] are worth while whenever they apply.

[10] Reference [3], pp. 21–22.

[11] F. B. Hilderbrand, "Methods of Applied Mathematics," Prentice-Hall, New York, N. Y., 1952, pp. 452–459.

[12] H. G. Elrod, "Improved Lumped Parameter Method for Transient Heat-Conduction Calculations," ASME paper No. 59—HT-28.

# Effect of Thermocouple Cavity on Heat Sink Temperature[1]

**JAMES V. BECK**
Associate Scientist

**H. HURWICZ**
Senior Staff Scientist
Research and Advanced Development Division, AVCO Corporation, Wilmington, Mass. Assoc. Mem. ASME

*An analysis is made of problems associated with prediction of and correction for temperature disturbance created by thermocouples placed beneath a surface of a heat sink (or calorimeter) exposed to heat flux during re-entry. Two of the important factors affecting temperature measurement are discussed:*

*(a) The disturbance created by the thermocouple itself, "hot spot."*

*(b) The fact that the thermocouple has to be placed at some distance from the heat flux surface and thus not measuring the surface temperature.*

*The magnitude of the surface hot spot caused by the presence of the thermocouple is determined, and optimum location of the thermocouple is found where the undisturbed surface temperature may be read with least over-all error.*

## Introduction

THE FLIGHT TEST EVALUATION of a re-entry vehicle performance requires the determination of the aerodynamic heating at the heat sink surface. Thermocouples may be placed near the surface of the heat sink to obtain a temperature history which then may be used to find the surface heat fluxes caused by aerodynamic heating. This analysis is concerned with the case in which the thermocouples possess a much lower conductivity than the surrounding heat sink; a valid approximation (which gives the maximum temperature disturbance) is to replace the thermocouples with an insulated cylindrical void. The thermocouple void would disturb the normally one-dimensional heat flow and in so doing would increase the surrounding temperatures. The surface heat flux determination would be affected by the increased thermocouple temperatures and also by the fact that the thermocouple has to be placed at some distance from the heat flux surface. Several analyses of these effects are presented to cover the geometries of interest. The results may be applied to produce more accurately the experimental data which are to be used to calculate heating rates.

The thermal effect of a void or an imperfection near the heat sink surface would be obtained from the same boundary conditions. The presence of the void would result in a hot spot at the surface of the heat sink. Though the results are for a cylindrical void which extends from just under the surface to the rear of the heat sink, they may be used as the (close) upper bound of the effect of a void which does not possess such a large depth. The determination of the magnitude of the surface hot spots due to voids may be used to formulate heat sink material fabrication specifications and to indicate permissible distribution and size of imperfections, voids, and occlusions near a heat sink surface.

[1] This work was performed under AF Contract AF-04(645)-30.

Contributed by the Heat Transfer Division of THE AMERICAN SOCIETY OF MECHANICAL ENGINEERS and presented at the ASME-AIChE Heat Transfer Conference, Storrs, Conn., August 9–12, 1959.

NOTE: Statements and opinions advanced in papers are to be understood as individual expressions of their authors and not those of the Society. Manuscript received at ASME Headquarters, May 25, 1959. Paper No. 59—HT-20.

## Discussion

A thermocouple embedded in a heat sink, which has a much higher conductivity than the thermocouple, disturbs the surrounding temperatures. The maximum temperature disturbance would be caused by replacing the thermocouple with an insulated cylindrical void placed just inside the heat sink and perpendicular to the heat sink surface, Fig. 1(*a*).

The effect of the assumption in which the thermocouple is replaced by a void is assessed at the end of this paper. Until the discussion of this assumption the thermocouple effect and void effect may be considered identical and a reference to an "upper bound" or "lower bound" will be considered in relation to whether the effect is respectively greater or smaller than the void effect. The upper or lower bounds would be caused by boundary conditions which approximate the disturbance caused by the void.

The boundary conditions [see Fig. 1(*a*)] for the insulated cylindrical void problem are

$$1)\quad k\frac{\partial T(0,r,t)}{\partial z} = -\phi(t)$$

$$2)\quad \frac{\partial T(L,r,t)}{\partial z} = 0 \qquad (r > R)$$

$$3)\quad \frac{\partial T(z,R,t)}{\partial r} = 0 \qquad (E < z < L)$$

$$4)\quad \frac{\partial T(E,r,t)}{\partial z} = 0 \qquad (0 < r < R)$$

$$5)\quad T(z,r,0) = 0$$

## Nomenclature

$E$ = distance of thermocouple tip below sink surface

$g = R/E$ = dimensionless ratio of position of thermocouple

$k$ = thermal conductivity of heat sink material

$L$ = thickness of heat sink

$\phi_s$ = heat flux at thermocouple tip

$\phi_0$ = surface heat flux

$r$ = radius

$R$ = thermocouple radius

$t$ = time

$t_r$ = response time

$T$ = temperature

$T_s$ = thermocouple tip temperature

$T_0$ = surface temperature above thermocouple

$T_{s\infty}$ = temperature at $E$ if thermocouple were not present

$T_{0\infty}$ = surface temperature if thermocouple were not present

$z$ = $z$-co-ordinate

$Z = E/L$ = dimensionless position of thermocouple tip

$\alpha$ = thermal diffusivity

$\tau_E = \dfrac{\alpha t}{E^2}$ = dimensionless time

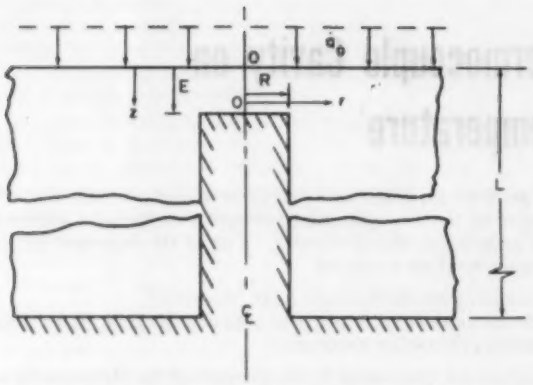


Fig. 1(a) Boundary conditions and dimensions for determining temperature disturbances caused by cylindrical void in a finite heat sink

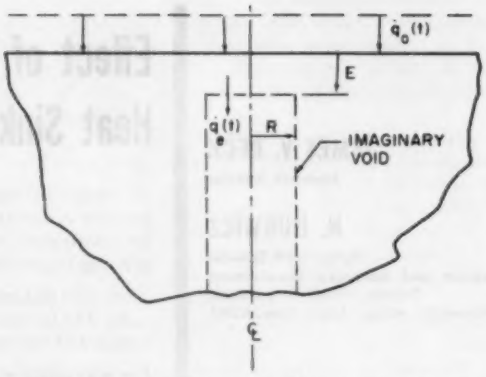


Fig. 1(b) Boundary conditions of one-dimensional heat flow in a semi-infinite slab with imaginary void

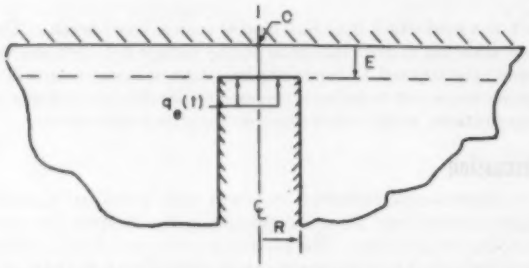


Fig. 1(c) Boundary conditions for the thermocouple error in semi-infinite slab

for the heat conduction equation in cylindrical co-ordinates

$$\frac{\partial^2 T}{\partial z^2} + \frac{1}{r}\frac{\partial}{\partial r} r \frac{\partial T}{\partial r} = \frac{1}{\alpha}\frac{\partial T}{\partial t} \tag{1}$$

**A Literature Review.** An upper bound of the temperature above the thermocouple junction is given by the fine paper by Masters and Stein [1][2,3] who effectively used the superposition principle. The heat sink with a surface heat flux was first considered with an imaginary void [Fig. 1(*b*)]. The heat flux $\dot{q}_e(t)$ which passes through the $z = E$ surface of the imaginary void was determined. Consider now the heat flux $\dot{q}_e(t)$ introduced in the negative $z$-direction at $Z = E$ [Fig. 1(*c*)] in an insulated semi-infinite body. If the heat fluxes at the boundaries in Figs. 1(*b* and *c*) are added, it may be observed that the boundary conditions for the thermocouple problem for a semi-infinite body are obtained. The temperature disturbances due to the void may then be obtained using the boundary conditions shown by Fig. 1(*c*). This change in boundary conditions still did not permit the analytical solution of the problem immediately. By allowing, however, the heat rejected by top of void to diffuse only in the infinite plate of thickness $E$, M and S were able to obtain an analytical solution.

In the M and S paper, the effect of several smooth analytical time-variable heat fluxes applied at the sink surface was obtained by determining the variation of these fluxes at the $E$-level in a semi-infinite body and then applying these latter heat fluxes at the thermocouple tip. The results at the sink surface hot spot (point $O$ in Fig. 1) for a uniform heat flux for $g(= R/E)$ of 0.25, 0.5, and 1 are shown by Figs. 2 and 3, and are quite similar to those obtained with variable heat inputs. It should be noted that in Fig. 2 the per cent change in hot-spot temperature has been divided by $g^2$ and in Fig. 3 the hot-spot temperature has been divided by $g$. Thus it is observed that per cent change in temperature due to the hot spot varies approximately as $g^2$ while the hot spot itself varies as $g$. Though the maximum error for $g = 0.25$ given by M and S is 1.5 per cent (which is quite small) it will be shown that usually the most advantageous position for the thermocouple is where $g = 1.1$ when the maximum per cent error given by M and S would be about 23 per cent which is rather large. The authors obtained the M and S curve for $g = 1$ using the given equation and found that the solution could not conveniently be extended beyond $\tau_E = 250$ since a large number of sensitive subtractions were involved.

In Fig. 2, it may be noticed that the maximum per cent error occurs approximately at $\alpha t/E^2 = 8$. For a typical thermocouple in a copper heat sink the maximum per cent difference would occur at about $^1/_{30}$ second when the temperature and heat flux level would be low. The determination of the thermocouple hot-spot effect is desired, however, at the time of maximum surface temperature which might occur several magnitudes of time later after the beginning of heating. From Fig. 3 the absolute hot-spot temperature error as given by M and S is seen to grow appreciably in time and to have no maximum. The use of the M and S results (Fig. 3) for time variable heat inputs which are discontinuous—such as might be caused by a change from laminar heating to much higher turbulent heating rates—is not apparent and may result in somewhat larger upper bounds.

It will also be shown that usually the most important state for the thermocouple disturbance is not a transient but a "steady" state which is said to exist when the disturbance is approximately proportional to the surface heat flux. This steady state is only possible in a semi-infinite heat sink but will be shown to be closely approximated in a finite heat sink; that a steady state exists should be emphasized since it is a fundamental point of the present paper and distinguishes it from the M and S work which emphasized the transient aspects. As a result of the steady-state disturbance concept, a "null" position is located where the thermocouple reads essentially the undisturbed surface temperature; the location of this position was not given by M and S. Bussell [2] also investigated and obtained a value for the hot spot with $R/E = {}^1/_2$ using a passive element analog; the results are shown by Figs. 2 and 3.

**B Calculations and Results.** To cover the complete range of interest, two analytical and two machine solutions were obtained. One analytical solution, which is particularly applicable for small voids ($g < 0.5$), employs a point heat source; transient and steady-state solutions are given. The other analytical solu-

[1] Numbers in brackets designate References at end of paper.

[2] Subsequent reference to Masters and Stein will use the abbreviations M and S.

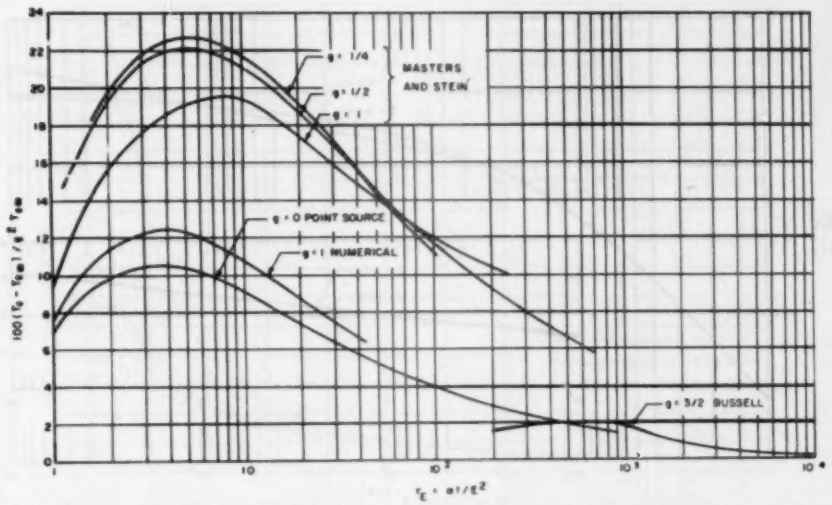


Fig. 2 Comparison of transient thermocouple hot-spot temperature results relative to the surface temperature or semi-infinite solid

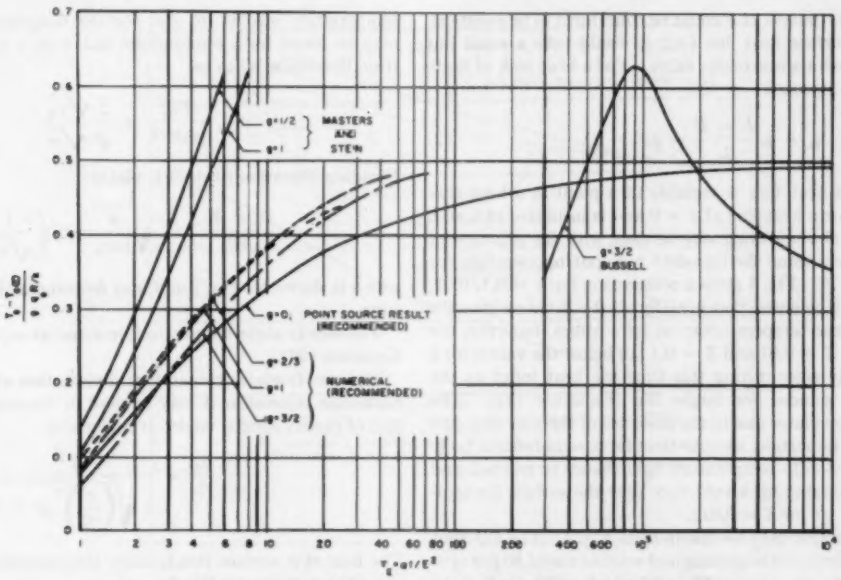


Fig. 3 Transient thermocouple hot-spot temperature results for a semi-infinite solid

tion (steady state only) gives reliable results for large $g$'s ($g > 2$); due to space limitations the solution will be outlined. The machine results have been obtained for the intermediate void or thermocouple sizes ($0.5 < g < 3$). Both steady and transient solution were obtained on a digital computer. All these solutions supplement one another and have their particular range of greatest accuracy. The results exhibit substantial agreement among themselves and all possess a steady-state solution in distinction to the data available in the literature. The point that each of these solutions has yielded a steady-state solution is important since the steady-state thermocouple errors are shown to be applicable to transient thermocouple measurements.

*1 Point Heat Source Analytical Solution.* As noted in the previous discussion of the M and S paper, the thermal effect of a void in a heat sink may be simulated by a heat input at the circular void surface equal to the negative of the undisturbed heat flux at that depth [Fig. 1(*c*)]. As the void becomes small in radius, the top of void approaches a point. In this case the thermal effect of the void would be approximated by a heat point source of strength equal to the heat that would be reflected at the tip of the void. This approach is very similar to that used by M and S who employed a disk heat source; the solution may not, however, be obtained directly from their treatment since a disk heat source in the limit (as $R$ approaches zero) does not approach the point source solution. This may be proved by noting that at the center of the disk source the temperature is always finite while at the point source the temperature is not bounded.

The void effect using the point heat source would be determined mathematically by solving Equation (1) for a point source of strength $\pi^2 R^2 q_s$ between two parallel insulated planes. $q_s$ is the undisturbed heat flux that would be caused at $E$ by a surface heat flux, $q_0$. To simplify initially the determination of the void

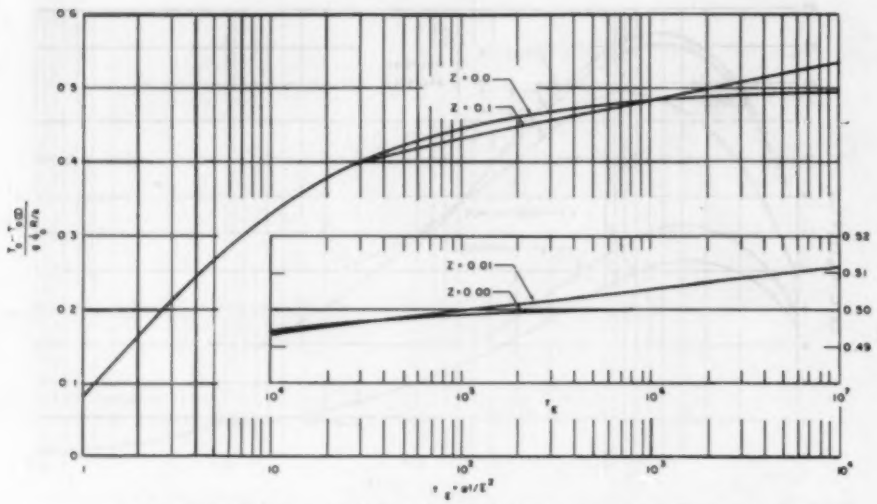


**Fig. 4 Effect of the rear surface of the finite heat sink upon the hot-spot temperature**

effect, the source strength at $E$ could be considered to be constant. For a uniform surface heat flux ($q_0$), $q_s$ would take a small but finite time to reach its maximum value. For a heat sink of finite thickness $q_s$ will approach

$$q_s = q_0 \frac{L - E}{L} = q_0(1 - z) \tag{2}$$

In reality, this heat flux is variable at a point in a heat sink which has a uniform heat flux at $z = 0$ and is insulated at $z = L$ [4]. Equation (17), however, may be used with the principle of convolution to determine the transient hot-spot temperature for various values of $Z$. Fig. 4 gives a comparison for $Z = 0.1$, 0.01, and zero. It may be noted that initially all the $Z$-values give the same dimensionless temperatures; at later times, however, the temperatures for $Z = 0.01$ and $Z = 0.1$ fall below the values for a semi-infinite body since during this time the heat input at the point source is reduced for larger $Z$'s [Equation (2)]. The situation is reversed later due to the presence of the rear sink surface. It is very important to note that for a semi-infinite body ($Z = 0$) a steady-state temperature disturbance is reached and is closely approximated for a void very near the surface for ordinary times ($\tau_E < 10^5$ for $Z = 0.01$).

A further conclusion may be drawn from Fig. 4. The hot-spot error grows rapidly at the beginning and reaches about 80 per cent of the steady-state value in $\alpha t/E^2 = 30$ which will be called the response time. For ordinary thermocouple placement this dimensionless response time indicates a very rapid temperature response at the void. For example, the response time in a copper heat sink for a 0.02-in. radius thermocouple, 0.02 in. below the surface, is computed to be about 0.08 second. This suggests that the steady-state calculation for a thermocouple located near the sink surface is sufficient for most cases.

For a semi-infinite sink heated with a uniform surface heat flux [and thus time-variable at the void, Equation (18)], the temperature disturbance caused by a point source is given by Equation (19).

For the hot spot (0, 0) the transient temperatures would be from Equation (19)

$$\frac{T_0 - T_{0\infty}}{gq_0R/k} = \frac{1}{2} \operatorname{erfc} \frac{1}{\sqrt{\tau_E}} \tag{3}$$

Equation (3) may be used to obtain the variation of the hot-spot temperature relative to the surface temperature. The latter may be found for a semi-infinite slab with a uniform heat input from Reference [4] to be

$$\frac{T_{0\infty}}{gq_0R/k} = \frac{2\sqrt{\tau_E}}{g^2\sqrt{\pi}} \tag{4}$$

Dividing Equation (3) by (4) yields

$$\frac{T_0 - T_{0\infty}}{g^2T_{0\infty}} = \sqrt{\frac{\pi}{16\tau_E}} \operatorname{erfc}\left(\frac{1}{\sqrt{\tau_E}}\right) \tag{5}$$

which is shown by Fig. 2 and may be compared with previous results.

The steady-state temperature increase at any point is given by Equation (20).

The steady-state temperature distribution at the surface is of particular interest as it may be used in determining the interaction of closely spaced voids; it is given by

$$\frac{T(r, 0)}{gq_0R/k} = \frac{1}{2\sqrt{\left(\frac{r}{R}\right)^2 g^2 + 1}} \tag{6}$$

The heat sink surface steady-state temperatures given by Equation (6) are shown by Fig. 5.

The temperature of the hot spot is of particular interest as its determination was one of the primary objectives of this investigation; from Equation (3) it is (see Fig. 6)

$$\frac{T_0 - T_{0\infty}}{gq_0R/k} = \frac{1}{2} \tag{7}$$

Equation (7) would be expected to apply to small values of $g$ (small radii for a given void depth).

**2 *Large g Analytical Solution.*** For large $g$ ratios the geometry may be broken into two parts: The finite cylinder of radius $R$ and thickness $E$ immediately above the void and a semi-infinite hollow cylinder of radius $R$. An exact solution may be obtained if the two cylinders have their boundary conditions properly matched at $r = R$ and $z = 0$ to $E$. This is not convenient to do; however, for large $g$'s it can be deduced that the temperature disturbance along this interface will be approximately constant. Klamkin [5] solved analytically the finite cylinder problem

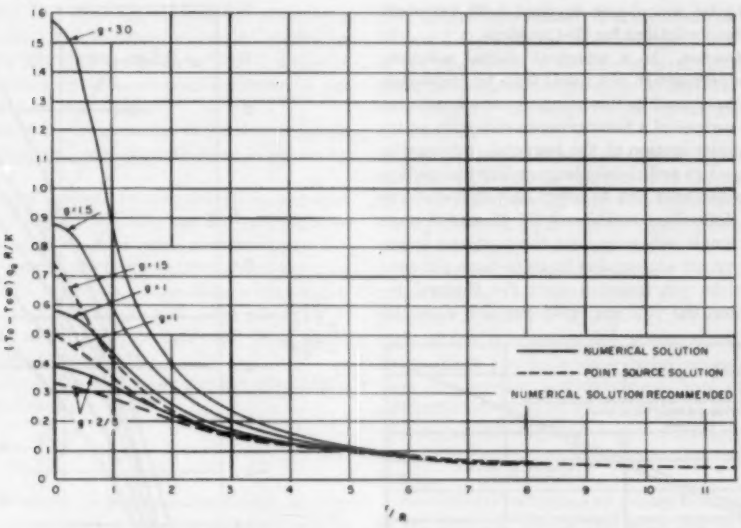


**Fig. 5 Steady-state numerical and point heat source solutions for the heat sink surface**

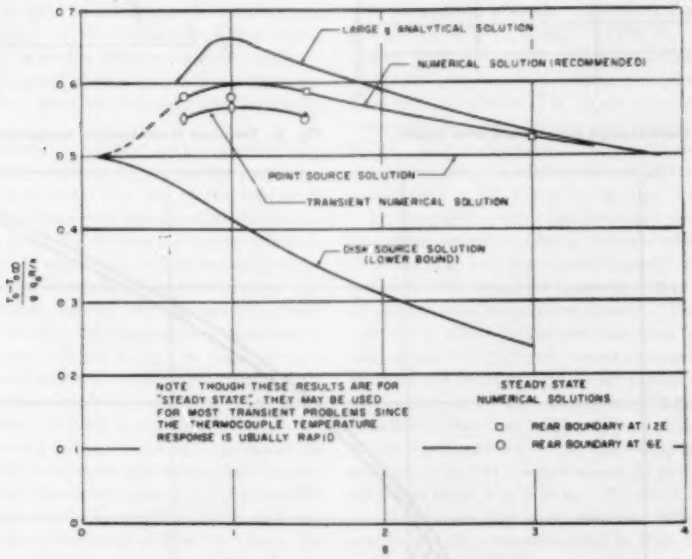
LARGE g ANALYTICAL SOLUTION
NUMERICAL SOLUTION (RECOMMENDED)
POINT SOURCE SOLUTION
TRANSIENT NUMERICAL SOLUTION
DISK SOURCE SOLUTION (LOWER BOUND)
NOTE THOUGH THESE RESULTS ARE FOR "STEADY STATE", THEY MAY BE USED FOR MOST TRANSIENT PROBLEMS SINCE THE THERMOCOUPLE TEMPERATURE RESPONSE IS USUALLY RAPID
STEADY STATE NUMERICAL SOLUTIONS
REAR BOUNDARY AT 12E
REAR BOUNDARY AT 6E
g

**Fig. 6 Steady-state hot-spot results**

which has the uniform heat flux $q_0$ at the $z = E$ surface and a constant temperature at $r = R$. The heat flux was then found at $r = R$ from $z = 0$ to $E$.

The semi-infinite cylinder also was solved analytically by Klamkin [6] for a uniform heat flux at $r = R$ from $z = 0$ to $E$; the temperature disturbance at the point $r = R$ and $z = 0$ only was obtained using a close upper bound approximation to evaluate a certain integral. With this later solution it was then possible using the principle of superposition to introduce the space variable heat flux at $r = R$ found from the disk. By then adding the temperature disturbance at $r = R$, $z = 0$ in the semi-infinite cylinder to the disturbances found in the finite disk, the steady-state temperature disturbances due to the void are obtained. The results for the hot spot, the thermocouple tip temperature disturbance, and the null point are shown by Figs. 6, 7, and 8 respectively; these results constitute an upper steady-state bound of the temperature disturbances.

*3 Digital Solutions.* The solution of the thermocouple problem was correctly thought by M and S to be somewhat difficult using a digital computer. Several considerations led to this conclusion. The thermocouple is a rather small device and the area above it occupies a very small part of the volume of the heat sink; this leads to a very small cell in the vicinity of the thermocouple which results in a large number of finite difference cells and in short computing intervals.

Another difficulty is adequate simulation of the boundaries. A finite section of the heat sink must be considered in a numerical solution while from the point source solution, it has been shown that the thermal effects are not strictly local. The authors have

successfully adapted digital techniques to yield both transient and steady-state numerical solutions for this problem.

**(a) Transient Digital Solution.** In a transient digital solution, a "direct" approach (superposition not used) may be employed.

The boundary conditions used in this solution were a uniform heat input at the front surface of a homogeneous slab with an insulated void. Since a finite section of the heat sink only can be considered in this approach, a sufficiently large cylindrical section of the heat sink was considered not to affect the temperatures about the void. The difficulties mentioned by M and S were overcome by (1) using small cells only near the void and larger cells elsewhere and (2) by not attempting to go to large physical times which actually were not required since the thermal response of the points about the void are rapid and also since the

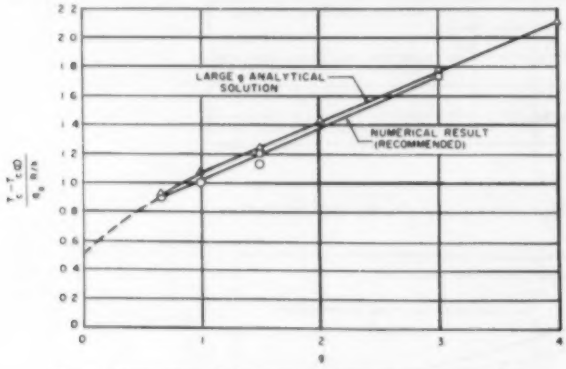


Fig. 7 Comparison of thermocouple temperature error results

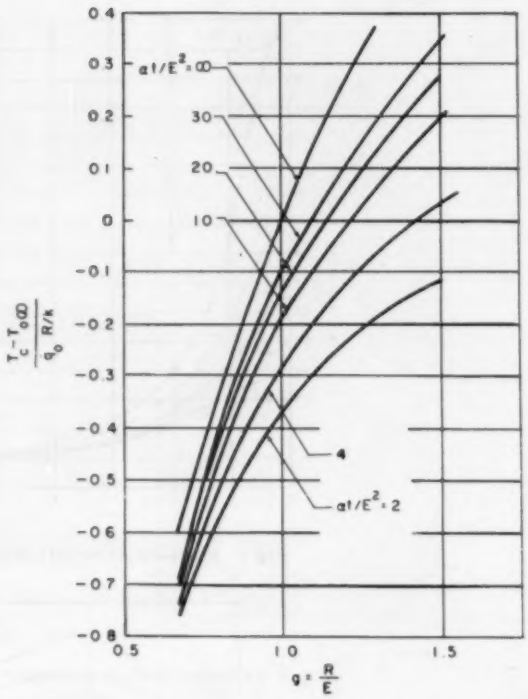


Fig. 9 Transient thermocouple temperatures for a semi-infinite solid

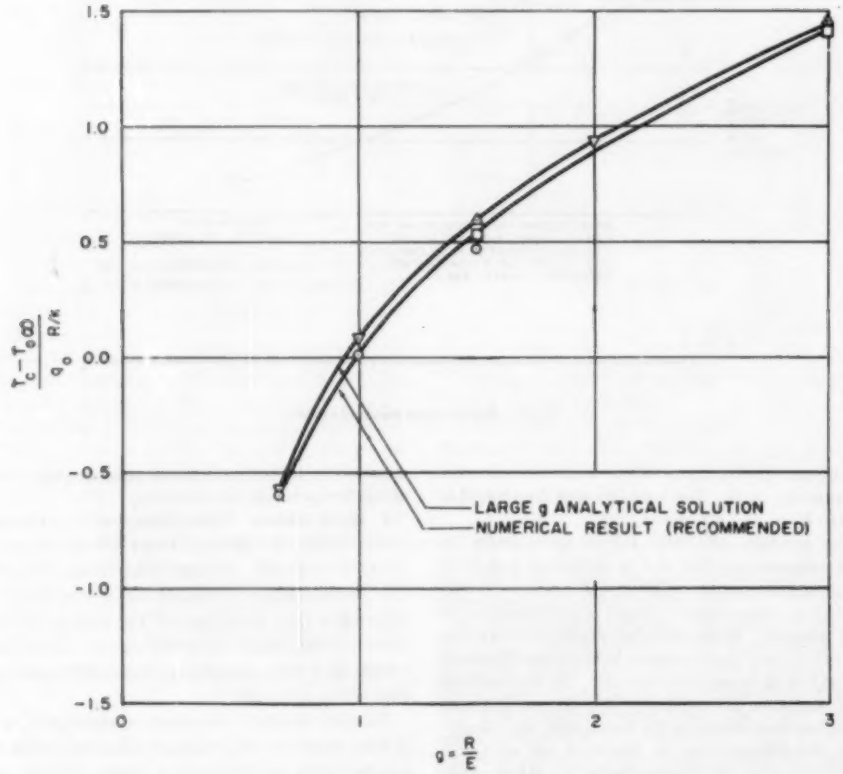


Fig. 8 Steady-state null point results

final values (steady state) for a semi-infinite sink are given by a separate numerical solution. The transient numerical results for $g = 3/4$, 1, and $3/2$ for the hot spot are given by Fig. 3 until the radial boundary temperature disturbance would increase 2 per cent according to the point source solution.

The transient variation of the temperature at the thermocouple tip relative to the undisturbed surface temperature is shown by Fig. 9.

In locating a thermocouple it would be desirable (if the hot-spot temperature were not excessive) to place the thermocouple so that the thermocouple reading would require a minimum correction. Provided the response of the temperatures about the void were rapid compared to the variations of the surface heat input, the thermocouple could be placed at the null point where $T_c - T_{0_\infty} \simeq 0$ (see Fig. 9). At $\alpha t/E^2 = 30$ the null point is within 10 per cent of its steady-state $g$ value of 1.0.

The response time for both the null point and hot spot might then be given by the dimensionless time

$$\frac{\alpha t_r}{E^2} = 30 \tag{8}$$

As given in a previous example, the response time $t_r$ is very rapid (0.08 sec) for a typical placement of a thermocouple in copper. In cases when this occurs, the thermocouple may be placed at the null point to read the surface temperature and the steady-state solutions may be used to determine the temperature errors about the thermocouple. If the surface heat flux varies widely in the response time, then the transient results could be used (see below). The "transient" thermocouple corrections are not usually required, however, since the response time is usually quite small.

**(b) Steady-state Digital Solution.** As has been observed the steady-state solution of this problem is frequently more important than the transient solution. One use of the *numerical* steady-state solution is to determine the steady state null point which cannot be accurately determined using the known analytical solutions. The steady-state numerical results cannot be conveniently obtained using the straightforward numerical approach, that have been described, because the temperature at any point is continually rising though the temperature disturbance reaches a maximum in a semi-infinite body. A superposition method would be desirable to obtain the steady-state temperature errors directly. Since it is known that the void effect extends to infinity, some mechanism must be used to simulate infinity.

The point source solution is, however, valid at large distances from the void. The boundary conditions used to simulate infinity were the point source temperature results given by Equation (20) at $r/R = 6$ and $z/E = 6$ for $g = 3/4$, 1, and $3/2$. For $g = 3$ and also $3/2$ the rear boundary was extended to $z/E = 12$. As in the point source solution, the front surface is insulated. The cylindrical void is insulated at its radial surfaces and has a uniform heat flux over the circular top surface of the void.

The numerical steady-state hot-spot temperatures are shown by Fig. 6. It may be observed from Fig. 6 that the numerical results for $g = 1.5$ with $z/E = 6$ is about 6 per cent below the value given using $z/E = 12$; the latter result is probably more accurate since then the boundary conditions obtained from the point source solution would have less effect at the hot spot. As small values of $g$ the numerical solution should approch the point source results; at larger $g$ values the numerical results approach the large $g$ *analytical* results.

The steady-state surface temperatures for $g = 0.667$, 1, 1.5, and 3 are shown by solid lines of Fig. 5. The point source solution [Equation (6)] is shown to approximate the numerical results more closely at [1] larger $r/R$'s for all $g$'s and for [2] smaller $g$'s at all $r/R$'s. The greatest disagreement, as would be expected, is in the immediate area above the void.

**4 Comparison of Results.** A comparison of the transient results of M and S the authors made in Figs. 2 and 3 indicates differences in the magnitude of the effects investigated. The hot-spot temperature disturbance given by M and S is larger than that given here (Fig. 2); the shape of the curves, however, given by Fig. 3 are similar.

The apparent lack of close agreement between the M and S and the present results is attributed to the analysis of the problem. M and S are concerned only with transient results and do not show steady hot-spot temperature. Also, they were interested only in the upper bound of the void effect.

In contrast, solutions presented here give the actual hot-spot temperatures and other effects and show the upper and lower bounds. In addition, through analysis of the transient and steady-state effects, it is shown that a steady-state solution is applicable to transient problems since rapid response times are involved. Such steady-state solutions have been obtained with a digital computer as well as by means of theoretical analytical approaches offering means of independent verification of results; the steady-state solutions in turn were verified by numerical transient calculations.

Since several solutions presented here demonstrate the validity of the authors' results and since the M and S solution is admittedly an upper bound, the results of the present investigation are recommended.

**5 Interpretation of Results.** Transient results for the hot spot are given for $g = 0$, $3/4$, 1, and $3/2$ (Fig. 3). The $g = 0$ values are obtained from the point source solution while the other were obtained by a numerical solution employing a digital computer. The authors' results (Fig. 3) are consistent and recommended to obtain the transient hot-spot temperature $(T_0 - T_\infty)$ from $y = 0$ to 1.5. The time-variation of the thermocouple tip temperature compared to the undisturbed surface temperature $(T_c - T_{0_\infty})$ is shown for $g = 3/4$, 1, and $3/2$ by Figs. 9 and 10.

In comparison with the transient results, steady-state results are given which require a decision which is the most accurate. A numerical solution would usually be preferred for a given problem with irregular geometry since it may approximate the boundary conditions most closely. The steady-state numerical solution is about 10 per cent less than the large $g$ *analytical* solution near $g = 1$ and even closer at larger $g$'s. If the transient results for the hot spot (Fig. 3) are extrapolated parallel to the point source solution, the steady-state results labeled "Transient Numerical Solution" (Fig. 6) are obtained. These results are about 5 per cent below the numerical results. The point source solution is on the average about 15 per cent below the numerical solutions from $g = 0$ to 4. The steady-state numerical solution appears to be the most accurate; the steady-state numerical results are then recommended in Figs. 5, 6, 7, and 8.

The null point is shown by the numerical solution of Fig. 8 to be $g = 1$. In locating a thermocouple at the null point of $g = 1$ several assumptions are made. The first is that the thermal conductivity of the thermocouple assembly is much less than that of the heat sink. If the thermocouple assembly thermal conductivity $(k_c)$ is of the same magnitude as the heat sink's conductivity $(k)$ then a larger $g$ should be used. A suggested $g$-correction factor, $C_{hc}$ would be

$$C_{hc} = \frac{k}{k - k_c} \tag{9}$$

The next consideration concerns the transient variation of the null point. The response is usually quite rapid for many thermocouples; there may be cases, however, when the thermocouple would be located relatively far from the surface or is in a relatively low conductivity material. Both of these effects would lengthen the response time and would cause the null point $g$ to be also larger (Fig. 9).

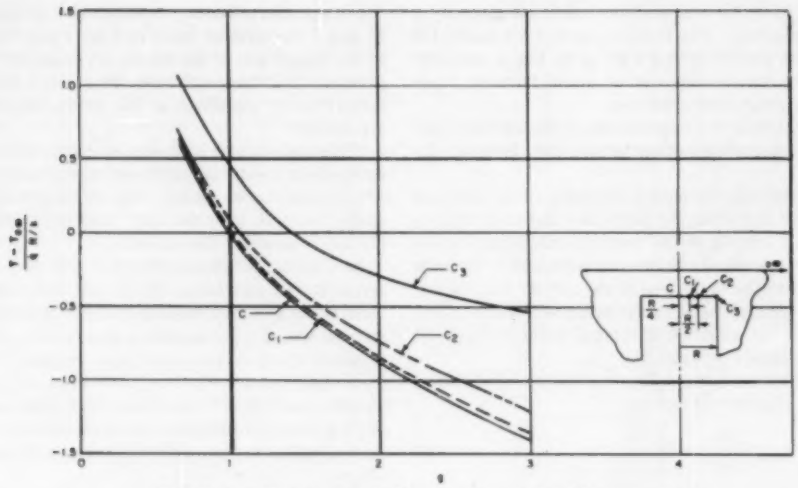


Fig. 10 Steady-state numerical temperatures at tip of thermocouple

The last point is explained by the fact that the determination of the null point was based only on the point at the tip of the thermocouple. Actually the thermocouple junction would integrate to find the average temperature of the void surface that it contacts. The contacting area probably would not be large but would again tend to increase the null $g$ value. Fig. 10 shows the variation of temperature along the top surface of the void. This figure indicates that the effect of the thermocouple junction extending over the tip area is small until $R/2$ when the null $g$ is 1.07. In summation, the null point $g$-value depends upon the actual problem though perhaps the best value for most cases would be about $g = 1.1$.

**C Applications.** The hot spot and null point have been found based on a uniform heat input while the heat sink would, in general, be exposed to a variable-in-time heat input. If the variation of the heat input in the response time, $\Delta q_0$, divided by the average $\dot{q}_0$ at that time is small, then the steady-state results may be used. The criteria would be

$$\frac{\Delta \dot{q}_0}{\dot{q}_0} < K \tag{10}$$

where $K$ would be less than some permissible value, probably about 0.1. It should be emphasized that the condition expressed by Equation (10) is usually satisfied, consequently, the steady-state thermocouple results may be used in an otherwise transient heat conduction problem.

To demonstrate that the steady-state solution may be used for a thermocouple which is placed in a heat sink exposed to a time-variable surface heat flux, consider the following problem. A 1-in. thick copper sink is exposed to a sine-squared shape heat input [7] for 12.5 sec with a maximum flux of 800 Btu/ft² sec. This heat input is similar to that which a re-entry vehicle might experience. The rear surface of the sink is insulated. It is desired to use a 0.044-in. diameter thermocouple to record the surface temperature accurately without causing the surface temperature hot-spot temperature to exceed the undisturbed surface temperature by 2 per cent. Calculations are needed to determine the location of the null point and to insure that the allowable hot-spot temperature is not exceeded. With $g = 1.1$, $E$ would be $E = R/1.1 = 0.022/1.1 = 0.02$ in. From Fig. 6 the steady-state hot spot $\Delta T$ would be

$$T_0 - T_{0_\infty} = \frac{1.1 \dot{q}_0 R}{k}(0.6) = \frac{1.1(0.6)(0.022/12)}{220/3600}\dot{q}_0 = 0.0198\,\dot{q}_0 \tag{11}$$

for $k = 220$ Btu/ft-hr-deg F. $\dot{q}_0$(Btu/ft² sec) is the surface heat flux at the time the hot spot $\Delta T$ is required. The undisturbed surface temperature is shown by Fig. 12 for constant properties and zero initial temperature ($\alpha_{C_u} = 4$ ft²/hr). The hot spot $\Delta T$'s computed using Equation (11) are also shown by Fig. 11.

The hot spot may also be expressed as per cent of the undisturbed surface temperature. This may be misleading as shown by Fig. 11 since the maximum per cent increase occurs at early times when the temperature level is quite low. Though at very early times the per cent temperature increase at the hot spot may be as high as 12 per cent (Fig. 2), the per cent is shown by Fig. 11 to decrease rapidly and to be about 0.6 per cent at the time of maximum surface temperature; the thermocouple hot spot then does not exceed the 2 per cent allowable temperature increase at the time of maximum surface temperature.

In using Fig. 6, two assumptions concerning transient effects were made. Use of the steady-state results assumes a small variation of $\dot{q}_0$ in the response time. From Equation (8) the response time may be computed for this case to be 0.075 sec. The permissible value of $K$ [Equation (10)] would not be exceeded for this response time for the given heat flux except at the lowest fluxes. This indicates that the steady-state results may be used to obtain the hot-spot temperatures for the variable-in-time heat flux in this example. The other assumption is that the $Z$ ratio (where $Z = E/L$) is such that the rear surface does not cause the hot spot to appreciably exceed its steady-state value (Fig. 4). The value of $\alpha t/E^2$ for the total heating time is 5000 and $E/L$ is 0.02. Since from Fig. 4 the $Z$-value of 0.1 does not exceed the point source steady-state value by more than 6 per cent at $\tau_E = 5000$ and since the $Z = 0.01$ value does not exceed the steady value until $\tau_E = 100{,}000$, it may be safely assumed that the steady-state value will be not appreciably exceeded in our example. The hot-spot results given by Fig. 11 would then be essentially the same using the steady-state solution (Fig. 6) or the transient solutions (Figs. 3 and 4).

For variable in-time heat inputs the principle of the convolution [8] may be used to sum results for uniform heat fluxes to obtain any desired variable heat flux. The steady-state results yields an upper bound for all cases except when the rear surface affects the hot-spot temperature (Fig. 4). In this case and also when the surface heat fluxes vary rapidly in time, the convolution may be applied; it is, however, more cumbersome than using the steady-state results.

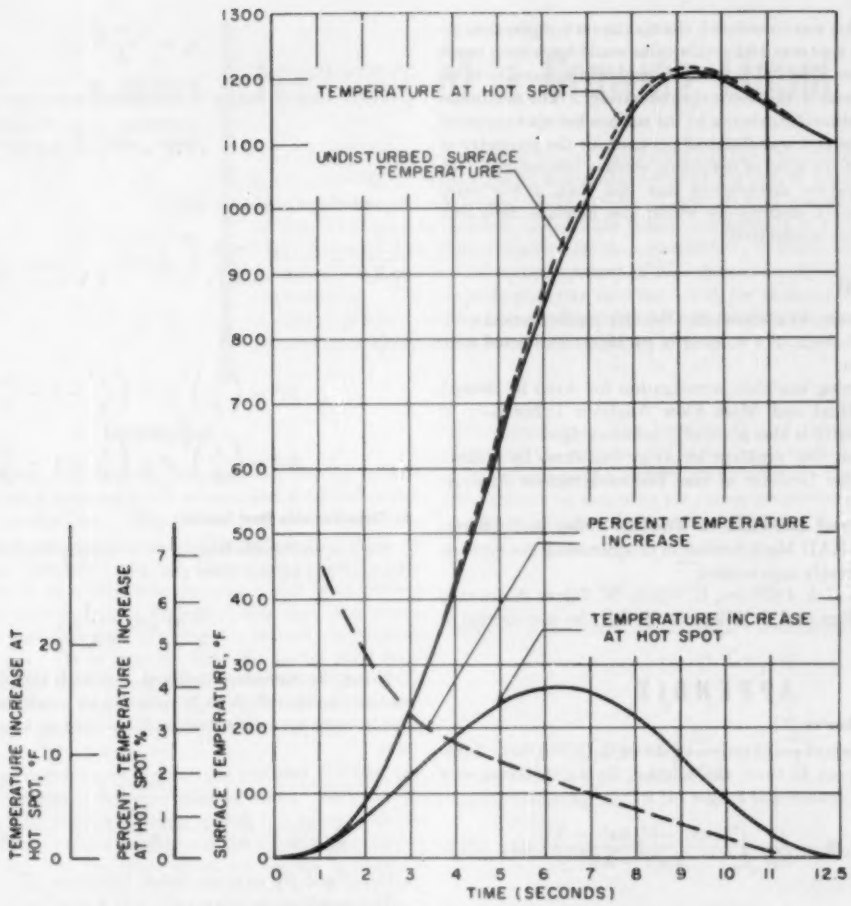


Fig. 11 Example showing the effect of the thermocouple upon the hot-spot temperature

## Summary and Conclusions

The temperature disturbances caused by a thermocouple placed normal to the heated surface of a heat sink or calorimeter are analyzed. The problem is similar to the determination of the temperature errors caused by an insulated cylindrical void near the surface since the effective thermal conductivity of the thermocouple is much lower than a heat sink material. The present report gives analytical and machine analyses, which investigate a comprehensive range of the important parameters. An important contribution of the present investigation is the inclusion of a steady-state as well as transient solutions.

**1 Hot-Spot Temperature Disturbance.** Though the temperatures are varying with time in the heat sink even for a constant in-time surface heat flux, it is demonstrated that the temperature disturbances caused by insertion of the thermocouple rapidly acquire values which are directly proportional to the surface heat flux; and when this occurs the disturbances are said to be in "steady state." Thus the temperature disturbances are usually given for transient temperature measurements by a steady-state solution. The transient surface hot-spot temperature for constant surface heat flux is shown by Fig. 3. For small voids ($g < 0.5$), the transient solution may be given by Equation (3) which indicates, as do the numerical solutions which are for larger voids, that the temperature disturbances near the thermocouple reach 80 per cent of the steady-state values when $\tau_E = 30$ which is called the response time. In most transient thermocouple measurements, it will be found that the surface heat flux does not vary significantly in the response time.

The steady-state hot-spot temperature disturbance is shown by Fig. 6 for various locations of the thermocouple tip relative to the heated surface. A convenient equation for the hot-spot temperature for small voids ($g < 0.5$) is Equation (7).

**2 Null Point.** Both the transient and steady-state solutions indicated that a minimum error in the thermocouple measurements of the undisturbed temperature would be present if the thermocouple were located at the null point. When the thermocouple is located at this poisition, the temperature disturbance at the thermocouple due to its presence equals the undisturbed temperature drop from the sink surface to the thermocouple tip. From the consideration of the null point, the optimum placement of the thermocouple was concluded to be when $g = 1.1$.

**Effect of Void Distribution.** The steady-state surface temperature disturbance for one void is given by Fig. 5 as a function of radial distance from the void. By properly superimposing the temperature disturbances found from this figure the effect of an arbitrary distribution of voids may be determined. For small voids the steady-state surface temperature disturbances may be approximated by Equation (6).

The order of magnitude of the hot-spot error depends upon the sink material and surface heat flux. For the typical case of a cop-

per heat sink which was considered, the maximum temperature increase at the hot spot was 16 F; this value could have been much higher for another material since the temperature increase is inversely proportional to the thermal conductivity. The maximum per cent temperature disturbance at the surface hot spot occurred at very early time and was about 12 per cent for the geometry of most interest; at the time of maximum surface temperature, the per cent temperature disturbance was less than 1 per cent. The per cent surface disturbance would also increase for a sink material of a lower conductivity.

## Acknowledgment

The authors desire to acknowledge the able mathematical solution by M. S. Klamkin of a number of problems connected with this investigation.

The initial analog machine investigation for Avco by Joseph Hlinka of the Heat and Mass Flow Analyzer Laboratory of Columbia University is also gratefully acknowledged.

Initial work on this problem at Avco was done by Robert Mascola and John Graham of the Thermodynamics Analysis Section.

The patience and assistance of Timothy Foley and Charles Sova of the Avco RAD Math Section in programming the numerical solutions is greatly appreciated.

The assistance of A. DiPietro, R. Elliot, W. Jarosz in drawing graphs and M. Ray and J. Wilkie in typing the manuscript is appreciated

## APPENDIX

### 1 Constant Heat Source [3]

Consider a constant point source of strength $Q$(Btu/hr). Integrating with respect to time, the solution for an instantaneous source given by Carslaw and Jaeger [4] is

$$T(x, y, z, t) = \frac{Q}{8\rho c}\int_0^t \frac{\exp\left[-b^2/4\alpha(t-\lambda)\right]}{[\pi\alpha(t-\lambda)]^{3/2}}\,d\lambda \qquad (12)$$

where

$$b^2 = (x - x_0)^2 + (y - y_0)^2 + (z - z_0)^2$$

The solution [4] of Equation (12) is

$$T(x, y, z, t) = \frac{Q}{4\pi kb}\operatorname{erfc}\frac{b}{\sqrt{4\alpha t}} \qquad (13)$$

The insulated surfaces at $z = 0$ and $L$ may be simulated by placing heat sources along the $z$-axis at $\pm E$, $\pm(2L - E)$, $\pm(2L + E)$, $\pm(4L - E)$, $\pm(4L + E)$, to give

$$T(r, z, t) = \frac{Q}{4\pi k}\sum_{n=-\infty}^{\infty}\left[\frac{1}{|b_1|}\operatorname{erfc}\frac{|b_1|}{\sqrt{4\alpha t}} + \frac{1}{|b_2|}\operatorname{erfc}\frac{|b_2|}{\sqrt{4\alpha t}}\right] \qquad (14)$$

where

$$b_1^2 = r^2 + (z - E - 2nL)^2$$

$$b_2^2 = r^2 + (z + E - 2nL)^2$$

For large times the heat flux $q_s$ at a point $E$ in a slab with a uniform heat flux $q_0$ at $z = 0$ and insulated at $z = L$ is

$$q_s = \frac{L - E}{L}\,q_0 \qquad (15)$$

For a void of radius $R$ the point source strength would be—

$$Q = \pi R^2 q_s = \frac{L - E}{L}\,\pi R^2 q_0 \qquad (16)$$

Equation (14) then becomes

$$\frac{T}{\rho q_0 R/k} = \frac{1 - Z}{4}\sum_{n=-\infty}^{\infty}\left[\frac{1}{|B_1|}\operatorname{erfc}\frac{|B_1|}{2\sqrt{\tau_E}} + \frac{1}{|B_2|}\operatorname{erfc}\frac{|B_2|}{2\sqrt{\tau_E}}\right] \qquad (17)$$

with

$$B_1^2 = \left(\frac{r}{R}\right)^2 + \left(\frac{z}{E} - 1 - \frac{2n}{Z}\right)^2$$

$$B_2^2 = \left(\frac{r}{R}\right)^2 + \left(\frac{z}{E} + 1 - \frac{2n}{Z}\right)^2$$

### 2 Time-Variable Heat Source

For a semi-infinite body with a uniform heat flux at its surface, the heat flux at any point $z = E$ is

$$\frac{q_s}{q_0} = \operatorname{erfc}\frac{1}{2\sqrt{\tau_E}} \qquad (18)$$

Using the procedure outlined, but with this variable heat flux and one image reflection to simulate an insulated plane at $z = 0$, the temperature disturbances for a void in a semi-infinite body are:

$$\frac{T}{\rho q_0 R/k} = \frac{1}{4}\left[\frac{\operatorname{erfc}\dfrac{|B_1| + 1}{2\sqrt{\tau_E}}}{|B_1|} + \frac{\operatorname{erfc}\dfrac{|B_2| + 1}{2\sqrt{\tau_E}}}{|B_2|}\right] \qquad (19)$$

with $B_1^2$ and $B_2^2$ as given below Equation (17) with $n = 0$.

The steady-state temperatures in a semi-infinite body are from Equation (19)

$$\frac{T(r, z)}{\rho q_0 R/k} = \frac{1}{4}\left(\frac{1}{|B_1|} + \frac{1}{|B_2|}\right) \qquad (20)$$

## References

1 J. L. Masters and S. Stein, "Effect of an Axial Cavity on the Temperature History of a Surface Heated Slab," *Review of Scientific Instruments*, vol. 27, 1956, pp. 1065–1069.

2 B. Bussell, "Analog Study of a Thermocouple Instrumentation Error," Dept. of Engineering, University of California, Los Angeles, August, 1957.

3 M. S. Klamkin, "Heat Transfer Due to Source Between Two Parallel Insulated Planes," AVCO RAD-2-TM-58-128, November, 1958.

4 H. S. Carslaw and J. C. Jaeger, "Conduction of Heat in Solids," Oxford University Press, London, England, 1947, p. 252.

5 M. S. Klamkin, "On a Heat Flux Determination in a Cylinder," AVCO RAD-U-58-12, April, 1958, p. 4.

6 Private Communication, August 9, 1957, M. S. Klamkin, AVCO RAD.

7 Private Communication, R. E. Mascola, AVCO RAD.

8 H. Hurwicz and M. S. Klamkin, "Conductive Heat Transfer in a Re-entry Body-Analysis of Computational Methods and Their Reliability," presented at this symposium.

G. HORVAY
General Electric Research Laboratory, Schenectady, N. Y. Mem. ASME

# Freezing of a Growing Liquid Column

*The one-dimensional problem is treated in which a liquid metal column, of the original temperature $\vartheta_0$, is supplied with additional metal at the top, of temperature $\vartheta_b$, at the rate $v$ ft/min. At the bottom of the column a heat sink of temperature $\vartheta_a$ is maintained. The case in which $\vartheta_a$ exceeds the fusion temperature is solved for $v$ = const, both rigorously and approximately; the case in which $\vartheta_a$ is below the fusion temperature so that a freezing front sweeps upward in the column is next treated by an approximate method. The foregoing analysis may represent, for instance, the filling stage of a casting process. The present analysis will be adapted to the more important continuous casting process in a succeeding paper.*

## I Introduction

DURING THE FILLING STAGES of a casting process heat flows, through a growing liquid column and solidified metal, to the heat sink at the base.[1] The difficulty of analytically handling this problem was pointed out by Chao and Weiner [1].[2] In their study they therefore restricted themselves to determining the temperature $\vartheta$ in a semi-infinite solid which is in perfect contact with a *perfectly mixed* liquid column (i.e., one whose temperature is uniform throughout); the column is growing linearly with time. (It is assumed that the initial solid temperature $\vartheta_a$ exceeds the freezing temperature of the liquid $\vartheta_f$. The liquid is poured at a temperature $\vartheta_b > \vartheta_a$.) In the Chao and Weiner paper the quantity of primary interest is the interface temperature of the liquid and solid.

In the present paper we reconsider the problem of Chao and Weiner from a somewhat different point of view. We drop the assumption that the fluid is perfectly mixed, but assume, on the contrary, that heat is transferred across the fluid by one-dimensional conduction. On the other hand, we assume in Sections II to V that the semi-infinite solid is replaced by a heat sink of fixed temperature $\vartheta_a$. In section VI we drop the assumption that $\vartheta_a > \vartheta_f$ (thus we allow freezing to take place), and also replace the fixed heat sink by a conducting slab of finite thickness. We treat the problem in an approximate manner, by the method of lumped parameters. This method, first introduced for this class of problems by London and Seban [2], was later generalized to problems of continuous casting by Horvay [3*a*], Glaever and Horvay [3*b*], and Horvay [4].

## II Rigorous Determination of the Temperature in a Growing Liquid Column

In Fig. 1 we illustrate the problem on hand. A plate (mold) of original temperature $\vartheta_a$ and isothermally maintained lower face, is brought in contact at the time $t = 0$, with a liquid column of original height $Y_0$ and original temperature $\vartheta_0$. Thereafter the height of the column is increased at the rate $v$ ft/hr by addition of liquid at temperature $\vartheta_b$. We seek to determine the temperature distribution $\vartheta$ in the liquid phase, in the frozen phase, and in the plate. The two most important quantities to be determined are: The location $X(t)$ of the frozen-liquid interface; and the temperature of the liquid surface.

If we assume the metal plate as infinitely thin, and the *ambient temperature as exceeding the fusion temperature*, then the mathematical problem reduces to that of solving the equation

$$\frac{\partial U}{\partial \tau} = \frac{\partial^2 U}{\partial \eta^2} \tag{1}$$

subject to the initial and boundary conditions[3]

$$\tau = 0: \quad U = U_b, H = 1 \tag{2a}$$

$$\eta = 0: \quad U = 0 \tag{2b}$$

$$\eta = H: \quad U_b \frac{dH}{d\tau} = U_1 \frac{dH}{d\tau} + \frac{\partial U}{\partial \eta} \tag{2c}$$

In the foregoing

$$U(\eta, \tau) \equiv \frac{c}{\lambda}(\vartheta - \vartheta_a), \quad U_b \equiv \frac{c}{\lambda}(\vartheta_b - \vartheta_a),$$

$$U_1(\tau) \equiv U(H, \tau) \tag{3a}$$

are dimensionless temperatures ($\lambda$ = latent heat of fusion,[4] $c$ = specific heat, $\gamma$ = specific weight, $k$ = conductivity, $\kappa$ = diffusivity = $k/\gamma c$)

$$\tau \equiv \kappa t / Y_0^2 \tag{3b}$$

is dimensionless time, and

$$\eta \equiv y/Y_0, \quad H \equiv Y/Y_0 \tag{3c}$$

[3] For simplicity we treat in this section only the problem in which the initial temperature $\vartheta_0$ of the column equals the pouring temperature $\vartheta_b$. In sections III to V we drop this restriction.

[4] When no freezing is involved then one may use for $\lambda$ any reference value which has the dimensions Btu/lb. When there is freezing then the use of the heat of fusion for $\lambda$ is mandatory.

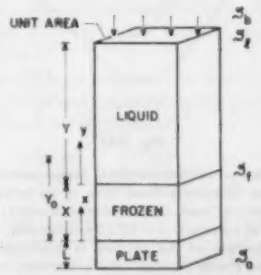


Fig. 1 Freezing of a growing liquid column

[1] We assume one-dimensional heat flow. The container side walls are assumed to be insulated.

[2] Numbers in brackets designate References at end of paper.

Contributed by the Heat Transfer Division of THE AMERICAN SOCIETY OF MECHANICAL ENGINEERS and presented at the ASME-AIChE Heat Transfer Conference, Storrs, Conn., August 9–12, 1959.

NOTE: Statements and opinions advanced in papers are to be understood as individual expressions of their authors and not those of the Society. Manuscript received at ASME Headquarters, May 14, 1959. Paper No. 59—HT-11.

are dimensionless distance and height of the liquid column, respectively. The dimensionless parameter, representing the pouring speed

$$p \equiv \dot{H} = \frac{Y_0}{\kappa}\frac{dY}{dt} \quad (\dot{H} \equiv dH/d\tau) \tag{4}$$

is usually referred to as the "Peclet number." The boundary condition (2c) means: The heat supplied to the liquid column at its surface (per unit time) equals the heat gained by the column through material growth, plus the heat gained by conduction.

It is shown in Appendix 1 that the solution of the problem (1), (2) is

$$U(\eta, \tau)/U_b = 1 - 2\sum_1^\infty B_k(\tau) \sin \zeta_k \eta \tag{5a}$$

where

$$\zeta_k(\tau) = \text{root of} \qquad \zeta H \cot(\zeta H) + H\dot{H} = 0 \tag{5b}$$

and

$$B_k(\tau) \equiv \frac{\dot{H}^2 + \zeta_k^2}{H(\dot{H}^2 + \zeta_k^2) + \dot{H}} A_k(\tau) \tag{5c}$$

$$A_k(\tau) \equiv \exp\left[-\int_0^\tau \zeta_k^2 d\tau\right] \int_0^\tau \zeta_k(\tau) \exp\left[\int_0^\tau \zeta_k^2 d\tau\right] d\tau \tag{5d}$$

For the case of linear growth of the liquid column,

$$H = 1 + p\tau \tag{6}$$

($p$ is the Peclet number) the use of the approximate $\bar{A}_k(\tau)$ formula (41a) in place of (5d) leads to results which, in a plot like Fig. 2(a), are indistinguishable from the true solution. In Table 2 of the Appendix we tabulate $\bar{A}_k(\tau)$ for the case $p = 1$. In Fig. 2(a) we plot, in full lines, the temperature $U(\eta, \tau)/U_b$ at $\eta = H(\tau)$ (the top of the liquid column), at $\eta = H/2$ (the mid-height of the column), and at $\eta = 1$ (the original height of the column). In dashed lines are shown the results for $\eta = H$, $H/2$ by the "approximate" method, Equation (11) of Section III. These latter curves are derived from the lumped circuit representation, Fig. 4(a), of the liquid column in Fig. 1; the agreement seems to be very satisfactory. In Fig. 3 we give the results by this method also for $p = 2, 4, 8, 1/2, 1/4, 1/8$.

In Figs. 4(b and c) we use still simpler lumped circuit representations for Fig. 1; we refer to these approximations as the "simplified" and "primitive" models. The dotted curve in Fig. 2(a) gives $U(H, \tau)/U_b$ by Equation (13b), Fig. 4(b). The latter approximation method is evidently inferior to that based on

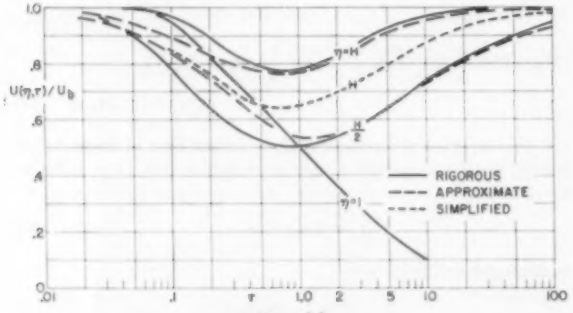

Fig. 2(a)

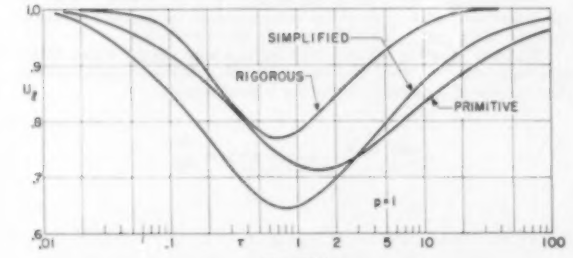

Fig. 2(b)

**Fig. 2 Determination of (dimensionless) temperature $U$ in the growing liquid column versus (dimensionless) time $\tau$, for initial value $U(\eta, 0) = U_b$ (pouring temperature) and initial (dimensionless) height $H(0) = 1$; at levels $\eta = H$ (top of column), $\eta = H/2$ (mid-height), and $\eta = 1$ (original height); when the bottom of the column is maintained isothermally at $U(0, \tau) = C$, and the Peclet number (dimensionless velocity of pouring) is 1**

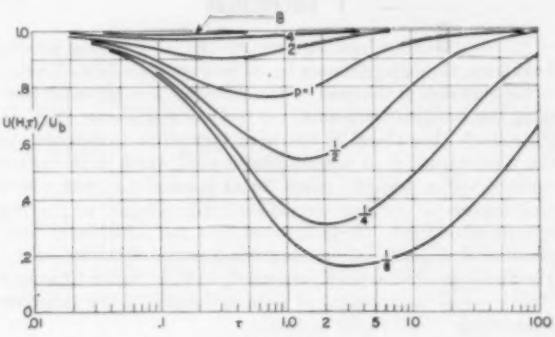

Fig. 3(a)

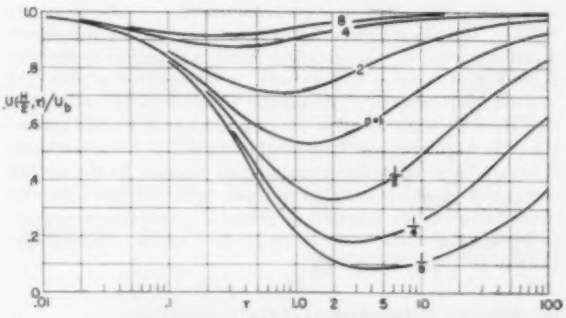

Fig. 3(b)

**Fig. 3 Variation of $U(H, \tau)$ and $U(H/2, \tau)$ with $\tau$ for various Peclet numbers. (Approximate method.)**

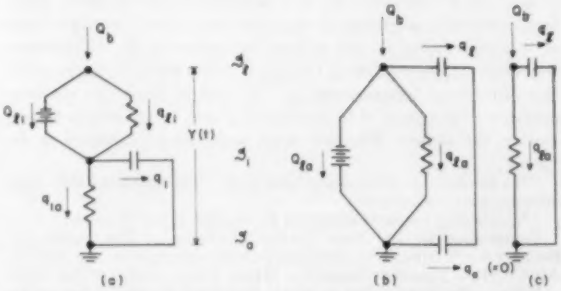

**Fig. 4(a) The "approximate" (2-node) model; (b) the "simplified" (1-node) model; (c) the "primitive" (1-node) model for the growing liquid column**

Fig. 4(*a*), but also simpler to program on a computer, and therefore will be adopted for the more complicated problem dealt with in Section VI, the combined growth and freezing of the liquid column. The solution by Equation (13*b*) is compared in Fig. 2(*b*) with the still poorer approximation, Equation (14*b*), Fig. 4(*c*).

Figs. 2 and 3 show that the temperature at the top of the liquid column begins to sink, from its original value, $U_1(0) = U_0$, to a minimum near $p\tau = 1$ (i.e., near the time at which the original column doubles its height; the conduction to the heat sink is most strongly felt in this early period, $p\tau < 1$);[5] then rises again toward $U_b$ as the column becomes very high, i.e., the conduction to the heat sink becomes vanishingly small. When pouring is done very slowly ($p \ll 1$) the minimum sinks close to the heat sink temperature ($U_{1,\min} \to 0$), when pouring is done very fast ($p \gg 1$) then the minimum of $U_1$ barely drops below $U_b$.

## III Approximate Solution

We assume that the entire heat absorbing capacity of the liquid column $\gamma cY$ (per degree) is concentrated at the mid-height. Then we obtain the two-node model illustrated in Fig. 4(*a*).[6] The lower terminal of the column is maintained at the constant temperature $\vartheta_a$. Kirchhoff's law of current balance applied to the nodes $\vartheta_i$ and $\vartheta_1$ states that

$$0 = Q_b - q_{in} - Q_{in} \tag{7a}$$

$$q_i = q_{in} + Q_{in} - q_{ia} \tag{7b}$$

where

$$Q_b = \gamma c(\vartheta_b - \vartheta_a)dY/dt \tag{8a}$$

is the heat supplied per unit time,

$$q_i = \frac{d}{dt}\left[\gamma c(\vartheta_i - \vartheta_a)Y\right] \tag{8b}$$

is the charging current,

$$q_{in} = 2k(\vartheta_i - \vartheta_1)/Y,\ q_{ia} = 2k(\vartheta_1 - \vartheta_a)/Y \tag{8c}$$

are the conduction currents, and

$$Q_{in} = (\vartheta_i - \vartheta_a)\frac{d(\gamma cY)}{dt} \tag{8d}$$

is the current due to mass transfer. [A more elaborate explanation of this term is given after Equation (27).]

Introducing (8) into (7*a*) and (7*b*) and multiplying through the equations by $cY_0/\lambda k$ yields, on using the notation (3)

$$0 = U_b\frac{dH}{d\tau} - \frac{2}{H}(U_i - U_1) - U_i\frac{dH}{d\tau} \tag{9a}$$

$$\frac{d(U_iH)}{d\tau} = \frac{2}{H}(U_i - U_1) + U_i\frac{dH}{d\tau} - \frac{2}{H}U_i \tag{9b}$$

Addition of the two equations leads to the single differential equation

$$\frac{d(U_iH)}{d\tau} + \frac{2}{H}U_i = U_b\frac{dH}{d\tau} \tag{10a}$$

The solution of this equation, for linear growth

$$H = 1 + p\tau \tag{6}$$

and initial value

$$U_i(0) = U_0 \tag{10b}$$

is

$$U_i(\tau) = \frac{\exp\left[\frac{-2\tau}{1+p\tau}\right]}{1+p\tau}U_0 + U_b\left[1 - \frac{\exp\left[\frac{-2\tau}{1+p\tau}\right]}{1+p\tau} + \frac{2}{p}\frac{\exp\left[\frac{-2\tau}{1+p\tau}\right]}{1+p\tau}e^{2/p}\left\{Ei\left(\frac{-2/p}{1+p\tau}\right) - Ei(-2/p)\right\}\right] \tag{11a}$$

From (9*a*) we then obtain

$$U_i(\tau) = \frac{pU_b + \frac{2}{1+p\tau}U_1}{p + \frac{2}{1+p\tau}} \tag{11b}$$

The curves $U_i(\tau)$, $U_1(\tau)$ are plotted in Figs. 3(*a* and *b*) for the initial value

$$U_0 = U_b \tag{12}$$

and the Peclet numbers 8, 4, 2, 1, 1/2, 1/4, 1/8.[7] It may be mentioned that the calculation of Figs. 3(*a* and *b*) took but a small fraction of the time required for calculation of the rigorous solution in Fig. 2 for the single Peclet number, $p = 1$.

## IV Simplified and Primitive Solutions

If, in contrast to Fig. 4(*a*), we approximate the liquid column by two capacities, one resistance, then we obtain the "simplified" model of Fig. 4(*b*). Since the lower capacity is maintained at the ambient temperature $\vartheta_a$, there is now effectively only a single node, $\vartheta_i$, involved in the problem. Proceeding as before we find the differential equation

$$\frac{1}{2}\frac{d(U_iH)}{d\tau} = U_b\frac{dH}{d\tau} - \frac{U_i}{H} - \frac{1}{2}U_i\frac{dH}{d\tau} \tag{13a}$$

The last term represents the heat flow due to mass transfer.

The solution for linear growth, $H = 1 + p\tau$, is

$$U_i(\tau) = \frac{\exp\left[\frac{-2\tau}{1+p\tau}\right]}{(1+p\tau)^2}U_0 + U_b\left[1 - \frac{2/p}{1+p\tau} - \frac{\exp\left[\frac{-2\tau}{1+p\tau}\right]}{(1+p\tau)^2}\left\{1 - \frac{2}{p} + \frac{4e^{2/p}}{p^2}\left[Ei\left(-\frac{2/p}{1+p\tau}\right) - Ei(-2/p)\right]\right\}\right] \tag{13b}$$

$U_i$ is plotted in Figs. 2(*a* and *b*) for $p = 1$, $U_0 = U_b$. It is seen that the one-node approximation is inferior to the approximation of Section III, but the results still may be used in a cautiously quantitative fashion.

An inferior 1-node approximation is illustrated in Fig. 4(*c*).[8] Here all the capacity is concentrated in the condenser at the top. The governing differential equation is

$$\frac{d(U_iH)}{d\tau} = U_b\frac{dH}{d\tau} - \frac{U_i}{H} \tag{14a}$$

[5] From Fig. 3(*a*): $p_\tau < 1$ at the minimum for small $p$, $> 1$ for large $p$.

[6] We follow the method developed by Gaever and Horvay in an earlier work [3*b*].

[7] In the figure we write $U(H, \tau)$, $U(H/2, \tau)$ in place of $U_i(\tau)$, $U_1(\tau)$.

[8] This "primitive" approximation offers no advantages in the present problem, but may do so in more complicated problems, see discussion of Fig. 11.

and the corresponding solution is, see Fig. 2(*b*)

$$U_1(\tau) = \frac{\exp\left[\frac{-\tau}{1+p\tau}\right]}{1+p\tau}\,U_0 + U_b\left[1 - \frac{\exp\left[\frac{-\tau}{1+p\tau}\right]}{1+p\tau}\right.$$

$$\left.\left\{1 - \frac{e^{1/p}}{p}\left[Ei\left(\frac{-1/p}{1+p\tau}\right) - Ei(-1/p)\right]\right\}\right] \quad (14b)$$

## V Multinode Approximation[9]

In Fig. 5 we illustrate the case of the $n+1$-node approximation, for $n = 3$. The Kirchhoff's equations now become

$$0 = U_b\frac{dH}{d\tau} - \frac{6}{H}(U_1 - U_1) - U_1\frac{dH}{d\tau} \quad (15a)$$

$$\frac{1}{3}\frac{d(U_1H)}{d\tau} = \frac{6}{H}(U_1 - U_1) - \frac{3}{H}(U_1 - U_2) + U_1\frac{dH}{d\tau} - \frac{2}{3}U_1\frac{dH}{d\tau} \quad (15b)$$

$$\frac{1}{3}\frac{d(U_2H)}{d\tau} = \frac{3}{H}(U_1 - U_2) - \frac{3}{H}(U_2 - U_3) + \frac{2}{3}U_1\frac{dH}{d\tau} - \frac{1}{3}U_2\frac{dH}{d\tau} \quad (15c)$$

$$\frac{1}{3}\frac{d(U_3H)}{d\tau} = \frac{3}{H}(U_2 - U_3) - \frac{6}{H}U_3 + \frac{1}{3}U_2\frac{dH}{d\tau} \quad (15d)$$

Because of the excellence of the two-node approximation there did not seem to be much point to working out a numerical example on the basis of Equations (15). Of greater interest is the establishment of the limiting form which equations of the type (15) assume for the case $n \to \infty$.

Equation (15c) may be written as

$$\frac{H}{3}\frac{dU_2}{d\tau} + U_2\frac{d\left(\frac{2}{3}H\right)}{d\tau} = \frac{3}{H}(U_1 - 2U_2 + U_3) + U_1\frac{d\left(\frac{2}{3}H\right)}{d\tau} \quad (16)$$

Denoting furthermore ($\lambda$ is not to be confused with the heat of fusion)

$$\frac{2}{3}H = \lambda H, \quad \frac{1}{3}H = Hd\lambda, \quad U_1 - U_2 = dU \quad (0 \leqslant \lambda \leqslant 1) \quad (17)$$

Equation (16) becomes

$$Hd\lambda\frac{\partial U}{\partial\tau} - \lambda dU\frac{dH}{d\tau} = \frac{d^2U}{Hd\lambda}$$

i.e.,

$$\frac{\partial U}{\partial\tau} - \frac{\lambda}{H}\frac{\partial U}{\partial\lambda}\frac{dH}{d\tau} = \frac{1}{H^2}\frac{\partial^2 U}{\partial\lambda^2} \quad (18)$$

subject to the initial and boundary conditions[10]

$$\tau = 0: \quad U = U_0(\lambda) \quad (19a)$$

$$\lambda = 0: \quad U = 0 \quad (19b)$$

$$\lambda = 1: \quad [U_b - U_1]\frac{dH}{d\tau} = \frac{1}{H}\frac{\partial U}{\partial\lambda} \quad (19c)$$

where $H$ is a prescribed function of $\tau$. Equation (18) was previously derived, in a different manner, by H. G. Landau [5].

Whereas the finite difference approximations (9) or (15), to (18), are very convenient both for numerical and for analog computations, the partial differential equation (18) is exceedingly awkward to use, and therefore no attempt was made to numerically verify that solution of the problem (18), (19) coincides with that of (1), (2).

## VI Freezing of a Growing Liquid Column

We represent the system of Fig. 1 by the 4-node circuit in Fig. 6. Heat enters at the top of the liquid column (which is of length $Y$ and original temperature $\vartheta_0$), then passes through the frozen column (of length $X$) and the mold (of length $L$), to the heat sink at the bottom, which is maintained at the ambient temperature $\vartheta_a$. $\vartheta_l$ is the temperature at the top of the liquid column, $\vartheta_f$ is the fusion temperature, $\vartheta_s$ the temperature at the bottom of the solidified portion, and $\vartheta_m$ the temperature at the center of the mold. The quantities whose time variation we want to determine are, in order of importance, $X$, $\vartheta_l$, $\vartheta_s$, and $\vartheta_m$.

Evidently, we are representing the liquid and frozen columns in Fig. 6 by the less accurate Fig. 4(*b*), the mold by the more

[9] Similar ideas are developed also by D. R. Otis, Proceedings, 1956, Heat Transfer Institute, Stanford, Calif.; and by W. D. Murray and F. Landis, JOURNAL OF HEAT TRANSFER, TRANS. ASME, series C, vol. 81, 1959, pp. 106–120, using the Landau equation (18) as starting point, and converting it into a system of difference equations.

[10] Condition (19c) results from (15a).

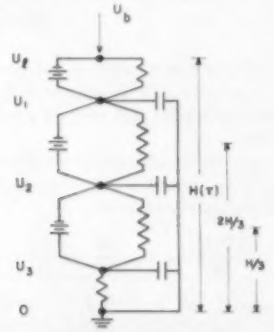


Fig. 5 The multinode model for the growing liquid column

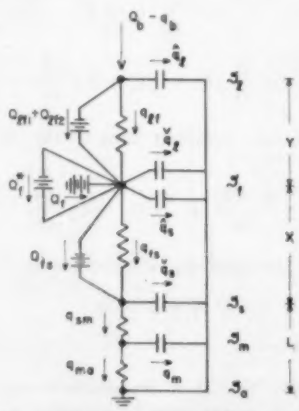


Fig. 6 Simplified circuit model for the freezing of a growing liquid column

accurate Fig. 4(*a*). Since our main interest is the development of the *simplest* circuit which represents the foregoing four quantities to correct orders of magnitude (so that the results may be used for semiquantitative predictions in continuous casting problems), we refrained from using the more elaborate Fig. 4(a) for the liquid and frozen portions.[11]

The Kirchhoff circuit laws at the four nodes give

$$\left.\begin{aligned} \vartheta_l:\ & q_l = Q_b - q_b - q_{lf} - Q_{lf'} - Q_{lf''} \\ \vartheta_f:\ & \check{q}_l + \check{q}_s = Q_f + q_{lf} - q_{fs} + Q_{lf'} \\ & \qquad + Q_{lf''} - Q_f^* + Q_f^* - Q_{fs} \\ \vartheta_s:\ & \check{q}_s = q_{fs} - q_{sm} + Q_{fs} \\ \vartheta_m:\ & q_m = q_{sm} - q_{ma} \end{aligned}\right\} \tag{20}$$

In the foregoing

$$Q_b = \gamma c(\vartheta_b - \vartheta_a)v \quad (v = d(X+Y)/dt) \tag{21}$$

is the heat supplied per unit time

$$q_b = h_r(\vartheta_l - \vartheta_a) \tag{22}$$

is the radiation loss from the liquid metal surface (for which we also allow in our analysis; $h_r$ is the heat-transfer coefficient to the ambient),

$$\left.\begin{aligned} q_l &= \frac{d}{dt}\frac{\gamma c(\vartheta_l - \vartheta_a)Y}{2}, \quad \check{q}_l = \frac{d}{dt}\frac{\gamma c(\vartheta_f - \vartheta_a)Y}{2} \\ q_s &= \frac{d}{dt}\frac{\gamma c(\vartheta_f - \vartheta_a)X}{2}, \quad \check{q}_s = \frac{d}{dt}\frac{\gamma c(\vartheta_s - \vartheta_a)X}{2} \\ q_m &= \frac{d}{dt}[\Gamma C(\vartheta_m - \vartheta_a)L] \end{aligned}\right\} \tag{23}$$

are the charging currents (we assume the metal properties to be the same in the liquid phase and in the solid phase; conductivity, density, and specific heat of the mold material are denoted by $K, \Gamma, C$),

$$Q_f = \gamma\lambda dX/dt \tag{24}$$

is the latent heat current produced during solidification, and

[11] That would have added two more nodes to our circuit representation, at the centers of the two sections. We state the equations for this more elaborate model in Appendix 2.

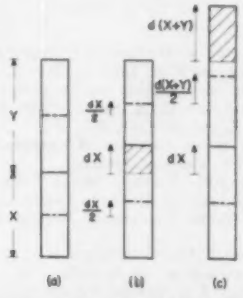


**Fig. 7 Explanation of the mass transfer terms due to freezing and to growth of column. See text after Equations (27).**

$$\left.\begin{aligned} q_{lf} &= k(\vartheta_l - \vartheta_f)/Y, \quad q_{fs} = k(\vartheta_f - \vartheta_s)/X \\ q_{sm} &= \frac{\vartheta_s - \vartheta_m}{\left(\frac{1}{K} + \frac{1}{K_s}\right)L/2}, \quad q_{ma} = \frac{K(\vartheta_m - \vartheta_a)}{L/2} \end{aligned}\right\} \tag{25}$$

are the conduction currents from $l$ to $f$, from $f$ to $s$, from $s$ to $m$ (here we included also a contact resistance term

$$\frac{1}{h_s} \equiv \frac{L}{2K_s} \tag{26}$$

to represent the airgap resistance between frozen metal and mold), and from $m$ to $a$. Finally,

$$\left.\begin{aligned} Q_{lf'} &= \frac{1}{2}\gamma c(\vartheta_l - \vartheta_a)v, \quad Q_{lf''} = \frac{1}{2}\gamma c(\vartheta_l - \vartheta_a)dX/dt \\ Q_f^* &= \gamma c(\vartheta_f - \vartheta_a)dX/dt, \quad Q_{fs} = \frac{1}{2}\gamma c(\vartheta_f - \vartheta_a)dX/dt \end{aligned}\right\} \tag{27}$$

are the mass-transfer terms.

The latter terms are more clearly illustrated in Fig. 7. The column in Fig. 7(*a*) represents the heat content in the frozen and liquid sections $X + Y$ at time $t$; dashed lines separate the heats assigned to the upper and lower condensers. In time $dt$ the freezing front progresses through a distance $dX$. The corresponding heat, $Q_f^* dt$ shown by cross-hatching in Fig. 7(*b*), is thus transferred from the lower liquid condenser to the upper solid condenser. (The two terms, $-Q_f^* + Q_f^*$, in the $\vartheta_f$ equation of (20) are self-canceling, because of the coincidence of the two condensers.) The lower liquid condenser regains heat $Q_{lf'}dt$ (it regains height $dX/2$) from the upper liquid condenser which, correspondingly, loses this amount of heat. Finally, $Q_{fs}dt$ represents the heat lost by the upper half of the frozen column to the lower half, because of the rise, by $dX/2$, of the separation line. Besides the changes brought about by the motion of the freezing front, there are additional changes caused by the rise of the liquid column surface by amount $d(X + Y)$. Clearly the separation line of the two halves of the liquid metal must be raised by $d(X + Y)/2$; thus the upper half loses to the lower half also heat $Q_{lf'}dt$.[12]

We now introduce, in addition to (3), also the notations

$$\Xi \equiv X/Y_0, \qquad \nu \equiv hY_0/k \ (= \text{Nusselt number})[13]$$

$$m = \frac{\Gamma CL}{\gamma c Y_0}, \quad \rho_1 = \frac{\left(\frac{1}{K} + \frac{1}{K_s}\right)L/2}{Y_0/k}, \quad \rho_2 = \frac{L/2K}{Y_0/k} \tag{28a}$$

and replace definition (4) of the Peclet number, in accordance with (21), by

$$p \equiv Y_0 v/\kappa = \dot{H} + \dot{\Xi} \tag{28b}$$

We also replace the radiation loss term (22) by the simpler expression

$$q_b = h_r(\vartheta_f - \vartheta_a) \tag{28c}$$

[12] Note that when there is melt-out, the direction of the $dX$ flow reverses; heat is transferred from the solid phase, at temperature $\vartheta_f$, to the liquid phase at the higher temperature $\vartheta_l$; the representative circuit element for mass transfer must therefore be a battery; see [3*b*].

[13] It would be equally appropriate to refer to $\nu$ as the "Biot number," since the conductivity of the liquid and solid phases is the same.

(Since the superheat is usually quite small, this change represents an insignificant error.)[14] On multiplying Equations (20) by $cY_0/\lambda k$ we are thus led to the governing equations for the system of Fig. 6 in nondimensional form:

$$\left.\begin{aligned}
\vartheta_l:\ & \frac{1}{2}\frac{d(U_l H)}{d\tau} = pU_b - \nu U_f - \frac{U_l - U_f}{H} \\
& \qquad - \frac{p}{2}U_l - \frac{1}{2}U_l\frac{d\Xi}{d\tau} \\
\vartheta_f:\ & \frac{p}{2}U_f = \frac{d\Xi}{d\tau} + \frac{U_l - U_f}{H} - \frac{U_f - U_s}{\Xi} \\
& \qquad + \frac{p}{2}U_l + \frac{1}{2}(U_l - U_f)\frac{d\Xi}{d\tau} \\
\vartheta_s:\ & \frac{1}{2}\frac{d(U_s\Xi)}{d\tau} = \frac{U_f - U_s}{\Xi} - \frac{U_s - U_m}{\rho_1} \\
& \qquad + \frac{1}{2}U_f\frac{d\Xi}{d\tau} \\
\vartheta_m:\ & m\frac{dU_m}{d\tau} = \frac{U_s - U_m}{\rho_1} - \frac{U_m}{\rho_2}
\end{aligned}\right\} \quad (29)$$

We shall adopt the system (29) in [4] to problems of continuous casting. This will involve replacement of some of the ordinary time derivatives in (29) by convective derivatives. In the present paper we restrict ourselves to exhibiting the principle features of the solution of Equations (29) for the very simple case where the column bottom (node $\vartheta_s$) is maintained at a temperature $\vartheta_s < \vartheta_f$ (the last two equations of (29) are thereby eliminated); the growth rate $v$ is a constant

$$\left.\begin{aligned}
& \dot{H} + \dot{\Xi} = p = \text{const} \\
& H = 1 + p\tau - \Xi
\end{aligned}\right\} \quad (30)$$

and the radiation loss ($\nu U_f$) is negligible. Then Equations (29) reduce to

$$\vartheta_l:\ \frac{H}{2}(U_l - U_f)^{\cdot} + \left(p + \frac{1}{H}\right)(U_l - U_f) = p(U_b - U_f) \quad (31a)$$

$$\vartheta_f:\ \frac{1}{2}(\Xi^2)^{\cdot}\left[1 + \frac{1}{2}(U_l - U_f)\right] + \Xi\left(\frac{p}{2} + \frac{1}{H}\right)(U_l - U_f) = U_f \quad (31b)$$

In Fig. 8 we show solution $\Xi(\tau)$, $U_l(\tau)/U_b$ of this equation system, obtained on the Reeves Electronic Analog Computer by R. Noorda, for the initial conditions

$$\Xi(0) = 0, \quad U_l(0) = U_b \quad (32a)$$

the supply speed

$$p = 1 \quad (32b)$$

and the parameter values

$$\left.\begin{aligned}
&(a) \quad U_b = 1.0, \quad U_f = 0 \\
&(b) \quad U_b = 1.70, \quad U_f = 1.60 \\
&(c) \quad U_b = 0.20, \quad U_f = 0.10 \\
&(d) \quad U_b = 1.60, \quad U_f = 1.60
\end{aligned}\right\} \quad (33)$$

Case ($a$) is identical with the problem treated earlier by the simplified solution, the growing liquid column, without any freezing ($\vartheta_s \geq \vartheta_f$). The excellent agreement between the calculated curve Figs. 2($a$ and $b$), and the computer curve Fig. 8($a$) is noted. Case ($b$) is representative for aluminum, with $\vartheta_b - \vartheta_f = 65$ deg superheat and $\vartheta_s = 170$ deg ambient ($k = 120$, $\gamma = 170$, $c = 0.26$, $\lambda = 170$, $\vartheta_f = 1220$; lb, ft, hr, Fahrenheit units); case ($c$) corresponds to aluminum with 65 deg superheat, and an ambient 65 deg below fusion temperature. In case ($d$) the bath is originally at the fusion temperature.

From (31$b$) one notes that for $\tau \ll 1$:

$$\Xi = 2\omega\sqrt{\tau} \quad (34a)$$

$$\omega^2 = \frac{\frac{1}{2}U_f}{1 + \frac{1}{2}(U_l - U_f)} = \frac{\frac{1}{2}\frac{c}{\lambda}(\vartheta_f - \vartheta_s)}{1 + \frac{1}{2}\frac{c}{\lambda}(\vartheta_l - \vartheta_f)} \quad (34b)$$

$\omega$ is known as the "solidification" parameter [6].[15]

In Fig. 8 curves $(\Xi^2)^{\cdot}/2U_b$ are also plotted. From their initial values $U_f \Big/ \left(1 + \frac{1}{2}U_b - \frac{1}{2}U_f\right)U_b$, at $\tau = 0$, the curves are seen to rise to a slight maximum around the $\tau$ value where $U_l/U_b$ is a minimum (conduction at this $\tau$ is most "effective", hence the temperature gradient across the liquid most conducive to speeding up the freezing front); thereafter $(\Xi^2)^{\cdot}$ drops slowly but continuously, because of the continuous replenishment of the superheat of the liquid. When pouring is at the fusion temperature, see Fig. 8($d$), then the replenishment is eliminated, $(\Xi^2)^{\cdot}$ = constant, and, so far as the freezing front is concerned, this moves as if the liquid column were semi-infinite; the $2\omega\sqrt{\tau}$ law holds now for all times.[16]

## Acknowledgment

I am indebted to Miss E. J. Miller for performing the tedious calculations for the curves of Figs. 2 to 13; and to R. Noorda of the Users Industries Sales Department for programming the curves of Fig. 8 on the REAC. The reading of the papers by London-Seban [2] and D. L. Cochran [7] contributed to a better understanding of the freezing problem, and suggested the approach used in [3$a$]. The technique of representing heat flow problems with variable masses by means of circuits of type Fig. 5 was first developed in conjunction with I. Giaever [3$b$].

## References

1 C. C. Chao and J. H. Weiner, "Heat Conduction in Semi-Infinite Solid in Contact With Linearly Increasing Mass of Fluid," *Quarterly of Applied Mathematics*, vol. 14, 1956, p. 214.

2 A. L. London and R. A. Seban, "The Rate of Ice Formation," TRANS. ASME, vol. 65, 1943, p. 771.

3$a$ G. Horvay, "Some Problems of Continuous Casting, I," to be submitted shortly to a technical journal.

3$b$ I. Ginever and G. Horvay, "Some Problems of Continuous Casting, II," to be submitted shortly to a technical journal.

4 G. Horvay, "Some Problems of Continuous Casting, III," in preparation.

5 H. G. Landau, "Heat Conduction in a Melting Solid," *Quarterly of Applied Mathematics*, vol. 8, 1950, p. 21.

6 G. Horvay and J. G. Henzel, "Freezing of Liquid Metal in a Mold," *Trans. AIME*, vol. 215, 1959, p. 258.

7 D. L. Cochran, "Rate of Solidification; Application and Extension of Theory," Stanford Univ. ONR Tech. Rept. No. 24, 1955.

[14] If desired, we may incorporate some of the change in a suitably redefined $h_r$.

[15] For $c(\vartheta_f - \vartheta_s)/\lambda = 0.2, 2.0$, Equation (34$b$) gives $\omega = 0.32, 1.0$ when $\vartheta_l = \vartheta_f$, and 0.30, 0.95 when $c(\vartheta_l - \vartheta_f)/\lambda = 0.2$; the rigorous solution from Fig. 4($a$, $b$, $c$), of [6] gives 0.31, 0.80, and 0.18, 0.73 for these cases. An improved expression for $\omega^2$, (46), is derived in Appendix 2.

[16] The jags in the $\Xi$ curves result from the inaccuracy of the square root generating circuit in the Analog Computer.

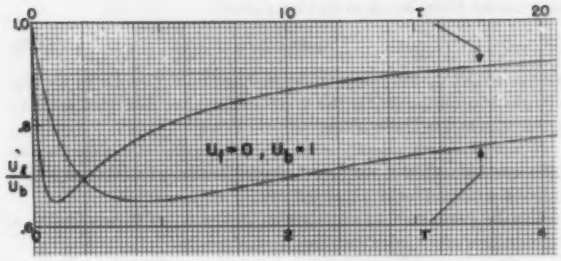


Fig. 8(a)

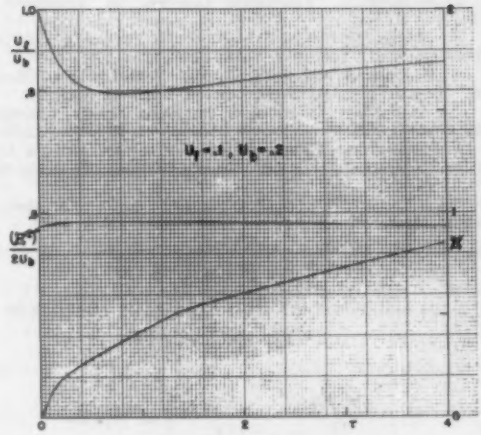


Fig. 8($c_1$)

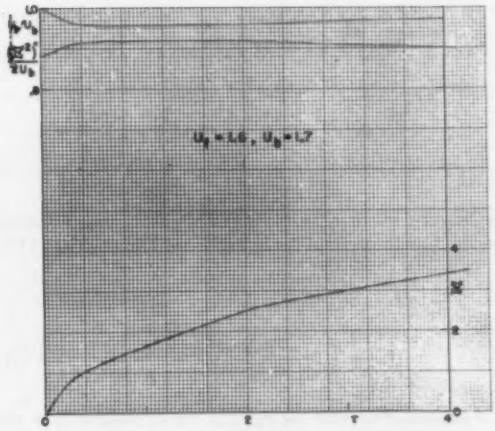


Fig. 8($b_1$)

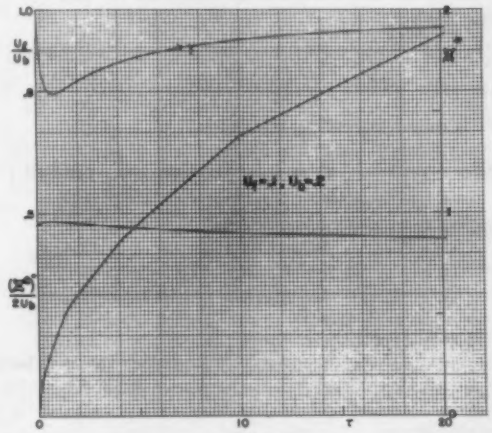


Fig. 8($c_2$)

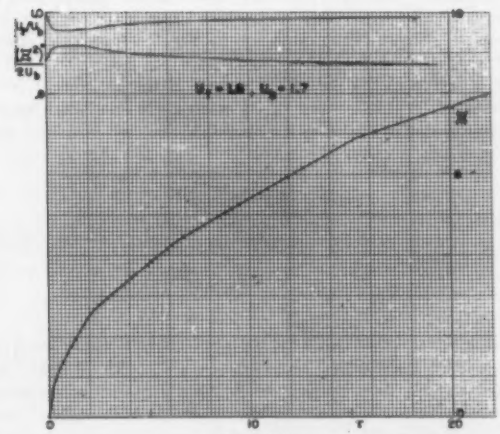


Fig. 8($b_2$)

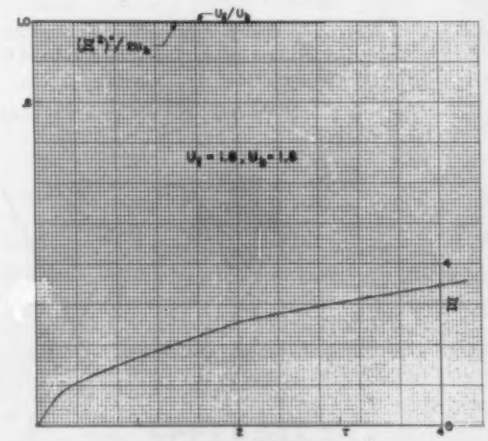


Fig. 8(d)

**Fig. 8 Motion $\Xi(\tau)$ of the freezing front, and the temperature $U_l(\tau)$ of the liquid top are illustrated for initial conditions $\Xi(0) = 0$, $U_l(0) = U_b$ (= pouring temperature), boundary condition $U(0, \tau) = 0$, Peclet number 1; and for the parameter values (a) $U_b = 1$, $U_f = 0$; (b), $U_b = 1.7$, $U_f = 1.6$; (c) $U_b = 0.2$, $U_f = 0.1$; (d) $U_b = U_f = 1.6$.**

**These cases are representative for aluminum when (a) ambient is above fusion temperature; (b) aluminum is poured at 65 deg superheat, ambient is at 170 deg; (c) aluminum is poured at 65 deg superheat, ambient is at 65 deg below fusion temperature; (d) aluminum is poured at fusion temperature, ambient is at 170 deg.**

8 I. N. Sneddon, "Functional Analysis," in "Handbuch der Physik," vol. II, Springer Verlag, Berlin, Germany, 1955.
9 W. Flügge, "Tables of Transcendental Functions," McGraw-Hill Book Company, Inc., New York, N. Y., 1954.
10 H. S. Carslaw and J. C. Jaeger, "Conduction of Heat in Solids," Oxford University Press, London, England, 1947.
11 H. E. Saltzer, "Method of Summing Slowly Convergent Series," *Journal of Mathematics and Physics*, vol. 33, 1955, p. 356.
12 T. R. Goodman, "The Heat-Balance Integral and Its Application to Problems Involving a Change of Phase," TRANS. ASME, vol. 80, 1958, p. 335.
13 P. L. Chambré, "On the Dynamics of Phase Growth," *Quarterly Journal of Mechanics and Applied Mathematics*, vol. 9, 1956, p. 224.

## APPENDIX 1

## Rigorous Solution of the Heat Conduction Equation in a Growing Liquid Column

On denoting

$$A_k(\tau) \equiv \int_0^H \left[1 - \frac{U(\eta, \tau)}{U_b}\right] \sin(\zeta_k \eta) d\eta \tag{35}$$

and taking the sine transform of Equations (1) and (2) there results (see e.g., Sneddon [8], pp. 309–312)

$$\frac{dA_k}{d\tau} + \zeta_k^2 A_k = \zeta_k, \quad A_k(0) = 0 \tag{36}$$

which is solved by

$$A_k(\tau) = \exp\left[-\int_0^\tau \zeta_k^2 d\tau\right] \int_0^\tau \zeta_k(\tau) \exp\left[\int_0^\tau \zeta_k^2(\lambda) d\lambda\right] d\tau \tag{37}$$

By the inversion theorem there follows

$$1 - \frac{U}{U_b} = 2 \sum_1^\infty \frac{\dot{H}^3 + \zeta_k^3}{H(\dot{H}^3 + \zeta_k^3) + \dot{H}} A_k \sin \zeta_k \eta \tag{38}$$

i.e., solution (5) of the text.

Formally (see e.g., Sneddon [8]) Equations (5) are identical with the solution of the heat conduction equation subject to the "radiative boundary condition;" only (5*b*) is replaced in the latter problem by

$$\alpha \cot \alpha + C = 0 \tag{39}$$

where $C$ is the heat-transfer coefficient from the ambient atmosphere to the conducting medium (which is assumed to be of fixed height). In the present problem

$$C \equiv H\dot{H} \tag{40a}$$

depends on time, hence so do also $\alpha_k$ and

$$\zeta_k \equiv \alpha_k / H \tag{40b}$$

For constant $\zeta_k$ the integrations in Equation (5) lead to an elementary formula for $A_k$; the nonconstant case does not seem to have been treated heretofore.

When $H$ varies linearly with time, as in (6) (the case we are interested in), then a very good closed-form approximation $\bar{A}_k(\tau)$ may be obtained for $A_k(\tau)$ as follows.

If it be permitted to visualize $\alpha_k$ in the $A_k(\tau)$ expression as a time-independent constant $\bar{\alpha}_k$, then

$$\bar{A}_k(\tau) = \bar{\alpha}_k \exp\left[-\bar{\alpha}_k^2 \int_0^\tau \frac{d\tau}{(1+p\tau)^2}\right] \int_0^\tau \frac{d\tau}{1+p\tau} \exp\left[\bar{\alpha}_k^2 \int_0^\tau \frac{d\lambda}{(1+p\lambda)^2}\right]$$
$$= -\frac{\bar{\alpha}_k}{p} \exp\left[\frac{\bar{\alpha}_k^2/p}{1+p\tau}\right] \int_{-\bar{\alpha}_k^2/p}^{-\bar{\alpha}_k^2/p(1+p\tau)} \frac{e^v dv}{v}$$
$$= \frac{\bar{\alpha}_k}{p} \exp\left[\frac{\bar{\alpha}_k^2/p}{1+p\tau}\right] \left\{- Ei\left(\frac{-\bar{\alpha}_k^2/p}{1+p\tau}\right) + Ei(-\bar{\alpha}_k^2/p)\right\} \tag{41a}$$

For values of $\tau$ where $\alpha_k^2/p(1+p\tau) > 10$, (41*a*) may furthermore be replaced by the asymptotic formula (see Flügge [9], p. 116)

$$\bar{A}_k(\tau) = \frac{1}{\bar{\alpha}_k}\left[1 + p\tau - \frac{p(1+p\tau)^2}{\bar{\alpha}_k^2} - \left(1 - \frac{p}{\bar{\alpha}_k^2}\right) \exp\left\{-\frac{\bar{\alpha}_k^2}{p} \frac{p\tau}{1+p\tau}\right\}\right] \tag{41b}$$

Is it permitted to treat the $\alpha_k(\tau)$ in the $A_k$ integrands as suitable constants $\bar{\alpha}_k$? We note from Table 1 (which extends the table in Carslaw-Jaeger [10], p. 378, for suitable values of $C$, to $k = 12$) that $\alpha_k$ varies from $(k - 1/2)\pi$ to $k\pi$ as $C = p(1 + p\tau)$ varies from 0 to $\infty$. Evidently $\alpha_1$ is the root of (39) most sensitive to variation in $\tau$. Let us write $A_k^*$, $A_k^{**}$, $\bar{A}_k$ for $\bar{A}_k(\tau)$ in formula (41) when we define $\bar{\alpha}_k$ by its smallest value $\alpha_k(0)$, by its largest value $\alpha_k(\tau)$, and by its mean value $[\alpha_k(0) + \alpha_k(\tau)]/2$, respectively, in the interval 0, $\tau$. In Fig. 9 we plot the curves $(A_1^* - \bar{A}_1)/\bar{A}_1$ and $(A_1^{**} - \bar{A}_1)/\bar{A}_1$, for the case $p = 1$. The error involved in the use of $\bar{A}_1$ instead of the rigorous $A_1(\tau)$ is represented by the *deviation of the mean of the two curves from 0*. Evidently, this deviation is less than 0.25 per cent for $\tau < 1$, and

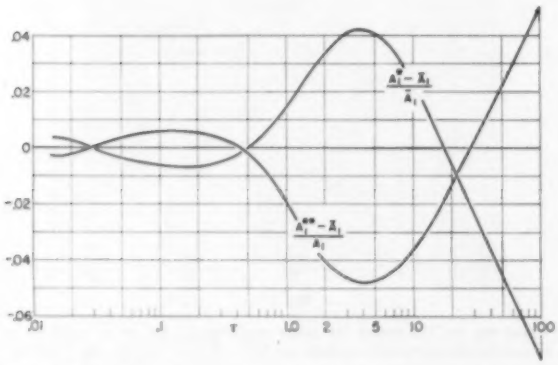


**Fig. 9 Illustration of the error involved in using a mean value $\bar{\alpha}_1$ instead of $\alpha_1(\tau)$ in formula (37). The deviation of the mean of the two curves from zero represents the error.**

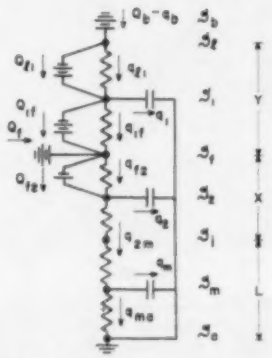


**Fig. 10 Approximate circuit model for the freezing of a growing liquid column**

**Table 1**

Roots $\alpha_k$ of $\alpha \operatorname{Cot} \alpha + C = 0$

| C \ k | 1 | 2 | 3 | 4 | 5 | 6 | 7 | 8 | 9 | 10 | 11 | 12 |
|---|---|---|---|---|---|---|---|---|---|---|---|---|
| 1.00 | 2.0288 | 4.9132 | 7.9787 | 11.086 | 14.208 | 17.336 | 20.469 | 23.604 | 26.741 | 29.879 | 33.017 | 36.156 |
| 1.02 | 2.0354 | 4.9169 | 7.9811 | 11.088 | 14.209 | 17.338 | 20.470 | 23.605 | 26.742 | 29.879 | 33.018 | 36.156 |
| 1.04 | 2.0419 | 4.9207 | 7.9835 | 11.090 | 14.210 | 17.339 | 20.472 | 23.606 | 26.743 | 29.880 | 33.019 | 36.157 |
| 1.10 | 2.0610 | 4.9318 | 7.9908 | 11.095 | 14.214 | 17.342 | 20.474 | 23.609 | 26.745 | 29.882 | 33.021 | 36.159 |
| 1.20 | 2.0917 | 4.9502 | 8.0028 | 11.104 | 14.221 | 17.348 | 20.479 | 23.613 | 26.749 | 29.886 | 33.024 | 36.162 |
| 1.40 | 2.1483 | 4.9862 | 8.0268 | 11.122 | 14.235 | 17.360 | 20.489 | 23.622 | 26.756 | 29.892 | 33.030 | 36.168 |
| 2.00 | 2.2889 | 5.0870 | 8.0962 | 11.173 | 14.276 | 17.393 | 20.518 | 23 647 | 26.779 | 29.912 | 33.048 | 36.183 |
| 4.00 | 2.5704 | 5.3540 | 8.3029 | 11.335 | 14.408 | 17.503 | 20.614 | 23.730 | 26.853 | 29.978 | 33.108 | 36.239 |
| 8.00 | 2.8044 | 5.6669 | 8.6031 | 11.599 | 14.637 | 17.703 | 20.805 | 23.896 | 27.000 | 30.111 | 33.228 | 36.348 |
| 15.00 | 2.9478 | 5.9080 | 8.8898 | 11.896 | 14.925 | 17.974 | 21.068 | 24.141 | 27.225 | 30.319 | 33.420 | 36.529 |
| 40.00 | 3.0651 | 6.1311 | 9.1987 | 12.269 | 15.342 | 18.418 | 21.454 | 24.520 | 27.584 | 30.649 | 33.715 | 36.779 |
| 100.00 | 3.1105 | 6.2211 | 9.3317 | 12.443 | 15.554 | 18.665 | 21.773 | 24.884 | 27.994 | 31.105 | 34.216 | 37.326 |

**Table 2**

$\bar{A}_k(\tau)$

| τ \ k | 1 | 2 | 3 | 4 | 5 | 6 | 7 | 8 | 9 | 10 | 11 | 12 |
|---|---|---|---|---|---|---|---|---|---|---|---|---|
| 1.00 | 0 | 0 | 0 | 0 | 0 | 0 | 0 | 0 | 0 | 0 | 0 | 0 |
| 1.02 | .03868 | .07731 | .09037 | .08320 | .07008 | .05848 | .04957 | .04313 | .03809 | .03410 | .03087 | .02819 |
| 1.04 | .07368 | .1256 | .1176 | .09222 | .07279 | .05978 | .05068 | .04397 | .03883 | 03477 | .03147 | .02874 |
| 1.10 | .1625 | .1918 | .1351 | .09829 | .07698 | .06321 | .05359 | .04650 | .04107 | .03677 | .03329 | .03040 |
| 1.20 | .2723 | 2280 | .1473 | .1071 | .08392 | .06892 | .05844 | .05072 | .04479 | .04010 | .03630 | .03316 |
| 1.40 | .4155 | .2665 | .1712 | .1247 | .09777 | .08032 | .06813 | .05914 | .05225 | .04678 | .04234 | .03867 |
| 2.00 | .6550 | .3680 | .2411 | .1768 | .1390 | .1144 | .09714 | .08436 | .07453 | .06675 | .06043 | .05521 |
| 4.00 | 1.122 | .6866 | .4615 | .3454 | .2741 | .2266 | .1929 | .1678 | .1484 | .1330 | .1206 | .1102 |
| 8.00 | 1.769 | 1.222 | .8726 | .6614 | .5333 | .4447 | .3804 | .3321 | .2944 | .2643 | .2398 | .2193 |
| 15.00 | 2.561 | 1.992 | 1.504 | 1.183 | .9569 | .8087 | .6971 | .6118 | .5444 | .4900 | .4454 | .4080 |
| 40.00 | 4.186 | 3.937 | 3.302 | 2.755 | 2.333 | 2.009 | 1.735 | 1.548 | 1.393 | 1.264 | 1.156 | 1.064 |
| 100.00 | 6.054 | 6.692 | 6.241 | 5.592 | 4.972 | 4.429 | 3.972 | 3.585 | 3.261 | 2.984 | 2.712 | 2.520 |

less than 2.5 per cent for $\tau < 100$; for higher $k$ the error of using $\bar{A}_k(\tau)$ instead of $A_k(\tau)$ is completely negligible. Thus it is demonstrated that $A_k$ may be replaced, for all practical purposes, by $\bar{A}_k$. The $\bar{A}_k(\tau)$ functions ($k = 1, \ldots, 12$) so determined are tabulated for $p = 1$ in Table 2. Once the $\bar{A}_k(\tau)$ are available, one readily determines $B_k(\tau)$ by (5c). Next the series (5a) is calculated, but one finds that the series converges very slowly, and the 12-term summation we used is insufficient. However, one easily extrapolates $\sum_1^{12}$ to $\sum_1^{\infty}$ by Saltzer's method [11] (a graphical extrapolation is adequate), and one then obtains the $U(\eta, \tau)/U_b$ plots, $\eta = H, H/2, 1$, shown in Fig. 2(a).

## APPENDIX 2

### Alternate Models for the Freezing Problem

In Fig. 10 we replace the 4-node representation of Fig. 6 by a more elaborate 6-node model. We now label the station at the interface of frozen metal and mold by $\vartheta_i$ rather than by $\vartheta_s$. The current balance equations are

$$
\left.\begin{aligned}
&\vartheta_i\text{:}\quad 0 = Q_b - q_b - q_{ii} - Q_{ii}\\
&\vartheta_1\text{:}\quad q_1 = q_{ii} - q_{if} + Q_{ii} - Q_{if}\\
&\vartheta_f\text{:}\quad 0 = Q_f + q_{if} - q_{fs} + Q_{if} - Q_{fs}\\
&\vartheta_2\text{:}\quad q_2 = q_{fs} - q_{si} + Q_{fs}\\
&\vartheta_i\text{:}\quad 0 = q_{si} - q_{im}\\
&\vartheta_m\text{:}\quad q_m = q_{im} - q_{ma}
\end{aligned}\right\}
$$

where

$$
\left.\begin{aligned}
&Q_b = \gamma c(\vartheta_b - \vartheta_a)d\,(X + Y)/dt, \qquad q_b = h_r(\vartheta_i - \vartheta_a) \simeq h_r(\vartheta_f - \vartheta_a)\\
&Q_f = \gamma\lambda dX/dt, \quad q_1 = d[\gamma c(\vartheta_1 - \vartheta_a)Y]/dt\\
&q_2 = d[\gamma c(\vartheta_2 - \vartheta_a)X]/dt, \qquad q_m = d[\Gamma C(\vartheta_m - \vartheta_a)L]/dt\\
&Q_{ii} = \gamma c(\vartheta_i - \vartheta_a)d(X + Y)/dt, \qquad Q_{if} = \gamma c(\vartheta_1 - \vartheta_a)dX/dt\\
&Q_{fs} = \gamma c(\vartheta_f - \vartheta_a)dX/dt\\
&q_{ii} = 2k(\vartheta_i - \vartheta_1)/Y, \quad q_{if} = 2k(\vartheta_1 - \vartheta_f)/Y, \qquad q_{fs} = 2k(\vartheta_f - \vartheta_2)/X\\
&q_{si} = 2k(\vartheta_2 - \vartheta_i)/X, \quad q_{im} = 2K(\vartheta_i - \vartheta_m)/L, \qquad q_{ma} = 2K(\vartheta_m - \vartheta_a)/L
\end{aligned}\right\} \tag{43}
$$

Nondimensionalizing Equations (42) gives

$$
\left.\begin{aligned}
&\vartheta_i\text{:}\quad 0 = pU_b - \nu U_f - \frac{2}{H}(U_i - U_1) - pU_1\\
&\vartheta_1\text{:}\quad (U_1H)^{\cdot} = \frac{2}{H}(U_i - U_1) - \frac{2}{H}(U_1 - U_f) + pU_i - \dot{\Xi}U_1\\
&\vartheta_f\text{:}\quad 0 = \dot{\Xi} + \frac{2}{H}(U_1 - U_f) - \frac{2}{\Xi}(U_f - U_2) + \dot{\Xi}U_i - \dot{\Xi}U_f\\
&\vartheta_2\text{:}\quad (U_2\Xi)^{\cdot} = \frac{2}{\Xi}(U_f - U_2) - \frac{2}{\Xi}(U_2 - U_i) + \dot{\Xi}U_f\\
&\vartheta_i\text{:}\quad 0 = \frac{2}{\Xi}(U_2 - U_i) - \frac{U_i - U_m}{\rho_1}\\
&\vartheta_m\text{:}\quad m\dot{U}_m = \frac{U_i - U_m}{\rho_1} - \frac{U_m}{\rho_2}
\end{aligned}\right\} \tag{44}
$$

When the interface temperature $\vartheta_i$ is maintained at a *fixed* value, then Equations $\vartheta_f$, $\vartheta_2$ of (44) reduce to

$$
\left.\begin{aligned}
&\frac{1}{2}(\Xi^2)^{\cdot}[1 + U_1 - U_f] = 2(U_f - U_2) - \frac{2\Xi}{H}(U_1 - U_f)\\
&\frac{1}{2}(\Xi^2)^{\cdot}(U_f - U_2) + \Xi^2(U_f - U_2)^{\cdot} + 2(U_f - U_2) = 2(U_2 - U_i)
\end{aligned}\right\} \tag{45}
$$

and one finds, similarly to (34) for $\tau \ll 1$:

$$
\left.\begin{aligned}
&\Xi = 2\omega\sqrt{\tau}, \quad \frac{U_f - U_2}{U_f - U_i} = \frac{1}{2 + \omega^3}\\
&\omega^3 = \left[1 + \frac{U_f - U_i}{1 + U_1 - U_f}\right]^{1/2} - 1 = \left[\frac{1 + \dfrac{c}{\lambda}(\vartheta_f - \vartheta_i)}{1 + \dfrac{c}{\lambda}(\vartheta_1 - \vartheta_f)}\right]^{1/2} - 1
\end{aligned}\right\} \tag{46}
$$

For $c(\vartheta_f - \vartheta_i)/\lambda = 0.2, 2.0$ this gives $\omega = 0.31, 0.86$, when $\vartheta_1(0) = \vartheta_f$, and $0.28, 0.80$ when $c[\vartheta_1(0) - \vartheta_f]/\lambda = 0.2$; in good agreement with the rigorous solution quoted in footnote 14, when $(\vartheta_1 - \vartheta_f)/(\vartheta_f - \vartheta_i)$ is small, and $c(\vartheta_f - \vartheta_i)/\lambda$ is not too large.[17]

Nevertheless, Equations (44) have some unpleasant shortcomings, in common with Equations (29). This is revealed most clearly by Equation $\vartheta_i$ where, at time $\tau = 0$, a current in the infinitesimal element $\Xi/2$ is equated to a current in the finite element $\rho_1$. (It is always desirable in circuit representations to employ sections of, roughly speaking, equal resistances. This, however, is patently impossible when one of the sections has zero thickness.) In consequence, our approximate analysis implies $U_2(0) = U_i(0)$, followed by a gradual, though rapid, separation of $U_2(\tau)$ from $U_i(\tau)$, whereas in an exact solution initial values $U_2(0) \neq U_i(0)$ are assumed, abruptly. Our approximate method therefore cannot furnish clearcut estimates for these initial values, which are frequently of great interest.[18] A more annoying disadvantage of the method is that expressions of type $0/0$, $0 \cdot \infty$ are very awkward to program on an analog computer, and what is gained by use of a more refined model may be more than lost through the inaccuracy generated by computer elements which inadequately reproduce $0/0$ or $0 \cdot \infty$ type quantities.

We may remedy the situation (at the expense of replacing the infinite rate $\dot{\Xi}$ at $\tau = 0$ by a finite rate) by lumping all the capacity of the frozen section $X$, Fig. 10, into a single node at $\vartheta_f$. (Compare Fig. 4(*c*), where the lumping is done into the node at $\vartheta_i$.) This is a particularly good approximation during the early times of the freezing process, where the thickness $\Xi$ is small.[19] Fig. 6 and Equations (29) are then modified to Fig. 11 and Equations (47):

$$
\left.\begin{aligned}
&\vartheta_i\text{:}\quad \frac{H}{2}\dot{U}_i + pU_i = pU_b - \nu U_f - \frac{U_i - U_f}{H}\\
&\vartheta_f\text{:}\quad \left(\frac{\dot{H}}{2} + \dot{\Lambda}\right)U_f = \dot{\Lambda} + \frac{U_i - U_f}{H} - \frac{U_f - U_m}{\Lambda} + \left(\frac{\dot{H}}{2} + \dot{\Lambda}\right)U_i\\
&\vartheta_m\text{:}\quad m\dot{U}_m = \frac{U_f - U_m}{\Lambda} - \frac{U_m}{\rho_2}
\end{aligned}\right\} \tag{47}
$$

where we used the abbreviation

$$
\Lambda \equiv \Xi + \rho_1 \qquad (\Lambda(0) = \rho_1) \tag{48}
$$

Fig. 10 and Equations (44) may be similarly simplified to Fig. 12 and Equations (49):

[17] Similar approximate expressions for $\omega^3$ were previously obtained by Goodman [12].

[18] Whatever estimate is obtained depends quite sensitively on the thickness of the finite element adjoining the infinitesimal element whereas, in reality, only the boundary conditions should matter.

[19] Many casting processes (coating processes) are never carried beyond this stage.

$$
\left.
\begin{aligned}
\vartheta_l\text{:}\quad & pU_l = pU_s - \nu U_f - \frac{2}{H}\,(U_l - U_i) \\
\vartheta_i\text{:}\quad & H\dot{U}_i + pU_i = pU_l + \frac{2}{H}\,(U_l - U_i) \\
& \qquad\qquad - \frac{2}{H}\,(U_i - U_f) \\
\vartheta_f\text{:}\quad & U_f\dot{\Lambda} = \dot{\Lambda} + \frac{2}{H}\,(U_i - U_f) - \frac{U_f - U_m}{\Lambda} + \dot{\Lambda}U_i \\
\vartheta_m\text{:}\quad & m\dot{U}_m = \frac{U_f - U_m}{\Lambda} - \frac{U_m}{\rho_2}
\end{aligned}
\right\} \qquad (49)
$$

Use of these equations will be made in [4].

NOTE: Because of the importance of formula (46) we also state it for the case in which the liquid metal properties $k_l$, $c_l$ differ from the solid metal properties $k_s$, $c_s$.[20] Writing

$$
\Xi \equiv X/Y_0 = 2\omega\sqrt{\tau}, \quad \tau \equiv k_s t/\gamma c_s Y_0^2 \qquad (50)
$$

one finds, by steps entirely analogous to (42) to (46), that at the incipience of freezing

[20] When $\gamma_l \neq \gamma_s$ then convection currents are set up, and the present analysis is not applicable without major modifications. See Chambré [13].

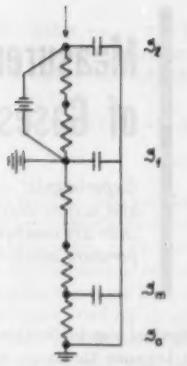


Fig. 11 Alternate model for the freezing of a growing liquid column

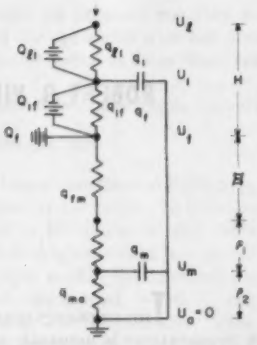


Fig. 12 Alternate model for the freezing of a growing liquid column

$$
\frac{\vartheta_f - \vartheta_2}{\vartheta_f - \vartheta_i} = \frac{1}{2 + \omega^2}
$$

$$
\omega^2 = \left[1 + \frac{c_s(\vartheta_f - \vartheta_s)/\lambda}{1 + c_l(\vartheta_i - \vartheta_f)/\lambda + (c_l - c_s)(\vartheta_f - \vartheta_i)/\lambda}\right]^{1/2} - 1 \qquad (51)
$$

It is noted that $\omega$ is (in our approximation) independent of $k_l/k_s$

ROBERT G. VINES[2]

# Measurement of the Thermal Conductivities of Gases at High Temperatures[1]

*Experimental results are reported for the thermal conductivities of air, argon, nitrogen, and carbon dioxide at temperatures up to 900 C, and of steam up to 560 C. These results are compared with values predicted from correlation formulas based on low temperature measurements.*

THE DETERMINATION of thermal conductivities at high temperatures is unusually difficult because the large heat losses produce thermal instability in experimental equipment. Investigations previously carried out in this laboratory have shown that measurements above 500 C are often liable to errors of up to 20 per cent. In the work reported here a system of high thermal capacity was employed, and consistent and reproducible results were obtained. It thus seems likely that the conductivity values given are substantially correct, and that reasonably accurate high temperature measurements have been achieved.

## Apparatus

At elevated temperatures a concentric cylinder apparatus is necessary to reduce the effects of "temperature jump." The conductivity cell was of novel design and was constructed entirely of platinum (see Fig. 1). The *emitter* (length ~5 cm) was a thick cylinder of 6 mm outside diameter (internal diameter <2 mm). A heater of fine platinum-rhodium wire, wound on a porcelain mandril (diam 1 mm) was inserted into the bore of the emitter and cemented in position with alundum cement. The cement was prepared with distilled water so that, at high temperatures, it still remained a good electrical insulator. Double leads (current and potential) were gold soldered to each end of the heater winding.

Two cylindrical *heat stations* (length 2.5 cm, other dimensions as above) were connected to the emitter by small thin-walled tubes, being separated from it by a distance of <1 mm. The heaters were "double wound" on hollow porcelain mandrils through which the leads to the emitter were taken. The leads from both the emitter and heat stations were then passed through porcelain insulators, and these were enclosed in short platinum tubes rigidly fixed to the ends of each heat station.

The *receiver* was a hollow cylinder 12.5 cm long and of 10 mm internal diameter (wall thickness ~1 mm). It was separated from the inner unit comprising the emitter and heat stations by two circular spacing pieces of fired "lava."

The completed conductivity cell was mounted vertically in a quartz tube directly connected to a glass vacuum system and gas supply. Eight thermocouples (Pt against Pt/10 per cent Rh)[3] were set in small flat pieces of gold and smoothly welded to the

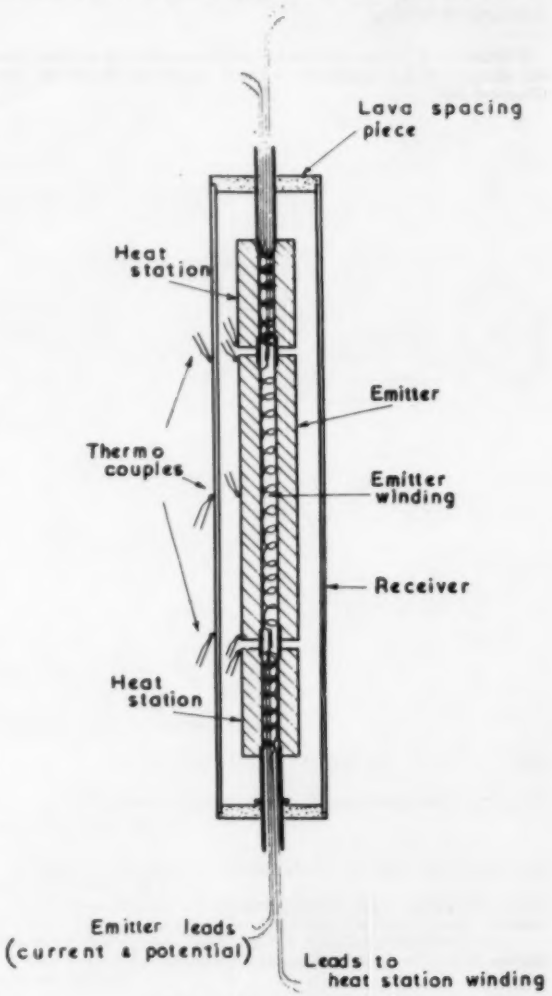


Fig. 1 High temperature cell

[1] This work was sponsored by Project SQUID which is supported by the Office of Naval Research, Department of the Navy, under contract Nonr 1858(25) NR-098-038. Reproduction in full or in part is permitted for any use of the United States Government.

Contribution from the Department of Chemistry, Massachusetts Institute of Technology. Results submitted in this article were obtained at M.I.T. by Mr. Robert G. Vines while on leave of absence from the C.S.I.R.O. Division of Tribophysics, University of Melbourne, Australia, during the period April to October of 1954.

[2] Member of the Commonwealth Scientific and Industrial Research Organization, Division of Industrial Chemistry, Melbourne, Australia.

Contributed by the Heat Transfer Division of THE AMERICAN SOCIETY OF MECHANICAL ENGINEERS and presented at the ASME-AIChE Heat Transfer Conference, Storrs, Conn., August 9–12, 1959.

NOTE: Statements and opinions advanced in papers are to be understood as individual expressions of their authors and not those of the Society. Manuscript received at ASME Headquarters, September 24, 1958. Paper No. 59—HT-2.

[3] Two sample thermocouples identical with those used were calibrated at the melting point of silver (960.8 C). During solidification of the silver, the temperature, as measured by the thermocouples, remained constant (to within better than 1/25 deg C) over a period of ten minutes. At this temperature the emf readings of the two thermocouples were 9115 $\mu$ volt and 9116 $\mu$ volt in good agreement with the value given in the U. S. National Bureau Tables (9120 $\mu$ volt).

cell at the positions shown in Fig. 1. External connections to the thermocouple (and heater) leads were made through Teflon seals in the glassware.

The quartz tube was itself completely surrounded by a thin, closely fitting nickel sheath (to help even out any temperature discontinuities) and placed in a *constant temperature furnace.* This was made from a porcelain cylinder (diam ~1 in. and somewhat less than one ft in length) wound with three sections of platinum ribbon—a long middle section with adjacent short windings to supply extra heat at each end. By manual adjustment of the heating currents (a-c with voltage regulation), it was possible to achieve uniformity of temperature along a considerable portion of the porcelain tube. The central winding was also connected to a stabilizing d-c circuit, the current in the circuit being regulated by a platinum resistance thermometer adjacent to the furnace; this provided thermostatic control when used in conjunction with a conventional resistance bridge, photocell circuit, and thyratron control unit.

The entire furnace was finally enclosed in a double-walled cylindrical brass case, filled inside with magnesium oxide and asbestos insulation. To provide a constant surrounding temperature of 100 C the outer compartment contained water which boiled when the furnace was at 500 C or higher. With careful adjustment of the electrical system the furnace could be maintained at any temperature between 200 and 1000 C for periods of an hour or more; over shorter intervals of time the maximum temperature variation was no more than a few thousandths of a degree.

## Calibration and Experimental Procedure

1 The thermocouples were annealed by heating "in situ" at 750 C for 36 hr in an atmosphere of argon.

2 In making measurements the furnace was first adjusted until the readings of all three thermocouples on the receiver agreed to within 1/30 deg C. Current (d-c) was then passed through the emitter and heat station windings. To minimize end effects and obtain reproducible (and accurate) results, it was necessary to keep the temperature differences between emitter and heat stations smaller than 1/20 deg C. This produced a nonuniform temperature distribution along the emitter, the center becoming slightly hotter than the ends.

3 The heat introduced to the emitter was determined from measurements of the potential difference across the winding when a known current was passed through it; the product of these two quantities gave the total heat input.

4 Conductivities were calculated from the measured dissipation of heat as determined with the apparatus under equilibrium conditions. Heat was lost by both conduction and radiation, but measurement of the corresponding heat dissipation when the apparatus was highly evacuated enabled corrections to be made for end conduction, radiation, and so forth; during these vacuum runs the temperatures of the emitter, receiver, and heat stations were maintained at roughly the previous levels. From a smoothed curve relating the radiation losses with temperature, appropriate corrections could be made to each experimental measurement.

5 The temperature difference ($\Delta T$) between emitter and receiver was usually between 5 and 10 C. The greatest accuracy was obtained when $\Delta T$ was large. Within experimental error, the results of the measurements at any temperature were independent of $\Delta T$. The "experimental temperature" was assumed to be the mean of the emitter and receiver temperatures.

6 The apparatus could not be operated at pressures higher than atmospheric. Convection effects appeared to be very small for, within experimental error, all results were independent of pressure over a wide pressure range. In general, measurements with gases were made at pressures close to atmospheric, though when water vapor was introduced the pressure was very much lower; since external portions of the apparatus were not heated, the pressure was only that of water vapor at room temperature (~2 cm Hg).

7 The cell constant as calculated from the simple formula

$$\text{const} = 2\pi L/\log r_2/r_1$$

does not take into account heat losses from the end surfaces of the emitter, edge effects, nonradial flow, and so forth. ($L$ is the length of the emitter, $r_1$ its radius, and $r_2$ the radius of the receiver.) As the constant so calculated is clearly somewhat low, it was arbitrarily increased by a few per cent so that the conductivities of air, argon, carbon dioxide, and nitrogen at ~250 C were in agreement with accepted values at this temperature. This adjusted constant was then used to calculate conductivities up to 900 C, small corrections merely being made to compensate for the expansion of platinum with temperature.

8 Calculation showed "temperature jump" effects to be unimportant with the present apparatus, except possibly for the steam measurements at 560 C; even in this case the error involved (~1 per cent) was less than the likely experimental error. Methods of estimating such effects are outlined in references [8][4] and [12].

9 In calculating conductivity coefficients the temperature difference between emitter and receiver must be accurately known. This requires knowledge of the variation of thermocouple emf with temperature. The factor $dE/dT$ was obtained by differentiating the equations relating $E$ and $T$, as given by the U. S. National Bureau of Standards; although this is not entirely satisfactory, no better method is available.

## Results

The results are shown in Table 1. The values listed at 900 C are probably less accurate than the other figures, not only because of the magnitude of the radiation correction but also because the apparatus was damaged at this high temperature. It is interesting to compare the conductivity values in Table 1 with those expected from extrapolation of low temperature data. Empirical correlation formulas have been developed previously [1] which reproduce experimental results obtained over a wide temperature range (−200 to 350 C). It may be seen that "high temperature conductivities" as calculated from such formulas are in excellent agreement with the present results for

[4] Numbers in brackets designate References at end of paper.

**Table 1 Thermal conductivities of selected gases**

$K \cdot 10^5 \cdot \text{cal cm}^{-1}\,\text{sec}^{-1} \cdot \text{deg}^{-1}$

| Temp C | 240 | 260 | 270 | 550 | 560 | 760[a] | 900[a] |
|---|---|---|---|---|---|---|---|
| Air | 9.76 | ... | .. | 14.06 | ... | 16.7 | 18.4 |
| Argon | ... | 6.82 | .. | 9.22 | ... | 10.4 | 11.7 |
| Nitrogen | ... | 9.92 | .. | 13.66 | ... | 16.1 | 17.8 |
| Carbon dioxide | ... | ... | 8.98 | 13.90 | ... | 17.5 | 19.4 |
| Steam | ... | ... | 9.65 | ... | 17.1 | .. | ... |
| $CO_2/N_2$ mixtures: | | 760 C | | | | | |
| % $CO_2$ | 0 | 33.5 | 47.1 | 65.9[b] | | 100 | |
| $K \cdot 10^5$ | 16.1[b] | 17.5 | 17.4 | 17.5 | | 17.1[b] | |

[a] At high temperatures the "blank" corrections (radiation, etc.) are large, being of the same magnitude as the conductivity values. As might have been expected, the radiation corrections appeared to vary roughly with the cube of the absolute temperature; with argon at 760 C approximately half the heat dissipated was accounted for in this way.

[b] This value for pure carbon dioxide is not quite in agreement with that given in the upper part of the table. Damage to the apparatus at 900 C, which took place before the measurements on mixtures were made, is the probable cause of the discrepancy.

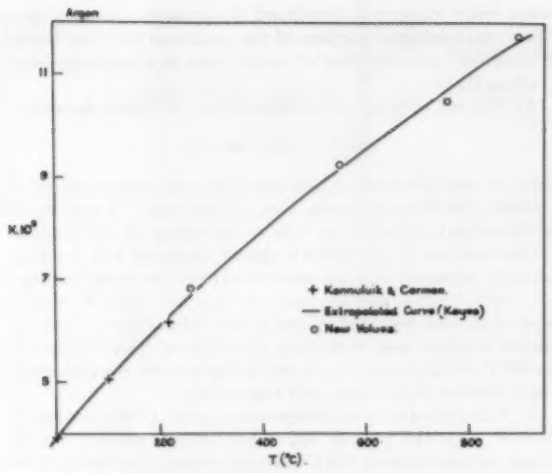


Fig. 2 Conductivity measurements for argon

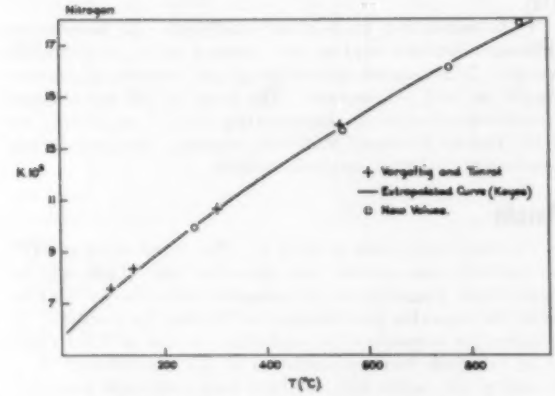


Fig. 3 Conductivity measurements for nitrogen

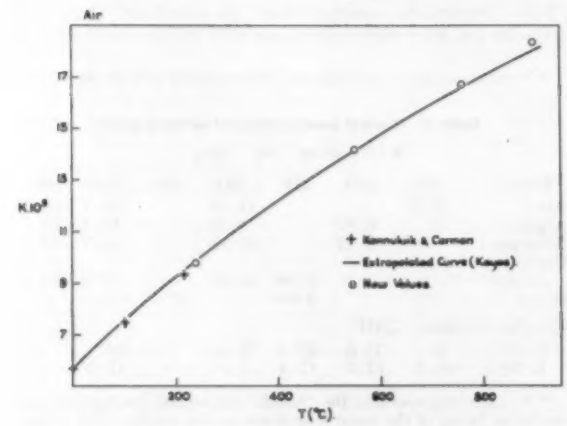


Fig. 4 Conductivity measurements for air

simple gases like argon, nitrogen, or air, but not with those for carbon dioxide.

**Argon.** The correlation equation[5] is

$$K \cdot 10^5 = \frac{0.388\sqrt{T}}{1 + \frac{186.7}{T} \cdot 10^{-12/T}}$$

where $T$ is in degrees absolute. Comparison with the earlier experimental results of Kannuluik and Carman [2] is shown in Fig. 2. There is close agreement between the predicted values at high temperatures and the present measurements. Reference to the literature indicates that there is excellent agreement with the results of Rothman and Bromley [9] at 600 C, and with those of Gardiner and Schäfer [13] at 200 and 300 C. Values listed by the National Bureau of Standards [14] agree well below about 600 C, but at 850 C are ~2½ per cent lower than the curve in Fig. 2 suggests.

For argon, reliable viscosity data are available. If these are used to calculate the ratio between conductivity and viscosity, a systematic decrease with increasing temperature is apparent in the value of the Chapman-Enskog transport factor—from 2.5 at 0 C to ~2.45 at 1000 C. Since the estimated experimental error is at least ±1 per cent this variation is scarcely significant; however, as reported earlier [3] helium and neon exhibit similar behavior which suggests the effect may be real. If so, it raises an interesting problem in kinetic theory which does not predict a variation of this kind.

**Nitrogen.** The results are shown in Fig. 3, together with those of Vargaftig and Timrot [4]. The correlation equation is

$$K \cdot 10^5 = \frac{0.604\sqrt{T}}{1 + \frac{224}{T} \cdot 10^{-12/T}}$$

It may be seen that the agreement between observed and predicted conductivity values is excellent.

Measurements reported by Rothman and Bromley [9] are uniformly ~4 per cent lower than the present results from 300 C to 800 C, and are not consistent with probable values for the conductivity of air—cf. the measurements in Figs. 3 and 4 which are reasonably self-consistent over a wide range. The results of Stops [15] are ~3½ per cent lower at 900 C, though the discrepancies are smaller at 500 C.

**Air.** The results are shown in Fig. 4, together with those of Kannuluik and Carman [5]. The correlation equation is

$$K \cdot 10^5 = \frac{0.632\sqrt{T}}{1 + \frac{245}{T} \cdot 10^{-12/T}}$$

Again, there is good agreement between observed and predicted values.

For air there are many measurements up to 500 C, and most of these are in accord with the present results. Values in the NBS Tables are in substantial agreement up to 750 C, but then become slightly *lower;* the curve estimated from the Lennard-Jones 6–12 potential, using accepted constants, also agrees to ~700 C, but is ~2 per cent *higher* at 900 C. Figures derived

[5] The constants used in the correlation equations are taken from reference [1].

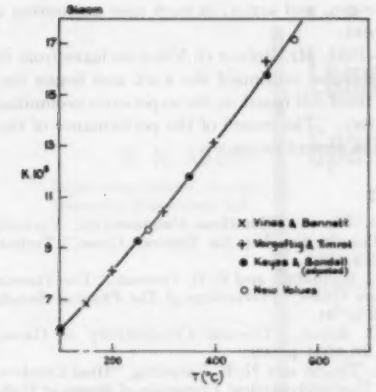


Fig. 5 Conductivity measurements for steam

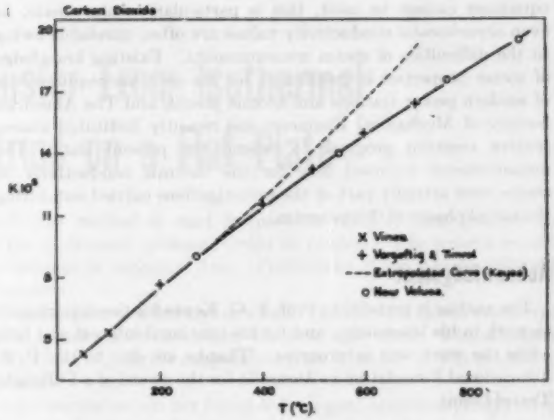


Fig. 6 Conductivity measurements for carbon dioxide

from the formula of Stops [15] are slightly lower at 500 C, but 2½ per cent lower at 900 C.

**Steam.** No satisfactory correlation equation has been formulated since measurement of the thermal conductivity of steam is very difficult; this is emphasized by the general lack of agreement between values obtained by different workers. Nevertheless, as may be seen from Fig. 5, the present results compare well with those of other recent investigations [4], [6], and [7].[4] Over the entire temperature range the curve in Fig. 5 is higher than values listed in the NBS Tables, being as much as 7 per cent higher at 450 C.

**Carbon Dioxide.** The results for carbon dioxide are interesting, for the values predicted from low temperature measurements (cf. also Vines [8]) are much in excess of those actually observed; the latter are, however, in excellent agreement with the recent results of Vargaftig and Timrot [4] (see Fig. 6). It is quite clear that the extrapolated curve in Fig. 6 is incorrect, for other experimental values of Stops [15], and Rothman and Bromley [9], which are reasonably consistent in themselves, are ~2 per cent lower than the present measurements at 400 C, and 5 per cent lower at 900 C. Again, the full curve in Fig. 6 is in excellent agreement with the NBS Tables—though these extend to only ~350 C.

The correlation equation for carbon dioxide (see reference [1]) was formulated from conductivity measurements in the range −50 to 300 C. Over this temperature range the heat capacity increases rapidly for, with carbon dioxide, the vibrational degrees of freedom become excited at quite low temperatures. Nevertheless, the heat capacity rises much less rapidly beyond 300 C, and since no allowance is made for this in the correlation equation, it is not surprising that the predicted high temperature conductivities are too large. With simpler gases the rate of increase in heat capacity is less marked at low temperatures; correlation equations should thus remain effective over a much greater temperature range—cf. the results given for argon, nitrogen, and air.

Measurements on carbon dioxide/nitrogen mixtures at 760 C are shown in Fig. 7. This illustrates the complexities likely to be encountered in conductivity measurements at high temperatures for, as reported earlier by Keyes [1] and Rothman and Bromley [9], the conductivity versus composition curve exhibits a well-defined maximum. At considerably lower temperatures

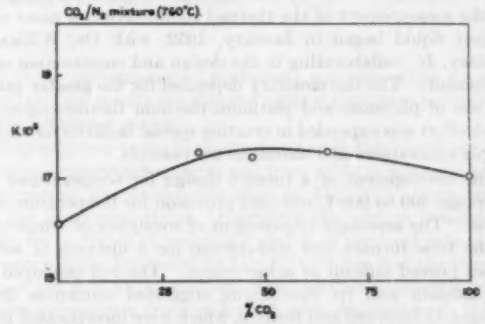


Fig. 7 Conductivity measurements for carbon dioxide/nitrogen mixtures at 760 C

the corresponding curves are roughly linear, the slight negative deviations observed near room temperature being in good agreement with the values predicted from the empirical equation of Lindsay and Bromley [10]—cf. Bennett and Vines [11]. It has been shown [11] that the maxima often observed in the conductivity versus composition curves for gaseous mixtures are due to differences in the polarity of the mixture constituents. On this basis, Fig. 7 suggests a definite lack of symmetry in the charge distribution within the carbon dioxide molecule at 760 C, in full accord with heat capacity measurements which indicate that, at this temperature, both the deformation and valence vibrations in carbon dioxide are activated.

## Conclusions

This investigation shows that the thermal conductivities of simple gases may be calculated accurately from low temperature measurements by the use of correlation equations (see also reference [16]). Even at very high temperatures up to 2000 C, values so estimated are unlikely to exhibit gross errors, as is clear from a study of Figs. 2, 3, and 4. This is of special importance to the engineer who can, with confidence, use extrapolated conductivity values in heat-transfer calculations for gases such as argon, neon, hydrogen, nitrogen, oxygen, and so on.

On the other hand, the method is not suitable for rather more complex gases possessing higher specific heats; here the use of correlation equations, based solely on low temperature measurements, could lead to enormous errors in the calculated high temperature values. Again in the case of water vapor, for which heat-transfer calculations are specially important, correlation

[4] These measurements of Keyes and Sandell for steam and nitrogen are known to be low at higher temperatures. If the results are adjusted so that there is agreement with accepted conductivity values for nitrogen over the whole range, the corresponding steam measurements are then in accord with the values for steam reported here (see Fig. 5).

equations cannot be used; this is particularly unfortunate, as even *experimental* conductivity values are often unreliable owing to the difficulties of steam measurements. Existing knowledge of steam properties is insufficient for the extreme requirements of modern power stations and atomic plants, and The American Society of Mechanical Engineers has recently instituted an extensive research program to extend the present data. The measurements reported here for the thermal conductivity of steam were actually part of the investigations carried out during the initial phases of this program.

## Acknowledgment

The author is grateful to Prof. F. G. Keyes for the opportunity to work in his laboratory, and for his continual interest and help while the work was in progress. Thanks are due to the U. S. Educational Foundation in Australia for the award of a Fulbright Travel Grant.

### Comments by Frederick G. Keyes

The attempt to actively develop high temperature equipment for the measurement of the thermal conductivity of gases under Project Squid began in January, 1952, with Dr. William T. Lindsay, Jr., collaborating in the design and construction of the equipment. The thermometry depended for the greater part on the use of platinum and platinum rhodium thermocouples and much effort was expended in creating special facilities for thermocouple calibrations and thermometry controls.

The development of a furnace design for temperatures over the range 300 to 900 C included provision for temperature regulation. The necessary requirement of constancy of temperature in the tube furnace and mid-portion for a distance of several inches proved difficult of achievement. The cell employed was of platinum and its functioning suggested numerous design changes, in both cell and furnace, which were incorporated in the equipment during 1953. The cell was entirely rebuilt and improvements made in temperature control apparatus. The thermocouple wire was increased in size from 0.1 mm to 0.2 mm because of inhomogeneities which developed in the finer wire. The alteration of the thermoelectric properties of wire caused by cold working was also reduced by the change to a larger size. A large variety of detail changes and improvements were incorporated in the second cell which underwent tests in June, 1953. In spite, however, of the care and attention to detail in construction of the second cell it was not altogether satisfying. A series of observations were made in vacuum and on air, argon, helium, and nitrogen. The highest temperature employed was 700 C. Different temperature distributions led to variations in results for air, nitrogen, and argon; in each case amounting to as much as ten per cent.

In April, 1954, Mr. Robert G. Vines on leave from the University of Melbourne continued the work and began the construction of the third cell based on the experience accumulated by Dr. W. T. Lindsay. The record of the performance of the third cell is given in the present paper.

## References

1 F. G. Keyes, "The Heat Conductivity, Viscosity, Specific Heat, and Prandtl Numbers for Thirteen Gases," Technical Report No. 37, April 1, 1952.

2 W. G. Kannuluik and E. H. Carman, "The Thermal Conductivity of Rare Gases," *Proceedings of The Physical Society*, series B, vol. 65, 1952, p.701.

3 F. G. Keyes, "Thermal Conductivity of Gases," TRANS. ASME, vol. 76, 1954, p. 809.

4 D. L. Timrot and N. B. Vargaftig, "Heat Conductivity, Viscosity, and Thermodynamical Properties of Steam at High Temperatures and Pressures," Transactions of Fourth World Power Conference, III, Lund-Humphries, London, 1952, p. 1642.

5 W. G. Kannuluik and E. H. Carman, "The Temperature Dependence of the Thermal Conductivity of Air," *Australian Journal of Scientific Research*, series A, vol. 4, 1951, p. 305.

6 R. G. Vines and L. A. Bennett, "The Thermal Conductivity of Organic Vapors. The Relationship Between Thermal Conductivity and Viscosity and the Significance of the Eucken Factor," *Journal of Chemical Physics*, vol. 22, 1954, p. 360.

7 F. G. Keyes and D. J. Sandell, Jr., "New Measurements of the Heat Conductivity of Steam and Nitrogen," TRANS. ASME, vol. 72, 1950, p. 767.

8 R. G. Vines, "The Thermal Conductivity of Organic Vapours: The Influence of Molecular Interaction," *Australian Journal of Chemistry*, vol. 6, 1953, p. 1.

9 A. J. Rothman and L. A. Bromley, "High Temperature Thermal Conductivity of Gases," *Industrial and Engineering Chemistry*, vol. 47, 1955, p. 899.

10 A. L. Lindsay and L. A. Bromley, "Thermal Conductivity of Gas Mixtures," *Industrial and Engineering Chemistry*, vol. 42, 1950, p. 1508.

11 L. A. Bennett and R. G. Vines, "Thermal Conductivities of Organic Vapor Mixtures," *Journal of Chemical Physics*, vol. 23, 1955, p. 1587.

12 R. G. Vines, "The Interchange of Energy Between Molecules During Collisions in the Gas Phase and at Solid Surfaces," *Reviews of Pure and Applied Chemistry* (*Australia*), vol. 4, 1954, p. 207.

13 W. C. Gardiner and K. Schäfer, "Transport Phenomena in Gases, and Intermolecular Forces," *Zeitschrift für Electrochemie*, vol. 60, 1956, p. 588.

14 "Tables of Thermal Properties of Gases," U. S. National Bureau of Standards, Circular 564, 1955.

15 D. W. Stops, "Effect of Temperature Upon the Thermal Conductivity of Gases," *Nature*, vol. 164, 1949, p. 966.

16 R. G. Vines, "Thermal Conduction in Gases," Proceedings of Conference on The Thermodynamic and Transport Properties of Fluids, The Institution of Mechanical Engineers, London, England, 1958, p. 120.

# Laminar Transfer From Isothermal Spanwise Strips on a Flat Plate

**H. H. SOGIN**
Engineering Division, Brown University, Providence, R. I.
Assoc. Mem. ASME

*The Rubesin-Klein-Tribus method is used to calculate rates of heat transfer by forced convection from two isothermal spanwise strips in tandem. The general results are applicable to either laminar or turbulent flow. Predictions of laminar transfer are based on Eckert's step function.*

*In experimentation, naphthalene cast in trays is used to simulate the isothermal strips while the inert material between them simulates the adiabatic wall. The velocities range from about 40 to 90 ft/sec, and the air temperature from 72 to 88 F. The boundary layer is shown to be laminar.*

*The theoretical and experimental results are found to be in good agreement, confirming the calculation method and Eckert's step function.*

*The experimentation is extended to an array of several equally spaced strips in tandem. Effects of roughness and spanwise diffusion are noted.*

## 1 Introduction

METHODS TO DEAL with surfaces of arbitrary temperature distribution have been developed by Chapman and Rubesin [1],[1] Lighthill [2], Rubesin [3], and others. An excellent review has been provided by Klein and Tribus [4] who have shown, also, how to calculate wall temperature distributions from prescribed distributions of heat flux. Of all the methods, the Rubesin-Klein-Tribus (RKT) probably is the most convenient in practice, and further simplification for engineering usage has recently been provided by Eckert, et al. [5, 6].

Eckert's [7] step function, which the RKT method uses for the laminar boundary layer has been confirmed by comparison of several theoretical solutions [5]. However, until now it has been only indirectly confirmed by experimentation [8, 9].

In the present investigation, the RKT method is employed to predict the performance of isothermal spanwise strips on a flat plate, and the results are checked against experimentation based on the heat-mass analog.

With reference to the flat plate sketched in Fig. 1(*a*), isothermal heating occurs from[2] $x_1'$ to $x_1$ and from $x_2'$ to $x_2$ as shown by the temperature distribution sketched in Fig. 1(*b*); these regions are the isothermal strips. Elsewhere the surface is adiabatic, as shown in Fig. 1(*c*), which is a sketch of the local rate of heat transfer $q''(x)$. Returning to Fig. 1(*b*), we see that the temperature of the fluid at the surfaces of the adiabatic elements rapidly decays downstream from each strip, as is shown later in the calculations. The areas under the curves AB and CD in Fig. 1(*c*) are proportional to the total rates of heat transfer from Strips 1 and 2, respectively. The rate of heat transfer at the leading edge of each strip is very high. One of the questions to be answered is whether or not the large rates of heat transfer at the leading edge of Strip 2 and of subsequent strips would possibly compensate for the loss of heated area between them.

[1] Numbers in brackets designate references at end of paper.

Contributed by the Heat Transfer Division of THE AMERICAN SOCIETY OF MECHANICAL ENGINEERS and presented at the ASME-AIChE Heat Transfer Conference, Storrs, Conn., August 9–12, 1959.

NOTE: Statements and opinions advanced in papers are to be understood as individual expressions of their authors and not those of the Society. Manuscript received at ASME Headquarters, April 6, 1959. Paper No. 59—HT-1.

[2] The prime (′) used with a symbol related to a length refers to the leading edge of a strip. The same symbol without the prime refers to the trailing edge of the strip. The prime used with $q$ or $m$ (rates of heat or mass transfer) refers to a unit span. Similarly, a double prime (″) refers to a unit area.

## Nomenclature

$A$ = area
$B_1, B_2$ = constants
$b$ = coefficient of mass transfer
$C$ = dimensionless coefficient
$c_p$ = specific heat at constant pressure
$\mathfrak{D}$ = coefficient of diffusion
$F$ = ratio of total rates of transfer
$h$ = coefficient of heat transfer by convection
$I_x$ = incomplete beta function
$K$ = dimensional coefficient, $Ck(U/\nu)^n$
$k$ = thermal conductivity
$l$ = chordwise length of a strip
$m$ = mass transfer
$\dot{m}$ = rate of mass transfer
$n$ = exponent
Pr = Prandtl number, $\nu/\alpha$
$p$ = pressure
$q$ = rate of heat transfer
$R$ = gas constant
Sc = Schmidt number, $\nu/\mathfrak{D}$
$s$ = $x^a$
$T$ = absolute temperature
$t$ = temperature
$U$ = velocity at outer edge of boundary layer
$u$ = velocity component in $x$-direction
$w$ = spanwise width of strip
$x$ = distance from leading edge
$y$ = distance from surface
$\alpha$ = exponent; thermal diffusivity
$\beta$ = exponent
$\delta$ = boundary layer thickness
$\theta$ = temperature excess
$\Lambda$ = defined by Equation (25)
$\nu$ = kinematic viscosity
$\xi$ = variable distance from leading edge when $x$ is considered constant
$\rho$ = density; concentration
$\sigma$ = $\xi^a$
$\tau$ = time
$\chi$ = defined by Equation (20)

**Subscripts**

$j$ = index of strip
$n$ = total number of strips
$v$ = vapor
$w$ = wall
0 = mainstream

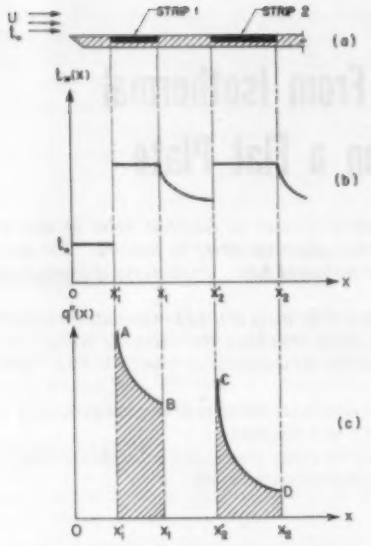


Fig. 1 Two isothermal strips in tandem

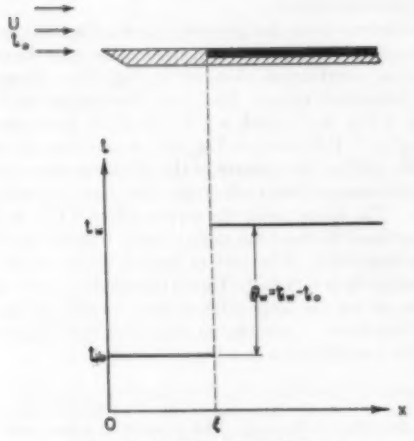


Fig. 2 Simple isothermal step

In the experimentation, trays of naphthalene are assembled on a flat plate, and rates of mass transfer are measured by weighing the trays before and after exposure to the air stream. Since the strips of naphthalene are virtually isothermal, their surface concentrations are very nearly uniform, and they simulate isothermal heated strips [10]. The advantage of employing the analog in this case is that thermal isolation can be completely simulated by inert surfaces and that a large variety of surface distributions, or "mosaics," can be tested without any modification of the instrumentation.

In Sections 2 through 4, which deal with the analysis and solution of the problem, a heated plate is considered, and the term "strip" is used for the longer term "spanwise isothermal strip." In Sections 5 through 8, which deal with the experimentation, the term strip refers to the analogical equivalent of the heated strip, namely, the naphthalene in the trays.

## 2 Analytical Statement of the Problem

It is assumed that the flow is steady, two-dimensional, and incompressible and that the temperature differences are sufficiently small to permit the use of constant values for the fluid properties. Since the flat plate is being studied, the pressure on the surface and throughout the boundary layer is uniform. Further, the velocity of the fluid is low enough so that effects of frictional dissipation may be neglected.

Under these assumptions we obtain the well-known system of equations which express the conservation of mass, momentum, and energy in the boundary layer. The only one that need concern us here is the energy equation

$$u\frac{\partial t}{\partial x} + v\frac{\partial t}{\partial y} = \alpha\frac{\partial^2 t}{\partial y^2} \tag{1}$$

For under the assumptions given, the equations are coupled unilaterally, the functions $u = u(x, y)$ and $v = v(x, y)$ being solutions only of the momentum and continuity equations. These functions may be tabulated, for instance, after the general Blasius solution.

The boundary conditions that $t = t(x, y)$ must satisfy have already been discussed in conjunction with Fig. 1. In regarding the distribution of the flux, it should be observed that $q''(x) = -k(\partial t/\partial y)_{y=0}$. Hence, in the first, third, and fifth intervals of $x$ in Fig. 1, $(\partial t/\partial y)_{y=0} \equiv 0$.

## 3 Scheme of the Calculations

The temperature distribution of a simple isothermal step is shown in Fig. 2. If $q''(x)$ denotes the rate of heat transfer per unit area at distance $x$ from the leading edge, then a local coefficient of heat transfer $h(\xi, x)$ may be defined by the equation

$$q''(x) = h(\xi, x)\cdot\theta(x) \tag{2}$$

where

$$\theta(x) = \left\{\begin{array}{ll} 0 & \text{for } x < \xi \\ \theta_w & \text{for } x > \xi \end{array}\right\} \tag{3}$$

and $\theta_w$ denotes the constant difference $t_w - t_0$.

The relation between the usual isothermal coefficient $h(0, x)$ and the coefficient $h(\xi, x)$ is taken to be of the form

$$h(\xi, x) = h(0, x)\cdot f\left(\frac{\xi}{x}\right) \tag{4}$$

Typically, for either laminar or turbulent transfer on a flat plate,

$$h(0, x) = \frac{k}{x}\cdot C\cdot\left(\frac{U_0\rho_0 x}{\mu}\right)^n \tag{5}$$

and

$$f\left(\frac{\xi}{x}\right) = \left[1 - \left(\frac{\xi}{x}\right)^\alpha\right]^{-\beta} = x^{\alpha\beta}[x^\alpha - \xi^\alpha]^{-\beta} \tag{6}$$

The coefficient $C$ is dimensionless; it depends upon the Prandtl number and the nature of the flow in the boundary layer. Also, the exponents $n$, $\alpha$, and $\beta$ are constants depending upon the nature of the flow.

Hence, for the simple step under particular flow conditions of a given fluid,

$$q''(x) = \left\{\begin{array}{ll} 0 & (x < \xi) \\ K\cdot\theta_w\dfrac{x^{\alpha-1}}{[x^\alpha - \xi^\alpha]^\beta} & (x > \xi) \end{array}\right\} \tag{7}$$

The coefficient $K$ has the units of $kx^{-n}$.

The significance of Rubesin's work [3] is that for an arbitrary distribution of the excess temperature at the wall, $\theta(x)$, the local rate of heat transfer can be computed by superposing the solu-

tions of infinitesimal as well as finite temperature steps. The formula has been concisely expressed as follows:

$$q''(x) = K \int_0^x \frac{x^{\alpha-1}}{[x^\alpha - \xi^\alpha]^\beta} d\theta(\xi) \tag{8}$$

the integration being performed in the Stieltjes sense.

The three exponents satisfy the relation

$$n = (1 - \beta)\cdot\alpha \tag{9}$$

Some sets of $n$, $\alpha$, and $\beta$ are tabulated here:

| Nature of the boundary layer | $n$ | $\alpha$ | $\beta$ | Reference |
|---|---|---|---|---|
| laminar | 0.5 | 3/4 | 1/3 | Eckert [7] |
| turbulent | 0.8 | 39/40 | 7/39 | Rubesin [3] |
| turbulent | 0.8 | 9/10 | 1/9 | Seban [11] |

The values for the turbulent boundary layer, which are based on semiempirical analyses, are quite well substantiated by experimentation. Some fairly recent comparisons have been made by Jakob in his communication regarding the work of Furber [12] and by Eckert, et al. [5].

As already mentioned, Klein and Tribus [4] provide a method to calculate the distribution of surface temperatures from a known distribution of the heat transfer $q''(x)$. Without repeating the details of the derivation, which may be found in [4], we may write on the basis of the power relations given that

$$\theta(x) = \frac{\alpha \sin \beta\pi}{K\pi} \int_0^x \frac{q''(\xi)d\xi}{[x^\alpha - \xi^\alpha]^{1-\beta}} \tag{10}$$[3]

The following minor transformation is introduced for convenience:

$$s = x^\alpha \quad \text{and} \quad \sigma = \xi^\alpha \tag{11}$$

Then (8) and (10) become

$$q''(s) = K \int_0^s \frac{s^{(\alpha-1)/\alpha} d\theta(\sigma)}{[s - \sigma]^\beta} \tag{12}$$

and

$$\theta(s) = \frac{\sin \beta\pi}{K\pi} \int_0^s \frac{q''(\sigma)\cdot\sigma^{(1-\alpha)/\alpha} d\sigma}{[s - \sigma]^{1-\beta}} \tag{13}$$

## 4 Application to the Isothermal Heated Strips

Equations (12) and (13) are used alternately as follows: First, (12) is employed to calculate the heat transfer from Strip 1. Second, (13) is used to calculate the temperature distribution at the adiabatic wall between the two strips. And third, (12) is again employed to calculate the heat transfer from Strip 2. It is assumed that the boundary layer is either laminar or turbulent.

Since the total instead of the local transfer is measured, an expression for the total rate of heat transfer from Strip $j$ per unit span is needed. It is obtained from the following relationships:

$$q_j' = \int_{x_{j'}}^{x_j} q''(\xi)d\xi = \frac{1}{\alpha} \int_{s_{j'}}^{s_j} q''(\sigma)\cdot\sigma^{(1-\alpha)/\alpha} d\sigma \tag{14}$$

The results of this calculation will be compared with the experimental results.

**4.1 Heat Transfer From Strip 1.** For Strip 1, (12) reduces to (7). Hence,

$$q_1''(s) = K\cdot\theta_w \frac{s^{(\alpha-1)/\alpha}}{(s - s_1')^\beta} \qquad (s_1' \leqslant s \leqslant s_1) \tag{15}$$

[3] In referring to [4] it may be useful to observe that $\Gamma(\beta)\cdot\Gamma(1-\beta) = \pi/\sin\beta\pi$.

After replacing $s$ with $\sigma$, sudstituting into (14), integrating, and eliminating $\alpha$ through (9),

$$q_1' = \frac{K\cdot\theta_w}{n}(s_1 - s_1')^{1-\beta} \tag{16}$$

In the particular case that heating begins from the leading edge

$$q_{01}' = \frac{K\cdot\theta_w}{n}\cdot s_1^{(1-\beta)} = \frac{K\theta_w}{n}\cdot C\cdot\left(\frac{U\rho x_1}{\mu}\right)^n \tag{17}$$

Hence

$$F_1 = q_1'/q_{01}' = \left(1 - \frac{s_1'}{s_1}\right)^{1-\beta} \tag{18}$$

**4.2 Distribution of the Wall Temperature Downstream of Strip 1.** Upon substitution into (13) for $q''(\sigma)$ in the interval $\sigma = 0$ to $\sigma = s_2'$,

$$\theta(s) = \theta_w \frac{\sin \beta\pi}{\pi} \int_{s_1'}^{s_1} \frac{d\sigma}{[\sigma - s_1']^\beta [s - \sigma]^{1-\beta}} \tag{19}$$

Introducing

$$\chi = \chi(s, \sigma) = \frac{\sigma - s_1'}{s - s_1'} \tag{20}$$

we obtain

$$\theta(s) = \theta_w \frac{\sin \beta\pi}{\pi} \int_0^{\chi(s, s_1)} \frac{d\chi}{\chi^\beta (1 - \chi)^{1-\beta}} \tag{21}$$

or, observing that the integral is the incomplete beta function,

$$\theta(s) = \theta_{w1}\cdot I_{\chi(s, s_1)}(1 - \beta, \beta) \qquad (s_1 \leqslant s < s_2') \tag{22}$$

For the laminar boundary layer $\beta = 1/3$. The normalized incomplete beta function $I_x(2/3, 1/3)$ has been calculated, and the results are presented in Table 1. It is evident that the wall temperature falls very abruptly downstream of Strip 1. Nevertheless, the theory continues on the assumption that the diffusion in the $x$-direction is zero everywhere.

**4.3 Heat Transfer From Strip 2.** Upon substitution into (12) for $\theta(\sigma)$ in the interval from $\sigma = 0$ to $\sigma = s_2$,

$$q_2''(s) = \theta_w K s^{(\alpha-1)/\alpha} \left\{ \frac{1}{[s - s_1']^\beta} + \int_{s_1}^{s_2'} \frac{\dfrac{d}{d\chi} I_{\chi(\sigma, s_1)}(1 - \beta, \beta) d\chi(\sigma, s_1)}{[s - \sigma]^\beta} + \frac{1 - I_{\chi(s_2', s_1)}(1 - \beta, \beta)}{[s - s_2']^\beta} \right\} \qquad (s_2' \leqslant s < s_2) \tag{23}$$

The integral is readily evaluated with the result that

$$q_2''(s) = \theta_w K s^{(\alpha-1)/\alpha} \left\{ \frac{I_{\Lambda(s)}}{[s - s_1']^\beta} - \frac{I_{\chi(s_2', s_1)}}{[s - s_2']^\beta} + \frac{1}{[s - s_2']^\beta} \right\} \tag{24}$$

where

$$\Lambda(s) = \frac{\chi(s_2', s_1) - \chi(s, s_1)}{1 - \chi_{(s, s_1)}} \tag{25}$$

and $I_x$ is used for the full expression $I_x(1 - \beta, \beta)$.

Table 1 $I_x\left(\frac{1}{3}, \frac{2}{3}\right) = \frac{1}{B\left(\frac{1}{3}, \frac{2}{3}\right)} \int_0^x \frac{d\lambda}{\lambda^{2/3}(1-\lambda)^{1/3}}$

| | 0 | 1 | 2 | 3 | 4 | 5 | 6 | 7 | 8 | 9 |
|---|---|---|---|---|---|---|---|---|---|---|
| 0.0 | 0.0000 | 0.1780 | 2246 | 2573 | 2835 | 3057 | 3251 | 3426 | 3585 | 3732 |
| 0.1 | 3869 | 3998 | 4119 | 4234 | 4344 | 4450 | 4550 | 4648 | 4742 | 4833 |
| 0.2 | 4921 | 5006 | 5090 | 5171 | 5250 | 5327 | 5403 | 5477 | 5550 | 5621 |
| 0.3 | 5691 | 5759 | 5827 | 5893 | 5959 | 6023 | 6087 | 6150 | 6212 | 6273 |
| 0.4 | 6334 | 6394 | 6453 | 6511 | 6570 | 6627 | 6684 | 6741 | 6797 | 6852 |
| 0.5 | 6908 | 6963 | 7017 | 7072 | 7126 | 7179 | 7233 | 7286 | 7339 | 7392 |
| 0.6 | 7445 | 7497 | 7550 | 7602 | 7654 | 7706 | 7758 | 7810 | 7862 | 7915 |
| 0.7 | 7967 | 8019 | 8072 | 8124 | 8177 | 8230 | 8283 | 8336 | 8390 | 8440 |
| 0.8 | 8498 | 8553 | 8609 | 8665 | 8722 | 8779 | 8837 | 8896 | 8957 | 9018 |
| 0.9 | 9081 | 9146 | 9212 | 9281 | 9353 | 9428 | 9508 | 9595 | 9691 | 9805 |
| 1.0 | 1.0000 | | | | | | | | | |

$B(\frac{1}{3}, \frac{2}{3}) = 3.62760$

In accordance with (14) the total rate of heat transfer from Strip 2 is

$$q_2' = \frac{K\theta_w}{n}\left\{[1 - I_{X(s_1', s_1)}][s_2 - s_2']^{1-\beta} + (1-\beta)\int_{s_1'}^{s_1} \frac{I_{A(\sigma)}}{[\sigma - s_1']^{\beta}}\, d\sigma\right\} \quad (26)$$

The first term in the braces represents the heat transfer that would occur if the wall temperature from $x = 0$ to $x = x_3'$ were uniformly $\theta_w \cdot [1 - I_{X(s_1', s_1)}]$. The second term represents the effect of the temperature gradient along the adiabatic portion. A closed expression for the integral has not been found. Calculations have shown that the contribution of the second term is relatively very small unless the distance between the two strips is quite short.

## 5 Description of the Experimental Apparatus

The *wind-tunnel* has an open circuit with a fan at the intake end. The test section is 32 in. wide by 22 in. high. The contraction ratio is approximately 7:1. The air speed is regulated by varying the pitch of the blades with the aid of a hydraulic mechanism that can be operated while the tunnel is running.

The mainstream turbulence intensity was measured by means of a hot-wire anemometer. Expressed as the ratio of the root-mean-square of the longitudinal velocity fluctuation to the mainstream mean velocity, its value was found to vary from 0.9 to 1.35 per cent, depending upon the station and the air speed. At 71 ft/sec, the velocity for most of the mass-transfer tests, the turbulence intensity varied from about 1.1 to 1.3 per cent.

The *flat plate* spanned the tunnel test section in a horizontal position. It was made of $^3/_8$-in. thick aluminum; its chord and over-all span were 15 and 38$^3/_4$ in., respectively. The leading-edge radius was $^1/_{16}$ in.

The plate, mounted on heavy stanchions outside the tunnel, could be rolled into and out of the test section through the vertical tunnel walls on special tracks. Thus the test mosaics could be installed and disassembled outside the tunnel, and the undesirable transient losses that occurred while the wind was being accelerated to or decelerated from test conditions were minimized.

Some details of the test plate are illustrated in Fig. 3. Test trays slide into the channels from the rear. The two rows of trays allow two simultaneous tests to be run at the same speed and temperature. Each row of trays is provided with two rows of diffusion guards, one row on each side of the channels. The configuration of the guards matches only one set of test mosaics.

The mosaics were assembled from steel trays of the type shown

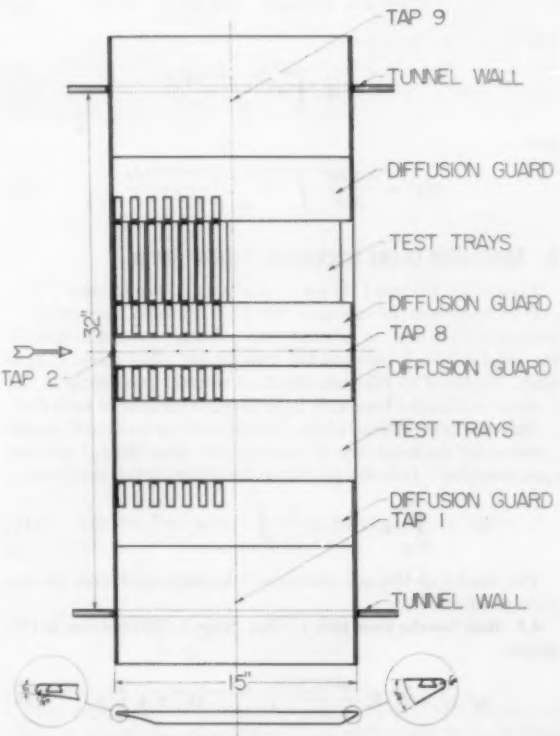


Fig. 3 Plan and profile views of the test plate

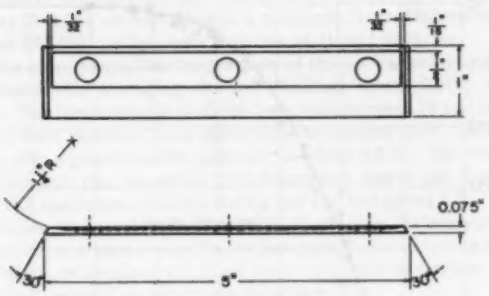


Fig. 4 Typical one-inch tray

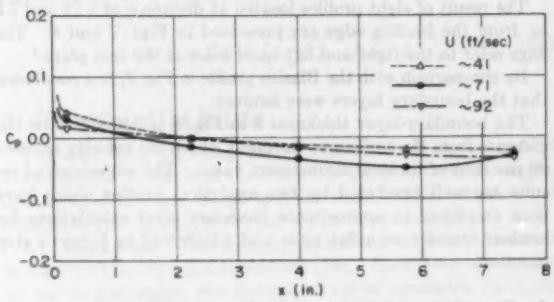


Fig. 6 Pressure distributions on the test plate

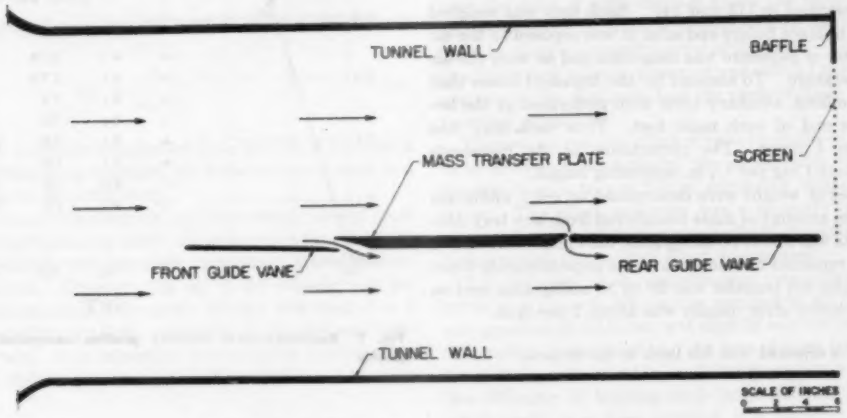


Fig. 5 Orientation of the test plate in the wind tunnel

in Fig 4. There were 14 trays 1.000 in. in length. Their effective spanwise widths were 4.754 in. ±1.1 per cent; the individual widths were used in the calculations. Blanks 1.000 in. in length were employed to introduce any additional inert (analogically unheated) lengths. Some longer trays are briefly described later.

A plate assembled from many individually machined and cast pieces must, of course, be expected to have a sort of waviness superposed on whatever roughness the basic materials possess. In the present case this difficulty is augmented by the regression of the naphthalene as it sublimes. This regression is not uniform, and one must expect that it impresses its peculiar type of roughness in different ways as time progresses during any run. The step-type roughnesses of contiguous trays was as much as 0.003 in., and in some cases the regression of the naphthalene appears to have been as much as 0.015 in. at the leading edges of some strips. But on the average the change of depth in a leading tray of $^1/_2$ in. subliming length was in the order of 0.001 in. A systematic effect of the surface roughness due to the protrusion of the naphthalene in the "as cast" (unsanded) condition was observed. The variation of the laminar transfer with respect to this roughness was small; and it was minimized by sanding the specimens flush.

It will be seen from the boundary-layer velocity profiles and the mass-transfer results themselves that, within the scope of the experiments, most of the assembled surfaces on the plate were smooth in the hydraulic sense.

The plate was oriented as shown schematically in Fig. 5. After establishing that the flow over the front guide vane was completely attached and laminar, the baffle was lowered until no separation occurred at the leading edge of the test plate.

Because the flow was split by the front guide vane, the mainstream velocity $U$ was measured above the test plate. In the region of the plate where the specimens were used (the leading 7.5 inches) the average value of the dynamic head was found to be 31.4 per cent of the total head, $p_0$, scattering within ±3 per cent over the entire range. This value was used to reduce the pressure distributions represented in Fig. 6.

The pressure coefficient is defined by

$$C_p = \frac{p - p_m}{p_{dm}} \tag{27}$$

where $p$ is the local pressure measured at taps along the center of the plate, $p_m$ is the mean static pressure over the main part of the plate, and $p_{dm}$ is the corresponding mean dynamic pressure, $0.314p_0$. Consequently,

$$C_p = 3.18\left(\frac{p}{p_0}\right) - 2.18 \tag{28}$$

Fig. 6 shows typical pressure distributions observed at velocities of about 41, 71, and 92 ft/sec. The drop in $C_p$ over the leading 12 in. is almost linear, and its value is about 0.045 $ft^{-1}$. In correlating the mass-transfer data, a mean velocity above each tray was used.

In order to ascertain that the boundary layer was laminar, velocity profiles were measured at several positions above the plate. The profiles were measured by means of a 0.035-in. thick total-pressure probe in conjunction with a Betz manometer. The trays were filled with clay and made smooth. In one test the clay in a leading tray was gouged to simulate a naphthalene specimen that would have sublimed for an exceedingly long time; the downstream flow exhibited no effect within the sensitivity of the instrumentation.

The result of eight profiles located at distances of 3.78 and 7.5 in. from the leading edge are presented in Figs. 7 and 8. The flags refer to the right and left-hand sides of the test plate.[4]

By comparison with the Blasius profile in Fig. 7, it is concluded that the boundary layers were laminar.

The boundary-layer thickness $\delta$ in Fig. 8 is defined to be the distance from the surface to the point where the velocity reached 99 per cent of its local mainstream value. The experimental results are well bracketed by two analytical profiles which have been employed in approximate boundary-layer calculations for laminar transfer on a flat plate and which lead to Eckert's step function.

## 6 Procedure and Scope of the Experimentation

The procedure employed in this investigation is essentially the same as that described in [13 and 14]. Each tray was weighed in an analytical balance before and after it was exposed to the air stream. The time of exposure was measured and so were the air speed and temperature. To account for the transient losses that occur during handling, auxiliary tests were performed at the beginning and the end of each main test. Thus each tray was weighed at least 4 times. The corrections for the transients amounted to about 1 mg per $^1/_8$ in. subliming length.

Since the losses of weight were determined to $\pm 0.1$ milligram and the minimum amount of mass transferred from any tray during the main tests was about 10 milligrams, the maximum relative error due to the repeated measurements was approximately 4 per cent. Usually, the net transfer was 20 to 30 milligrams, and so the maximum relative error usually was about 2 per cent.

[4] The observer is oriented with his back to the stream.

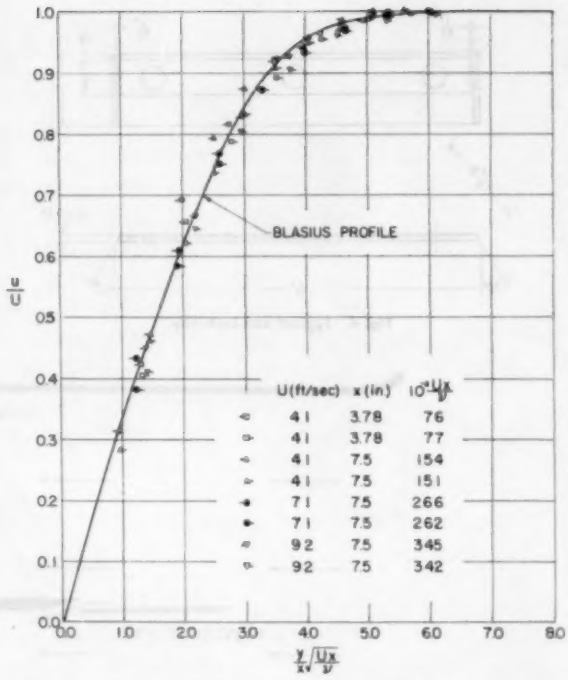


Fig. 7 Boundary-layer velocity profiles compared with the Blasius profile

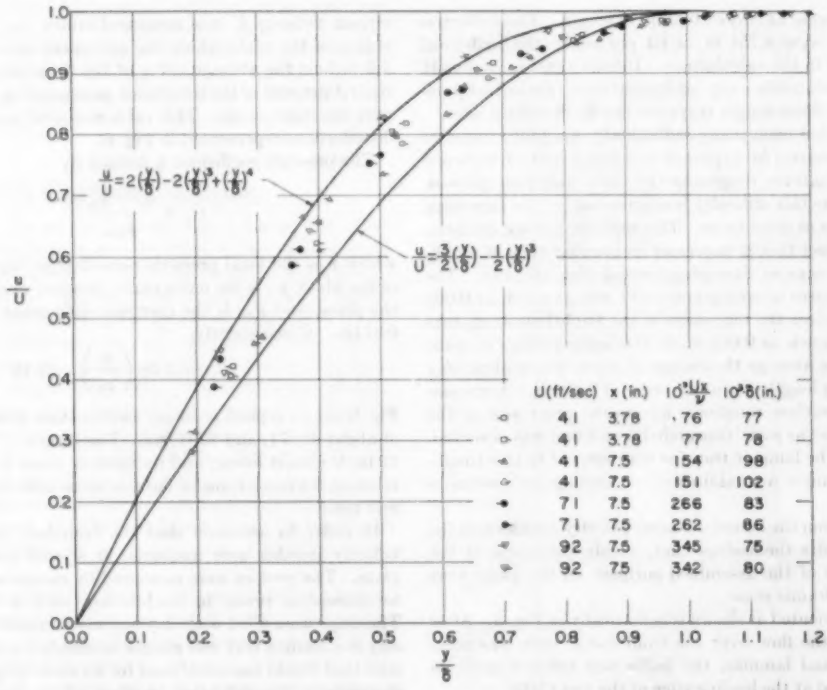


Fig. 8 Boundary-layer velocity profiles compared with polynomial approximations

Most of the tests were performed at a mainstream velocity of about 71 ft/sec corresponding to a maximum Reynolds number of about 250,000. A few tests were run at 41 and 92 ft/sec.

The mean stagnation temperature of the air was evaluated by arithmetically averaging the emf readings taken during each run. The temperatures of all the tests were between 72 and 88 F. They were measured with calibrated thermocouples in conjunction with a potentiometer, accurate to within 0.2 F. The rate of temperature rise was about 0.15 Fahrenheit degree per minute, and the maximum variation during any run was about 3 F. The exposure times were varied from 6 to 20 minutes. In some cases, the specimens were exposed more than once.

Data were obtained for single trays, two trays in tandem, and multiple (more than two) trays in tandem.

## 7 Reduction of the Data

The observed rate of mass transfer per unit span of the $j$th tray or strip is

$$\dot{m}_j' = \frac{\Delta m_j}{w_j \cdot \Delta\tau} \tag{29}$$

where $\Delta m_j$ is the net mass transferred from the $j$th strip after a correction for the handling transient, $\Delta\tau$ is the exposure time, and $w_j$ is the spanwise width of the strip.

In order to compare the observed and theoretical rates of mass transfer, and, in particular, to check the simple step function (18) for the total transfer, the so-called "absolute" transfer ratio $\dot{m}_j'/\dot{m}_{0j}'$ was formed. The quantity $\dot{m}_{0j}'$ is the transfer rate per unit span that would occur if the entire surface area from $x = 0$ to $x = x_j$ were subliming at the conditions of velocity and temperature in the test. It is calculated according to the following equation, which defines the average coefficient of mass transfer $b(0, x_j)$.

$$\dot{m}_{0j}' = b(0, x_j) \cdot x_j \cdot (\rho_{v,w} - \rho_{v,\delta}) \tag{30}$$

The factors in the right-hand member are evaluated as discussed in the next paragraphs.

The mass-transfer coefficient is calculated by means of the equation

$$\frac{b(0, x_j)}{U} \cdot \mathrm{Sc}^{2/3} = \frac{C}{\left(\dfrac{U x_j}{\nu}\right)^n} \tag{31}$$

where $U$ is the velocity observed at the outer edge of the boundary layer. From Pohlhausen's theory, $C = 0.664$ and $n = 0.5$. The distance $x_j$ is measured from the forward tip of the plate to the trailing edge of the $j$th strip.

The vapor pressure in the mainstream is nil, and so $\rho_{v,\delta} = 0$. The vapor at the surface of the subliming wall is assumed to be in equilibrium with the solid and, also, to be thermally perfect. Thus

$$\rho_{v,w} = \frac{p_{v,w}}{R_v T_w} \tag{32}$$

where

$$\log_{10} p_{v,w} = B_1 - \frac{B_2}{T_w} \tag{33}$$

As in [13], Sc = 2.5 and $R_v = 12.05$ ft lb/lb$_M$ F; $B_1 = 11.884$ and $B_2 = 6713$ for absolute temperature in degrees Rankine and pressure in lb/ft$^2$. Further, the wall temperature is taken to be equal to the observed temperature; for the effects of cooling by sublimation and heating by friction are both small and, besides, virtually cancel themselves at the air temperatures and speeds employed in these experiments. Hence (30) may be written

$$\dot{m}_{0j}' = 0.361 \cdot \left(\frac{U x_j}{\nu}\right)^{0.5} \cdot \rho_{v,w} \cdot \nu \tag{34}$$

## 8 Discussion of the Results

The main tests are comprised of runs in which the specimens were sanded. In the next three sections the results on the single, double, and multiple strips are discussed. The influences of roughness and lateral (spanwise) diffusion are noted.

**8.1 Single Strips.** The results of the leading strips are presented in Fig. 9. The solid line represents (18). Except for the results on the longest strips, the theoretical curve correlates the main data within the expected scatter due to experimental error.

The effect of the roughness of the unsanded specimens is to raise the rates of mass transfer above the theoretical values. It was particularly large for a specimen which was made to protrude 0.005 in. above the general level of the plate. The deviation from the theoretical value in that case was about 7 per cent. The effect systematically diminished as the protuberance regressed during repeated exposures.

There was a residual effect of velocity in the experimental setup. It is shown particularly by the abnormally high rate of mass transfer from a tray of 6.5 in. subliming length (Tray 10) at 41 ft/sec. The effect evidently was a property of the tunnel and of mounting the plate independently of the guide vanes. At the higher speeds the residual effect disappeared.

The deviation of the experimental points from the theoretical curve at $x_1'/x_1 = 0.926$ may be ascribed to the fact that the pressure gradient at 92 ft/sec was slightly adverse as shown in Fig. 6, thus reducing the shear and the rate of mass transfer. The scatter of the points at $x_1'/x_1 = 0.038$ probably is a consequence of the difficulty of keeping such large surfaces free of waviness, which could have been avoided, it is believed, if the trays had been made deeper.

The lateral diffusion increased the rate of mass transfer by thinning the diffusional boundary layer. Since its influence could be most easily found if it were acting along large chordwise distances, Tray 10 was run with a reduced width, the edges being filled flush with an inert clay. The result is shown by the partially shaded point marked "$w \approx 2.5$ in." which lies about 5 per cent higher than the theoretical value. Accordingly, the corresponding deviation for the wider strip would be less than 5 per cent, but a definite conclusion cannot be drawn on account of the afore-mentioned scatter.

With regard to the trays of $^1/_2$ in. length, simultaneous tests on guarded and unguarded strips and on strips of 4.75 in. and 2.5 in. span show no significant differences in the rates of mass transfer from corresponding specimens. In view of these results and of those on the long tray, it is concluded that the effect of the lateral diffusion from the $^1/_2$-in. trays is considerably less than 5 per cent. Hence, for the present purpose it has been neglected, and the $^1/_2$-in. specimens are regarded as though they are strips of infinite span. Further, two strips in tandem as well as the single strips can be viewed in this way.

**8.2 Two Strips in Tandem.** As soon as two strips in tandem are used, the number of possible mosaics becomes very large. In order to keep the program within bounds, only two sets of such mosaics, comprised of $^1/_2$-in. strips, were tested.

In one set of tests the distance between them was kept at $^1/_8$ in., and they were moved together from one position to another in different runs. The results are shown in Fig. 10, where the abscissa is the distance to the center of the configuration expressed in units of the subliming length.

A noticeable effect of the roughness in the interposed steel blanks was observed when the trays were at their greatest dis-

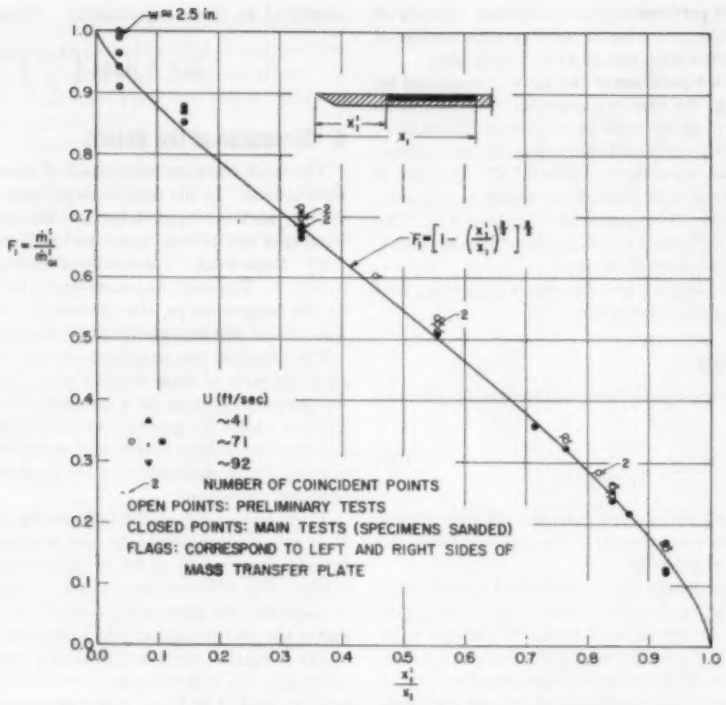


**Fig. 9 Comparison of experimental and theoretical results for single strips**

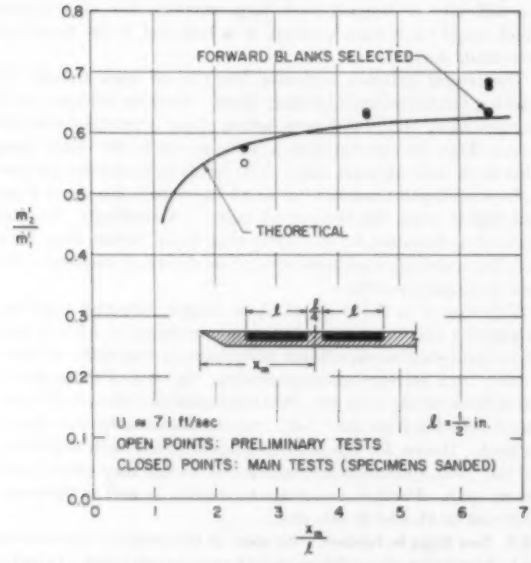


**Fig. 10 Comparison of experimental and theoretical relative ratios (fixed distance between strips)**

tance downstream. Thus, when the 1-in. blanks were carefully selected so that the forward inert length was smooth to the sense of touch, the experimental result fell in good agreement with the theory, as shown by the lowest point at $x_m/l = 6.5$.

In the second set of tests on two $^1/_2$-in. strips in tandem, Strip 1 was held fixed at $x_1 = 0.75$ in. and Strip 2 was moved to different positions downstream. The results are shown in Figs. 11 and 12 where the abscissas are distances between the strips measured in units of the length of one strip.

The ordinate in the graph of Fig. 11 is the relative mass transfer ratio $\dot{m}_2'/\dot{m}_1'$. Interestingly, the theory shows that the mass transfer from Strip 2 is increased 20 per cent when it is moved to the distance $l$ downstream. It reaches a maximum at about $2.5l$ and thereafter it hardly changes. The experimental results substantially verify the results predicted by the theory. Again, the low-speed runs appear high. The scatter is somewhat greater than it was for the single strips, especially for the preliminary results, undoubtedly because the roughness of both strips influences the transfer process.

The absolute mass-transfer ratios, $\dot{m}_2'/\dot{m}_{2_0}'$, for the same series of tests is presented in Fig. 12. Theoretically, the absolute ratio reaches a maximum when the distance between the trays is $l/2$, and again the agreement between the experimental and theoretical results is good.

**8.3 Multiple Strips in Tandem.** Several tests were performed on mosaics comprised of seven $^1/_2$-in. strips in tandem. In each test the inert distance to the leading edge of the first strip was $x_1' = 0.25$ in., and the total distance to the trailing edge of the last strip was $x_7 = 6.75$ inch. The inert distances between the strips were $^1/_2$ in., and each strip was situated on an individual tray. The velocity was approximately 71 ft/sec in all the tests.

In order to determine whether the nature of the flow in the boundary layer was grossly altered by the changing roughness, the pressure behind the last strips was continually observed by laying the impact tube flat on the test surface. A pressure variation occurred during the first few minutes of each initial exposure, but its magnitude was quite small and no particular significance could be attached to it. In one instance a complete boundary-layer velocity profile, measured about $^1/_2$ hour after the sublimation test had ended, virtually coincided with the profiles described previously. Hence, it was concluded that within

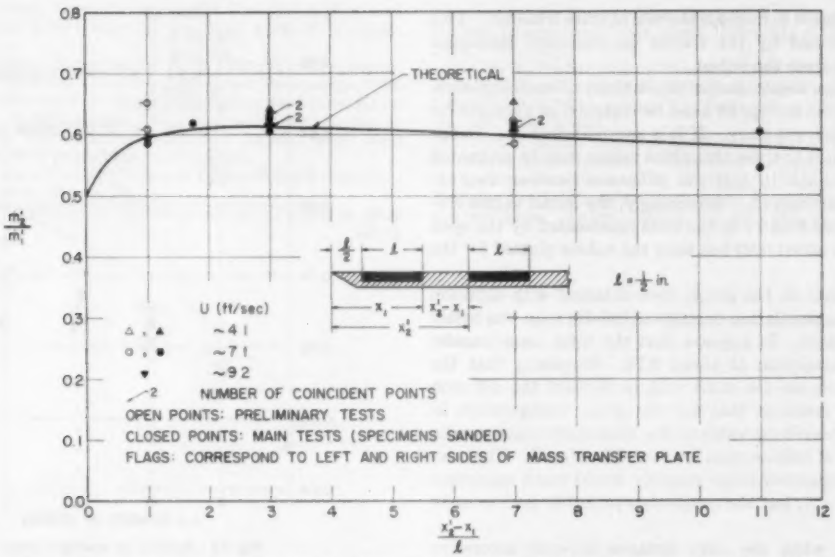
THEORETICAL
U (ft/sec)
△ , ▲ ~41
○ , ● ~71
▼ ~92
2 NUMBER OF COINCIDENT POINTS
OPEN POINTS: PRELIMINARY TESTS
CLOSED POINTS: MAIN TESTS (SPECIMENS SANDED)
FLAGS: CORRESPOND TO LEFT AND RIGHT SIDES OF MASS TRANSFER PLATE
ℓ = ½ in.

**Fig. 11 Comparison of experimental and theoretical relative ratios (fixed leading strip and variable distance between strips)**

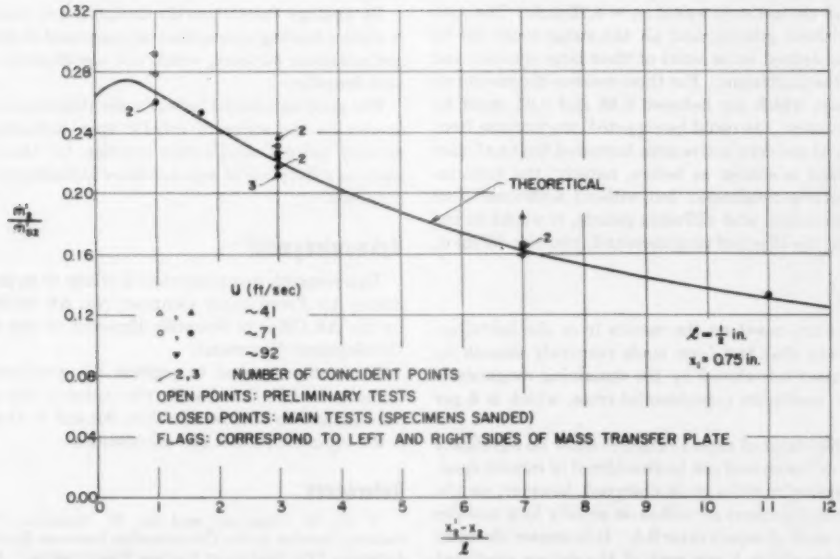
THEORETICAL
U (ft/sec)
△ , ▲ ~41
○ , ● ~71
▼ ~92
2,3 NUMBER OF COINCIDENT POINTS
OPEN POINTS: PRELIMINARY TESTS
CLOSED POINTS: MAIN TESTS (SPECIMENS SANDED)
FLAGS: CORRESPOND TO LEFT AND RIGHT SIDES OF MASS TRANSFER PLATE
ℓ = ¼ in.
x₁ = 0.75 in.

**Fig. 12 Comparison of experimental and theoretical absolute ratios (fixed leading strip and variable distance between strips)**

the limitation of the instrumentation the profiles remained substantially laminar during the main tests and that no major change in the nature of the boundary layer occurred during ablation. However, significant changes probably would have been found with finer instrumentation as indicated by the mass-transfer results themselves.

In Fig. 13 the total mass-transfer ratio $\sum_{j=1}^{n} \dot{m}_j'/\dot{m}_{on}'$ is plotted against the number of strips from $n = 1$ to 7. Curves are not drawn through the points because the functional relationship is discontinuous. The dotted curve represents the upper bound of the experimental results of very rough specimens, details of which are omitted from the graph in order to avoid obscuring the pertinent features. Almost all exposure times were 10 minutes. The suffixes A and B refer, respectively, to the first and second exposure. The points are staggered to indicate the side of the test plate on which the strips were situated.

Clearly, there is a remarkable spread of the results, increasing as the number of the strips is increased. This spreading is ascribed to the effect of the changing roughness.

The results of the second exposure are almost consistently higher than those of the first, the possible exception being those at Strip 1. Hence, as one expects intuitively, the effect of the

increasing roughness is to increase the rate of mass transfer. This is similarly confirmed by the results on unsanded specimens which were rough from the outset.

Since the surfaces ablate during the entirety of each exposure, the results presented in Fig. 13 must be regarded as averages for the duration of each exposure. If it is assumed that the change is linear with respect to time, the initial values may be estimated by extrapolating back to half the difference between two exposures on the same mosaic. Accordingly, the initial values corresponding to Strips 6 and 7 in the tests represented by the open symbols would be about 0.02 less than the values plotted for the first exposure.

The lowest points on the graph were obtained with diffusion guards, so that the simulation to strips of infinite span was better than with the others. It appears that the total mass-transfer ratio reaches a maximum of about 0.74. Supposing that the effects of roughness are the same with or without the diffusion guards, we may conclude that for the given configuration in laminar flow the maximum value of the total mass-transfer ratio for smooth strips of infinite span is about 72 per cent. The relatively smooth, unguarded strips possibly would reach maximum values beyond $n = 7$, but the rough ones probably lead to early transition.

What happens when the inert distance between successive strips is reduced? Tests were performed on the single aluminum tray with 11 strips 0.100 in. apart (Tray 11). Like the 7-strip mosaic, the leading edge of the first strip was at $x_1' = 0.25$ in. and the trailing edge of the last strip was at $x_{11} = 6.75$ inch. The data were obtained without guards, and all the strips could not be finished as well as desired on account of their large number and of the softness of the aluminum. For these reasons the results on the 11-strip mosaic, which lay between 0.88 and 0.95, must be regarded as preliminary. As could be expected, the increase from a nominally 50 to 80 per cent active area increased the total mass transfer. The trend is similar as before, namely, the ratio increases with increasing roughness; but without additional tests using smoother specimens and diffusion guards, it would be impossible to separate the effects of roughness and spanwise diffusion.

## 9 Conclusions

The conclusions are based on the results from the initial exposures of specimens that had been made relatively smooth by sanding. The scatter introduced by the remaining roughnesses is well within the maximum experimental error, which is 5 per cent.

Single and double strips of aspect ratio 9.5 show no significant effect of spanwise diffusion and can be considered of infinite span. The influence of spanwise diffusion is observed, however, on the long narrow subliming surfaces as well as on equally long mosaics of multiple strips, each of aspect ratio 9.5. It increases the total rate of mass transfer about 5 per cent of the values predicted for a single strip of the same length but of infinite span. No attempt has been made to account for the lateral diffusion by correlating against the aspect ratio in a general way. Here, a theory is needed that would, also, account for the fact that the thermal diffusivity of the air is considerably greater than its diffusivity with respect to naphthalene vapor.

The results on 7 equally spaced strips of virtually infinite span indicate that an active area of nominally 50 per cent would yield about 72 per cent of the mass transfer from a surface of uniform concentration functioning otherwise under like conditions. Some preliminary results on 11 strips indicate, however, that when the active area along the same distance is increased to nominally 80 per cent, the corresponding mass transfer is in the order of 85 per cent. Clearly, the surface discontinuities of concentration and flux due to the short inert surfaces between the strips neither

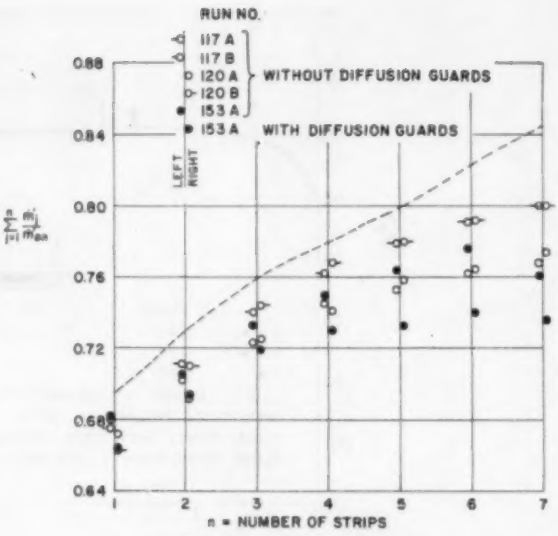


Fig. 13 Results on multiple strips

considerably deter nor appreciably improve the rate of mass transfer.

By analogy the surface discontinuities of temperature and flux in similar heating arrangements, comprised of alternate isothermal and adiabatic surfaces, would not significantly affect the rate of heat transfer.

The good agreement between the theoretical and experimental results on the strips of infinite span indicates that the RKT method using Eckert's step function for the laminar boundary layer on a flat plate at zero incidence is satisfactory for engineering purposes.

## Acknowledgment

This research was supported in whole or in part by the United States Air Force under Contract No. AF 49(638)-46 monitored by the AF Office of Scientific Research of the Air Research and Development Command.

The author wishes to express his gratitude to Messrs. C. Cometta and E. Schafranik, who aided in the design of the apparatus, and to Messrs. Cho-Yen Ho and V. Oskay, who assisted in the experimentation and calculations.

## References

1 D. R. Chapman and M. W. Rubesin, "Temperature and Velocity Profiles in the Compressible Laminar Boundary Layer With Arbitrary Distribution of Surface Temperature," *Journal of the Aeronautical Sciences*, vol. 10, 1949, pp. 341–348.

2 M. J. Lighthill, "Contributions to the Theory of Heat Transfer Through a Laminar Boundary Layer," *Proceedings, Royal Society of London*, series A, vol. 202, 1950, pp. 359–377.

3 M. W. Rubesin, "The Effect of an Arbitrary Surface Temperature Variation Along a Flat Plate on the Convective Heat Transfer in an Incompressible Turbulent Boundary Layer," NACA Technical Note 2345, 1952.

4 J. Klein and M. Tribus, "Forced Convection From Non-Isothermal Surfaces," Heat Transfer Symposium, Engineering Research Institute, University of Michigan, 1952.

5 J. P. Hartnett, E. R. G. Eckert, R. Birkebak, and R. L. Sampson, "Simplified Procedures for the Calculation of Heat Transfer to Surfaces With Non-Uniform Temperatures," WADC Technical Report 56-373, 1956.

6 E. R. G. Eckert, J. P. Hartnett, and R. Birkebak, "The Calculation of the Wall Temperature Along Surfaces Which Are Exposed to a Fluid Stream When the Local Heat Flow Through the Surface is Prescribed," WADC Technical Report 57-315, 1957.

7 E. R. G. Eckert, "Introduction to the Transfer of Heat and Mass," McGraw-Hill Book Company, Inc., New York, N. Y., 1950, pp. 88–92.

8 R. D. DeLauer, "Experimental Heat Transfer at Hypersonic Mach Number," PhD thesis, California Institute of Technology, 1953.

9 W. J. Christian and S. P. Kezios, "Experimental Investigation of Mass Transfer by Sublimation From Sharp-Edged Cylinders in Axisymmetric Flow With Laminar Boundary Layer," 1957 Heat Transfer and Fluid Mechanics Institute, Pasadena.

10 M. Jakob, "Heat Transfer," volume I, John Wiley & Sons, Inc., New York, N. Y., 1949, Chapter 28.

11 S. Scesa, "Experimental Investigation of Convective Heat Transfer to Air From a Flat Plate With a Stepwise Discontinuous Surface Temperature," MS thesis, University of California, Berkeley, 1949.

12 B. N. Furber, "Some Heat and Mass Transfer Experiments on Humid Air in Turbulent Flow Over a Plane Containing an Isolated Cooled Region," *Proceedings, The Institution of Mechanical Engineers*, vol. 168, 1954, p. 860.

13 H. H. Sogin, "Sublimation From Disks to Air Streams Flowing Normal to Their Surfaces," TRANS. ASME, vol. 80, 1958, pp. 61–67.

14 Shoa-Yen Ko and H. H. Sogin, "Laminar Mass and Heat Transfer From Ellipsoidal Surfaces of Fineness Ratio 4 in Axisymmetrical Flow," TRANS. ASME, vol. 80, 1958, pp. 387–390.

**R. V. DUNKLE**
Associate Professor of Mechanical Engineering, University of California, Berkeley, Calif.

**F. EHRENBURG**
Associate in Nuclear Engineering, University of California, Berkeley, Calif.

**J. T. GIER**
Professor of Engineering, University of California, Los Angeles, Calif.

# Spectral Characteristics of Fabrics From 1 to 23 Microns

## Introduction

THE EVALUATION of the heat transfer to and from clothing requires a knowledge of the absorptance, reflectance, transmittance, and emittance of the cloth. Such information may consist of total radiant property measurements which are applicable only for specific conditions, or it may consist of spectral data which can be utilized to predict the total radiant properties for sources of any spectral distribution. This investigation was concerned with the determination of the spectral reflectance of several types of natural, synthetic, and regenerated textiles used as clothing materials. The types of textiles are defined by the fibers used in their construction. Natural fibers are those which are derived directly from animals, plants, or insects, e.g., wool, cotton, silk. Synthetic fibers are produced in the laboratory from simple chemical units and have no relationship to natural fibers. Nylon and Orlon are two examples of this type. Regenerated fibers are made from relatively complex chemical units, e.g., cellulose or protein, and are frequently made by treating natural fibers chemically to produce a new type of fiber. Rayon and acetate are examples of regenerated fibers. Table 1 lists the samples tested, groups them into their main categories, gives a short description, and indicates whether the samples were the same on both sides.

The work described in this paper was performed at the University of California at Berkeley as an outgrowth of a research project sponsored by the United States Army Quartermaster Corps Research and Development Center. The spectral reflectance as reported here is actually the system reflectance, since, in addition to energy reflected from the sample, it also includes energy that passes through the sample and is reflected from the low reflectance background and transmitted back through the sample. A low reflectance background was used in these tests; as a consequence, the effect of the background was negligible except in the region of 1.0 to 3.0 microns where the textile material is relatively transparent to infrared radiation. It was found experimentally, for the materials reported in this paper, that three layers were sufficient to eliminate the effect of the background, so data were reported for both single and triple layers of cloth.

Contributed by the Heat Transfer Division of THE AMERICAN SOCIETY OF MECHANICAL ENGINEERS and presented at the ASME-AIChE Heat Transfer Conference, Storrs, Conn., August 9–12, 1959.

NOTE: Statements and opinions advanced in papers are to be understood as individual expressions of their authors and not those of the Society. Manuscript received at ASME Headquarters, May 4, 1959. Paper No. 59—HT-9.

**Table 1 Description of cloth samples**

| Fig. | Material | Class | Color | No. of layers run | Remarks |
|---|---|---|---|---|---|
| 3 | Cotton | Natural | | 1 & 3 | Close weave avg. of samples, dyed, and undyed |
| 4 | Cotton | Natural | Medium gray | 1 & 3 | Sateen, treated w/Carboxy Methyl cellulose and impregnated with carbon |
| 4 | Cotton | Natural | Dark gray | 1 & 3 | |
| 4 | Cotton | Natural | Deep black | 1 & 3 | |
| 4 | Milium | Natural | Aluminum | 1 & 3 | Aluminized cloth, close weave |
| 5 | Linen | Natural | Blue | 1 & 3 | Close weave, thin |
| 6 | Wool | Natural | Spotted pink | 1 & 3 | Close weave, thin |
| 7 | Wool-nylon (85-15) | Nat.-syn. | Dark green | 1 | Close weave, thick |
| 7 | Wool-cotton (50-50) | Natural | White | 1 & 3 | Close weave, thick |
| 8 | Silk | Natural | White | 1 & 3 | Close weave, thin |
| 9 | Acetate | Regenerated | White | 1 & 3 | Close weave, thin |
| 10 | Arnel | Synthetic | Rust | 1 & 3 | Close weave, thin |
| 11 | Rayon | Regenerated | Green | 1 & 3 | Med. weave, thin |
| 12 | Dacron | Synthetic | White | 1 & 3 | Med. weave, thin |
| 12 | Dacron | Synthetic | Green | 1 & 3 | Med. weave, thin |
| 13 | Orlon | Synthetic | White | 1 | Fuzzy surface, suit material |
| 13 | Orlon | Synthetic | Blue | 1 | Fuzzy surface, suit material |
| 14 | Nylon | Synthetic | White | 1 & 3 | Med. weave, thin |
| 14 | Nylon | Synthetic | Green | 1 & 3 | Med. weave, thin |

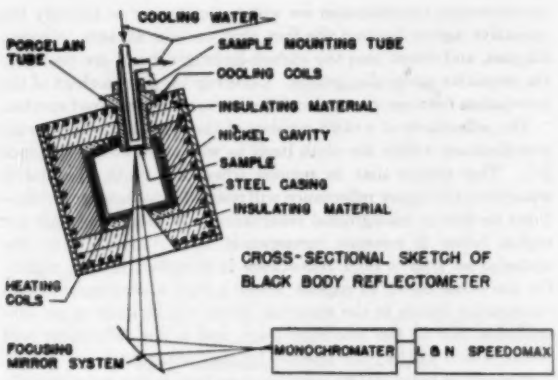


Fig. 1(a) Sketch of hohlraum

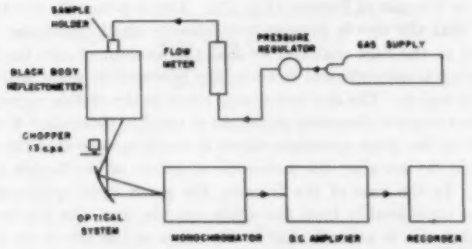


Fig. 1(b) Block diagram of system

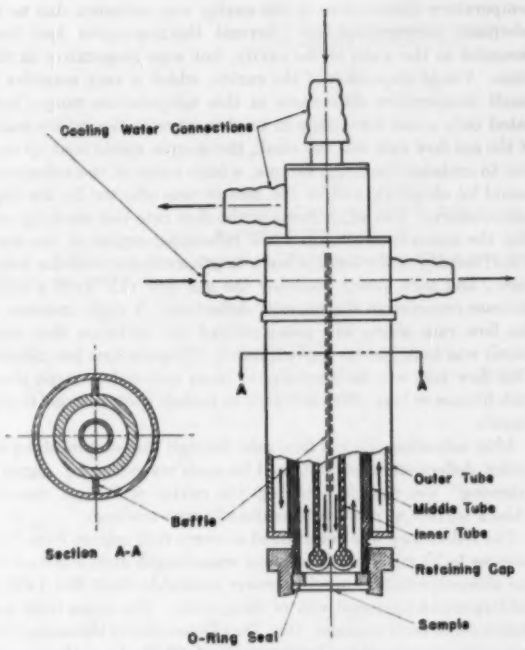


Fig. 1(c) Sketch of sample holder

## Apparatus and Equipment

A Gier-Dunkle black body reflectometer [1][1] is used, which operates by exposing the sample to black body radiation within a "hohlraum" at a temperature of approximately 1400 F, Fig. 1(*a*). Since the sample is cooled to approximately detector temperature, the reflectance can be evaluated from the ratio of the radiosity of the sample to the radiosity of the hohlraum. The radiosity is defined as the flux density leaving a surface, and includes transmitted, reflected, and emitted radiation. For opaque materials, the radiosity is equal to the sum of the emitted and reflected radiation fluxes. A block diagram of the system is shown in Fig. 1(*b*). Radiation from the black body is sent through the optical system to the Perkin-Elmer monochromator where a prism breaks the infrared radiation into its spectrum. The radiation is detected by means of a sensitive vacuum thermocouple, the signal of which is transmitted through an amplification system and then to a recorder.

A slight modification was made in the sample cooling method described in reference [1], Fig. 1(*c*). The center tube of the sample holder which normally directs water on the rear of a metal sample, was connected to a tank of gas through a flow-metering system. This allowed gas to flow through the cloth samples, thus cooling them by convection.

An inert cooling gas, which is transparent to thermal radiation, and is relatively inexpensive, is desirable for this purpose. The majority of texts were run using dry nitrogen as a coolant.

## Experimental Procedure

The reflectance of the sample holder was taken without a sample in place to provide some basis for evaluating the background effect. The reflectance is found to be reasonably constant over the wave-length range from 3 to 23 microns (see Fig. 2). The variations shown in the figure are attributed to the existence of surface films on the central cooling tube in the sample holder The central tube was constructed of copper and had an enlarged end built up of solder to direct the water flow onto the sample for normal operation with metallic samples. This tube should have been blackened for use with the cloth samples to reduce reflections, but this was not done. The nature of the corrosion products in this tube was not known, but they were present in small amounts. The effect of the variations in the constancy of the background reflectance is negligible.

Samples used were cut from large swatches of material and trimmed to a circular shape of $^{7}/_{8}$ in. diameter. These were placed in the retaining cap and held in place by an O-ring.

The gas flow was started and the sample holder inserted in the black body reflectometer. The coolant gas entered the sample holder at room temperature, which was controlled at 68 F. The sample temperature could not be relisbly measured with the cool gas flowing through it while exposed to the high radiation flux on one side. The gas flow rate through the sample was found to be critical. If the flow rate was too large, the bottom of the cavity would be cooled, resulting in a low value for the reflectance. The

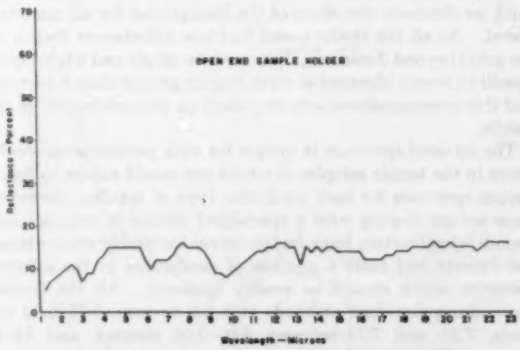


Fig. 2 Reflectance, open end of sample holder

[1] Numbers in brackets designate References at end of paper.

temperature distribution in the cavity was unknown due to inadequate instrumentation. Several thermocouples had been mounted in the walls of the cavity, but were inoperative at this time. Visual inspection of the cavity, which is very sensitive to small temperature differences in this temperature range, indicated only small variations in brightness over the cavity walls. If the gas flow rate was too small, the sample would heat up and, due to emission from the sample, a high value of the reflectance would be obtained, and/or the sample was affected by the high temperature. The adjustment of the flow rate was made by setting the monochromator in a low reflectance region of the spectrum (usually at the longest wave length available with the prism used), and then slowly reducing the gas flow rate until a slight increase occurred in the recorder deflection. A slight increase in the flow rate above this point yielded the optimum flow rate, which was found to be approximately 0.3 cubic feet per minute. This flow rate was satisfactory for most materials, except those with fibrous or fuzzy surfaces, such as mohair (not included in this paper).

After adjusting the gas flow rate through the sample, three recorder deflections were obtained for each wave length; namely, "viewing" the sample, viewing the cavity wall, and viewing a black surface at room temperature (a zero reading).

The reflectance was determined at every 0.25 micron from 1.25 microns to 23 microns. The lower wave-length limit was fixed by the monochromatic emissive power available from the 1400 F hohlraum and the sensitivity of the system. The upper limit was chosen for several reasons: One, that 78 per cent of the energy lies below 23 microns for a temperature of 60 F; two, the energy from the black body became so small that the slit widths used became too large for good spectral resolution; and three, the uniformity of the curves in the far infrared indicated the possibility of extrapolation to longer wave lengths with a small amount of error. This method of taking data at 0.25 micron intervals was determined by Gier, Dunkle, and Bevans [1] to be the most feasible since it allowed the amplifier gain and slit widths to be adjusted for maximum deflection, thus affording less error than would be the case with a continuous scanning and comparison process. Because of a fairly high noise level the recorder deflection was rounded off to the nearest integer on the scale of 100.

In addition to the error in the recorder reading there are small errors due to emission from the cloth and cooling of the bottom of the hohlraum cavity. The error is not computed as a percentage, but only as units of reflectance (see Appendix).

## Discussion of Results

The spectral reflectance curves for the various materials tabulated in Table 1 are plotted in Figs. 3 to 14. For most materials, two curves are plotted, one for a single layer of cloth with the low reflectance sample holder as a background (Fig. 2), and a second curve for a triple layer of cloth which was found to be sufficiently thick to eliminate the effect of the background for all materials tested. As all the cloths tested had low reflectances (below 50 per cent) beyond 3 microns, the curves for single and triple layers should be nearly identical at wave lengths greater than 3 microns, and this correspondence acts as a check on the consistency of the results.

The infrared spectrum is unique for each particular molecule, hence in the textile samples observed one would expect to find a unique spectrum for each particular type of textile. However, since we are dealing with a specialized section of organic compounds where certain basic molecules are inevitably encountered, one expects and finds a number of similarities in the infrared spectrum which should be readily apparent. All the textiles show absorption lines or bands at 3–3.5 microns, 5.75–6.00 microns, 7.25 and 7.75 microns, 7.00–9.00 microns, and 14–17 microns. Since this investigation is not concerned with infrared spectroscopic identification we will not endeavor to identify the causative agents beyond the fact that certain alkanes, alkenes, alkynes, and esters, and the carbon-hydrogen bond are probably the causative molecular groups. Colthrup [3] gives a chart of the correlation between the molecular structure and infrared spectra.

The reflectance of a cloth consists of the contributions from interreflections within the cloth itself as well as surface reflectance [6]. This means that in regions where the cloth material is transparent a higher reflectance will result due to these interreflections or due to background reflectance. In most materials the region below 2 microns corresponds to a "window" in the material so that a high reflectance is observed in this region. On the other hand, in regions where a high absorptance occurs (absorption bands in the material) there will be little or no contribution due to the interreflections, and a low reflectance will result, which will be little affected by the background.

*It should be noted that the use of dyes on textiles does not materially affect the infrared spectrum past 3 microns on any of the textiles* except in the case of Dacron (Fig. 12). This is primarily due to the fact that the dye is present in relatively small quantities compared to the base material so that the amount of dye the fiber takes up is not sufficient to cause any perceptible effect in the infrared region. The dye has a large effect in the visible region due to the resonant electronic structure of the dye molecule. From a study of the gross spectrum shown it would appear that the dyes present do not alter the molecular structure of the textile molecule. In the case of the Dacron, the green dyed specimen deviates considerably from the white sample, and it is not known whether this is actually due to the effect of the dye or to a difference in the chemical structure of the two types of Dacron.

It should also be noted that several other processes on textiles do change the infrared spectrum considerably. Metallizing the cloth by coating the fiber of the fabric with some metal such as aluminum, gold, or silver causes the cloth to exhibit more of the properties of the metal than of the basic textile. This is evidenced by the almost constant, relatively high, reflectance of Milium (aluminized cloth, Fig. 4) from 1 to 23 microns, broken only in portions of the spectrum by the strong carbon hydrogen bands. Cloth samples impregnated with carbon black (Fig. 4) show effects through the complete infrared region as well as the visible. The effect of carbon black is to minimize by absorption the contribution of the interreflections within the cloth, so that the principle result is to reduce the reflectance in regions where the reflectance is high.

It is also of interest to note that the three main classifications of textiles (i.e., natural, regenerated, and synthetic) show certain basic *similarities and differences* in their infrared spectra.

For example, in the natural textiles two major maxima occur in the reflectance curve at approximately 5.25 and 11.5 microns. The regenerated fibers also have two maximums, although they are located at 4.25 and 12.75 microns. The synthetic textiles differ in their spectral characteristics from the regenerated and natural groups and also differ from each other.

From the nature of these basic similarities and dissimilarities it is easy to classify an unknown textile sample into one of the three major groups.

The spectral reflectance curves can be used to compute the total emissivity of the cloth [4, 5]. The curves can also be utilized to compute the reflectance for sources of any temperature or energy distribution [4]. If the spectral reflectance curves are extended through the visible region, it is found that the reflectance in this region is determined almost exclusively by the type of dye used on the cloth. These data can be used to calculate the reflectance of materials for solar radiation. A paper is now under preparation describing apparatus for direct measurements of solar transmittance and reflectance of textiles. Good agreement is obtained between the measured and calculated solar reflectances.

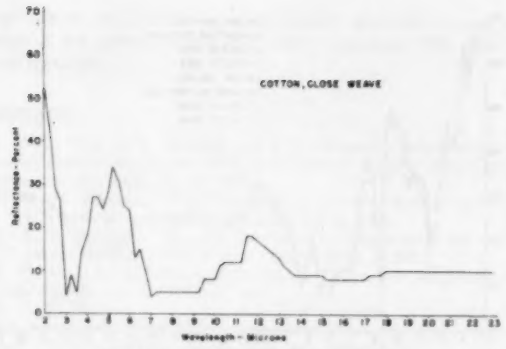


Fig. 3 Reflectance, cotton, close weave

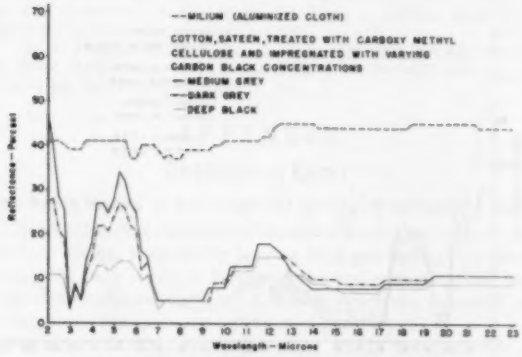
—MILIUM (ALUMINIZED CLOTH)
COTTON, SATEEN, TREATED WITH CARBOXY METHYL CELLULOSE AND IMPREGNATED WITH VARYING CARBON BLACK CONCENTRATIONS
— MEDIUM GREY
— DARK GREY
— DEEP BLACK
Reflectance - Percent
Wavelength - Microns

Fig. 4 Reflectance, Milium and carbon-impregnated

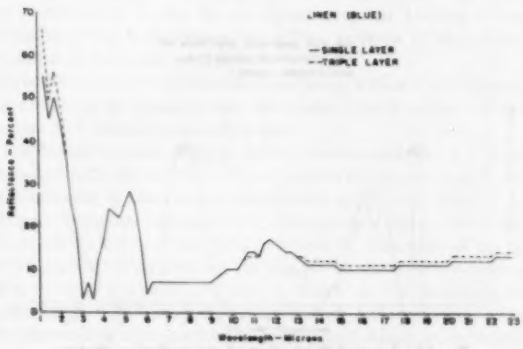


Fig. 5 Reflectance, linen

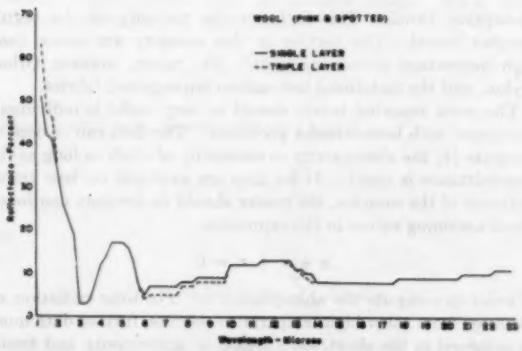


Fig. 6 Reflectance, wool

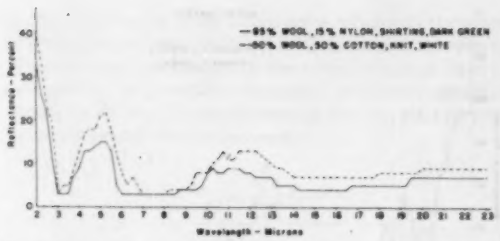


Fig. 7 Reflectance, 85 per cent wool, 15 per cent nylon; 50 per cent wool, 50 per cent cotton

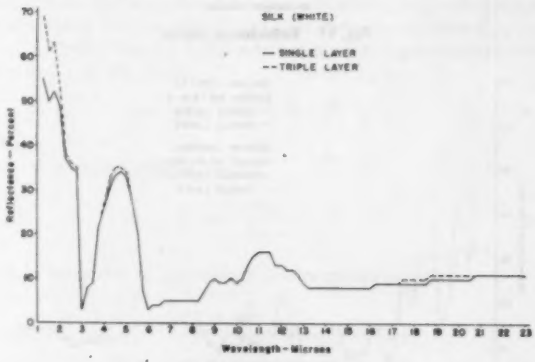


Fig. 8 Reflectance, silk

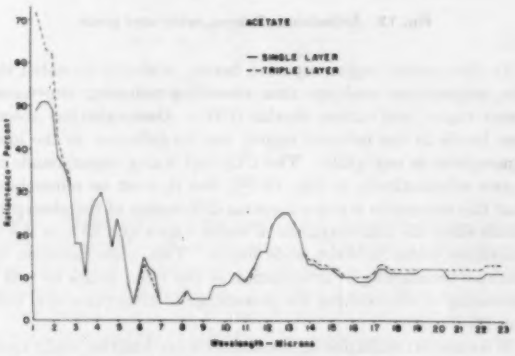


Fig. 9 Reflectance, acetate

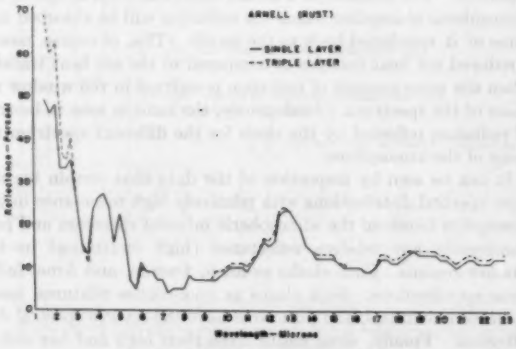


Fig. 10 Reflectance, Arnel

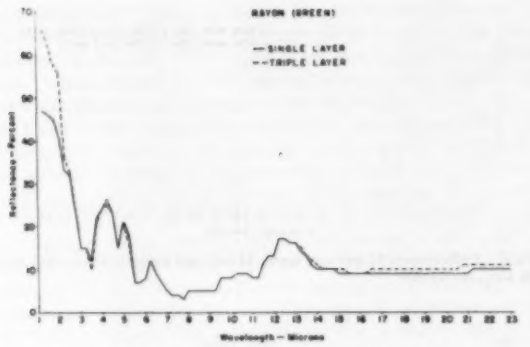


Fig. 11 Reflectance, rayon

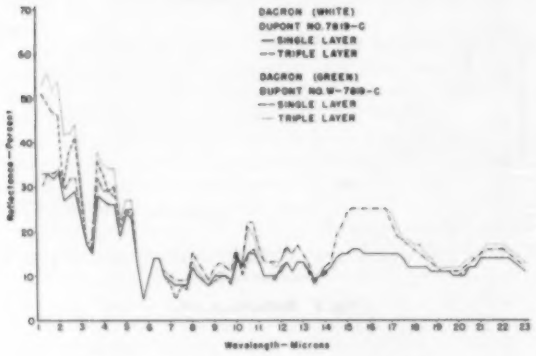


Fig. 12 Reflectance, Dacron, white and green

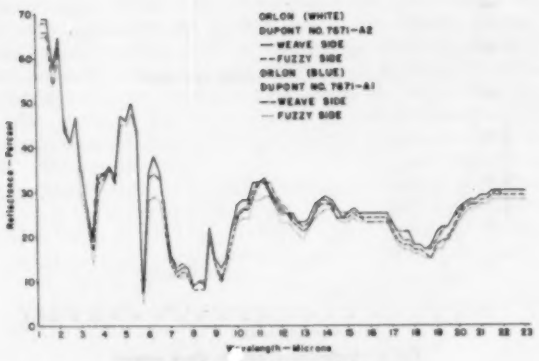


Fig. 13 Reflectance, Orlon

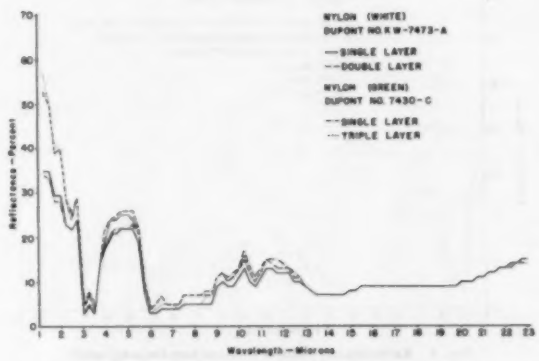


Fig. 14 Reflectance, nylon

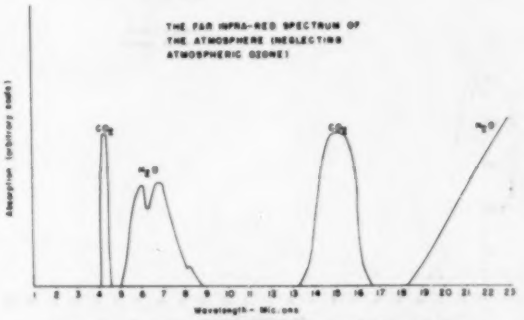


Fig. 15 Spectral distribution of atmospheric radiation

In the spectral region reported herein, it should be noted that the atmosphere contains two absorbing-radiating substances, water vapor, and carbon dioxide ($CO_2$). Ozone also has absorption bands in the infrared region, but its influence in the lower atmosphere is negligible. The $CO_2$ and water vapor bands are shown schematically in Fig. 15 [2], but it must be remembered that this schematic is not a rigorous delineation of the absorption bands since the concentration of water vapor and $CO_2$ in the atmosphere varies between wide limits. This wide variation can produce broadening or attenuation of the band limits as well as increasing or diminishing the percentage of absorption and emission [2].

If we neglect radiation in the shorter wave lengths (night time), such as solar radiation, we see that the net gain or loss of heat from the textile is strongly influenced by the atmospheric infrared spectrum. For instance, if a textile emits radiation in one of the atmospheric absorption bands the radiation will be absorbed and some of it reradiated back to the textile. This, of course, means a reduced net heat transfer as compared to the net heat transfer when the same amount of radiation is emitted in the window regions of the spectrum. Analogously, the same is seen to be true of radiation reflected by the cloth for the different spectrum regions of the atmosphere.

It can be seen by inspection of the data that certain textiles have spectral distributions with relatively high reflectance in the absorption bands of the atmospheric infrared spectrum and predominately low relative reflectance (high emittance) in the window regions. Such cloths as linen, Dacron, and Arnel fulfill these specifications. Such cloths as wool-cotton mixtures, wool-nylon combinations, and pure wool have the reverse spectral distribution. Finally, some cloths have their high and low reflectance bands distributed randomly in and out of the atmospheric absorption bands. This includes the majority of the textile samples tested. The textiles in this category are cotton (and high percentage cotton mixtures), silk, rayon, acetate, Orlon, Nylon, and the metallized and carbon impregnated fabrics.

The work reported herein should be very useful to individuals concerned with heat-transfer problems. The data can be used to compute [4] the absorptivity or emissivity of cloth as long as the transmittance is small. As no data are available on true transmittance of the samples, the reader should be strongly cautioned about assuming values in the expression

$$a + r + \tau = 0$$

in order to compute the absorptance, $a$. For solar radiation, or radiation from other high temperature sources, further data must be obtained in the short wave region in absorptivity and transmissivity. This region was not covered in this paper as the cloth

properties in this spectral range are highly dependent upon the nature of the dyes used and are readily measured with conventional methods.

## References


1 J. T. Gier, R. V. Dunkle, and J. T. Bevans, "Measurement of Spectral Reflectivity From 1.0 to 15 Microns," *Journal of the Optical Society*, vol. 44, 1954, pp. 558–562.

2 W. M. Elsasser, "Heat Transfer by Infrared Radiation in the Air," Harvard Meteorological Studies, no. 6, 1942.

3 N. B. Colthrup, "Spectra Structure Correlations in the Infrared," *Journal of the Optical Society*, vol. 6, 1950, p. 397.

4 R. V. Dunkle, "Thermal-Radiation Tables and Applications," TRANS. ASME, vol. 76, 1954, p. 549.

5 J. T. Bevans, J. T. Gier, and R. V. Dunkle, "Comparison of Total Emittances With Values Computed From Spectral Measurements," TRANS. ASME, vol. 80, 1958, pp. 1405–1416.

6 R. V. Dunkle, J. T. Gier, J. T. Bevans, and D. K. Edwards, "Study of the Various Modes of Heat Transfer From and Through Clothing Materials," Report Series 80, Issue 1, Project 92-06-001, University of California, Berkeley, Calif.

7 R. V. Dunkle and J. T. Bevans, "An Approximate Analysis of the Solar Reflectance and Transmittance of Snow," *Journal of Meteorology*, vol. 13, 1956, p. 121.


# APPENDIX

## Discussion of Errors

### Errors Due to Heating of the Sample and Cooling of the Cavity

Two significant temperature-dependent errors can occur when the cloth sample is cooled by passing inert gas through it. One error arises as a result of increased thermal emission from the sample if its temperature rises. A second error is due to cooling of the bottom of the hohlraum by the inert gas.

Two other radiation errors can occur within the black body. One error is due to net radiation exchange between the sample 1 and reference area 2. This error can be shown to be very small. The fourth error is due to the opening in the bottom of the hohlraum which is important for diffuse surfaces of high reflectance but is normally negligible.

In order to analyze the radiation exchange within the hohlraum, it is necessary to break up the boundaries into a number of isothermal and constant radiosity zones.

The sample is designated as 1, the reference area on the top of the cavity as 2, the view port in the bottom of the cavity as 3, and the remainder of the zones on the cavity walls from 4 to $N$. In taking reflectance measurements, the optical system first views the sample 1, and then the reference area 2. The ratio of the recorder reading when viewing the sample to the recorder reading when viewing the reference area is taken as the measured reflectance $r_m$. (Zero readings are also taken and corrected.) The recorder reading is proportional, at a given slit width, wave length, and amplifier gain, to the difference in radiosity between the radiation source viewed and the chopper blade. Thus, the measured reflectance can be expressed:

$$r_{\lambda m} = \frac{J_{\lambda 1} - J_{\lambda 3}}{J_{\lambda 2} - J_{\lambda 3}} \tag{1}$$

The spectral radiosities of surfaces 1 and 2 are:

$$J_{\lambda 1} = \epsilon_{\lambda 1} E_{\lambda 1} + r_{\lambda 1} \sum_{n=1}^{N} F_{1-n} J_{\lambda n} \tag{2}$$

and

$$J_{\lambda 2} = \epsilon_{\lambda 2} E_{\lambda 2} + r_{\lambda 2} \sum_{n=1}^{N} F_{2-n} J_{\lambda n} \tag{3}$$

Although any cooling of the wall or bottom of the hohlraum due to the inert gas will be greater on the sample side of the cavity, the form factors of the cooled areas relative to the sample and reference are not greatly different. The sample and reference area are located symmetrically in the cavity top, and have the same geometrical relationship with regard to the exit opening.

If equations (2) and (3) are substituted into (1), the expression for the measured reflectance becomes:

$$r_{\lambda m} = \frac{\epsilon_{\lambda 1} E_{\lambda 1} + r_{\lambda 1} \sum_{n=1}^{N} F_{1-n} J_{\lambda n} - J_{\lambda 3}}{\epsilon_{\lambda 2} E_{\lambda 2} + r_{\lambda 2} \sum_{n=1}^{N} F_{2-n} J_{\lambda n} - J_{\lambda 3}} \tag{4}$$

Rearrangement of equation (4) with a little algebraic juggling, which is not included here for reasons of brevity, the assumption of symmetry for the sample and reference area so that $F_{1-n} = F_{2-n}$, and with the aid of the relationship for opaque substances that $a + r = 1.0$, yields:

$$r_{\lambda m} - r_{\lambda 1} = \delta_1 + \delta_2 + \delta_3 + \delta_4 \tag{5}$$

where

$\delta_1$ = error due sample heating

$$\delta_1 = \frac{\epsilon_{\lambda 1}(E_{\lambda 1} - J_{\lambda 3})}{J_{\lambda 2} - J_{\lambda 3}} \tag{6}$$

$\delta_2$ = error due to nonuniform hohlraum temperatures

$$\delta_2 = -\frac{\epsilon_{\lambda 2} r_{\lambda 1} \sum_{n=4}^{N} (E_{\lambda 2} - J_{\lambda n}) F_{2-n}}{(J_{\lambda 2} - J_{\lambda 3})} \tag{7}$$

$\delta_3$ = error due to view port opening in bottom of hohlraum

$$\delta_3 = -\frac{r_{\lambda 1} \epsilon_{\lambda 3} F_{1-3} (J_{\lambda 2} - J_{\lambda 3})}{(J_{\lambda 2} - J_{\lambda 3})} \tag{8}$$

$\delta_4$ = error due to radiation exchange between sample and reference area

$$\delta_4 = -\frac{r_{\lambda 1} r_{\lambda 2} F_{1-2} (J_{\lambda 2} - J_{\lambda 1})}{(J_{\lambda 2} - J_{\lambda 3})} \tag{9}$$

**Error 1.** The effect of sample heating is to increase the measured reflectance above the actual reflectance. This error is proportional to the spectral emittance and is a maximum for materials of low reflectance. The value of $\delta_1/\epsilon_{\lambda 1}$ is plotted in Fig. 16 as a function of wave length for a 50 F rise in sample temperature and a hohlraum temperature of 1400 F. This error is negligible at wave lengths less than about 10 microns. If the zero reading surface is at the sample temperature and black, this error is zero.

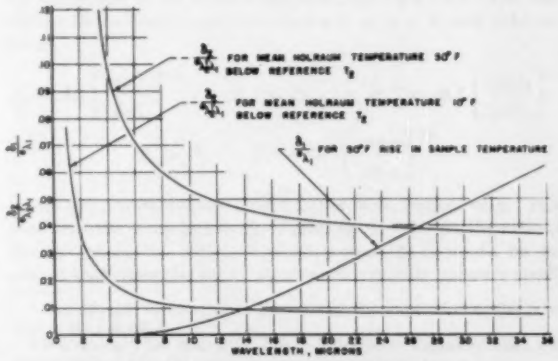
FOR MEAN HOHLRAUM TEMPERATURE 50°F BELOW REFERENCE $T_2$
FOR MEAN HOHLRAUM TEMPERATURE 10°F BELOW REFERENCE $T_2$
FOR 50°F RISE IN SAMPLE TEMPERATURE
WAVELENGTH, MICRONS

Fig. 16 Reflectance errors occurring in hohlraum

**Error 2.** The effect of cooling the bottom part of the hohlraum is to reduce the irradiation of both the sample and the reference area, which causes the measured reflectance to be low. It is seen that this error tends to oppose the first error. This error is proportional to the reflectance of the sample and to the emittance of the reference area. This indicates that a polished metal reference area would be advantageous, although the rest of the hohlraum should have a high emittance. The part of equation (7) within the summation represents the effect of cavity wall cooling. If the walls were all black at the same temperature as the reference area, this term would be zero. The magnitude of this error is shown in Fig. 16 for the case where the cooling of the walls is equivalent to a 50 F drop in temperature relative to the reference area of 1400 F. This error is seen to increase rapidly in the short waves. A curve is also given for a 10-deg F temperature difference.

**Error 3.** The effect of this error is also to reduce the measured value of the reflectance. As $J_{\lambda 3}$ is nearly equal to $J_{\lambda 0}$, this error becomes independent of hohlraum temperature,

$$\delta_3 = -r_{\lambda 1} e_{\lambda 3} F_{1-3} \tag{10}$$

The value of $F_{1-3}$ is about 0.022 for the cavity, so this represents the limiting error for a diffuse reflector with $r_{\lambda 1} = 1$ and $e_{\lambda 3} = 1$. The error is only important for diffuse reflectors and is negligible for specular reflectors. The reason for this is that the diffuse surface views the opening with a firm factor of 0.022, whereas a specular surface only includes radiation reflected from the hohlraum interior.

**Error 4.** The effect of direct radiation exchange between the sample and reference area is negligible for the present design.

#### Other Sources of Error

*Noise Level:* The noise level of the detection amplification and recording system was of the order of 1 per cent of full scale deflection. This resulted in a possible error in reflectance of ±0.01.

*Scattered Energy:* This error is of the greatest magnitude at the two ends of the spectral range covered when the spectral energy in the beam is small and hence the contribution due to scattered energy may be significant. This source of error was controlled in the short waves by use of a plexiglas filter and was shown to be small at 23 microns by use of a NaCl filter.

Most of the scattered energy is of wave lengths less than 15 microns; hence, if a sodium-chloride filter is placed in the beam while the monochromator is set at 23 microns, the energy reaching the detector should be zero as sodium chloride is opaque at this wave length. Any signal from the system would then represent scattered short wave energy.

*Effect of Background of Sample:* This error cannot be accurately defined since no data are available on the true transmittance of the samples; however, from the Final Clothing Report [6] it is seen that for a single layer of cloth with a low reflectance background of magnitude $r_b$ (Fig. 2):

$$r_s = r_m - r_b \tau^2/(1 - r_b r_s)$$

whence it should be apparent, since $r_b < 0.15$ and in practically no case is $r_m > 0.40$ and is generally much lower, that:

$$r_m - r_s \leqq (\tau^2/6.7)$$

and in the single layer case where as a worst case we assume $\tau = 0.60$

$$r_m - r_s \leqq 0.05$$

and in the triple layer case where it would be unusual for $\tau = 0.20$ to occur,

$$r_m - r_s \leqq 0.006 \text{ (negligible)}$$

Therefore as a first approximation we can assume that in the triple layer case the reflectance measured is very close to the actual reflectivity of the 3 layers of cloth and that due to interreflections from the low reflectance background the system reflectance of thinner samples will closely approach the reflectance of the triple layer samples. This is seen to be true from the measured results, and indicates that the background is negligible for the triple layer of cloth.

#### Summary of Error

The actual data error is estimated to be on the order of ±0.03 in the reported reflectance.

#### Nomenclature

- $e_\lambda$ = spectral emittance
- $E_\lambda$ = black body spectral emissive power Btu/(hr ft²μ)
- $F$ = form or configuration factor
- $J_\lambda$ = spectral radiosity (Btu/(hr ft²μ)
- $r_\lambda$ = spectral reflectance
- $\tau$ = transmittance of cloth sample

#### Subscripts

- 0 = chopper blade
- 1 = sample
- 2 = reference area
- 3 = opening in base of hohlraum
- $b$ = background of sample
- $m$ = measured value of reflectance
- $n$ = zone on boundaries of hohlraum
- $S$ = sample corrected for background effect

Journal of HEAT TRANSFER — Technical Briefs

This section consists of contributions of 750 words or less (about 2½ double-spaced typewritten pages, including figures). Technical Briefs will be reviewed and approved by the specific division's reviewing committee prior to publication. After approval such contributions will be published as soon as possible, normally in the next issue of the Journal.

# The Effect of Vapor Drag on Rotating Condensation

E. M. SPARROW[1] and J. L. GREGG[1]

## Introduction

In the analysis of film condensation on external surfaces, it is common to assume that the entire process is governed by force and energy balances within the condensed liquid, and that the vapor plays a very passive role. In particular, it is almost standard to suppose that the vapor offers no shearing resistance to the condensate flow and, hence, the shear stress at the liquid-vapor interface is zero. To lift this assumption and attack the problem in a rigorous way would require *simultaneous* solution of the flow problem in both the liquid and vapor. This poses an exceedingly difficult task which has not heretofore been carried out.[2]

Here, we consider the problem of laminar film condensation on a cooled rotating disk. The centrifugal force field associated with the rotation sweeps the condensed liquid outward over the disk surface—in much the same way as gravity causes the condensate to flow downward in a natural condensation process. Our goal is to formulate and solve this problem without imposing restricting assumptions on the interfacial shear—and this will lead to simultaneous consideration of the flow problem for the liquid and vapor.

A detailed treatment of the condensation problem for a rotating disk has already been presented in a previous paper (reference [2]);[3] but there, the assumption of zero shear at the interface was used. The present work thus constitutes an extension and, to achieve a concise treatment here, we will lean heavily on the material contained in reference [2]. The analysis is carried out for condensation of a pure, saturated vapor at temperature $T_{sat}$ on an isothermal disk at temperature $T_w$. The only motions in the vapor are those induced by the rotation of the disk.

## Analysis

The condensation process is governed by the basic conservation laws of mass, momentum, and energy as given by equations (1) through (5) of reference [2]. These laws apply equally well in the vapor and in the liquid.

The fluid motions which are induced in the vapor will, in turn, affect the flow within the liquid; and this mutual interaction requires simultaneous solution of the equations of motion in the liquid and vapor. But, since we are dealing with saturated vapor, the vapor temperature is essentially constant,[4] and the energy equation need not be considered in the vapor. So, once the velocity solutions are known, we can attack the energy equation for the liquid and obtain the heat-transfer results.

The first step in the analysis is to obtain solutions for the flow. Noting that $z$ represents the distance measured normal to the disk surface, the velocity problem may be formulated as follows: In the condensate layer, which extends from $z = 0$ to $z = \delta$, the mass and momentum conservation equations (1) through (4) of reference [2] are used with fluid properties appropriate to the liquid. In the vapor region, which extends from $z = \delta$ to $z = \infty$, the same equations apply, but now the properties are those of the vapor. At the interface, $z = \delta$, there are conditions of continuity which tie together the liquid and vapor velocities and their derivatives. Using subscripts $l$ and $v$ to denote liquid and vapor, these conditions are:

1 Conservation of mass across interface: $(\rho V_z)_l = (\rho V_z)_v$
2 Equality of tangential velocity: $(V_\phi)_l = (V_\phi)_v$
3 Equality of radial velocity: $(V_r)_l = (V_r)_v$
4 Continuity of tangential shear: $(\tau_{z\phi})_l = (\tau_{z\phi})_v$
5 Continuity of radial shear: $(\tau_{zr})_l = (\tau_{zr})_v$

Finally, the statement of the problem is completed by giving the boundary conditions:

$$\left.\begin{aligned} V_r = V_z = 0 \\ V_\phi = r\omega \end{aligned}\right\} z = 0 \text{ (liquid)} \qquad \left.\begin{aligned} V_r = 0 \\ V_\phi = 0 \end{aligned}\right\} z \to \infty \text{ (vapor)}$$

where $\omega$ is the angular velocity of the disk.

The formidable mathematical problem just outlined is made tractable by use of von Karman's transformation, which reduces the partial differential equations to ordinary differential equations. The transformation consists of a new independent variable $\eta$ and new dependent variables $F$, $G$, and $H$ which have the following definitions

$$\eta = (\omega/\nu)^{1/2}z, \quad F(\eta) = V_r/r\omega, \quad G(\eta) = V_\phi/r\omega, \quad H(\eta) = V_z/(\omega\nu)^{1/2}$$

The transformation applies to both the liquid and vapor provided that appropriate fluid properties are used and additional subscripts $l$ and $v$ are affixed. So, the transformed conservation equations (7) and (8) of reference [2] apply to the liquid when subscript $l$ is added and to the vapor when subscript $v$ is added. The conditions at the liquid-vapor interface $\eta = \eta_\delta$ ($z = \delta$) now take the form[5]

$$H_v = H_l\left[\frac{(\rho\mu)_l}{(\rho\mu)_v}\right]^{1/2}, \qquad H_v' = H_l', \qquad H_v'' = H_l''\left[\frac{(\rho\mu)_l}{(\rho\mu)_v}\right]^{1/2}$$

$$G_v = G_l, \qquad G_v' = G_l'\left[\frac{(\rho\mu)_l}{(\rho\mu)_v}\right]^{1/2}$$

where the primes denote differentiation with respect to $\eta$. It is seen that the jump in velocity functions depends on the ratio of the $\rho\mu$ products. From physical reasoning, it would be expected that when the vapor density and viscosity are very small,

[1] NASA Lewis Research Center, Cleveland, Ohio. Assoc. Mem. ASME. E. M. Sparrow is now Professor of Mechanical Engineering at the University of Minnesota.

[2] An estimate of the effects of vapor drag in the vertical plate problem has been made by Rohsenow, Webber, and Ling (ref. [1]); but their method continues to deal only with the liquid film to which there is applied arbitrary amounts of interfacial shear.

[3] Numbers in brackets designate References at end of paper.

Contributed by the Heat Transfer Division of The American Society of Mechanical Engineers.

Note: Statements and opinions advanced in papers are to be understood as individual expressions of their authors and not those of the Society. Manuscript received at ASME Headquarters, November 13, 1959.

[4] The change in saturation pressure in the vapor due to the rotation is very small.

[5] We also use the fact that $F = -H'/2$ from Equation (1a), reference [2].

the vapor drag would play a minor role. Conversely, the effects of vapor drag should increase as $(\rho\mu)_l/(\rho\mu)_v$ decreases. The boundary conditions may also be transformed into the new variables as follows:[6]

$$\left.\begin{matrix} H = H' = 0 \\ G = 1 \end{matrix}\right\} \eta = 0 \text{ (liquid)} \qquad \left.\begin{matrix} H' = 0 \\ G = 0 \end{matrix}\right\} \eta \to \infty \text{ (vapor)}$$

So, with this, the simultaneous velocity problem for the liquid and vapor is reduced to a form where solutions can be obtained on an electronic computer. Before the numerical integration of the governing equations can be undertaken, it is necessary to specify values for two parameters: (1) The dimensionless film thickness, $\eta_\delta$; (2) the ratio $(\rho\mu)_l/(\rho\mu)_v$, which relates the liquid and vapor velocities at the interface.

With the velocity problem now formulated, we turn to the energy equation (5*a*) for the liquid. The velocity solutions are needed as input data to this equation and, in addition, the Prandtl number Pr must be prescribed. So, there are thus a total of three parameters which characterize each solution of our condensation problem. In reference [2], it is shown that $\eta_\delta$ can be replaced by the more convenient group: $c_{pl}(T_{sat} - T_w)/h_{lg}$ where $h_{lg}$ is the latent heat. With this, the governing parameters may be stated as: $(\rho\mu)_l/(\rho\mu)_v$, Pr, $c_{pl}\Delta T/h_{lg}$.

## Results

Since there are three parameters to be prescribed for each case, care must be exercised in choosing cases to be studied in order to keep the computations within reasonable bounds. Table 1 gives[6] the cases which have been considered, as well as the results for the heat-transfer coefficient $h$ and for the torque $M$ required to rotate the disk. As a point of departure in making these choices, cognisance was taken of the experiments on rotating condensation by Nandapurkar and Beatty [3], who worked with methanol, ethanol, and freon −113 at atmospheric pressure. The $\rho\mu$ ratio of 150 which appears in Table 1 is typical of these experiments, but it also applies to other fluids; e.g., water near atmospheric pressure. The choice of Pr = 10 is made to typify ordinary liquids (i.e., nonmetals), and it is not expected that the precise choice of Pr (for Pr > 1) will significantly influence the comparison between results with and without drag. The range of $c_p\Delta T/h_{lg}$ covers current practice. To test the effect of decreasing $\rho\mu$ ratio (e.g., for water, this ratio decreases as saturation temperature increases), a value of 50 was used, while maintaining $c_p\Delta T/h_{lg}$ at a practical value. Finally, a typical operating condition for liquid metals was studied.

To provide perspective for the results to be presented, it is useful to note the following characteristics of the vapor drag: First, the tangential component of the vapor drag always opposes the rotational motion of the condensate. So, taking account of the vapor drag will give rise to a larger prediction for the torque requirement $M$, and this is demonstrated numerically in the last two columns of Table 1. Since the rotational motions do not transport energy, the effect of the tangential drag upon the heat transfer is felt only indirectly through modification of the radial and axial velocities. Secondly, depending on the operating conditions and on the film thickness in particular, the radial component of the vapor drag may either retard the radial flow of the condensate or else may augment it. It is expected that the retardation would occur for thicker films and the augmentation for thinner films. Since the radial flow in the condensate is directly involved in the transfer of heat to the surface, it is seen that accounting for vapor drag may either increase or decrease the heat transfer, depending on operating conditions. This is illustrated in Table 1. The first entry is for very thin films and shows an increased heat transfer. The other entries are for thicker films and show a decreased heat transfer. To understand the interesting behavior of the radial drag, we recall that the radial velocity is zero both at the disk surface (no slip) and in the ambient fluid. So, a maximum value occurs somewhere between, and it is at this point that the direction of the radial shear force changes sign ($\tau_{sr} \sim \partial V_r/\partial z$). For very thin condensate layers, the velocity maximum occurs in the vapor; and under this condition, the vapor exerts a positive radial shear force on the condensate layer. For thicker condensate layers, the velocity maximum occurs within the condensate. In this event, the vapor exerts a negative (retarding) shear force.

Now, looking in greater detail at the heat-transfer listing of Table 1, we first turn our attention to the results for Pr = 10 (nonmetallic liquids). For all the cases considered, the effects of vapor drag on heat transfer are seen to be quite small. At the fixed $\rho\mu$ ratio of 150, larger effects were found for either thin films ($c_p\Delta T/h_{lg} \to 0$) or very thick films ($c_p\Delta T/h_{lg} = 0.855$). The change of the $\rho\mu$ ratio from 150 to 50 (at a fixed value of $c_p\Delta T/h_{lg}$ and Pr) had almost no effect on the case considered, although larger effects might conceivably have occurred at the extremes of thick and thin films. For the single liquid metal case considered (Pr = 0.008), the effect of vapor drag was larger than that for the nonmetallic liquids. This finding is associated with the fact that the liquid metal case had the largest (dimensionless) film thickness of all the entries of the table. Apparently, this was sufficient to override the expected tendency of the high $\rho\mu$ ratio (650) to diminish the coupling between liquid and vapor.

The experiment of reference [3] corresponded approximately to the second entry in the table. Since the effect of vapor drag on the *analytical prediction* of heat transfer as given in reference [2] is not significant, the 30 per cent deviation between theory and experiment must be laid to other causes.

## References


1 W. M. Rohsenow, J. H. Webber, and A. T. Ling, "Effect of Vapor Velocity on Laminar and Turbulent Film Condensation," Trans. ASME, vol. 78, 1956, pp. 1637–1649.

2 E. M. Sparrow and J. L. Gregg, "A Theory of Rotating Condensation," Journal of Heat Transfer, Trans. ASME, Series C, vol. 81, 1959, pp. 113–120.

3 S. S. Nandapurkar and K. O. Beatty, Jr., "Condensation on a Horizontal Rotating Disc," Preprint 112, presented at the Third National Heat Transfer Conference, ASME-AIChE, Storrs, Connecticut, August, 1959.


[6] Unsubscripted properties are those of the liquid.

**Table 1 Effects of vapor drag**

| $[(\rho\mu)_l/(\rho\mu)_v]^{1/2}$ | $c_p\Delta T/h_{lg}$ | Pr | $\frac{h(\nu/\omega)^{1/2}}{k}\left[\frac{c_p\Delta T/h_{lg}}{\text{Pr}}\right]^{1/4}$ | | $\frac{2M}{\pi r_0^4 \rho(\nu\omega^3)^{1/2}}$ | |
|---|---|---|---|---|---|---|
| | | | No drag[b] | Drag | No drag[b] | Drag |
| 150 | →0[a] | All | 0.903 | 0.9147 | ... | ... |
| 150 | 0.170 | 10 | 0.924 | 0.9176 | 0.041 | 0.08005 |
| 150 | 0.855 | 10 | 0.995 | 0.9654 | 0.126 | 0.2174 |
| 50 | 0.172 | 10 | 0.924[+] | 0.9208 | 0.041[+] | 0.08283 |
| 650 | 0.00244 | 0.008 | 0.836 | 0.7431 | 0.31 | 0.4627 |

[a] Thin film theory, Appendix, reference [2].
[b] Interpolated values from reference [2].

# Radiation Fin Effectiveness

J. G. BARTAS[1] and W. H. SELLERS[2]

## Introduction

POWER PLANTS operating in space for long periods of time have one heat sink, space, and one means of transferring heat to the heat sink, a radiator. This radiator is a "true" radiator in that all heat leaving its surfaces does so by radiation. There is, apparently, no reference in the available literature which provides a rapid method for estimating the radiator effectiveness and for optimizing fin designs.

This analysis considers the radiator configuration shown in Fig. 1. In this design, parallel pipes are joined by webs, which act as radiation fins. Heat flows by conduction from the pipes down the fin and radiates from both surfaces. The fin surface may "see" other portions of the radiator if the radiator is conical, cylindrical, spherical, and so forth. The radiator may see a sun or other body, as well as deep space. The absorbed incident energy from these sources can be determined, and a mean "space" temperature $T_s$ can be computed. Thus the problem is reduced to consideration of a fin which radiates to a constant temperature environment $T_s$.

Results for radiator fin effectiveness have been computed for a limiting class of radiation fins—the case where the radiator is perfectly flat, i.e., there is no spacial interference of radiation by the pipes. This situation also is mathematically equivalent to a condition where the pipes are perfect specular reflectors.

## Assumptions

The following assumptions are made:

1 Material properties $k$, $\epsilon$ are independent of the temperature.

2 Emissivity $\epsilon$ is independent of the angle.

3 The fin thickness $2b$ is constant.

4 The fin base temperature $T_R$ is constant across the base of the fin.

5 The fin base temperature $T_R$ is constant along the pipe axis. Conduction heat flow is one-dimensional.

6 The surface heat transfer is entirely by radiation.

The foregoing assumptions are those made in conventional fin analyses, except for the added restrictions due to the radiation effects and the lack of convection.

## Energy Balance Equation

Consider the geometry shown in Fig. 2. The energy balance equation for the element $dx$ is

$$Q_c + Q_{R\,IN} = Q_c + \frac{dQ_c}{dx}\,dx + Q_{R\,OUT} \tag{1}$$

Conduction heat flow $Q_c$ is

$$Q_c = -kA_x \frac{dT}{dx} \tag{2}$$

where the cross-sectional flow area $A_x$ is equal to $2b$ per unit fin depth. The *net* radiant heat flux is given by

$$Q_{R\,OUT} - Q_{R\,IN} = \sigma\bar{\epsilon}dA_s(T^4 - T_{SR}^4)$$

where $\bar{\epsilon}$ is the emissivity function, and $dA_s$ is the incremental surface area $2dx$. The parameter $T_{SR}$ is defined here as

$$T_{SR}^4 \equiv T_S^4(1 - F) + T_R^4 F$$

where $T_S$ is the space temperature, $T_R$ is the fin root temperature, and $F$ is the radiant interchange configuration factor of the element surface $dx$ with respect to the two nearest pipes. The net radiant heat flux equation is, therefore,

$$Q_{R\,OUT} - Q_{R\,IN} = \sigma\bar{\epsilon}dA_s[T^4 - T_s^4(1 - F) - T_R^4 F] \tag{3}$$

Combining Equations (1), (2), (3), and canceling common terms, we have

$$kb\frac{d^2T}{dx^2} = \sigma\bar{\epsilon}[T^4 - T_s^4(1 - F) - T_R^4 F] \tag{4}$$

Equation (4) is subject to the boundary conditions

at

$$x = 0 \qquad \frac{dT}{dx} = 0 \tag{5a}$$

at

$$x = L, \qquad T = T_R \tag{5b}$$

Equation (4) is nondimensionalized to

[1] Senior Heat Transfer Engineer, General Electric Company, West Lynn, Mass. Assoc. Mem. ASME.

[2] Supervisor, Calculations and Special Problems Unit, General Electric Company, West Lynn, Mass.

Contributed by the Heat Transfer Division of THE AMERICAN SOCIETY OF MECHANICAL ENGINEERS and presented at the ASME-AIChE Heat Transfer Conference Storrs, Conn., August 9–12, 1959.

NOTE: Statements and opinions advanced in papers are to be understood as individual expressions of their authors and not those of the Society. Manuscript received at ASME Headquarters, November 26, 1959. Condensed from paper No. 59—HT-17.

Fig. 1 Schematic radiator tube sheet

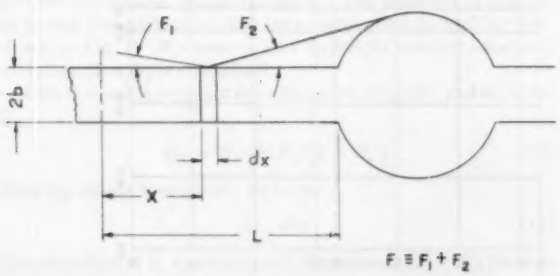


Fig. 2 Radiation fin geometry designations

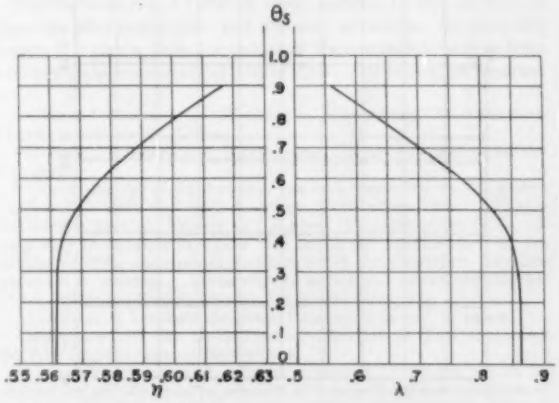


Fig. 3 Radiator fin effectiveness versus parameter λ

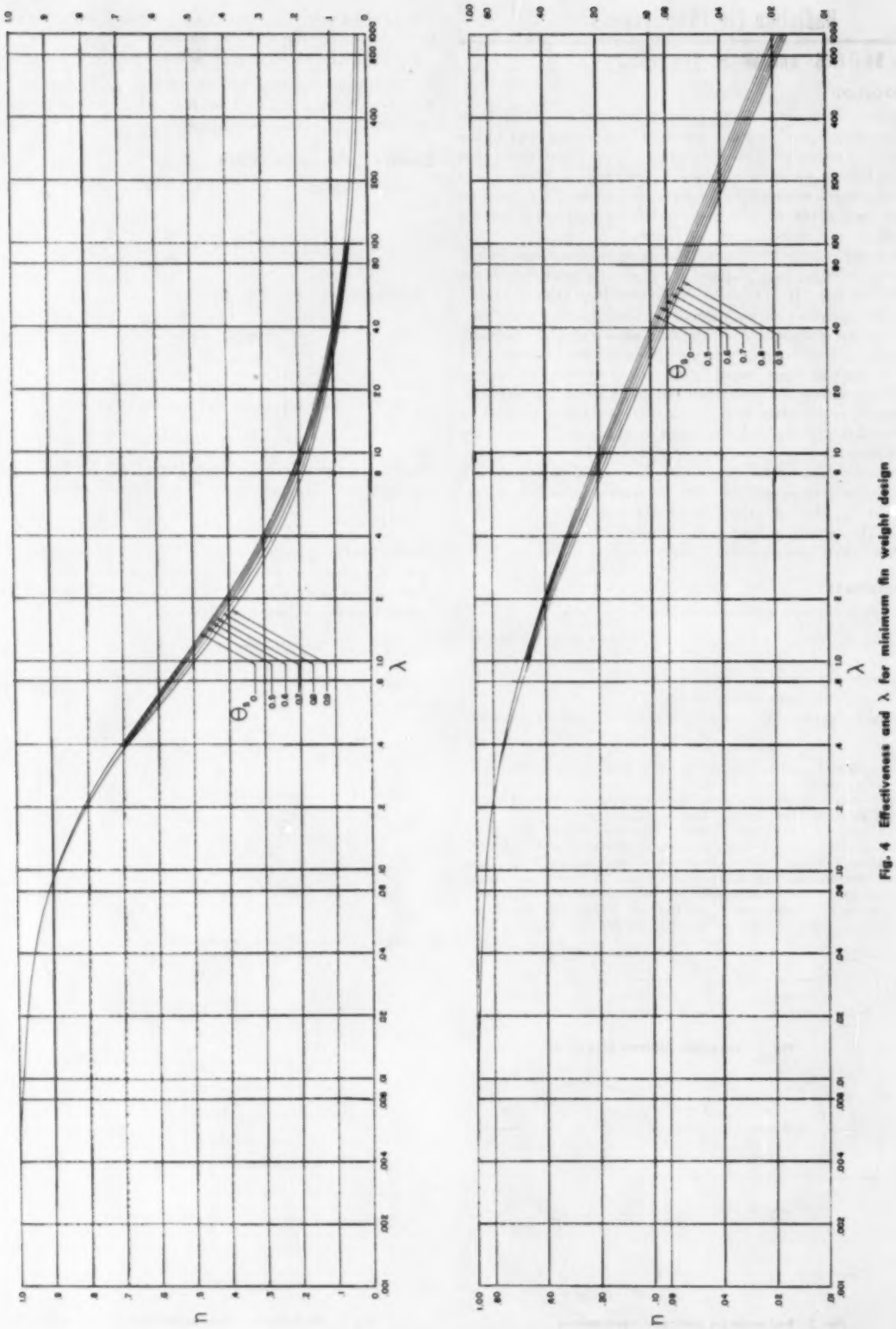


Fig. 4 Effectiveness and λ for minimum fin weight design

$$\frac{d^2\theta}{d\rho^2} = \lambda[\theta^4 - \theta_s^4 - F(1 - \theta_s^4)] \tag{6}$$

where

$\theta = T/T_R$
$\rho = x/L$
$\lambda = \sigma\bar{\epsilon}L^2T_R^3/kb$

The boundary conditions are

at

$$\rho = 0, \quad \frac{d\theta}{d\rho} = 0 \tag{7a}$$

at

$$\rho = 1, \quad \theta = 1 \tag{7b}$$

### Effectiveness

The fin effectiveness $\eta$ is defined as

$$\eta \equiv \frac{Q_A}{Q_I} \tag{8}$$

where $Q_A$, and $Q_I$ are the actual and ideal heat flows, respectively. The actual heat flux is evaluated at $x = L$

$$Q_A \equiv \left| -kA_s\left(\frac{dT}{dx}\right)_{x=L}\right|$$

or

$$Q_A \equiv \left| -k2b\,\frac{T_R}{L}\left(\frac{d\theta}{d\rho}\right)_{\rho=1}\right| \tag{9}$$

The ideal heat flux is defined by assuming the entire fin is at the fin root temperature and radiates without interference,

$$Q_I = \sigma\bar{\epsilon}A_s[T_R^4 - T_s^4]$$

or

$$Q_I = \sigma\bar{\epsilon}2LT_R^4[1 - \theta_s^4] \tag{10}$$

Combining Equations (8), (9), (10)

$$\eta = \frac{\left(\frac{d\theta}{d\rho}\right)_{\rho=1}}{\lambda(1 - \theta_s^4)} \tag{11}$$

### Results

A limiting case of radiator design has been analyzed in detail. It was assumed that $F = 0$. That is, there is no special interference of the radiation by the pipes.

Equations (6) and (11) were solved numerically on an IBM 704 digital computer. The results for the fin effectiveness are plotted in Fig. 3.

### Optimum Fin Geometry

The premium for weight saving in space hardware makes it imperative to optimize radiator designs. The following is limited to finding the optimum design for a rectangular fin such as that shown in Fig. 2. We assume that fin weight remains constant, while heat flow $Q_A$ is maximized.

With $F$ equal to zero, combine Equation (8), (10), and solve for $Q_A$

$$Q_A = N\sigma\bar{\epsilon}2LT_R^4(1 - \theta_s^4) \tag{12}$$

Since fin weight is constant, we have

$$bL = c' \tag{13}$$

The definition of $\lambda$, combined with Equations (12), (13), leads to

$$Q_A = \eta\lambda^{1/3} \times \text{constant} \tag{14}$$

where the constant is equal to

$$2T_R^4(1 - \theta_s^4)[\sigma^2\bar{\epsilon}^2kc']^{1/3}$$

We can plot $Q_A$ versus $\lambda$ and find the maximum $Q_A$ directly, $\eta$ being a function of $\lambda$ as shown in Fig. 3.

A graph of the effectiveness $\eta$ and parameter $\lambda$ that correspond to a minimum weight fin at any $\theta_s$ is plotted in Fig. 4.

### Concluding Comment

Note the relationship between the present parameter $\lambda$ and the parameter $ml$ in conventional convection fin analyses.

$$\lambda = \sigma\bar{\epsilon}T_R^3\,\frac{L^2}{kb}$$

$$(ml)^2 = h\,\frac{L^2}{kb}$$

It is apparent that

$$h \sim \sigma\bar{\epsilon}T_R^3$$

This result is expected, since the equivalent radiation heat-transfer coefficient is commonly defined as

$$h_r \equiv \sigma\bar{\epsilon}T_R^3$$

if $T_R \to 0$.

The radiation fin performance curve follows the classical pattern but with considerable variation due to the mode of heat transfer. It is unfortunate that the profuse data available on convective fins are not convertible to the evaluation of radiation fins.

## A Tabulation of the Function exp $X^2$ erfc $X$

**J. E. SUNDERLAND[1] and R. J. GROSH[2]**

THE FUNCTION exp $X^2$ erfc $X$ is tabulated for values of the argument running from 0.10 to 7.00 in increments of 0.01. The values reported were obtained by hand and machine computation and are given to four, five, or six significant figures with an error of plus or minus one in the last figure. For values of the argument less than 0.10 or greater than 7.00, convenient expressions are given for the function. The tabulation of the function has been placed on file at the American Documentation Institute.[3]

The function exp $X^2$ erfc $X$ often appears in the solution of transient heat conduction and diffusion problems. Carslaw and Jaeger [1][4] give a table for values of the argument ranging from 0.00 to 3.00 in increments of 0.05 or 0.10. The values are reported

[1] Assistant Professor of Mechanical Engineering, Northwestern University, Evanston, Illinois.

[2] Professor of Mechanical Engineering, Purdue University, Lafayette, Ind.

[3] The tabulation of the function has been deposited as Document number 6157 with the ADI Auxiliary Publications Project, Photoduplication Service, Library of Congress, Washington 25, D. C. A copy may be secured by citing the Document number and by remitting $1.25 for photoprints, for $1.25 for 35 mm microfilm. Advance payment is required. Make checks or money orders payable to: Chief, Photoduplication Service, Library of Congress.

[4] Numbers in brackets designate References at end of paper.

Contributed by the Heat Transfer Division of THE AMERICAN SOCIETY OF MECHANICAL ENGINEERS.

NOTE: Statements and opinions advanced in papers are to be understood as individual expressions of their authors and not those of the Society. Manuscript received at ASME Headquarters, December 9, 1959.

with four significant figures. Radau [2] tabulated $\sqrt{\pi}/2 \exp X^2 \operatorname{erfc} X$ to twelve significant figures for integral values of $X^2$ from 3 to 16. The function $\sqrt{\pi}/2 \exp X^2/2 \operatorname{erfc} X/\sqrt{2}$ has been tabulated by Sheppard [3] to twenty-four places for values of $X$ ranging from 0.00 to 10.0 in increments of 0.01, and by Mills [4] to five places for values of $X$ ranging from 0.00 to 4.00 in increments of 0.01, 4.00 to 5.00 in increments of 0.05, and 5.00 to 10.0 in increments of 0.10. All these functions are, of course, related. The purpose of the tabulation reported here is to provide a convenient and accurate table of the function $\exp X^2 \operatorname{erfc} X$. Before the results are given, the functions will be defined, the method of calculation described, and certain useful, but not original approximations indicated.

The symbol $\exp X^2$ is defined as the value of the number 2.71828 ($e$) raised to the $X^2$ power.

The symbol $\operatorname{erfc} X$ is defined as the complement of the error function with argument $X$, $\operatorname{erf} X$; that is

$$\operatorname{erfc} X = 1 - \operatorname{erf} X$$

where

$$\operatorname{erf} X = \frac{2}{\sqrt{\pi}} \int_0^x \exp(-u^2) du$$

It follows that

$$\operatorname{erfc} X = \frac{2}{\sqrt{\pi}} \int_x^\infty \exp(-t^2) du$$

Finally, it can be remarked that these integrals are closely related to the probability or Gauss error integral [5, 6].

Rather than make use of the previous tabulations, which differ from the results reported here by constants in the argument and/or preceding the function, it was found more convenient to use an ElectroData digital computer for obtaining values of the function when $X$ was in the range 0.10 to 3.00. The programming routine employed polynomial expansions for the exponential and error functions.

For values of $X$ in the range 3.00 to 7.00 the function was evaluated by means of the twelve to eighteen place tables given in references [7 and 8].

The consistency of the table was checked by a simple differencing technique which involved taking the first and second differences between each successive number on the table. Where the second differences showed no abrupt changes, the table was considered to be consistent.

For values of $X$ greater than one the function can be determined from the expansion

$$f(x) = \frac{1}{x} \frac{1}{\sqrt{\pi}} \left[ 1 - \frac{1}{2x^2} + \frac{1.3}{2^2 x^4} - \ldots + (-1)^{n-1} \frac{1.3.5 \ldots (2n-3)}{2^{n-1} \quad x^{2n-2}} \right]$$

and the error is less than the last term used. As $X$ becomes larger, the series converges faster and for values of $X$ greater than seven, the error is less than 1 per cent when only the first term of the expansion is used. Using two terms of the expansion, the error is less than 0.04 per cent.

For all finite values of $X$ it is noted that

$$f(x) = \exp(x^2) \left[ 1 - \frac{2}{\sqrt{\pi}} \sum_{n=0}^{\infty} \frac{(-1^n) x^{2n+1}}{(2n+1)\, n!} \right]$$

For values of $X$ less than 0.1, using only the first term of the series expansion, the function becomes

$$f(x) = \exp(x^2) \left[ 1 - \frac{2}{\sqrt{\pi}} x \right]$$

and gives an error of less than 0.05 per cent.

The tabulation of the function is on file at the American Documentation Institute.


## Acknowledgments

The writers gratefully acknowledge support from the Office of Ordnance Research, U. S. Army; the use of an ElectroData digital computer made available by Purdue University; the hand computations performed by Mr. James Matchett.


## References


1 H. S. Carslaw and J. C. Jaeger, "Conduction of Heat in Solids," The Clarendon Press, Oxford, England, 1948, p. 373.

2 R. Radau, "Tables of the Integral $f(x) = \sqrt{\pi}/2 \exp X^2 \operatorname{erfc} X$," *Annals de l'Observatoris de Paris, 1885 Memoires*, vol. 18, pp. B 1–25.

3 W. P. Sheppard, "The Probability Integral," *British Association for the Advancement of Science, Mathematical Tables*, vol. VII, 1939, pp. 1–22.

4 J. P. Mills, "Table of the Ratio: Area to Bounding Ordinate, for Any Portion of Normal Curve," *Biometrika*, vol. 18, 1926, pp. 395–400.

5 H. B. Dwight, "Tables of Integrals and Other Mathematical Data," The Macmillan Company, New York, N. Y., revised edition, 1954, p. 129.

6 M. Jakob, "Heat Transfer—Volume I," John Wiley & Sons, Inc., New York, N. Y., 1955, p. 253.

7 Federal Works Agency, Work Projects Administration, "Tables of the Exponential Function," National Bureau of Standards, 1939.

8 Federal Works Agency, Work Projects Administration, "Tables of Probability Functions—Volume I," National Bureau of Standards, 1941.

Journal of HEAT TRANSFER

# Information for Authors

• Manuscripts should be submitted in final form to the Editor. Each manuscript must be accompanied by a statement that it has not been published elsewhere nor has it been submitted for publication elsewhere. A paper which would occupy more than 8 pages of the Journal may be returned to the author for abridgment.

• The author should state his business connection, the title of his position, and his mailing address. A short abstract (50 to 100 words) should be included on the first page immediately preceding the introductory paragraph of the paper.

Three copies of the manuscript are required. One of these must be a carefully prepared printer's copy, typed in double spacing, on one side of the page only, with wide margins, on $8^1/_2$ by 11-in. opaque white paper. Mimeographed manuscripts, if prepared with exceptional care, can be accepted provided they are completely edited.

• As far as possible, all mathematical expressions should be typewritten. Greek letters and other symbols not available on the typewriter should be carefully inserted in ink. Care should be taken to distinguish between capital and lowercase letter, between zero (0) and the letter (*O*), between the numeral (1) and the letter (*l*), etc. A letter representing a vector cannot be printed with an arrow above or below it. The letter should be underscored with a single wavy line, wherever it appears in the text, to designate boldface type.

• A list of symbols carefully marked for the use of the editor (thus: $\kappa$, Greek l.c. kappa), if it has not been included in the body of the paper, should accompany the manuscript on a separate page.

• Before preparing a manuscript the author should study printed articles in the Journal, with special attention to the form and style of mathematical expressions, tables, footnotes, references, and abstract. Numbers that identify mathematical expressions should be enclosed in parentheses. Numbers that identify references at the end of the paper should be enclosed in brackets. Care should be taken to arrange all tables and mathematical expressions in such a way that they will fit into a single column when set in type. Equations that might extend beyond the width of one column (fractions that should not be broken or long expressions enclosed in parentheses) should be rephrased to go on two or more lines within column width. Fractional powers are preferred to root signs and should always be used in more elaborate formulas. The solidus should be used instead of the horizontal line for fractions wherever possible.

• A normal paper should not exceed 8 pages in the Journal. It is about 8000 words or 20 double-spaced typewritten pages exclusive of drawings. A Technical Brief should not exceed 750 words or about one page in the Journal inclusive of drawings.

• Originals and two copies of figures must accompany the manuscript. Line drawings should not be larger than $8^1/_2 \times 11$ in. and should be planned for reduction to column width. Lettering should be large enough to be clearly legible when the illustration is reduced. The originals of line drawings must be in India ink on white or pale blue tracing paper or tracing cloth. Photographs of equipment or test specimens must be glossy prints and should be used sparingly. Captions for figures should be typed double-spaced and included as the last page of the manuscript. The figure number and author's name should be written in the margin or on the back of each illustration.

• Titles of papers should be brief.

• Authors can obtain copies of the ASME Manual MS-4, "An ASME Paper," from the Editor and are urged to do so before drafting their papers in final form.

• Papers published in Journals of the Transactions of the ASME must be presented at a Meeting, either in person or by title.

• An author is entitled to 25 preprints free of charge ( in the case of two authors, 15 each; three or more authors, 10 each). Larger quantities of preprints or reprints can be ordered from Editorial Department, The American Society of Mechanical Engineers, 29 West 39th Street, New York 18, N. Y. Quotations will be sent on request.

Please address all communications to:

**Editor, ASME,**

**29 West 39th Street,**

**New York 18, N. Y.**

**ASME Publications Committee**

# New Publications

## STRUCTURAL DAMPING

In this book engineers and scientists will find a wealth of information useful in engineering design, such as:

the discussion concerning the principal mechanisms by which structure dissipates damping energy;

the identification and classification of the various types of material and system mechanisms;

the reviews of current research in energy dissipation through interfacial slip at contact surfaces of structure and machine joints;

a method for analyzing systems composed of viscoelastic and elastic materials applied to an elastic plate, along with specific results for a number of damping treatments such as, automotive undercoat, damping tape, and sandwich plates with dissipative cores;

the results of a preliminary experimental study of vibrational energy dissipation at the support junctions of built-in beams and plates;

details of structural damping measurement methods and the limitations that are imposed by the assumptions associated with each method;

a fatigue strength damping criteria for selecting the proper structural materials for the design of members which are subjected to fluctuating resonant stresses;

a hundred references to articles on structural damping, arranged alphabetically according to authors and chronologically for a given author.

***This information was prepared by authorities in the field and presented at a colloquium held at the 1959 ASME Annual Meeting.***

**Paper Binding, 165 Pages $4.25***

## SPRAY LITERATURE ABSTRACTS

Here, for the first time, is a comprehensive source-book on the multitudinous applications of sprays and their scientific, technical and industrial aspects. The compilation comprises over 1300 items collected from the technical literature of 24 countries, published from 1880 to 1958 inclusive. The abstracts are detailed, contain full bibliographic data, as well as information on the affiliation of each author wherever available. Entries include:

fuel sprays for furnaces, internal combustion engines, gas turbines, and rockets;

sprays in industrial processes for evaporation, drying, humidification, cooling, air conditioning, and chemical reactions;

atmospheric sprays, as rain, fog, haze, sleet and snow, their formation, evaporation and freezing;

agricultural sprays for sprinkling, pest, fungus, and weed control;

fire-fighting sprays, as in sprinkler systems and in fire-smothering fogs;

aerosols for medical, disinfecting, therapeutic, and air conditioning purposes;

sprays and fogs for military purposes in defense and attack.

Other entries direct attention to published information having a bearing on the theoretical and experimental study of sprays; in particular:

mathematics, ranging from arithmetics to statistics and probability theory;

physics and chemistry, dealing with the properties of liquids and gases, especially the science of colloids and other disperse systems;

hydro-, aero-, and thermodynamics, and rheology, dealing with the motion of liquids in spray-generating devices, the breakup of liquid stream into drops, and their motion in air, their evaporation and combustion;

optical and electronic devices for the experimental study of sprays;

branches of mechanical and production engineering concerned with the design, production, and testing of pumps, nozzles, and other elements of spray generating equipment;

borderline and associated disciplines, such as the science and technology of powders and dusts.

**Cloth Binding 384 Pages $12.00***

## SUCCESSFUL TECHNICAL WRITING

This is a comprehensive treatment that can be used profitably by engineers, scientists, and technicians who wish to improve their skill and effectiveness as well as by those who have never written before. It shows how to look for ideas, how to evaluate them, how to build an idea into an outline, how to write-up the idea, and how to work with editors and publishers in getting the idea into print. In addition to sections on technical articles, reports, and books, including text books and handbooks, this book also gives useful material on military and industrial training manuals and industrial advertising.

**By arrangement with the publisher, McGraw-Hill Book Company, ASME members may purchase copies from the Society at a 20% discount.**

**Cloth Binding 294 Pages $5.50***

## ILLUSTRATIONS FOR PUBLICATION AND PROJECTION

With the help of this American Standard clear, legible, and effective illustrations can be prepared with a minimum of effort. Here will be found descriptions of preferred illustrations and layout practices, a discussion of the factors influencing legibility of reproductions, suggestions on the preparation of illustrations suitable for technical publications, recommendations on preparing copy for either still projections or publications, and general guidance information on drafting practices and on material useful in illustration work.

**ASA Y15.1–1959 $2.00***

***20% discount to ASME members**

**OF THE AMERICAN SOCIETY OF MECHANICAL ENGINEERS**
**29 West 39th Street, New York 18, N. Y.**